The use of a UK Alum Water Treatment Sludge as a Supplementary Cementitious Material – Characteristics, Hydration and Performance

Mubarak Yahaya Shamaki

Submitted in accordance with the requirements for the degree of Doctor of Philosophy

The University of Leeds
School of Civil Engineering

January 2021

The candidate confirms that the work submitted is his own, except where work which has formed part of jointly authored publications has been included. The contribution of the candidate and the other authors to this work has been explicitly indicated below. The candidate confirms that appropriate credit has been given within the thesis where reference has been made to the work of others.

Parts of the works reported in chapters 4, 5 and 6 have been jointly published in a journal or proceedings of conferences as follow:

- M. Shamaki, S. Adu-amankwah, L. Black, Reuse of UK alum water treatment sludge in cement-based materials, Constr. Build. Mater. 275 (2021) 122047.

- M. Shamaki, L. Black, Characterization and pozzolanic activity of UK alum water treatment sludge, Proceedings of the RILEM International Conference on Sustainable Materials, Systems and Structures (SMSS): New Generation Construction Materials, Rovinj, Croatia, 2019, pp. 19-26.

- M. Shamaki, M. Lock, S. Adu-Amankwah, L. Black, Hydration and strength development of ternary cement blends containing calcined alum water treatment sludge and limestone powder, Proceedings of the 39th Cement and Concrete Science Conference, Bath, 2019, pp. 87-91.

Acknowledgements

I'd like to start by expressing my profound gratitude to my supervisor, Professor Leon Black. This research project was only possible through his valuable recommendations, support and guidance. I'll forever be grateful for his constant help and encouragement. I must also give thanks to my co-supervisor Dr. Samuel Adu-amankwah for his technical support and contributions during this project.

My thanks and appreciation go to Civil Engineering technical staff Lucy, Les, Karen, Steve and Marvin for their valuable training and support in the laboratories.

To my past and present colleagues Suraj, Joseph, Shola, Ahmad, Diletta, Tiemo, Saleh, Jamiu, Mustafa, Mohammad, Hong and Ali, I say a huge thank you for all the knowledge sharing, morale support and for listening to my numerous complaints about research challenges.

To my beloved Mother, Father and Sisters, thank you for the encouragement and support through this journey. This thesis is dedicated to you.

Abstract

The use of supplementary cementitious materials (SCMs) offers a viable solution to partially substitute Portland cement and reduce carbon emissions associated with cement production. However, concerns over the future availability of traditional SCM sources, such as fly ash and slag, have left the concrete industry in need of alternatives. Water treatment plants generate large volumes of waste alumina-rich sludge in the purification of water for potable supplies. In the UK, the commonly used long-term disposal method is landfilling but this is being actively discouraged due to limited landfill spaces and increasing landfill costs. To address this disposal challenge and the need for alternative sources of SCMs, this thesis assesses the suitability of alum sludge as an additive in cement. A clear understanding of the physical and chemical impact of binder materials is fundamental to predicting performance and durability. Consequently, this work investigates the physical, chemical, and mineralogical properties of alum sludge and its calcination products, and their impact on the hydration, phase assemblage, microstructural development and engineering performance of blended cements.

Alum sludge was calcined at 475-1100^{o}C and then characterized to correlate thermal changes with cementitious activity and engineering performance. Alum sludge calcined at 825^{o}C transforms to poorly crystalline η-alumina (eta) and has the best cementitious activity. It is found that the reactivity of the sludge leads to the massive precipitation of ettringite at very early age which impairs the ability of gypsum to control C_3A hydration leading to an undersulfated cement which inhibits alite hydration. The poorly crystalline η-alumina is metastable, transforming to highly crystalline α-alumina (alpha) at 1100^{o}C, whereupon alite hydration is enhanced because undersulfation is avoided and the alumina provides nucleation sites, leading to improved performance. The results obtained highlight the main properties of calcined sludge, explaining their influence on calcined sludge reactivity, cement hydration and the microstructure of the matrix.

Synergistic interactions of calcined sludge in blended cements containing slag (amorphous silicon oxide source) and/or limestone (calcium carbonate source) were explored. Results show that coupled substitutions of slag and calcined sludge (at

825^{o}C) also resulted in an undersulfated condition due to reduction of gypsum contained in PC and the increased Al^{3+} concentration contributed by both slag and sludge leading to significant inhibition of alite hydration. Consequently, slag hydration was also hindered, leading to further reduction in performance. However, a synergistic interaction between limestone and η-alumina from sludge calcined at 825^{o}C was confirmed. Calcined sludge provides aluminates, increasing the aluminate-sulfate ratio and enhancing limestone reaction. This reaction leads to the formation of mono- or hemicarboaluminate hydrates instead of monosulfoaluminate hydrate and stabilizes ettringite, leading to enhanced mechanical strength. This synergistic effect produced comparable strength to neat PC within 7 days with Strength Activity Indices up to ~98%. The lower pH of calcined sludge favoured limestone dissolution which enhanced Al^{3+} reaction, which is limited by gypsum dissolution in the absence of limestone. Hence, with an increase in the calcined sludge content, the chemically reactive portion of limestone increased. However, the degree of alite hydration decreased and undersulfation was evident at higher doses of calcined sludge. At later ages, the hydration of clinker phases in the neat PC system progresses at a faster rate leading to slightly lower Strength Activity Indices in the ternary calcined sludge-limestone cements.

The findings of this study show that clinker hydration and mechanical strength are strongly influenced by Al_2O_3/SO_3 ratio in the calcined sludge-blended cements. To avoid an undersulfated condition, it is proposed that optimal doses of gypsum and limestone powder can help control the accelerator effect of 825^{o}C sludge on C_3A hydration while exploiting reaction synergies with limestone. In this way, the higher reactivity of the 825^{o}C sludge can be better utilized for improved performance. This study provides a fundamental base and a promising direction for further studies and the widespread utilisation of calcined alum sludge in the cement industry.

Table of Contents

List of Tables

List of Figures

List of Abbreviations

Cement Nomenclature:

A = Al_2O_3	K = K_2O
C = CaO	M = MgO
C = CO_3	N = Na_2O
F = Fe_2O_3	S = SiO_2
H = H_2O	$= SO_3

Clinker Phases and Hydrated assemblages

Alite	$3CaO.SiO_2$
Belite	$2CaO.SiO_2$
Calcium Aluminate Silicate Hydrate	$CaO\text{-}Al_2O_3\text{-}SiO_2\text{-}H_2O$
Calcium Silicate Hydrate	$CaO\text{-}SiO_2\text{-}H_2O$
Ettringite / AFt	$3CaO.Al_2O_3.3CaSO_4.32H_2O$
Gypsum	$CaSO_4.2H_2O$
Hemicarboaluminate / Hc	$3CaO.Al_2O_3.0.5Ca(OH)_2.0.5CaCO_3.11.5H_2O$
Hydrotalcite / Ht	$Mg_6Al_2(OH)_{16}.CO_3.4H_2O$
Monocarboaluminate / Mc	$3CaO.Al_2O_3.CaCO_3.11H_2O$
Monosulfoaluminate / Ms	$3CaO.Al_2O_3.CaSO_4.12H_2O$
Portlandite/ CH	$Ca(OH)_2$
Stratlingite	$2CaO.Al_2O_3.SiO_2.8H_2O$
Tricalcium Aluminate	$3CaO.Al_2O_3$
Tetracalcium alumino- ferrite	$4CaO.Al_2O_3.Fe_2O_3$

Techniques

BSE	Back-Scattered Electron
DSC	Differential Scanning Calorimetry
DTA	Differential Thermal Analysis
EDX	Energy Dispersive X-Ray Spectroscopy
EMPA	Electron Microprobe Analyzer
FTIR	Fourier Transform Infrared Spectroscopy
ICC	Isothermal Conduction Calorimetry
SEM	Scanning Electron Microscopy
SEM-IA	Scanning Electron Microscopy Image Analysis
STA	Simultaneous Thermal Analysis
TEM	Transmission Electron Microscope
TGA	Thermogravimetric Analysis
TG-MS	Thermogravimetric and Mass Spectrometry
XRD	X-Ray Diffraction

Materials / Properties

AWTS	Alum Water Treatment Sludge
GGBS	Ground Granulated Blast Furnace Slag
PC	Portland Cement
NA	Nano- alumina
SP	Superplasticiser
WTS	Water Treatment Sludge
W/B	Water – Binder Ratio
W/C	Water – Cement Ratio

Chapter I: Introduction

1.1 Background and Problem Statement

The manufacture of cement is an energy intensive process contributing an estimated 5-7% of global CO_2 emissions [1]. Considerable progress has been achieved in lowering the environmental impact of cement production through increasing energy efficiency and the use of alternative fuels in the clinkering process. However, about 60% of the 0.8-1 tonnes of CO_2 emitted per tonne of clinker is related to the thermal decomposition of limestone into quicklime [2]. Conventional supplementary cementitious materials (SCMs), such as fly ash and ground granulated blast furnace slag (GGBS) are viable partial replacements for Portland Cement (PC). The use of such materials, where no additional clinkering process is required, provides considerable reduction in CO_2 emissions as well as a way of valorising industrial by-products. However, shortages in the supply of SCMs in some locations, plus threats to worldwide availability by, for example, the move away from burning coal for electricity generation, hinders their continued extensive use. This has encouraged researchers to work on finding alternative SCMs from industrial by-products. The valorisation of such by-products and waste materials in cement-based materials could offer (i) environmental advantages from reduced abiotic depletion, prevention of waste, energy savings and reduced CO_2 emissions ii) economic advantages from the use of lower cost construction materials and iii) technological improvement in rheological and mechanical properties of mortars and concretes.

The purification of raw water obtained from surface and groundwater sources involves a coagulation/flocculation process where chemical coagulants are added to agglomerate contaminants, thereby aiding sedimentation and filtration of the pollutants from the liquid phase. Aluminium sulfate is widely used in the UK as a chemical coagulant for the purification of raw waters [3]. When added to the raw water, it hydrolyses to form an amorphous or poorly crystalline gelatinous precipitate of aluminium hydroxide. The precipitate flocculates colloidal and suspended impurities into heavier clumps that allows them to settle easily. The resulting residue is an alumina-rich waste known as alum water treatment sludge (AWTS) or alum sludge. The most common long-term disposal route for this waste is landfilling but this is actively being discouraged due to limited landfill spaces and rising landfill costs [4].

The physical and chemical properties of alum sludge is mainly influenced by the dosage of coagulant and the source water characteristics which is influenced by catchment bedrock minerals and any pollutants discharged into the water source [5]. The variability in treatment processes and source water quality is responsible for the differences in the characteristics of alum sludge samples from one treatment facility to another and even for a specific plant over time [6]. Thus, it is necessary to characterize sludge samples for recycling and reuse purposes.

Alum sludge mainly comprises clay minerals removed and precipitated from untreated water along with residues of the alum coagulant used during water treatment [5]. These constituents make alum sludge a rich source of silica and alumina which can potentially drive pozzolanic reaction in blended cement. It is well-known that clays usually have a fixed lattice structure in their original state where aluminate and silicate sites have minimal reactivity [7]. Thermal treatment can induce the disorder in their structure and potentially lead to enhanced pozzolanic reactivity. On this basis, a few researchers have investigated the incorporation of calcined alum sludge in cement and have found similar or improved performance to neat cement systems [8,9]. However, an understanding of the underlying factors governing calcined sludge interactions in cementitious materials is limited. Moreover, the determination of optimum calcination temperature is not straightforward due to their mineralogical variety and often the optimum calcination temperature has been reported from performance-based trial and error methods. Pertinent questions remain as to the origin of the improved performance and the factors that drive it.

A synergistic interaction exists between alumina from SCMs, such as slag and fly ash, with limestone powder, leading to higher mechanical strength [10–12]. Aluminates react with carbonates to form AFm phases mono- and hemi-carboaluminates thereby stabilising ettringite. This leads to an increase in the volume of hydrates which ensures better space filling and a well-refined pore structure leading to improved strength and durability [13]. The high alumina content in alum sludge makes this an interesting area for research. Although calcined alum sludge is potentially a source of reactive alumina, there have been no studies into its effectiveness in limestone blended cements.

There is a recognition that landfilling of alum sludge is not environmentally sustainable, so it is important that other uses are explored. Given the role of aluminates in the hydration of cement, there is potential for the use of alum sludge as

an SCM. Understanding the physical and chemical impact of binder materials is fundamental to predict performance and durability. To optimise the reuse potential of alum sludge, the characteristics of raw and calcined sludges and their impact on the hydration, phase assemblages, microstructural evolution and engineering performance of composite cements must be well understood.

1.2 Scope of research

The aim of this project is to assess the suitability of UK alum sludge as an SCM by understanding its characteristics and impact on the hydration, phase assemblages, microstructural evolution and engineering performance of blended cement systems. An understanding of sludge characteristics and the underlying factors describing its interaction in blended cement systems provides a means for predicting performance and finding solutions to problems of reduced strength, durability and poor mixture workability that are commonly associated with the use of pozzolans as SCMs [14]. The objectives of this project are outlined as follows:

i) Characterisation of as-received and calcined alum sludge in terms of chemical and mineralogical composition, thermogravimetric behaviour and particle properties (fineness, porosity and morphology). These characteristics are conducive to assessing the reactivity of SCMs in cement-based materials.

ii) Investigating the effect of incorporating alum sludge on the hydration, microstructure and engineering properties of blended cement pastes and mortars. This will be achieved via the following sub-objectives:

- Understanding the influence of calcination temperature on the cementitious reactivity of alum sludge.
- Establishing the influence of calcined sludge on the reactivity of limestone powder.
- Quantifying the hydration of calcined sludge-blended cement systems and understanding how hydration is influenced by the physical, chemical and mineralogical characteristics of the constituent materials.
- Evaluating relationships between hydration, microstructure and engineering performance of calcined sludge-blended cement systems.

1.3 Experimental approach

The experimental work to achieve the aforementioned objectives are summarised herein. The as-received alum sludge collected for this work was in its as-produced form, which required material processing including drying and grinding to produce a suitable powdered sample. Hereinafter, the dried and ground as-received alum sludge will be referred to as raw sludge.

Thermogravimetric and mass spectrometric (TG-MS) analysis was performed on raw sludge to understand how thermal treatment affects phase decomposition and to determine suitable calcination temperature(s). Based on TG-MS data, calcination temperatures were selected ranging from 475^{o}C to 1100^{o}C at a holding time of 2 hours to ensure complete calcination at any temperature. The raw and calcined sludge samples were then characterized by a variety of experimental techniques, namely XRF for chemical composition, pycnometry for particle density, laser diffraction for particle size analysis, BET for particle surface area and porosity, SEM for particle morphology, XRD and FTIR for mineralogical composition.

The pozzolanic activity of the raw and calcined sludges was assessed by determining their Strength Activity Indices (SAI) in accordance with ASTM C618 [15]. Based on SAI results, sludge calcined at selected temperatures was blended variously with GGBS and limestone to monitor the hydration and performance of the composite systems. Hydration of cement pastes was monitored by SEM, XRD, FTIR, TGA and isothermal calorimetry and performance was assessed by workability and compressive strength in mortars.

Based on the aforementioned step, ternary mixes incorporating limestone powder and calcined sludge at the optimum calcination temperature were formulated. Paste hydration and microstructural development in cement pastes were assessed by SEM, XRD, TGA, FTIR and isothermal calorimetry. Performance was evaluated by determining compressive strength, sorptivity and gas permeability in mortars.

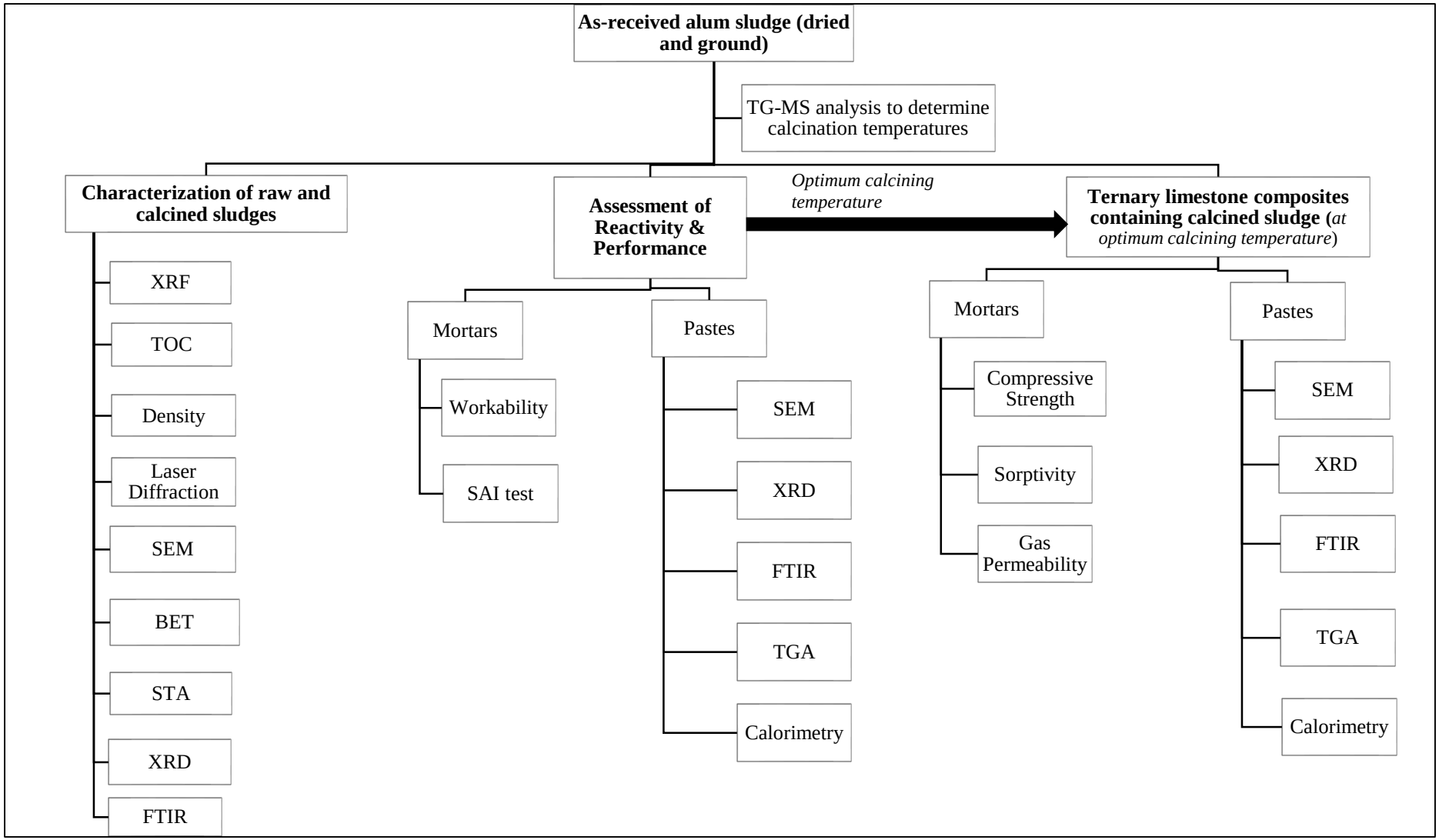

Figure 1- 1: An overview of the structure of this study

1.4 Organisation of thesis

- Chapter 2 presents a literature review related to this research with a focus on the following aspects: the hydration and microstructure of clinker phase assemblages; the influence of SCMs such as GGBS, limestone and calcined alum sludge on the hydration, microstructural and strength development of blended cements; and key factors affecting the hydration of mentioned cementitious materials.
- Chapter 3 describes details of materials and methods used in this research.
- Chapter 4 presents the results of the characterization of the raw materials used in this study with a focus on the raw and calcined sludge samples. The goal was to provide an understanding of how heat treatment affects the physical, chemical and mineralogical properties of the sludge samples. These properties are conducive to assessing the potential reactivity of SCMs and their behaviour in fresh and hardened cement mixtures.
- Chapter 5 presents an evaluation of the pozzolanic reactivity of raw and calcined sludges in various blended cement systems. The goal here was to understand the physical and chemical effects of calcined sludge on the hydration and microstructural development of cement composites.
- Chapter 6 presents the investigation into the hydration and engineering properties of ternary blends containing limestone powder and calcined sludge. The goal was to investigate the hydration, microstructural development and engineering properties of ternary blends incorporating calcined sludge and limestone powder.
- Chapter 7 summarises the main findings in this research and draws conclusions. Recommendations for future studies are also given.

Chapter II: Literature Review

2.1 Ordinary Portland Cement

Portland cement (PC) is a finely ground hydraulic binder commonly used for the preparation of cement paste, mortar and concrete. It is produced by heating a mixture of calcareous materials such as limestone or chalk and argillaceous materials such as shale or clay at temperatures up to 1450^{o}C. The resulting clinkers are then ground and mixed with gypsum to form the dark grey powder that we know as Portland cement. About 2-5% of calcium sulphate (often as gypsum, $CaSO_4.2H_2O$) is added to control its rapid setting and influence the rate of strength development [16]. Classic PC clinker is composed of four main minerals [17]:

- Tricalcium silicate, $3CaO.SiO_2$ (C_3S in cement nomenclature), known as alite, comprising 50-70% by mass;
- Dicalcium silicate, $2CaO.SiO_2$ (C_2S in cement nomenclature), known as belite, comprising approximately 15-30% by mass;
- Tricalcium aluminate, $3CaO.Al_2O_6$ (C_3A in cement nomenclature) known as aluminate, comprising approximately 5-10% by mass;
- Tetracalcium aluminoferrite $4CaO.Al_2O_3.Fe_2O_3$ (C_4AF in cement nomenclature) known as ferrite, comprising approximately 5-15% by mass.

Strength gain in Portland cements is mainly due to the hydration of calcium silicates, although aluminate phases may also contribute. As indicated by the composition of the principal phases, the main chemical elements present are calcium, silicon, aluminium and minor amounts of iron. Cement composition is usually expressed in terms of elemental oxides. Table 2-1 shows the typical range of oxides present in Portland cement [18]. The total fraction of reactive CaO, and SiO_2 in CEM cement is at least 50% by mass with a CaO/SiO_2 ratio greater than 2 [17]. Mineral oxides such as magnesia (MgO) are limited to 5% due to the related adverse long-term expansions in hardened concrete. SO_3 is limited to 3.5% while the amount of alkalis (K_2O and Na_2O) are also limited due to concerns over alkali silica reactions.

Table 2- 1: Typical chemical analyses of CEM I cements

Oxide	Proportion (% wt.)
SiO_2	19-23
Al_2O_3	3-7
Fe_2O_3	1.5-4.5
CaO	63-67
MgO	0.5-2.5
K_2O	0.1-1.2
Na_2O	0.07-0.4
SO_3	2.5-3.5
Mn_2O_3	0.03-0.08
P_2O_5	0.07-0.23
TiO_2	0.20-0.31
Free lime	0.5-2.1
LOI	0.7-1.7
Density kg/m^3	3120-3150
Surface Area (m^2/kg)	343-443

2.2 Hydration of Portland cement

The hydration of Portland cement occurs upon contact with water. Anhydrous cement clinker phases undergo a series of endothermic and exothermic reactions that lead to setting, hardening and strength development in the cement paste. The clinker phases react at different rates and can influence each other. The kinetics of cement hydration are influenced by many factors including phase composition of the cement and the presence of foreign ions within individual clinker phases; the fineness of the cement; the water-cement ratio used; the curing temperature; the presence of chemical admixtures; the presence of additives, etc. [19]. Of particular importance to this study is the influence of SCMs on the hydration of the main clinker minerals and the reactivity of the SCMs themselves. In slag-blended cements, the hydration of cement produces portlandite thereby enabling the dissolution and hydration of slag constituents. Calcium carbonate from limestone react with aluminates from SCMs to produce carboaluminates. Carbonates from limestone are known to react aluminates

from C_3A and slag (and possibly alum sludge) to form carboaluminates. The hydration of the main clinker minerals and the impact of SCMs and other factors are hereby reviewed.

2.2.1 C_3S hydration

The hydration of silicates and in particular, alite (C_3S), as the main strength contributing clinker phase in Portland cement is of immense interest. Upon contact with water, calcium ions and hydroxide ions are quickly dissolved from the C_3S grain surface and within a few minutes, the pH rises above 12. After an initial rapid rate of C_3S hydration, the rate slows down very quickly. When the calcium and hydroxide ions reach a critical level, C-S-H and portlandite are formed and the C_3S hydration continues more rapidly. The hydration reaction of alite may be described by [19,20]:

$$C_3S + (3 - x + y)H \rightarrow C_xSH_y + (3 - x)CH$$

Where 'x' refers to the Ca/Si ratio, which is ~1.7-1.8 in neat PC systems [21]. 'y' refers to the water content and is assumed to be equal to 4 in saturated conditions, but is sensitive to changes humidity and possible dehydration [20,22].

C-S-H is the main hydrate formed along with portlandite and are major contributors to strength development in cement paste. C-S-H clusters are formed on the surface of cement particles. After several minutes, these clusters increase in size and become fibrillar clumps. The nucleation and growth process of C-S-H is well supported as the mechanism controlling its formation [23]. This process involves the formation of nuclei on the surface of hydrating cement which begin to grow at a rate controlled by the kinetics of the process occurring at the solution-crystal interface.
Alite is the impure form of C_3S modified with foreign ions such as Mg^{2+}, Al^{3+} and Fe^{3+}. MgO, Fe_2O_3 and Al_2O_3 have been reported to affect the early hydration kinetics of C_3S [24,25]. Valenti et al.[26] doped triclinic C_3S with 1% MgO, Al_2O_3 and Fe_2O_3, observing a lower degree of hydration than in pure C_3S. This decrease was more significant for Al- and Fe- and less noticeable for Mg-doped alite. Stephan et al. [24] reported a similar trend where MgO influenced hydration only slightly while Al and Fe-doped C_3S had a more significant retarding effect, increasing with dopant concentration.

The partial replacement of cement clinker by SCMs is an effective route to reduce greenhouse emissions associated with the manufacture of Portland cement. However, many SCMs are alumina-rich and this can retard hydration of C_3S [25,27,28]. A number of mechanisms have been proposed to describe the delay in hydration of silicates in the presence of aluminium. One mechanism involves the action of aluminates on the dissolution of silicates. In this case, surface poisoning is proposed on pre-existing etch pits or by covalent bonding between aluminate ions and the surface of silicates. Another suggestion is that C-S-H containing aluminium is a poor nucleating site for growth of additional C-S-H. Begarin et al. [28] observed that Al-bearing C-S-H formed during alite hydration does not nucleate C-S-H growth, thereby retarding hydration. Quennoz and Scrivener [29] attributed the inhibition of alite hydration to the presence of aluminate hydrates in the space available for the nucleation and growth of C-S-H as well as a poisoning of alite by aluminium. Pustovgar et al. [25] studied the influence of aluminates on the hydration kinetics of C_3S pastes by mixing C_3S with $NaAlO_2$ solutions of different concentrations. It was found that the addition $NaAlO_2$ solution inhibited the hydration of C_3S and increasingly so with higher concentrations of aluminates in solution. Although, C_3S hydration was retarded when aluminates were present, the maximum heat release rate and total cumulative heat increased with aluminate concentration, implying a higher degree of hydration of C_3S. However, increasing the pH by addition of NaOH seems to cancel the inhibiting effect of aluminates. By molecular dynamics simulations, the authors observed that below pH 13 aluminates adsorb directly to the surface of C_3S grains, mainly through strong ionic interactions between aluminate and calcium ions. As hydration continues and pH increases, the binding strength of aluminates to the C_3S surface reduces, which weakens its passivating and retarding effect.

2.2.2 C_2S hydration

Belite usually exists in a monoclinic β form in cement and is the second most abundant phase in clinker. Upon contact with water, it hydrates similarly to C_3S but at a much slower rate. It has been observed that some unreacted β-C_2S still remained in 20-year cement hydrated paste samples [30]. At early ages, the Ca^{2+} concentration in the pore solution increases, decreasing later and becoming stable after about 30 mins. It has been widely reported that the delayed hydration of β-C_2S is due to the formation

of calcium-rich barrier around the anhydrous particle[31,32]. Hence, β-C_2S hydration proceeds when calcium ion concentration in the pore solution drops significantly. The hydration of belite can be described as [19,20]:

$$C_2S + (2 - x + y)H \rightarrow C_xSH_y + (2 – x)\ CH$$

2.2.3 C_3A hydration

In the absence of calcium sulfate, C_3A reacts rapidly with water to form calcium aluminate hydrates thereby causing undesirable setting [33]:

$$2C_3A + 21H \rightarrow C_4AH_{13} + C_2AH_8 \rightarrow 2C_3AH_6 + 9H$$

C_4AH_{13} and C_2AH_8 are metastable hydrates which finally transform to C_3AH_6 i.e. hydrogarnet. The formation of C_4AH_{13} and C_2AH_8 during C_3A hydration is controlled by the CH concentration in solution. It is suggested that solutions with low calcium ion concentrations will lead to the preferential precipitation of C_2AH_8 while solutions with high concentrations will form C_4AH_{13} [34]. At early age of hydration, the presence of CO_2 hinders the formation of hydrogarnet [35]. Dissolved aluminates will also react with carbonates to form hemi and/ mono-carboaluminates thereby stabilizing ettringite. The reaction of C_3A upon contact with water is highly exothermic, potentially leading to the rapid setting of cement paste called flash set. Calcium sulfates in the form of gypsum, anhydrite and hemihydrate are therefore usually added to cement during grinding to control C_3A hydration. C_3A reacts with sulfate ions to form ettringite [19]:

$$C_3A + 3C\$H_2 + 26H \rightarrow C_6A\$_3H_{32}$$

It usually happens that unreacted C_3A remains when the sulfate ions are depleted. The remaining C_3A consumes ettringite and water to form the AFm phase, monosulfoaluminate [19]:

$$2C_3A + C_6A\$_3H_{32} + 4H \rightarrow 3C_4A\$H_{12}$$

Microstructural properties of hydrated C_3A are reported in literature according to gypsum content [36] :

- In under-sulfated systems, a foil-like amorphous covering on C_3A particles was reported within the first few minutes of reaction [37]. As C_3A reaction progresses, irregular plates of calcium aluminium hydrates are observed.
- In well-sulfated systems, only the formation of ettringite crystals is observed.
- For systems with intermediate sulfate content, AFm phases were observed on the C_3A particles upon contact with water [34] and the subsequent precipitation of ettringite rods and the development of hexagonal platelets near C_3A particles [37].

2.2.3.1 Mechanisms of C_3A hydration

Two main mechanisms have been proposed to explain the mechanisms by which C_3A reaction is retarded by the presence of calcium sulfate [36]. The first one proposes that C_3A reaction in well-sulfated systems is controlled by diffusion through a hydrate layer. However, different views exist on the nature of this layer. Various authors have suggested that C_3A hydration is inhibited by the formation of a coating of ettringite crystals on C_3A particles [38,39].

- Corstanje et al. [40] suggested an aluminate gel coating on C_3A particles containing calcium and sulfate ions.
- Other authors suggested hydration is inhibited by the formation of AFm platelets and ettringite on the C_3A particles [41].
- Scrivener observed a composite coating consisting of AH_3 and ettringite which could also contain C_4AH_{19} and monosulfoaluminate and/or their solid solutions [42].

The second school-of-thought proposes that the adsorption of sulfate ions on the C_3A particles is the basis of the inhibition of C_3A hydration:

- While Feldman and Ramachadran [43] proposed that the adsorption of sulfate ions on C_3A particles reduces the dissolution rate of C_3A, Collepardi et al. [39] observed that the sulfate compounds such as Na_2SO_4 has no effect on C_3A hydration
- Skalny and Tadros [44] suggested that dissolved calcium and sulfate ions from gypsum are the origin of the inhibition of C_3A hydration. Calcium ions are

chemisorbed on the C_3A particles thereby creating a positively charged surface that enables sulfate ions to be adsorbed. This is then followed by the adsorption of sulfate ions on active dissolution sites

2.2.4 C_4AF hydration

The hydration products formed by C_4AF hydration are similar to C_3A, with Fe^{3+} partly substituting Al^{3+}. As the Fe content increases, hydration becomes slower due to the formation of iron hydroxides gel that coat active reaction sites on the C_4AF grains [23]. Beaudoin and Ramachandran [45] found that the compressive strength contribution of C_4AF was greater than that of alite within the first 10 days of hydration. However. Plowman and Cabrera [46] found that hydration of C_3A occurred at seven times the rate of hydration of C_4AF. This further suggests that the Al/Fe ratio is an important factor controlling the reactivity of C_4AF. The reaction of ferrite phase with or without gypsum can be described as:

$$C_4AF + 3C\$H_2 + 21H \rightarrow C_6(A,F)\$_3H_{32} + (F,A)H_3$$

$$C_4AF + C_6(A,F)\$_3H_{32} + 7H \rightarrow 3C_4(A,F)\$H_{12} + (F,A)H_3$$

2.2.5 Cement hydration kinetics

As earlier discussed, the anhydrous clinker phases react upon contact with water. This hydration is exothermic and a plot of heat release against time by isothermal calorimetry is a simple way of presenting the kinetics of hydration (Figure 2-1).

2.2.5.1 Initial reaction

Figure 2-1 shows the stages of early cement hydration by isothermal calorimetry. The *initial reaction* is rapid and takes place as the cement comes in contact with water. This stage is characterized by a strong exothermic reaction where the reaction of C_3A with water to form aluminate gel is dominant. Sulfate ions dissolve in water and react with the aluminate gel to form ettringite, which are rod-like crystals (Figure 2-2). This period of rapid heat release ceases within 15 minutes as ettringite formation slows down the hydration of C_3A as described earlier.

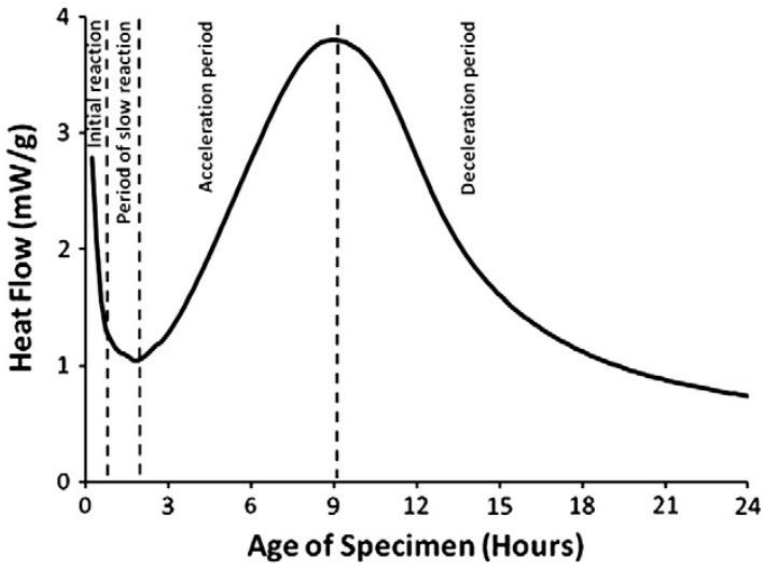

Figure 2- 1: Stages of early age hydration by isothermal calorimetry measurements [31].

2.2.5.2 Induction Period or Period of Slow Reaction

After the initial reaction, the induction period follows, in which few reactions occur. The reason behind this period remains unclear. It has been attributed to nucleation control where a certain concentration of ions in solution needs to be achieved before crystal nuclei form from the hydration products that grow [23]. CH crystallizes and metastable C-S-H develops forming a coating around the cement particles. This theory has been disputed by the suggestion that the induction period is caused by a retardation in C_3S dissolution due to super-undersaturation of the pore solution [47]. The end of the induction period determines the initial set of cement as further hydration reactions occur and hardening begins.

2.2.5.3 Acceleration Period

The induction period is followed by the accelerating period where metastable C-S-H on the surface of the cement grain converts to C-S-H gel, which has a higher porosity thereby enabling free water to react with anhydrous cement particles [31]. The rapid heat release during the accelerating period is due to the hydration of C_3S, and lasts for about 24 hours. During this period, C_3S reacts to form C-S-H gel and CH (i.e. portlandite) and the cement grains connect with each other. The C-S-H forms in the space which is initially filled with water and is described as *outer-product* (Fig 2-

2). This period determines the final set and the rate of initial hardening of cement paste. At the end of this period, about a third to half of all cement is hydrated.

2.2.5.4 Deceleration Period

Following the final setting of cement paste, the rate of hydration slows down over the *deceleration period* which lasts over the service life of concrete. During this period, the hydration of C_3S and C_3A continue, as C_2S hydration starts. C_2S hydration is slow but contributes to the strength gain up to years after initial casting of cement paste. It is at this stage that *inner-product* C-S-H starts to form within the shells of cement grains. Any ettringite that forms during this stage will be consumed by remaining C_3A to form monosulfoaluminate. Continued hydration leads to an increase in density of outer product C-S-H and a refinement of pore structure.

2.2.6 Microstructure of Hydrated Cement Paste

As earlier stated, the terms ‘inner’ and ‘outer’ products are used to classify C-S-H according where they are formed. The inner product forms in the space initially occupied by clinker grain and has a homogenous morphology[48]. The outer product forms within the matrix in the space originally occupied by water and has either a fibrillar or foil-like morphology [48]. The main hydrates formed are C-S-H, CH, AFm, and AFt (Figure 2-2).

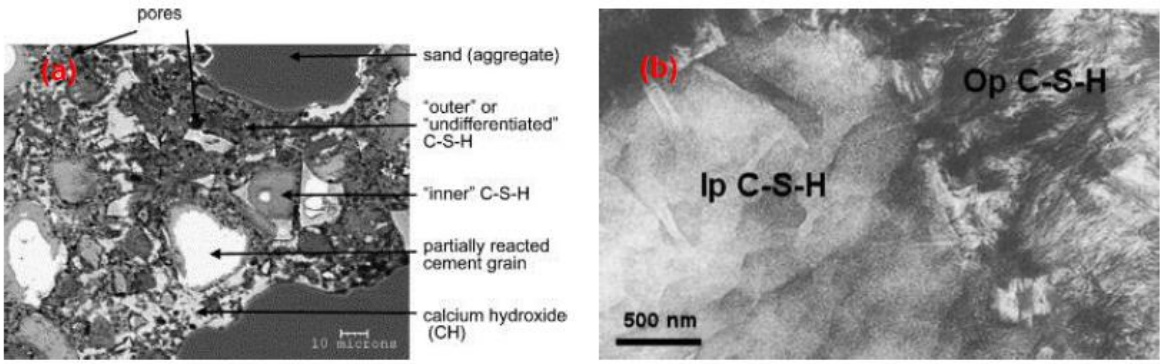

Figure 2- 2: (a)BSE image showing the microstructural characteristics of neat PC mortar [49]; (b)TEM image showing inner and outer product C-S-H [50].

The microstructural evolution during the hydration of clinker is illustrated in Figure 2-3 [42]. Soon after mixing with water, the aluminate phase in clinker reacts with sulfates and water to form amorphous aluminate-rich gel and ettringite rods. It

was observed that in the presence of little calcium sulfate, large hexagonal plates of C_4AH_{19} were formed causing flash setting [42]. On the other hand, an excess of hemihydrate led to the formation of large lathlike crystals of gypsum which caused false setting [42]. After 10 hours of hydration, outer-product C-S-H precipitated on the ettringite rods. The formation of a reaction rim around the hydrating grains is characteristic of the microstructural evolution of cement pastes. These rims were first reported Barnes et al. [51], who called them ‘Hadley grains’.

After about 16 hours of hydration, long AFt rods were found to have grown through the secondary hydration of C_3A while C-S-H inner product is formed on the hydration rim. Within 1 to 3 days of hydration, hexagonal AFm platelets are formed from the consumption of AFt by the C_3A. By 14 days, the rim around the hydrating cement grain is filled with inner-product C-S-H.

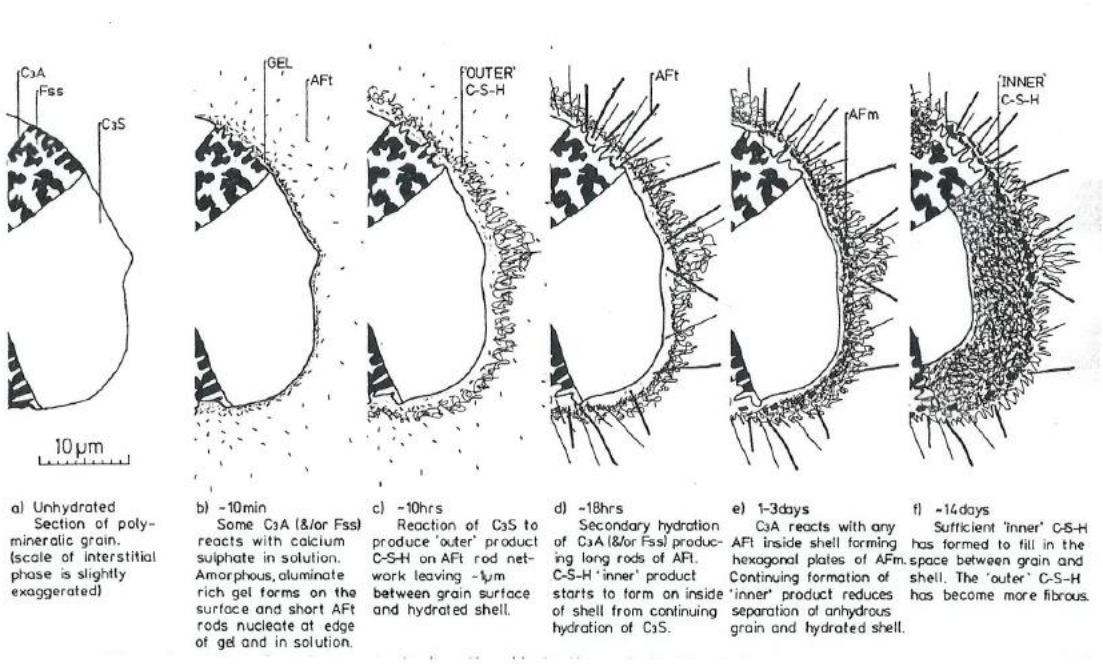

Figure 2- 3: Development of microstructure during the hydration of Portland cement [42,52]

2.3 Parameters Influencing Nucleation and Growth Mechanisms

A number of parameters are understood to affect the kinetics of reactions taking place during the acceleration stage. Their influence are hereby reviewed relating to the nucleation and growth processes [53].

2.3.1 Particle Size of Cement Particles

The fineness of cement particles has a huge effect on the rate of hydration. Scrivener [54] found that smaller cement particles, less than 5μm, had a 100% hydration degree within the first few hours of contact with water, while larger particles had only achieved partial hydration after several days. Fernandez [55] observed this effect more so at early age and reported that it is proportional to the surface area of the particles.

2.3.2 Mechanical Mixing

Juilland [56] reported on the influence of mechanical mixing on the hydration kinetics. Higher mixing speeds had a significant effect on early hydration kinetics, where the induction period is shortened, and the acceleration period is earlier and steeper. The microstructure of the paste mixed at a higher speed was more homogenous and denser than at lower speed. Simulations verified the suggestion that mechanical mixing leads to the development of more nuclei for the formation of hydrates.

2.3.3 Temperature

The early age hydration is accelerated with increasing temperature [19]. A few authors have observed heterogeneously distributed hydration products with temperature, caused mainly by an increase in C-S-H density [57]. This leads to development of a porous microstructure which is detrimental to strength and durability. Higher curing temperatures of neat PC have been observed to negatively impact later age hydration leading to decreased mechanical strength at 28 days [58]. Below 50^{o}C, the nucleation and growth processes of C-S-H control the kinetics of hydration.

2.3.4 Water Reducers and Superplasticisers

Superplasticizers are commonly used to improve the rheological performance of concrete. This improvement is due to the dispersion of agglomerated constituents in cement mixtures. A number of recent studies have focused on polycarboxylate-based (PCE) superplasticizers and it is observed that they invariably retard hydration. [59]. It is suggested that this is attributed to the adsorption of polymers on the surface of the cement particles and due to growth kinetics and morphology of hydration products form at early age [60,61]. Although it is suggested that PCE with more carboxylate groups have a more significant retarding effect on cement hydration, the precise reason and mechanism for retardation, particularly on how it is linked to the molecular structures of superplasticisers is still not understood [59].

2.3.5 Mineral Additions

A wide range of industrial by-products and natural materials are more frequently used in the cement industry to lower the reliance on cement clinker. As discussed earlier (*Section 2.2.1*) these additions could contain foreign ions that would affect cement hydration kinetics. Each SCM could have a wide range of chemical compositions and the solubility of phases present is dependent on the temperature and pH of the system [62]. In addition to the chemical effect of SCMs on cement hydration, their physical presence imparts a *filler effect* that enhances the hydration of clinker phases. This effect is attributed to the additional nucleation sites provided by the extra surface of the mineral additions.

2.3 Supplementary Cementitious Materials

Supplementary cementitious materials (SCMs) are commonly used in the cement industry in an attempt to reduce the greenhouse emissions during the manufacture of cement. The use of SCMs such as ground granulated blast furnace slag (GGBS), a by-product from pig iron production, or fly ash from coal combustion, are viable partial replacements for Portland cement. The utilization of such materials that do not require clinkering leads to reduced greenhouse emissions and provides a way for the valorisation of industrial by-products that could otherwise pose environmental problems. SCMs could also bring cost reductions, energy savings, as

well as technological benefits such as improved workability, strength and durability [62].

Most of the studies on the use of alternative materials in blended cement are focussed on the mechanical properties. There is currently limited knowledge on the link between the composition of an SCM and the phase assemblage and microstructural development of blended systems. As discussed earlier, clinker phases react with water to form C-S-H, portlandite, ettringite and AFm phase. When SCMs are incorporated in Portland cement, they react inter-dependently to form a complex system of hydration products. The reaction of most SCMs is slower than that of cement clinker phases and following hydration of many SCMs is often complicated because of their disordered or partially ordered structure. The kinetics of the blended cement hydration depends on the characteristics of constituent materials such as chemical composition, particle fineness and amount of reactive phases present as well as composition of the pore solution [62]. There is currently little knowledge on the detailed effect of these factors due to difficulty in measuring the reactivity of SCMs in blended systems.

2.3.1 Composition of C-S-H in Blended Cements

As shown in shown in Figure 2-4A, the chemistry of most SCMs is characterized by lower calcium contents than neat PC. This results in variations in the hydration products formed which also affects strength and durability. The hydration of a blended system results in a complex system where hydration occurs simultaneously, and the different binders affect the reactivity of one another. Figure 2-4B shows a ternary diagram of hydration products formed in the CaO-SiO_2-Al_2O_3 system. The illustration points to C-S-H having a variable composition. It is well established that the C-S-H in systems with a silica or alumina-rich is significantly different to C-S-H in Portland cements.

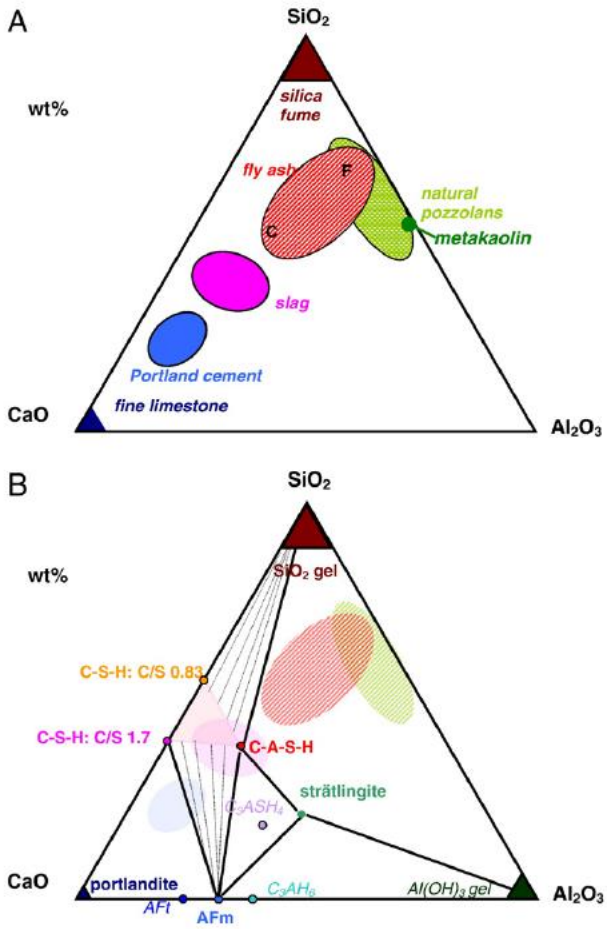

Figure 2- 4: A) Compositional map of cementitious materials; B) Probable hydration products [62].

Of particular importance to this study is the influence of alumina-rich SCMs (i.e. alum sludge and slag) on the hydration of blended systems. The incorporation of aluminium in C-S-H increases with increasing aluminium concentration in the solution and with the Si/Ca ratio of the C-S-H [62]. The boundaries shown in Figure 2-4B are just an estimation because limits on pore solution concentration are not well understood, particularly relating to aluminium uptake. Qualitatively, blending PC with fly ash will reduce the portlandite content and increase the amount of C-S-H with a lower Ca/Si ratio and AFm phases, as fly ash is rich in alumina. The formation of C-S-H with low Ca/Si ratio results in higher incorporation of aluminium in the C-S-H [63]. SCMs such as ground granulated blast-furnace slag (GGBS), metakaolin and fly ash have a high aluminium content and are known to produce high Al/Si ratios (~0.17) in the resulting C-A-S-H phases [30,64]. Aluminium is incorporated in C-S-H mainly at bridging sites in the silicate chains [63]. The incorporation of aluminium ions in C-S-H

may be detrimental to the cohesion of C-S-H in cement paste, so it is important to understand how much aluminium is incorporated and what governs its uptake. The cohesion of cement paste is attributed to the attractive electrostatic forces between charged C-S-H particles so aluminium incorporation could affect the cohesive forces [65]. Furthermore, recent investigations on the mechanisms of sulfate attack have indicated that aluminium is mobilized from C-A-S-H phases in hardened pasted made with PC/fly ash and contributes to the formation of ettringite [66,67]. Mullauer [67] and Ding et al.[68] observed a clear correlation between the increase in ettringite content and a decrease in Al/Si ratio of C-A-S-H during long-term storage tests of hydrated blended cements in sulfate solutions. Thus, the composition and reactivity of an SCM could also influence the amount of amount of ettringite formed as well as amount and kind of AFm phases.

Quennoz et al. [29] found considerable variations in the time over which sulfates are depleted in pure C_3A and C_3S/C_3A systems, meaning that C-S-H affects the sulfate content in these systems. The S/Ca ratio in C-S-H was between 0.04 and 0.1 before the aluminate peak in C_3S/C_3A systems. However, the sulfate content in C-S-H decreased by 75% after the aluminate peak. Berodier and Scrivener also observed a change in C-S-H morphology due to sulfate adsorption [69]. By comparing the early hydration of LC3 and PC-limestone systems, Zunino & Scrivener [70] found that the sulfate balance of blended systems is related to the additional surface area (filler effect) rather than the aluminium content of the SCMs. The acceleration of C_3S reaction due to filler effect increases the rate of precipitation of C-S-H thereby increasing the sulfate adsorption. When gypsum in the system is depleted, sulfate is released from the C-S-H following a decrease in pore solution and can react to form additional AFt.

2.3.2 Factors Affecting Hydration Kinetics of Blended Cements

2.3.2.1 Composition of SCM

The chemical composition of the different types of SCMs can vary over a wide range. For a given pH and temperature, the dissolution rate of the phases in SCMs present will vary. Roelofs & Vogelsberger [71] found that nano-alumina (γ-phase) quickly dissolved upon contact with an aqueous solution at a pH of 11and the actual aluminium concentration increased intensely until maximum concentration. The

alkaline solution in hydrating cement is conducive to the dissolution of aluminates which would chemically influence the reaction of aluminate during the early hydration [72].

2.3.2.2 Replacement Level

Due to differences in the reactivity of SCMs, the replacement levels required to achieve desired strengths will be vary. The very high surface areas of SCMs such as silica fume and metakaolin will accelerate hydration due to the availability of additional nucleation sites as well as pozzolanic reaction. However, high substitution rates will reduce pH of the system which will in-turn reduce reaction rates [73].

2.3.2.3 Solution pH

The dissolution of amorphous silica and aluminates is dependent on pH of the system. The higher the pH, the faster the rate of reaction [73]. In blended cements, the highly alkaline environment is attributed to alkali hydroxides and portlandite, with pore solution pH quickly rising in the early hours of hydration as sulfate ions are removed from pore solution due to reaction with aluminates. As long as there are sufficient hydroxyl ions in the system to keep the system pH highly alkaline, the hydration of SCMs will continue.

2.3.2.4 Temperature

Both the pozzolanic and latent hydraulic slag hydration rates are influenced by temperature, reacting more slowly than Portland cements at temperatures under 15 °C while rates are increased at temperatures above 27 °C [73,74]. Higher temperatures produce a more porous microstructure in neat cement but less-so for slag cements due to its pore–refining characteristic [75].

2.4 Composite Cements

Composite or blended cements are prepared by the use of at least one SCM in combination with PC. Composite cements are commonly used in the UK, a result of the unrelenting drive towards a sustainable cement industry, by the use of industrial by-products to partially replace cement clinker. The use of such materials, where no

additional clinkering is required, results in cost and energy savings as well as the reduction in greenhouse gas emissions associated with the production of neat PC.
A range of formulations incorporating SCMs in Portland cement has been provided in BS 197-1 [76]. The permissible SCMs include GGBS fly ash, limestone and burnt shale. These SCMs have a wide range of compositions as previous shown in Figure 2-4 and their availability is geographically sensitive. These SCMs are hydraulic or pozzolanic i.e. they become reactive either when the pH reaches a critical level or directly react with portlandite formed from hydration of clinker phases respectively. This has an effect on the hydration of SCMs which in turn impact clinker hydration. The following section reviews current knowledge on the hydration, microstructure and engineering performance of composite cements incorporating slag and/or limestone. This is followed by a review of the characteristics, reactivity and performance of alum sludge-cement composites.

2.4.1 GGBS

Slag is an industrial by-product generated during the manufacture of pig iron. It is estimated that for every tonne of iron produced, about 300kg of slag is generated [33]. GGBS suitable for use as an SCM is obtained by rapidly cooling and quenching a molten stream from a blast furnace with water, which solidifies as glass. The resulting material formed is an amorphous granulated material with a glass content typically in excess of 90% [77] Although not all slags are utilized as SCMs, it is the most abundant SCM both in the UK and internationally [77].

The physical properties of slag such as particle size distribution and specific surface area have significant effects on the rheological properties and characteristics of hardened cement. Finer slags tend to increase workability due to reducing size and volume of voids in fresh mix. Oner et al. [78] found that the compressive strength of slag-blended cement increased with decreasing particle size. However, the authors suggested that a higher clinker fineness than slag is more effective in achieving a desired strength.

The main chemical constituents in GGBS are CaO, SiO_2, Al_2O_3, and MgO. Minor phases include TiO_2, MnO, FeO, S^{2-}, Na_2O, and K_2O [79]. Compared to cement, slags are richer in all the major phases, except CaO, as highlighted previously in

Figure 2-4. In the UK, slag must meet the specifications of BS EN 197-1 [76]; the most pertinent of which are:

- $\frac{\mathrm{CaO+MgO}}{SiO_2} \geq 1$
- At least two-thirds (by wt.) of the slag must be amorphous and have hydraulic properties upon activation
- The CaO, SiO_2 and MgO content combined should equal at least two-thirds of the slag.

The improvement in strength and chloride binding capacity in slag-blended cements has been related to the high alumina content of slags [80]. In addition, slags with alumina contents between 8 to 12 % are reported to have considerable effect on hydration kinetics while higher contents up 16% had insignificant effects. However, it has also been suggested that the alumina content of slags has an insignificant impact on the hydration kinetics, hydrates formed and compressive strength after 28 days [81]. Wang et.al [82] observed that there is a strong correlation between the Al_2O_3 and CaO content, where slags with a higher aluminium content were more reactive if the CaO content was above 37%.

2.4.1.1 Hydration of Slag in Blended Cements

The highly alkaline environment required for slag hydration is provided by calcium hydroxide and alkalis. The reaction of C_3S with water releases calcium and silicate ions thereby providing the alkaline environment required for slag hydration. Slag hydration typically produces C-S-H and hydrotalcite, although other hydrates such as stratlingite can also form. The formation stratlingite is more likely at higher aluminium contents [83]. In the presence of sulfates, slag reaction could also lead to the formation of ettringite.

In blended cements, the hydration of slag is slow relative to neat PC. Its hydration can be accelerated by increasing the water cement ratio, the curing temperature and slag fineness[84]. Higher replacement levels can however inhibit reactivity [85]. Lumley et al. [84] reported a degree of slag hydration of 30-55% after 28 days for slags cured at 20^{o}C with water-binder ratios of 0.4 to 0.6. This range for degree of slag hydration is typical in blended systems [85,86].

2.4.1.2 Characteristics of Hydrates in Slag-Blended Cements

The hydration of slag composite cements can be observed in a backscattered electron image by the formation of a reaction rim around the edges of a slag grain in Figure 2-5.

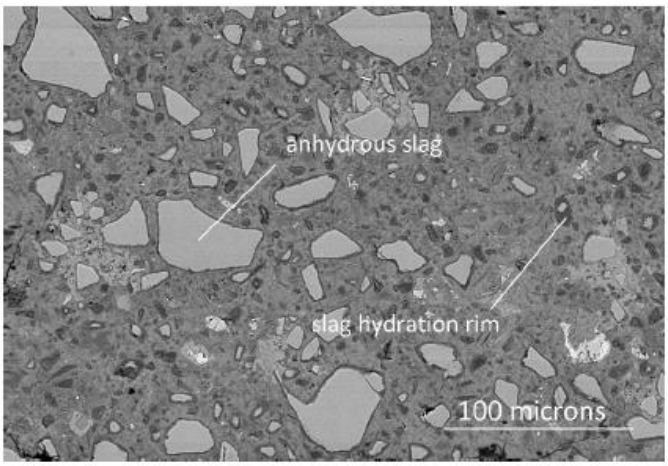

Figure 2- 5: SEM-BSE image of slag cement paste with 70% slag, cured at 180 days [87]

The substitution of clinker with slag is expected to produce less AFt, AFm and portlandite than 100% clinker although the addition aluminates in slag may lead to the formation of AFm phases [88]. Literature reports on the consumption of CH by slag are somewhat contradictory. Kocaba [89] and Luke & Glasser [90] reported insignificant consumption of CH, while other others have reported consumption of CH even at early age [88]. Escalante et al. [85] observed that the CH content increased to maximum during hydration and then steadily decreased with time. Taylor et al. [30] compared slag-blended samples cured for 2 and 20 years. The authors found that the 20 year samples had depleted CH owing to the presence of slag.

The C-S-H formed in slag-blended cement differs in composition to that present in neat PC. The lower calcium content and higher alumina content in slag leads to the formation of C-S-H with lower calcium content. Consequentially, aluminium will be incorporated in C-S-H [87]. The Ca/Si ratio in the outer product (Op) C-S-H, inner product (Ip) C-S-H and C-S-H in the reacted slags are similar while the Al/Si ratio of C-S-H in reacted slag is greater [91]. Richardson [48] studied the microstructural evolution of slag-blended cement and found that the change in C-S-H composition led to a change in its morphology. Calcium-rich C-S-H has a fibrillar morphology which gradually changes to a foil-like morphology with increasing slag content, similar to the C-S-H found in alkali activated systems [21].

2.4.1.3 Impact of Slag on Clinker Hydration

The early-age hydration of clinker can be accelerated by the addition of fine inert filler material like quartz. This effect could also be achieved by the use of slag in the provision of additional nucleation sites for the precipitation of hydrates [86]. This effect on clinker hydration by the physical presence of mineral additions is known as the filler effect, as shown in Figure 2-6. The figure shows the cumulative heat for binary blends where clinker is substituted with either 40% slag or quartz. The difference in cumulative heat evolved per gram of cement between plain clinker and cement-quartz blend is attributed to the filler effect. Accordingly, the difference in heat evolved between slag-cement paste and quartz-cement paste is attributed to slag hydration [89].

While the cement substitution with slag will provide nucleation sites for cement hydration, slag reacts at a much slower rate than cement. Consequently, with the same water/binder ratio, slag substitution for cement will increase the free water available to react with cement particles thereby having a dilution effect. This results in a higher degree of cement hydration as confirmed in many studies [87].

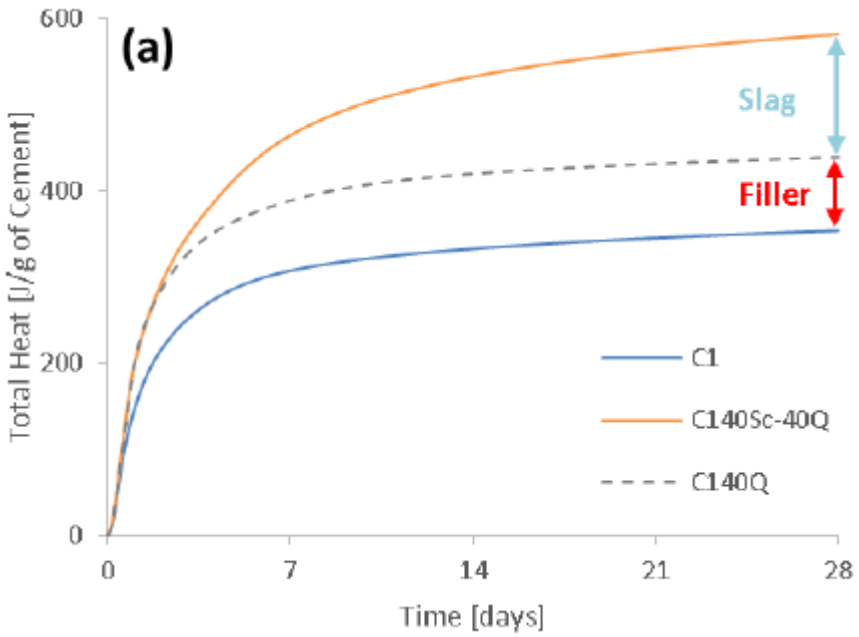

Figure 2- 6: Total Heat of a Neat Cement Paste and a Slag Cement Paste with 40% Slag, W/B = 0.5 [92]

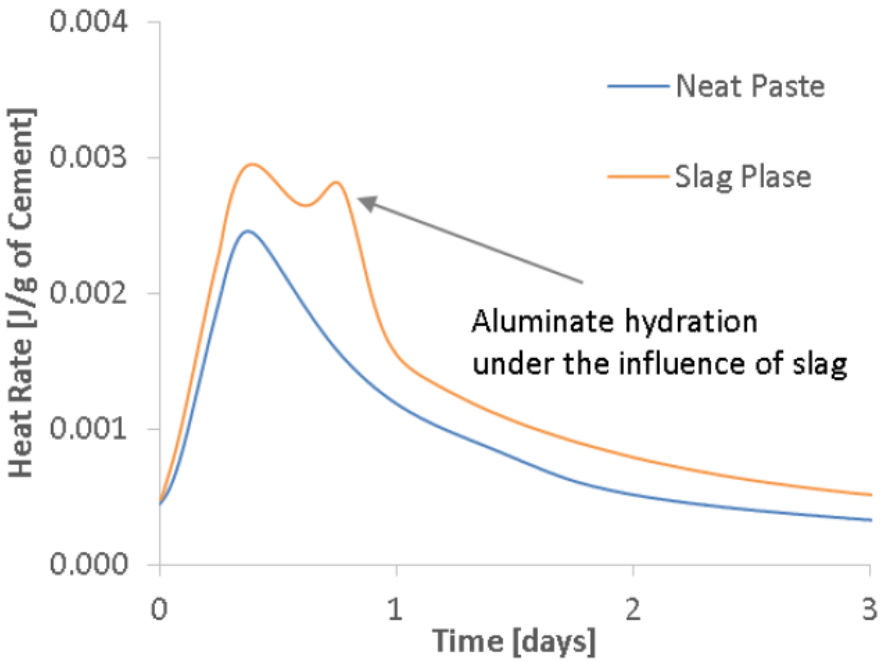

Figure 2- 7: Heat Rate of a Neat Cement Paste and a Slag Cement Paste with 40 % Slag, W/B = 0.5 [92]

Peak intensities in the heat rate curve (Figure 2-7) are largely dependent on the fineness of cement and slag. The filler effect contributed by slag has been attributed to the aluminate hydration peak which forms after the silicate main hydration peak [89,93]. Berodier and Scrivener [69] supported this view and suggested that slag was inert over the first 35 hours. Similarly, Cetin et al. [94] reported higher silicate reaction peak intensities with finer slags while coarser slags produced broader peaks with lower intensities.

2.4.2 Limestone

Limestone is a carbonate sedimentary rock mainly composed of decayed marine organisms and minerals such as calcite, aragonite, vaterite and/or magnesium carbonates. Most limestones have a granular texture, but could also exist in massive, crystalline or clastic forms depending on the method formation. Its powder form is a by-product of limestone quarrying and is widely used as a construction material.

Production of Portland limestone cement, using limestone powder as partial substitution to clinker is a current trend in the cement industry, particularly in European countries, due to the technological, economic and environmental benefits from reduced cement production as well as improved cement properties. BS EN 197-1 [76] identifies two types of Portland limestone cements: Type II/A-L containing 6–20% and

Type II/B-L containing 21–35% limestone addition. In addition, the inclusion of 5% of filler material that can be calcareous is accepted in all cements in BS EN197-1.

The substitution of cement clinker with limestone powder has several effects on the physical and chemical properties of cement paste and hardened mortar. The addition of limestone powder could accelerate the early hydration of Portland cement [95,96] and may reduce the total porosity and retard the initial and final setting times as well [97]. In addition, fine limestone can chemically react with aluminates present in cement clinker and SCMs to form carboaluminates [98,99]. This reaction leads to the stabilization of ettringite thereby increasing the total volume of hydrates, decrease porosity and consequently increase strength [100].

Different mechanisms have been used to describe the action of limestone powder in cement-based materials. The effects of limestone have been reported to alter the properties of cement-based materials through the proposed mechanisms of filler, nucleation, dilution and chemical effects [98]. Thus, it is important to clarify the action mechanisms of fine limestone in order to understand its effects on the hydration and microstructure of cement-based materials. A description of each mechanism and their potential implication on the hydration and performance of cement composites are discussed in the following section [98].

2.4.2.1 Hydration Mechanisms of Fine Limestone

2.4.2.1.1 Filler Effect

The filler effect of fine limestone in hydrating pastes is due to its particle size. The incorporation of finer limestone will fill the voids between cement particles and increase the packing density of cement-based materials. This will lower the water requirement of concrete and enhance its strength and durability [101]. However, limestone has a high surface area so the incorporation of very fine limestone will reduce the workability of concrete. The workability of ultra-high performance concrete (UHPC) reduced by 27% with the addition 3% nano-limestone [102].

2.4.2.1.2 Nucleation Effect

After Soroka and Setter [103] first reported the nucleation effect of limestone, several authors have established that fine limestone provides additional nucleation sites for the precipitation of hydrates [104], acceleration of hydration reactions [105]

and enhancement of the degree of hydration in cement [101]. The particle size, surface structures and limestone content in cement-based materials are factors that could affect its nucleation effects [98].

Calorimetric measurements showed that the use of very fine limestone with a median particle size of 0.7μm produced an alite peak 15% higher and 25% earlier than a neat PC mixture. The incorporation of more coarse limestone led to similar heat release curves to neat PC [106]. With regards to hydration kinetics, Poppe and Schutter [107] observed the shortening of the induction period and aluminate reaction peak as well as a more pronounced alite hydration peak in binary clinker-limestone blends. In binary cement-quartz blends, however, the shortening of the induction period was not observed, implying that the difference was due to the presence of limestone providing a better nucleation sites of C-S-H [69]. Furthermore, the acceleration of clinker hydration has been correlated with w/c ratio [108]. At low w/c ratio, a portion of clinker remains unreacted hence acting as a filler material. At w/c ratio greater than 0.42, there is enough space in the matrix for hydrate growth. The space added space for growth of hydrates and the provision nucleation sites is responsible for the high early strength [109]. However, less hydrates are formed by increased limestone addition.

The surface energy and adsorption capacity of limestone particles increases with decreasing particle size [98]. Rode et al. observed that the precipitation of C-S-H on the surface of limestone is favourable due to the identical planar configuration of Ca and O atoms in calcite and CaO layers in C-S-H [110]. This characteristic makes calcite more favourable to the precipitation of hydrates than aragonite where no O atoms were detected [111].

Furthermore, increasing the limestone content provides more nucleation sites for precipitation of hydrates, thereby increasing the hydration degree of cement mixtures. For limestone contents up to 10%, greater release of heat was observed than neat Portland cements. However, there is still uncertainty as to which factor most controls the nucleation effect of limestone.

2.4.2.1.3 Dilution Effect

The dilution effect of limestone powder is dependent on its content in the cement matrix. For a given water-to-powder ratio (w/b), increasing the limestone

replacement results in greater cement dilution. Since limestone does not have cementitious properties, the dilution results in a higher w/c ratio as more free water is available for cement hydration. This leads to increased degree of cement hydration at earlier ages as well as increased initial porosity [112]. The 48hr total hydration heat of mixtures incorporating coarse limestone (maximum particle size of 20μm) was seen to be lower than that of neat PC and it decreased with increasing limestone content [113].

2.4.2.1.4 Chemical Effect

The chemical reactivity of limestone is dependent on its fineness plus the alumina content (from C_3A and C_4AF in clinker as well as SCMs). The rate of carbonate dissolution increases with decreasing limestone particle size. C_3A, C_4AF and SCMs are aluminate sources, which promote the reactivity of limestone. Redundant C_3A and C_4AF reacts with carbonate ions to form AFm phases [98]. Aluminate phases in clinker react with carbonates to form AFm phases monocarboaluminate and hemicarboaluminate instead of consuming ettringite to form monsulfoaluminate. This leads to a higher volume of hydrates, decreased porosity and increased strength at modest levels of limestone addition.

Monosulfoaluminate is a cement hydrate produced during the hydration of cements with $CaCO_3$ content less than 1% by the reaction between earlier produced ettringite and the residual C_3A [114,115]. Several studies have shown that limestone favours the formation of carboaluminates instead of monosulfoaluminate [116,117], leading to increased ettringite content. The high affinity between calcium aluminate and carbonate ions to produce carboaluminates has been reported by Feldman et al. [43] and Bensted [118]. This has led some authors to investigate the potential substitution of $CaSO_4$ with $CaCO_3$. It has been reported that depending on the fineness of clinker and sulfate content, $CaCO_3$ can substitute up to 25% of $CaSO_4$ without any change in the hydration of the system [18,118]. Hence, the addition of limestone may lead to the reduction of the optimal gypsum content, which may reduce the costs of raw materials. Another benefit of limestone addition is a reduction of the expansion that occurs during sulfate attack, which is most commonly observed in cements with high C_3A content [119].

The aluminate phase in clinker is however limited, so the reactivity of limestone powder in cement systems is small. The additional aluminates provided by alumina-rich SCMs such as fly ash, metakaolin and slag could promote limestone reactivity [10]. The extent of chemical reactivity of limestone is dependent on the sulfate and aluminate content in the system. Above a critical sulfate to aluminate ratio, limestone acts as an inert filler [120]. It is well established that calcium sulfates are more soluble than carbonates[121]. Hence, the initial SO_3/Al_2O_3 will control which carbonates will react. The dissolution of SCMs increases with aluminate concentration which will therefore promote the reaction of limestone.

Figure 2-8 presents the calculated phase assemblages that will normally appear in hydrated neat PC and their dependence on initial sulfate (SO_3/Al_2O_3) and carbonate ratios (CO_2/Al_2O_3) [83,122]. In limestone-blended cements, AFt and monocarboaluminate are important stable hydrated phases that occur. Monosulfoaluminate is unstable in the presence of monocarboaluminate and is unlikely to remain in cements with a carbonate ratio greater than 0.5. PC with low amount of calcite will form hemicarboaluminate as an additional AFm phase but this hydrated phase is not stable at 25^{o}C in the presence of excess calcite. Calcite is completely reacted in area I, II, III and IV, but remains unreacted in regions V and VI. Because the carbonate content in AFm phases is limited and the total contents of phases containing alumina, AFm and AFt is also small, little amount of calcite is required to achieve area V and VI. Gypsum is usually depleted in hydrated cement pastes, so the phase assemblages defined in area VI are highly unlikely. The bold dividing line between areas IV and V represents undersaturated and saturated calcite concentrations respectively. Accordingly, the left of the bold boundary represents compositions where calcite completely reacts while compositions to the right represent an excess of calcite which act as an inert filler. C_4AH_x is metastable and will not occur when the initial sulfate ratio is higher than 0.5 and is unstable in the presence of monocarboaluminate.

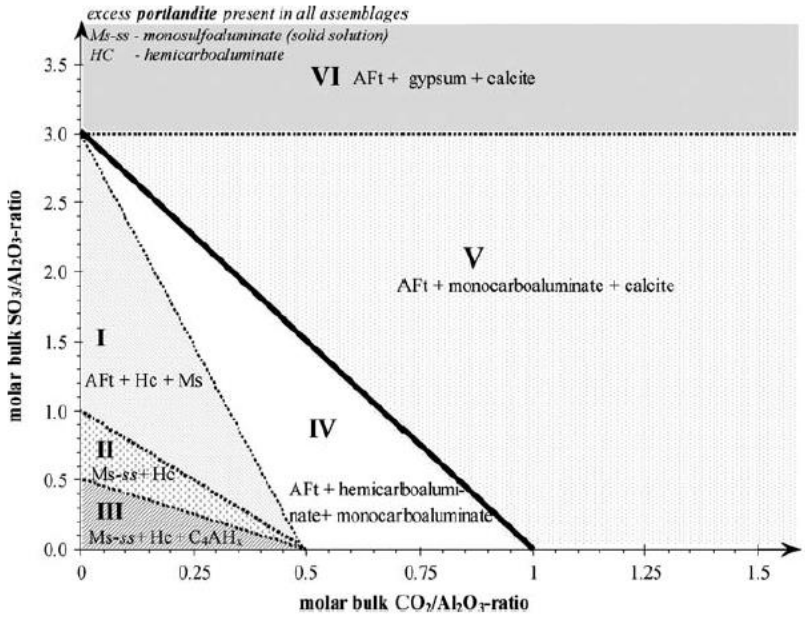

Figure 2- 8: Calculated phase assemblages of a hydrated mixture consisting of C_3A, portlandite and varying initial sulfate (SO_3/Al_2O_3) and carbonate ratios ($CO_2/Al2O_3$) at 25°C [83].

Bentz [123] used a hydration model to study the combined filler, nucleation and chemical effects of limestone at substitution levels up to 20%. He confirmed the observations of Bonavetti et al. [108] that acceleration of clinker hydration occurred at w/c ratios < 0.4. It was found that the formation of carboaluminates was enhanced after sulfate depletion. However, only one-quarter of the 20% limestone content was consumed after 180 days of curing.

Ternary blends of clinker, limestone and alumina-rich SCMs such as fly ash, slag or calcined clay have been the subject of considerable research [106,124,125]. The major oxides in these SCMs are silica and alumina. The additional aluminates provided by these SCMs react with carbonates to form carboaluminates. This prevents the conversion of ettringite into monosulfoaluminate [120]. Calcium monocarboaluminate has been detected in mixes containing limestone-blended cements as early as 1 day [126] or 3 days [95] after casting, and the amount continued to increase up to 28 days.

This synergy between aluminates and carbonates has recently been elucidated [127] to show that composite cements containing up to 5% limestone perform similarly to neat Portland cement mixtures. Damidot et al. [128] showed with thermodynamic modelling that the increase in solid volume in ternary blends of cement –limestone – pozzolan can be attributed to the reactive aluminates provided by the pozzolan.

Mounanga et al. [129] observed that for a fixed clinker to SCM ratio, modifying the proportion of slag and limestone had insignificant effect on heat flow even though the SCMs had different nucleation effects (Figure 2-9). The evolved heat in the ternary blends was higher than 50:50 cement-slag blend. At early stages of hydration, both SCMs provide nucleation sites for the precipitation of C-S-H, thereby accelerating clinker hydration [85,108]. Since the hydration of slag requires a highly alkaline environment (~ pH 12) it is assumed that the heat released due to slag reaction will be influenced by the amount of slag in the system. In addition, carboaluminate formation will have an impact the calorimetric heat release. It is worth pointing out that the limestone used in this study was much coarser than the slag so the reaction of sulfates was favoured at the expense of calcite. Hence, the observed chemical effect of limestone was less significant.

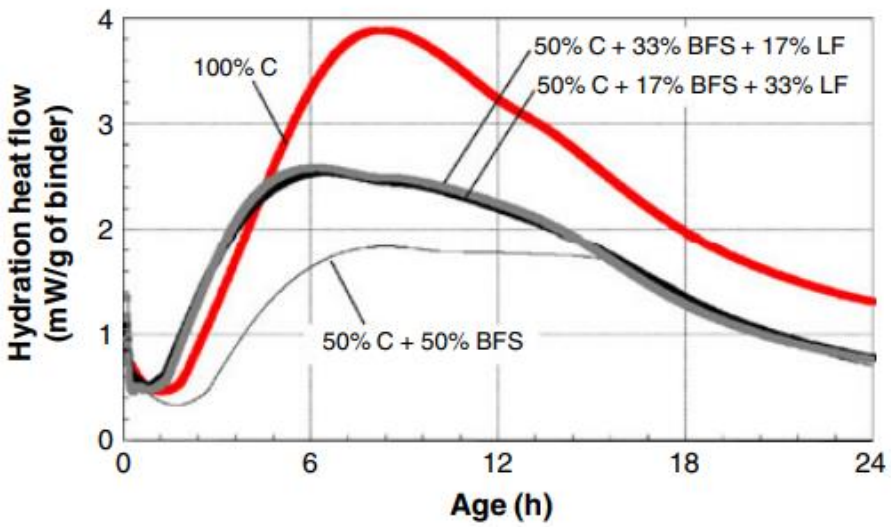

Figure 2- 9: Heat flow measured by isothermal calorimetry for PC-slag-limestone blend [129]

In composite limestone cements, the CO_3^{2-}/Al_2O_3 ratio also has a significant influence on the synergistic reaction between aluminates and carbonates [130]. The improved reactivity of SCMs in composite limestone blends could be attributed to the accelerating effect of both slag and limestone on C_3S hydration (through the provision of additional nucleation sites). Enhanced C_3S hydration means increased portlandite content which would activate slag hydration at early ages.

2.4.2.2 Transport Properties of Limestone-blended Cements

The early age hydration and microstructural development in cement systems are important in understanding mechanical and durability properties. Permeability largely depends on size, interconnectivity and tortuosity associated with the internal structures of materials through which deleterious substances may percolate. The microstructure of hydrating cement paste undergoes significant conversion from a viscous suspension of cement grains in water to a hardened, porous mass. The strength and durability properties of the hardened mass is dependent on the internal structure of the cement paste. The spatial and topological setting of the anhydrous and hydrated cement phases is responsible for strength and durability properties [131].

An important topological feature is the interconnectivity of the different phases within the microstructure. Using a three-dimensional digital image-based simulation model of cement hydration, Bentz & Garboczi [131] demonstrated that a total capillary porosity of about 18% is required to achieve capillary pore discontinuity at any given w/c ratio. However, experimental findings suggests a capillary porosity of about 20-40% for pore discontinuity in cement pastes [132]. Assuming a capillary porosity of 18%, Powers' model was used to demonstrate that disconnected porosity can be achieved at w/c ratios under 0.5 and 0.42 for neat PC pastes and cement pastes containing 20% limestone replacement respectively [133]. Increasing limestone additions will lower the w/b ratio required to attain disconnected porosity due to its dilution effect. For limestone substitutions of 5, 10, 20 and 35% by weight, Irassar [104] found that discontinuity in porosity can be achieved for maximum w/b ratios of about 0.50, 0.48, 0.43 and 0.34 respectively. This means that for the same w/b ratio, additional limestone contents will produce higher porosity in cement paste. The described trend therefore applies to cement systems where limestone reactivity is minimal. This trend is supported by experiments by Gonzalez et al. [134] on concretes (w/b ratio 0.4) exposed to chloride solution. Their work revealed that the chloride penetration was deeper at 45 days for mixtures with increased limestone contents.

The aforementioned scenario does not always occur due to the additional physical and chemical effects of limestone, particularly when blended with high C_3A cements and alumina-rich SCMs. However, the constant 18% porosity for pore discontinuity allows the described trend in porosity with changes in limestone content to be applied

to permeability of cement-based materials. In binary PC-limestone blends, it is expected that a lower limestone content will lead to more hydrates being formed which would decrease porosity as well as pore interconnectivity and the overall permeability. On the other hand, when limestone content is higher, there is lesser amount of cement to form hydrates and a bulk of the limestone only contributes a filler effect. This leads to increased capillary porosity, which will consequently increase interconnectivity and the overall permeability.

The permeability behaviours described have been backed by water penetration and sorptivity tests reported by Ramezanianpour et al. [135] and Dhir et al.[136] on concretes having w/b ratios between 0.37-0.79 and limestone contents between 0-45%. There was decreasing water penetration and sorptivity results at low limestone substitutions (5-15% depending on w/b ratio) while considerable increases were found for substitutions of 20-45% up to 180 days of curing. Elsewhere, Tsivilis et al. [137] carried out gas and water permeability tests on concretes with w/b ratios of 0.62 and 0.70. They found that gas permeability was greater in samples containing limestone while water permeability was lower for all levels of limestone addition. These atypical observations were elucidated by Pipilikaki & Beazi-Katsioti [138], who observed that the addition of limestone modifies the pore structure of cement paste by increasing the capillary pores (related to gas permeability) from 20nm to 40nm for 35% limestone addition (the maximum substitution allowed by EN 197-1 [76]). This is associated with an exponential decrease in 'threshold diameter', i.e. the minimum diameter for continuous pores (related to water permeability). Thus, even though the dilution effect of limestone may increase the total porosity of cement paste, better particle packing will lower the mean size of interconnected pores thereby restricting overall transport of fluids [139]. Although this explains the observations of Tsivilis et al.[137], further research is required for more understanding on how limestone affects the pore structure of blended cement pastes.

2.4.3 Alum Water Treatment Sludge

Water Treatment Sludges (WTSs) are the residues generated from conventional water treatment processes which involves chemical coagulation, flocculation, filter backwash, filtration and disinfection [4]. For typical water treatment plants, about 60 – 90% of the residues are generated from the coagulant/flocculation

unit process with the remainder coming from the backwashing and sedimentation processes [140]. The coagulation and flocculation processes are used to remove both the organic and inorganic impurities present in surface and ground waters. This is achieved by the addition of chemical coagulants to agglomerate particles to a size that can be removed by settlement, flotation, or filtration.

Aluminium sulfate, $Al_2(SO_4)_3$. $18H_2O$, is commonly used in the UK as a coagulant for the treatment of surface water. Solid aluminium sulfate is added to water, which is hydrolysed to form an amorphous or poorly-crystalline gelatinous precipitate of aluminium hydroxide which carries colloidal and suspended impurities down to the bottom. The reaction of cationic Al^{3+} is summarized as [3]:

$$Al^{3+}\ (aq) + 3H_2O \rightarrow Al(OH)_3\ (s) + 3H^+\ (aq)$$

The solids settle under gravity and are removed continuously from the bottom of the basin by rakes or blades that scrape the sludge into an outlet. The collected material is known as alum water treatment sludge. The amount of sludge generated is about 3-5 percent of the untreated water entering a water treatment plant [140] and depends how much raw water is processed, the quality and dosage of coagulant used and the amount of suspended solids in the source water [5]. The sludge produced has a water content of 94-99.5%. To reduce transportation costs, the sludge is thickened and dewatered using mechanical gravity thickeners, which increases the solid content to about 2-6% [141]. In tropical zones, the water content of the sludge can be further reduced by drying in filter beds. However, the sludges are dewatered by mechanical means in the UK.

2.4.3.1 Characteristics of Alum Sludge

2.4.3.1.1 Chemical Composition

The elemental constituents of alum sludge do not vary significantly, but the relative abundances are site specific and dependent on [142]:

1. Characteristics of source water: This is influenced by the catchment bedrock minerals and any impurities discharged into the river.
2. Coagulant type used and the dosage applied
3. Any other relevant plant operating conditions.

The variability in water quality and treatment processes is responsible for the differences in the properties of alum sludge from one treatment plant to another and even for a particular plant over time. Alum sludge is made of organic and inorganic substances in the solid, liquid and gaseous states, whose composition differs in terms of physical, chemical and biological properties [143]. The composition of WTS reported in literature are presented in Table 2-2. Typically, SiO_2 constitutes a major part of the sludge followed by Al_2O_3 and Fe_2O_3 while other oxides including CaO, MgO, Na_2O, K_2O, P_2O_5 and TiO_2 are present in trace amounts. The amount of Al_2O_3 is also related to the dose of coagulant applied ($Al_2(SO_4)_3$, and the concentrations of aluminium present in impurities that get concentrated into the sludge volume during the purification process [143].

Table 2- 2: Chemical analysis of alum water treatment sludge from literature (wt. %) [143].

SiO_2	Al_2O_3	Fe_2O_3	CaO	MgO	Na_2O	K_2O	P_2O_5	TiO_2	Reference
53.36	15.28	21.01	1.20	-	-	5.41	0.83	1.38	[144]
54.1	28.84	9.92	3.1	0.64	0.30	0.75	-	1.28	[145]
64.3	21.2	10.4	2.05	1.06	0.17	0.79	-	-	[146]
52.75	20.15	6.75	0.3	-	0.872	3.69	-	-	[147]
53.6	20.9	6.6	0.3	1.9	-	-	-	-	[148]
24.68	30.39	11.59	0.16	0.17	-	0.35	-	0.90	[149]
29.63	17.57	5.18	11.85	2.15	6.09	2.85	0.94	0.56	[150]
49.2	26.3	6.6	0.8	1.0	0.6	3.2	-	-	[151]
40.61	27.36	6.99	2.62	1.89	1.05	1.28	-	-	[152]

Due to its vast availability and similar chemical compositions with clay, particularly alumina, silica and iron, WTS has been studied for the preparation of various building and construction materials. It has been used in the preparation of bricks and ceramic products with most studies showing increasing sludge content led to a decline in strength and increased water absorption of bricks [153,154]. Furthermore, preliminary characterization on the geotechnical and geoenvironmental properties of WTS have shown some promise for use as backfill material [155]. However, calcination is required to remove organics for better compatibility with traditional filler materials.

The use of calcined alum sludge as an SCM gained research interest due to move towards the use of sustainable materials. Alum sludge usually contains clay

minerals that yield reactive alumina and silica when heated between 700 and 850^{o}C [156]. The heat treatment also burns off any organic and inorganic impurities that may negatively influence concrete properties. A major limitation with alum sludge utilisation in cement composites involves identification of the heat treatment process required to convert the raw sludge into a product with optimum reactivity. This is strongly dependent on the chemical and mineralogical compositions of the raw sludge and its calcination products. Section 2.4.3.2 reports studies on the performance of calcined alum sludge-blended cement systems.

2.4.3.1.2 Mineralogy

Although pure $Al(OH)_3$ is known to have a regular crystalline structure, XRD analysis of alum sludge shows no distinct peaks, suggesting poorly ordered particles and the absence of crystalline aluminium hydroxide phase [143]. The mineralogy of alum sludges is mainly influenced by the catchment bedrock minerals where the raw water is sourced. Quartz has been identified as the most abundant mineral in calcined alum sludge with feldspar and kaolinite to a lesser degree [8,9,157–159]. The solid phase of alum sludge comprises amorphous phases of aluminium and organic matter [160]. Rodriguez et al. reported an amorphous content of 35.2% by mass in raw alum sludge [161]. Calcination will vary the amorphous content in sludge samples due to the combustion of organics and the dehydroxylation of mineral phases. Reactive components in clay minerals are obtained between the dehydroxylation and recrystallization temperatures, usually between 700-850^{o}C [162]. In this sense, the works reported have heat treated alum sludge mainly at 600-800^{o}C to activate its pozzolanic reactivity. There is currently no understanding on the evolution of mineral phases in alum sludge with calcination. This is important for understanding hydration in blended cement systems.

2.4.3.1.3 Fineness and Grading

Calcined alum sludge ground for use as an SCM can achieve a well-graded particle size distribution, similar to Portland cement. Selected literature data [157,158,161] suggest that ground calcined sludge falls within the silt (2.5-62.5μm) size fraction, with mean diameters ranging from 9.8-24μm. The BET surface area of sludges increased with calcination temperature. Raw sludge and those calcined at 600

and 800ºC had BET surface area of 3.29, 27.70 and 46.94 m^2/g respectively [9,157,161]. The marked variation compared to typical ordinary Portland cement (BET 0.5-1.5m^2/g [163]) could be due to the amorphous content and porous microstructure associated with calcined aluminas [164,165] (discussed later). Morphological characterization suggests that sludge particles have irregular shapes with rough surface textures [8,166]. Further work is required to understand the changes in microstructure of sludge particles upon various degrees of heat treatment. These properties are conducive to understanding changes in the performance when sludge is incorporated in cement mixtures.

2.4.3.2 Influence of Raw and Calcined Alum Sludge on the Properties of Cement Mixtures

Rodriguez et al. [161] evaluated the potential of adding spray-dried atomized alum sludge as a pozzolanic addition in cement mortars. The replacement of 10-30% of Portland cement with atomized sludge led to substantial retardation of hydration rates, even in samples with 10% sludge. The authors suggested that this could be due to the hydrophobic fatty acids present in the sludge preventing cement dissolution. However, FTIR analysis suggested that the presence of fatty acids could induce the formation of amorphous ettringite. Mortars with 10-30% atomized sludge showed a significant decline in slump and lower compressive than neat PC, with 28d strength activity indices (SAI) of 30-50%.

It is well established that heat treatment at 800ºC induces the pozzolanic activity of clays such as kaolinite [162]. In this sense, a number of authors have heat-treated alum sludges to rid them of any organics and induce the pozzolanic activity of any clays present. It was observed that the incorporation into cement of sludge calcined at 800ºC significantly increased water demand [8,167,168]. Some studies have suggested that alum sludges have irregular particles with large specific surface areas, which could increase the water absorption and thus increase the water demand to maintain the standard consistency [8]. This has often necessitated the use of superplasticisers to control the consistency of cement mixtures. Ahmad et al. [167] reported that 20% replacement of PC with calcined sludge had negligible effect on the initial setting time but final setting time was retard by one hour compared to neat PC mixes. A 28d SAI of 80% was achieved, exceeding the 75% minimum requirement for

pozzolans. Increasing incorporation of calcined sludge led to a steady decline in compressive strength although 28d strength activity indices of 80% was observed [169]. Lower strengths were attributed to the higher water requirement induced by the sludge particles, producing more permeable voids.

Gastaldini et al. [9] investigated the optimal calcination temperature and residence time to attain maximum reactivity in calcined sludges. Using the Chappelle test, which measures the amount of fixed calcium hydroxide in blended $Ca(OH)_2$-sludge mixtures, it was concluded that the best pozzolanic results are obtained with a calcination temperature of 700 °C for 30 min. However, calcining at 700^{o}C for 1 hour produced the highest 28-day SAI of 125% , consistent with the findings of Hagemann et al. [157]. This is not far off from the optimum conditions of 750^{o}C for 1 hour reported by Gabriel et al. [166]. By calcining at 700 °C for 30 min, the compressive strengths in concrete mixtures were determined for substitution levels ranging from 5% to 30% for three different w/b ratios (0.35, 0.5 and 0.65). For the same w/b ratios, concrete mixes containing calcined sludge showed improved strength, ranging from 3-30% relative to neat PC mixes. A comparison of the performance of mixes prepared using the same content of calcined sludge, more conventional SCMs such as rice husk ash and silica fume as a substitution for cement showed that the values obtained using calcined sludge ash are higher, which attests the viability of using the material. However, rice husk ash and silica fume produced higher fixed calcium hydroxide than calcined sludge, which indicates that the test cannot be used to rule out a mineral addition. The higher silica contents in rice husk ash and silica fume react with CH to form C-S-H.

Owaid et al. [8] investigated the mechanical strength in binary and ternary blends containing alum sludge calcined at 800^{o}C, silica fume (SF), palm oil fuel ash (POFA) and GGBS. In binary systems, the incorporation of up to 15% calcined sludge produced higher strength than the neat PC. Higher substitutions led to a decline in strength with 28-d SAI of 93%. The compressive strength of ternary mixtures containing calcined sludge and the mentioned pozzolanic materials was higher than binary blends with the same calcined sludge replacement. The PC + calcined sludge + SF mix exhibited the highest strength, followed by PC + calcined sludge + POFA and calcined sludge + GGBS. In another study, the same authors investigated the durability performance of these mixes by water absorption, sorptivity and sulfate and chloride resistance showing a similar trend to the earlier studied mechanical properties [168]. The results indicate that the binary blends with 15% calcined sludge showed

better durability performance compared to the control and 20% calcined sludge concrete mixtures. Similarly, all ternary blended mixes performed better than the binary blends with calcined sludge at the same substation levels. Further work is required to elucidate the underlying chemistry responsible for the strength and durability characteristics.

It is well established that a synergistic interaction exists between limestone and alumina-rich SCMs that leads to enhanced strength and durability [124]. In this sense, Hagemann et al.[157] recently investigated the potential synergy between calcined sludge and limestone powder. A response model was used to study the effect of each factor or combination of factors affecting the behaviour of cementitious mixtures. The results for mixes with coupled substitutions of calcined sludge and limestone showed that the most significant factors influencing compressive strength were w/b ratio, calcined sludge content, and the interaction between them. Although limestone was not considered a significant factor in the compressive strength model, experimental results showed that ternary mixes composed of 15% calcined sludge and 7.5% of limestone showed compressive strength values higher than the reference concretes at the same w/b ratios (0.35, 0.50, and 0.65). However, hydration studies are required to establish a synergistic interaction in ternary calcined sludge-limestone mixtures.

2.4.3.3 Availability and Practical Use of WTS in Cement

There are several sources of SCMs which have been well studied, but their availability is not in the range of the huge cement production (Figure 2-10). The global availability of slag is around 5-10% of the amount of cement produced [170]. In the UK, an estimated 2.2 Mt of slag was produced in 2013 but this may decrease in the future as only two main steel producing facilities remain (Port Talbot and Scunthorpe) [171]. The drive towards more sustainable manufacturing processes could result in facilities shutting down or being replaced with more modern Electric Arc Furnaces which do not produce Slag. Figure 2-10 shows that the global availability of fly ash is somewhat higher (around 30% relative to cement). UK production of fly ash was about 5.8Mt in 2013 but this is likely to decline as the UK Government has announced plans to close all unabated coal-fired power plants by 2025 [171]. Similar moves are being discussed in other European countries which could affect the availability of these SCMs.

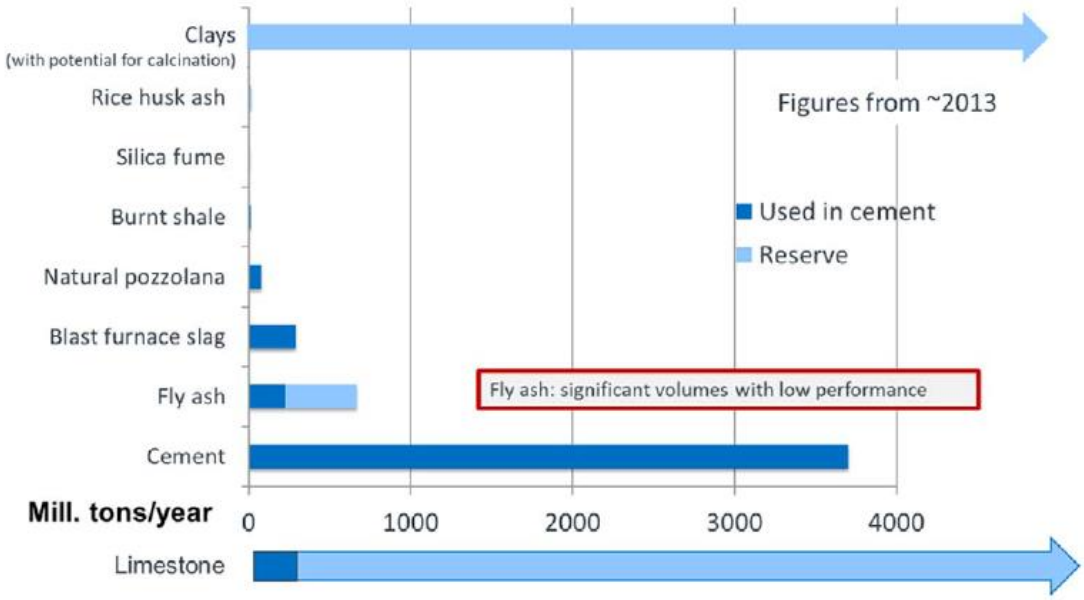

Figure 2- 10: Global Availability of Common SCMs [170]

Due to the limited availability of conventional SCMs, it is essential to find new types and sources of SCMs. Estimates of WTS generated per annum are sparsely reported as local authorities usually publish the waste statistics in a broad category instead of specifying each waste type. Fig. 2-11 shows the WTS generation in different countries [172]. UK production of WTS in 2013 was approximately 131,000 tonnes dry solids. This consists of 44% alum sludge, 32% ferric sludge and 18.5% softening sludge [173]. Preliminary studies assessing the technical viability of calcined alum sludge as an SCM are promising [8,9]. Calcination temperatures are much lower (~800^{o}C) than clinker (1450^{o}C) leading to lower energy costs. Based on the quantities of alum sludge generated in the UK in 2013 and assuming a loss of ignition of ~22% [174], 44,960 tonnes of SCM can realistically be produced. This amount is significantly lower than quantities of slag (2.2Mt) and fly ash (5.8Mt) produced in the same year. However, Figure 2-11 shows that annual WTS generation in a country is proportional to population size due to the varying demand for potable water. Thus, considerably more WTS should be available for recycling purposes in countries with population growth.

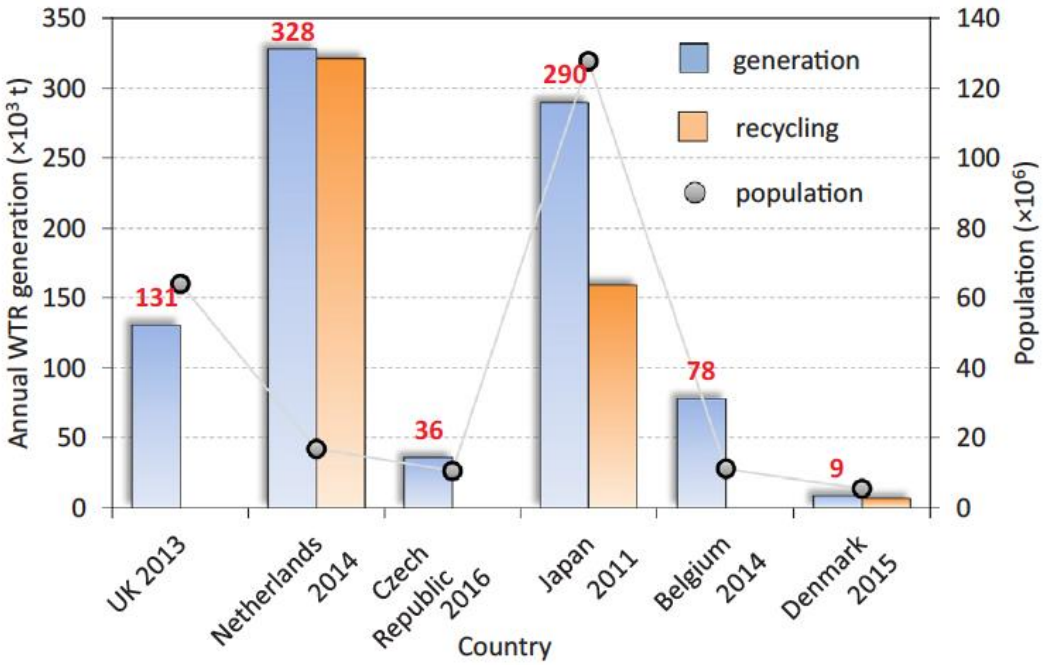

Figure 2- 11: Annual WTS generation (dry mass) and recycling statistics [172]

2.4.4 Properties of Aluminium Hydroxides and Oxides

As earlier stated, alum water treatment sludge is an amorphous aluminium hydroxide precipitate formed from the reaction between the $Al_2(SO_4)_3$ and the natural alkalinity of raw water, which usually arises from calcium bicarbonate. The dehydration of $Al(OH)_3$ gel produces metastable aluminium oxides. These materials have gained research interest; with their preparation and properties being of theoretical and applied interest. They are commonly used directly or indirectly in almost every major industry from ceramics and refractories to plastics and pharmaceuticals. Of particular importance to this study are the characteristics of raw and calcined sludges. This is investigated experimentally with inferences drawn from available scientific knowledge on the chemical, structural and surface characteristics of aluminium hydroxides and oxides. The following section briefly describes relevant theoretical knowledge on the synthesis, physical and mineralogical characterization of aluminium hydroxides and oxides. For a comprehensive overview of the properties of aluminas, refer to the works of Hudsson et al. [175], Hart [3] and Wefers & Misra [176].

2.4.4.1 Synthesis and Properties of Aluminium Hydroxides

A general classification of the variations of aluminum hydroxides is shown in Figure 2-10 [175]. The well-defined crystalline forms are the three trihydroxides, $Al(OH)_3$: gibbsite, bayerite, and nordstrandite, and two modifications of aluminum oxide hydroxide, AlOOH: boehmite and diaspore. Gelatinous hydroxides may consist of mostly amorphous aluminium hydroxide or pseudoboehmite. The XRD pattern of the latter shows broad bands that coincide with strong reflections of the well-crystallized oxide hydroxide boehmite.

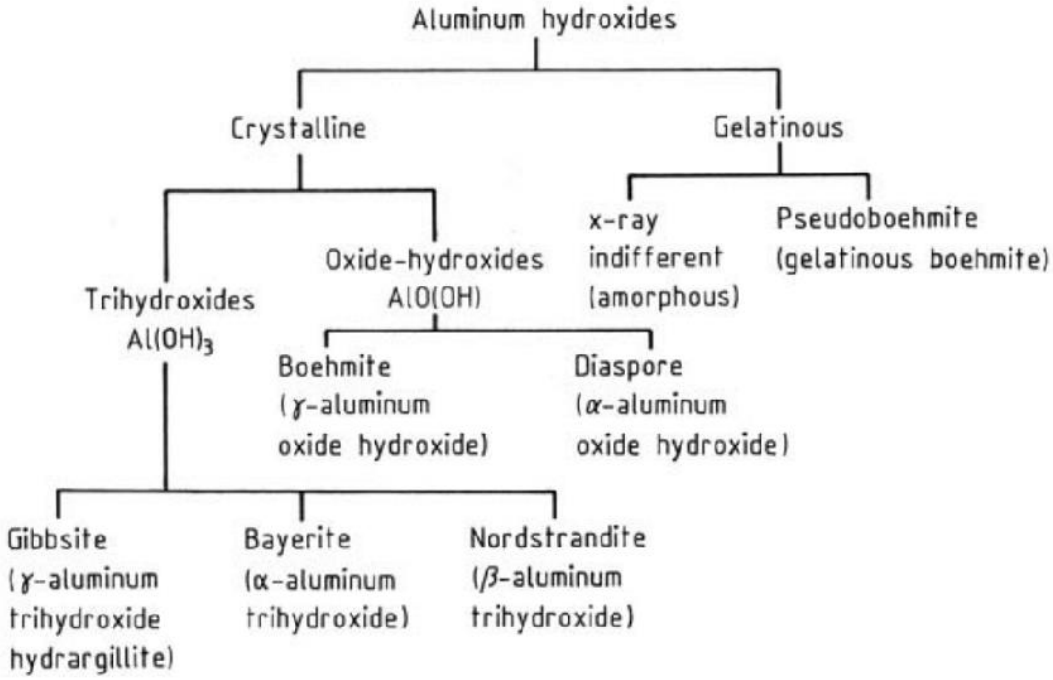

Figure 2- 12: Classification of aluminium hydroxides [175].

Several methods are available for the preparation of aluminas such as the sol-gel route, co-precipitation, organic gel assisted citrate complexion, hydrothermal route, flame spray pyrolysis and combustion route [164,165,177,178]. Similar to alum sludge generation, the sol–gel process consists of the preparation of a colloidal suspension from the controlled hydrolysis and condensation of aluminum salts to obtain an aluminum hydroxide precipitate [179]. Another route is through the rapid neutralisation of aluminium salt solutions with bases such as NaOH, urea, ammonia, Na_2CO_3, ammonium carbonate and sodium aluminate[178]. In both cases, the initial amorphous $Al(OH)_3$ precipitate is usually colloidal and coagulates to a gel. Many factors determine the crystallinity and chemical composition of alumina gels, such as temperature, rate

of precipitation, final pH, ionic composition, concentration of starting solutions and time of ageing (transformation of the solid phase to ordered aluminium hydroxide) [176]. By infrared analysis, it was reported that gels precipitated in the presence sulfates and carbonate ions had a retarding effect on the ageing of alumina gels [180]. In addition, Sato et al. [181] observed that the precipitate formed, whether amorphous $Al(OH)_3$, boehmite or bayerite.was dependent on the final pH.

Aluminium hydroxide gel is synthesized by the neutralisation of concentrated aluminium salt solutions at temperatures below 290K [176]. The rate of ageing is very slow at this pH and temperature. The strong interaction of alumina gels with ions of precursor solutions imparts impurities in the system which may vary the structure of the product formed. Bhattacharya et al. [178] prepared aluminium hydroxide gel precipitate through wet chemical precipitation involving the hydrolysis of aluminium sulfate by ammonia at a pH 7-7.2, normal temperature and pressure. Similarly, Pradhan et al. [177] prepared aluminium hydroxide gel by the base hydrolysis of aluminium sulfate solution and urea at room temperature and a pH of ~6.7.

Pseudoboehmite or gelatinous boehmite can be synthesized by ageing aluminium hydroxide gel [176]. Ageing at temperatures below 350K transforms pseudoboehmite into crystalline boehmite. Thus, pseudoboehmite is an intermediate phase in the ageing of $Al(OH)_3$ gels. It has been suggested that presence of structural water is the difference between boehmite and pseudoboehmite [176]. Rajabi and Derakhshan [182] prepared boehmite particles by the neutralisation reaction of aluminium nitrate solution with NaOH. Characterization of the samples suggested that bayerite was initially formed upon mixing precursor materials at room temperature, which was rapidly converted to boehmite. Boehmite crystals were obtained by hydrothermal treatment.

Bayerite can be prepared by the immersion of amalgamated aluminium in pure water at room temperature. Another method is the neutralisation of aluminium salt solutions by ammonium hydroxide at temperatures below 325K and pH 8 to 9.

2.4.4.2 Thermal decomposition of aluminium hydroxides and oxides

The dehydration of gelatinous aluminium hydroxides occurs through metastable phases such as η, θ, γ, δ and ultimately thermodynamically stable α-alumina. However, the degree of structural ordering, thermal conditions, starting materials and method of synthesis have significant effects on the formation of metastable phases and the ultimate α-alumina [176,183]. Metastable phases of aluminium oxide called 'transition aluminas' are used adsorbents, coatings, soft abrasives and catalyst supports because of the unique characteristics such as high surface area, porosity and chemical activity [184]. These materials make use of aluminas with different levels of transformation to α-alumina, ranging from 5-100% [176]. The temperature and rate of transformation is highly dependent on contaminants and other mineral addition. This means that although inferences can be made from commercially synthesized aluminas, the characteristics of raw and calcined sludges are likely to differ. A review of the effect of calcination on the physical and mineralogical properties of aluminium hydroxide gels is provided below.

Stumpf et al. [185] developed the generally accepted sequence of transition aluminas shown in Figure 2-11. The schematic was based on the results of a wide XRD study which showed that during the thermal transformation of aluminium hydroxides, the series of transition aluminas formed was based on the starting material and temperature of calcination. However, some authors disagree about the XRD identification of some phases and the existence of others, arguing that the transition sequence is also affected factors such as heating rates and the presence of impurities [178,186].

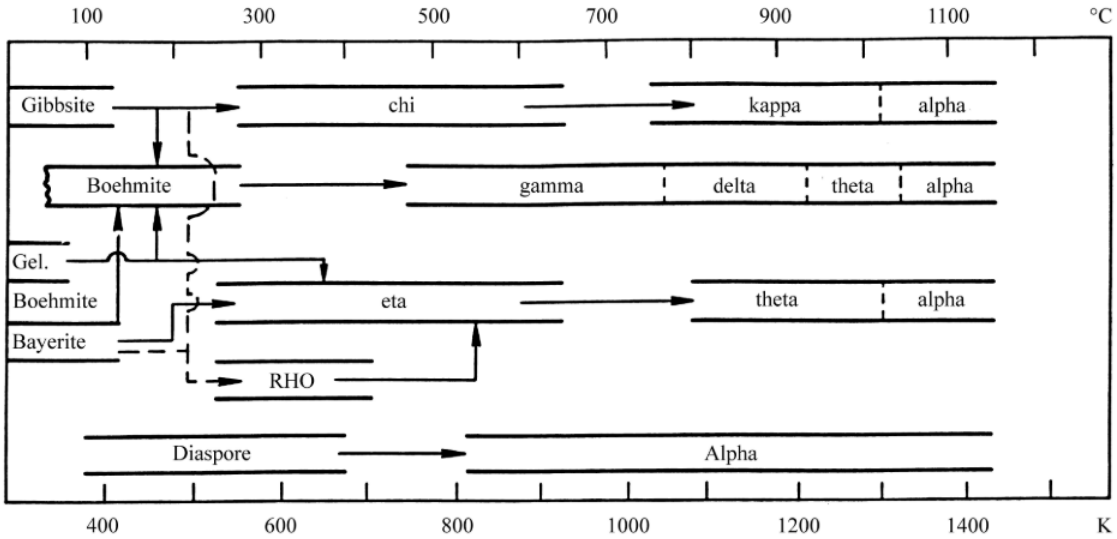

Figure 2- 13: Thermal transformation sequence of aluminium hydroxides [175]

During the thermal decomposition of aluminium hydroxides, their compositional and structural characteristics are modified before ultimately transforming into α-Al_2O_3. This heat-induced conversion is topotactic. A mass loss 15% or 24% by weight occurs for trihydroxides or oxide hydroxides, respectively due to the removal of considerable amount of free water, adsorbed water and chemically bound water, with little change in particle shape. This creates significant internal porosity that may increase the specific surface area of the material. This describes the main dehydroxylation stage of aluminas. Transition aluminas are then formed, although not thermodynamically stable, are reproducible under the same thermal conditions and synthesis method.

Bhattaacharya et al. [178] prepared aluminium hydroxide gel by hydrolysing an aqueous solution of aluminium sulfate with ammonia at normal temperature and pressure. FTIR, XRD and TGA were used to characterize the thermally treated samples. Calcining the aluminium hydroxide gel up to 800^{o}C maintained the amorphous structure of the material. At 900^{o}C, the η- alumina phase was detected by XRD. This structure was maintained until 1100^{o}C whereupon it converted to α-alumina. TGA of the aluminium hydroxide gel indicated two distinct mass losses, at 250^{o}C and 900^{o}C. The first was attributed to dehydration or dehydroxylation with the second attributed to desulphurisation of the samples. It was found that the surface area of the calcined product was highest at 900^{o}C. The phase transitions and variation in surface area were consistent with the works of Pradhan et al. [177] and Das et al. [187] who also produced Al(OH) gels derived from aluminium sulfates. It is worth

noting that the XRD patterns of γ-alumina and η-alumina are almost identical. Characterisation was primarily on the basis that the η-alumina has a spinel-cubic structure with a regular cubic-oxygen lattice of lattice parameter a= 0.79 nm while γ-alumina is of the spinel-tetragonal type with lattice parameters a=0.796, c=0.781 nm [176,177].

Castruita et al. [179] compared transition phases obtained from calcining pseudoboehmites derived from three different salts: $AlSO_4$, $Al(NO_3)_3$ and $AlCl_3$. During the treatment, the three samples showed similar routes to α-alumina as follows: Pseudoboehmiteà η-Al_2O_3 → θ-Al_2O_3 → α-Al_2O_3. However, the sample from the sulfate showed the highest α-Al_2O_3 alumina content at temperatures below 1200^oC. This was attributed to sulfate salts reducing the transformation temperature. The removal of sulfate salts provides space that enhance atomic rearrangement thereby lowering the energy for conversion to α-Al_2O_3. Furthermore, SEM analysis showed that the $Al(NO_3)_3$ and $AlCl_3$-derived gels calcined at 1200^oC had identical coarse vermicular microstructures with higher porosities while calcination of sulfate-derived gel developed a finer vermicular morphology.

The increase in porosity and associated high surface area of transition aluminas have been attributed to the rapid loss in mass without a change in the external dimensions of hydroxide particles[176]. A number of authors have attempted to relate specific surface area, size and shape of pores, pore volume to the characteristics of the precursor and calcination conditions. The large surface area developing during the dehydration process has been attributed to a collection of slit-shaped pores with pore diameters below 2nm [176]. Sun et al.[188] prepared boehmite gel from the base hydrolysis of aluminium chloride solution and ammonia. Mesoporous alumina (MA) of different pore sizes and crystalline structures were prepared by heat treatment at 550^oC and over (Figure 2-12). At 550^oC, MA remains amorphous. Upon calcination at 800^oC, γ-alumina is formed. At 1100^oC, however, both θ- and α-Al_2O_3 are formed. Above 1100^oC, there is a drastic reduction in surface area, indicative of α-Al_2O_3 formation. Pore sizes increased with temperature while total volume decreased at temperatures between 550^oC and 1100^oC.

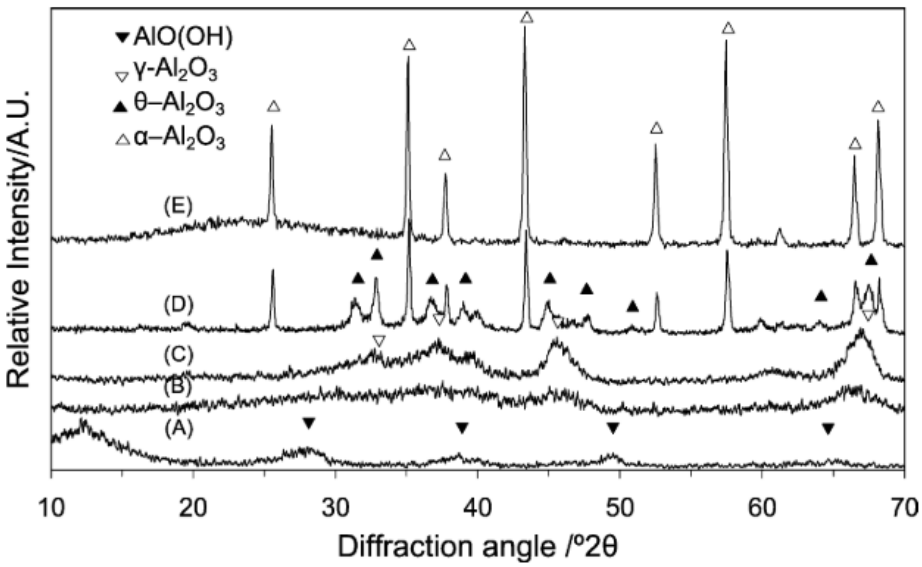

Figure 2- 14: XRD patterns of (A) boehmite gel, calcined aluminas at (B) 550ºC (C) 800 ºC (D) 1100 ºC and (E) 1300 ºC [188].

The dehydration, with changes in porosity, specific surface area and density with calcination temperature in aluminium hydroxides of different particle size are illustrated in Figure 2-13 [165]. Samples heated at 300ºC transitioned into boehmite. The particles became denser and showed a significant increase in the surface area and total volume compared to the as-received material. Further calcination up to 900ºC produced denser particles which was followed by an intense reduction in specific surface area. This behaviour is due to the continuous reordering and consolidation of the solid. At 1100º C, the stabilization of density and the intense reduction in surface area and total pore volume indicate initial signs of sintering and transition to α-Al_2O_3. These trends are consistent with the observations of Hudson et al. [175] and Sun et al.[188], although maximum surface area were observed at 400ºC and 550ºC respectively.

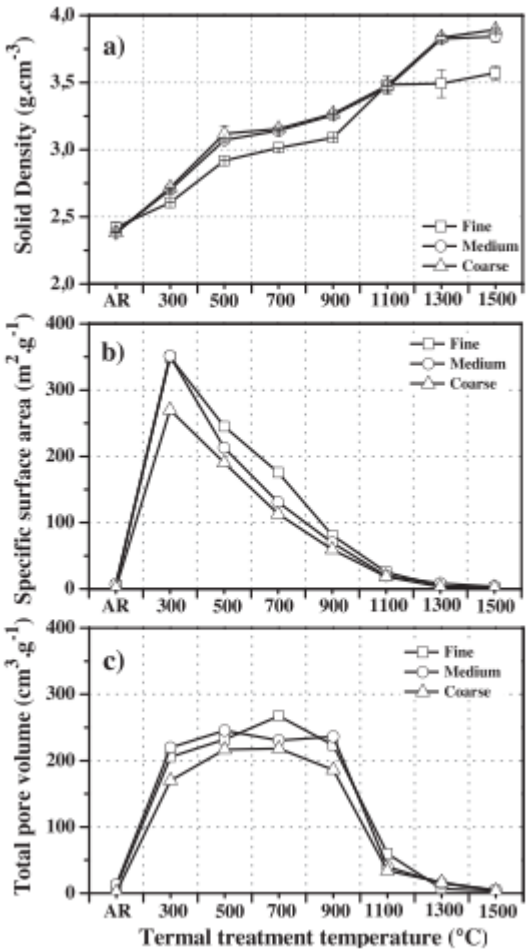

Figure 2- 15: a) Solid density, b)Specific surface area and c) Total pore volume of $Al(OH)_3$ [165].

2.5 Influence of nano-alumina on the properties of cement mixtures

Advances in nanotechnology and practical use of nano-materials in many industries has encouraged research into their viability in cementitious materials. A number of nano-materials have shown promise in cement-based materials for the enhancement of certain characteristics (physical, mechanical or durability properties). For example nano-silica [189,190] has been used to enhance strength and durability in cementitious materials due to its high reactivity and nano-Fe_2O_3 [191] has been suggested to provide self-sensing abilities and promote mechanical performance. Similarly, some researchers have investigated the potential use of nano-alumina (NA) in cement to improve its properties. Compared with other transition aluminas, it was found that the γ- (gamma) phase has the lowest surface energy and higher reactivity [192], which could assist cement hydration. As a result, its potential use has drawn the

interest of researchers. This section provides a review of research investigation the influence of γ- alumina on the properties of cement mixtures.

Zhan et al. [193] reported on the effect of nano γ- alumina additions up to 4% by wt. of cement on the hydration and strength development of cement pastes. Calorimetric measurements indicated that the presence of nano-alumina accelerated the silicate and aluminate phase reactions in PC. The formation of the AFm phase seemed to start earlier and overlapped with the aluminate reactions in paste prepared with 4% NA. Acceleration of the alite peak was attributed to the additional high surface area provided by NA particles for the precipitation of hydrates. This was confirmed by SEM analysis which showed that Al/Si ratio of outer-product C-S-H in NA-modified pastes was 30% higher than in neat cement. This could mean that the NA acted as seeding for outer C-S-H. However, no new phases were detected in NA-modified pastes. Addition of 1 and 2 wt% NA led to only a slight increase in strength while 4% incorporation of NA led to up to 56% increase in strength compared to neat PC mixes. Similar accelerated alite hydration was reported elsewhere [72], increasing with NA content and was attributed to both filler- and chemical effects. The chemical effect arose from nano-alumina dissolution in pore solutions which led to a dramatic decrease in aqueous sulfate concentration. The initially dissolved nano-alumina reacted with sulfates at very early age, with rapid ettringite formation. This however consumed sulfates, thereby accelerating C_3A reaction. Shao et al. [194] related the reduction in the SO_3/Al_2O_3 ratio with an increase in monosulfate content. It was suggested that the monosulfate converted to monocarbonate with time in NA-modified pastes. Although not confirmed in the study, the presence of monocarbonate could also be an indication of limestone-NA reaction. These hydrates resulted in a reduction in porosity and refinement of pore structure which led to improved strength at later ages.

Chen et al. [195] reported that nano-γAl_2O_3 additions in calcium aluminate cements (CAC) can contribute to the formation of hydrated calcium aluminate and alumina gels. This led to a shortening of the induction period and an acceleration of the CAC hydration. XRD results indicated that increasing NA content enhanced the relative intensities of the characteristic peaks of CAH_{10} and C_2AH_8 indicating that NA contributes to the nucleation and growth of hydrate crystals. This led a denser microstructure and improved strength.

Al_2O_3 is a precursor material for the production of mullite, a compound that enhances the mechanical properties of ceramics. Mullite is a stable aluminosilicate which is formed at calcination temperatures of about 1100 and 1350^oC from the reaction between alumina and silica [196]. As a result, a few authors have investigated the properties of NA-cement mixes at elevated temperatures. Farzadia et al. [197] prepared mortars with 1, 2, 3% NA as cement replacement and exposed them to temperatures ranging from 100-1000^oC. The results from gas permeability tests indicated that 1% NA produced the most impermeable of the mixes prepared, particularly at room temperature, 300^oC and 600^oC. At these temperatures, 1% NA decreased gas permeability by 38%, 31% and 21%. At room temperature, 1 % NA increased compressive strength by 16% while higher NA replacements led to decreasing strength. The reason for the strength loss with NA addition might be due to the agglomeration of excess NA particles which may coat sand particles thereby loosen the interfacial transition zone [198]. At elevated temperatures, all samples experienced strength loss which may be related to the decomposition of CH and C-S-H.

2.6 Influence of aluminate-based accelerators on the properties of cement mixtures

Over the last few decades, tunnel construction has become more common in railway and highway projects. For safety reasons, accelerating admixtures or accelerators are used to prepare ‘sprayed concrete’ to offer support to unstable ground and prevent fresh materials from falling from overhead area [199]. These accelerators promote rapid setting of cement-based materials and enhance the early strength development by altering the kinetics and mechanisms of cement hydration. Alkaline and alkali-free accelerators are mainly composed of sodium aluminate and aluminium sulfate respectively. In alkaline environment of cement mixes, Al^{3+} ions are converted to $Al(OH)_4$, which can further react with Ca^{2+} and SO_4^{2-} in the liquid phase to form AFt and AFm phases, which lead to shortened setting times of the matrix [200,201]. C_3A hydration then occurs in an undersulfated system and C-A-H phases might also be formed. The primary mechanism of accelerators is to accelerate the formation and growth of ettringite by accelerating the hydration of C_3S and C_3A [202]. The interaction between clinker phases and dissolved aluminates have received research attention

due to the viable industrial application in the preparation of accelerators. This section provides an overview of studies on influence of aluminate-based accelerators on the hydration of C_3S, C_4A as well as setting and strength development in cement-based materials.

Tan et al. [203] studied the influence of AS on the hydration of C_3S pastes by XRD, NMR TEM and isothermal calorimetry. The presence of AS shortened the induction period and accelerated C_3S hydration (Figure 2-14). According to the authors, the dissolved sulfates and aluminium from AS immediately react with Ca^{2+} ions to form ettringite which provide nucleation seeds that promote the formation of hydrates as illustrated in Figure 2-15. Then again, the formation of ettringite consumes the Ca^{2+} ions in the system and advances the dissolution of Ca^{2+}, thereby speeding up the dissolution of the C_3S + AS system. The ettringite initially formed away from the C_3S grains, promotes the precipitation of C-S-H gel. This leads to an increase in the volume of hydrates and better filling of pores plus a denser microstructure, which translates to higher strength. Compared to neat C_3S mix, the addition of 4% AS led to an increase in compressive strength by 64.56% and 42.73% at 1 and 28 days. The improved performance at all ages is consistent with the findings of Yang et al.[201], where more significant alite acceleration was observed as well as a higher maximum heat flow in pastes with 7% and 9% accelerator compared to the alite peak of the reference paste.

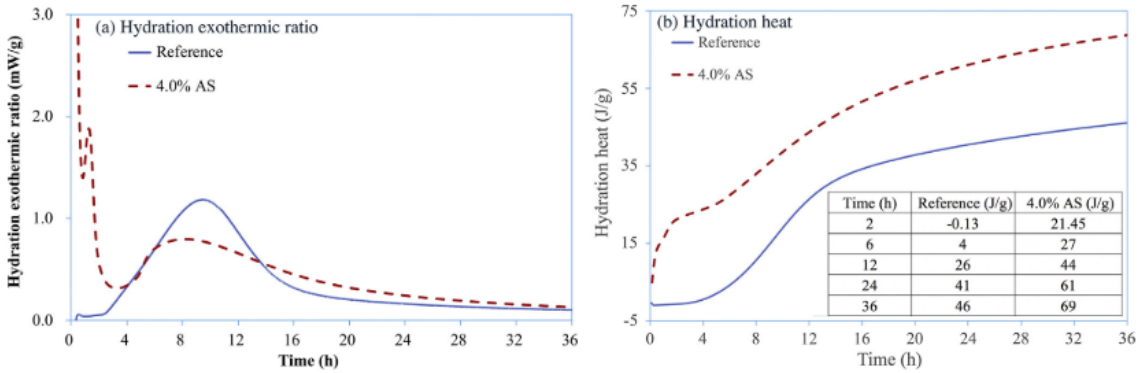

Figure 2- 16: Effect of AS on hydration heat of C_3S [203].

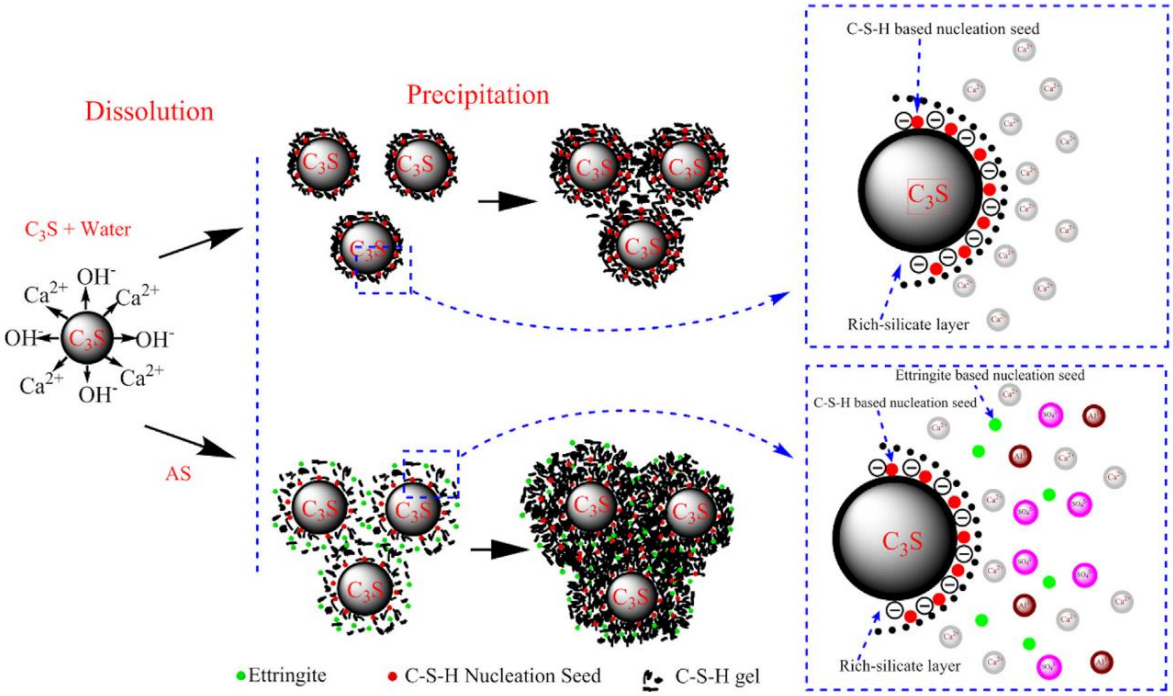

Figure 2- 17: Hydration mechanism of C_3S with AS [203].

Although, Han et al. [204] also reported that increasing AS content can effectively accelerate setting and enhance compressive strength at early age (1 day), impaired compressive strength was observed at later ages compared to neat PC. AS was found to accelerate the hydration of C_3A but inhibit the hydration of C_3S. AS consumed sulfate and calcium ions to form ettringite thereby enhancing C_3A hydration. The resulting undersulfated condition allows the consumption of ettringite by unreacted C_3A to form monosulfoaluminate. This consumption of ettringite was also expedited by the slow dissolution of anhydrite. On the other hand, the enhanced amount of ettringite acted as a barrier to the hydration of C_3S. It was suggested that the water binding property of ettringite could limit the free water available for C_3S hydration. Thus, the observed impaired strength at later ages.

The molar aluminate-to-sulfate ratio (C_3A/SO_3) is the main factor controlling the accelerator reaction. Ettringite is the main hydrate formed when the sulfate-to-aluminate ratio is between 0.6 and 0.9 [205]. This is rarely so in accelerated systems due to the extra aluminate ions contributed by accelerators which creates an undersulfated situation where the sulfate-to-aluminate ratio is greater than 0.9. In this case, C_3A consumes ettringite to form monosulfoaluminate [29,206]. The formation monosulfoaluminate early-on coats cement grains and fills up the spaces present. This

reduces the rate and degree of alite reaction which leads to lower compressive strength at later ages [205]. To avoid this scenario, sulfate balance needs to be maintained. Although AS contains additional sulfate ions, accelerated cement mixes could still experience an undersulfated condition. Therefore, additional sulfates may be required to regulate the hydration of C_3A and C_4AF.

Salvador et al. [200] and Xu and Stark [207] observed that accelerators based on sodium aluminate solutions quickly deplete dissolved sulfates. Gypsum is depleted within 20 minutes of hydration and further C_3A reaction occurs as in undersulfated systems. The main aluminate hydrates detected are ettringite, monosulfoaluminate and C-A-H. It was found that AFm and C-A-H, which are primarily less soluble and more thermodynamically stable than alite, block C_3S dissolution sites and prevent its continued reaction. As indicated by in-situ-XRD and calorimetric measurements, this leads to reduced dissolution of alite and lower degree of hydration at later ages.

Herrera-Mesen [208] studied the influence of gypsum content on the hydration and mechanical properties of accelerated mixes. The increase in sulfate content by the addition of sulfate led to faster formation of ettringite at early age due to the induced reactivity of accelerator admixtures. This led to increased early age compressive strength. An optimally sulfated system is necessary for optimum accelerator reaction and compressive strength both in the short and long term. The authors observed maximum performance in mixes with aluminate-to-sulfate ratio of 0.66. On the other hand, it was found that over-sulfated systems inhibits alite dissolution due to the common ion (Ca^{2+}) effect. The considerable formation of ettringite occupies the space available for precipitation of hydrates before the alite hydration occurs. Thus, high accelerator reaction restricts alite reaction which leads to lower strength at later ages. Li et al. [209] observed that the accelerated C_3S hydration at the early stage leds to the adsorption of SO_4^{2-} by C-S-H and the formation of ettringite mainly at the surface of the C_3S grains. This hindered the further hydration of C_3S which led to a decrease in 28-day compressive strength with increasing dosage.

Maltese et al.[210] investigated the effect of AS and different setting regulators (anhydrite, gypsum, α-hemihydrate and β-hemihydrate) on the setting behaviour and hydration of Portland cement. The study found that the efficiency of AS was influenced by the instantaneous dissolution rate of the setting regulators and observed that the lower the instantaneous dissolution rate (anhydrite < gypsum < α-hemihydrate < β-hemihydrate), the more efficient the accelerator. The reason for this could be related

with the different morphology of ettringite formed during the first minutes of reaction, changing from round mass to prismatic needle along with the decrease of instantaneous solubility rate of setting regulator.

Salvador et al. [205] found that limestone filler enhanced accelerator reactivity when gypsum was the calcium sulfate source. Results suggest a synergistic reaction between limestone and accelerators. Al^{3+} from the accelerator reacts with calcium carbonate forming hemi- and monocarboaluminate. The acidity of accelerators was found to be conducive to limestone dissolution, thereby promoting Al^{3+} reaction, which is restricted by gypsum dissolution in Portland cement pastes. Because the dissolution rate of hemihydrate is higher than gypsum, it retards the dissolution of limestone by the common ion (Ca^{2+}) effect, restricting its efficiency. In addition, it was found by SEM analysis that limestone powder provides nucleation sites for the precipitation of aluminate hydrates formed from accelerator reaction. Thus, limestone retards the rapid sulfate depletion in accelerated pastes by restricting C_3A reaction thereby enhancing its reactivity. The authors recommend the use of both limestone and calcium sulfate whilst ensuring the C_3A-to-sulfate ratio in the system is between 0.67 and 0.9.

2.7 Summary of key literature and approach to address gaps

The use of SCMs offers a viable solution to reducing the adverse environmental impact of cement production. However, due to shortages of conventional SCMs in some locations, plus threats to worldwide availability by, for example, the move away from burning coal for electricity generation, their continued extensive use is limited. This forms the basis of this study, which aims to investigate the potential use of UK alum water treatment sludge as an SCM. A review of the literature has shown how components in blended systems affect the hydration of one another. While the influence of slag and limestone on the hydration, microstructural development and engineering performance of composite cements has received extensive research, alum sludges remain sparsely studied. Literature has shown an improvement in strength when calcined sludge is incorporated in blended systems. However, little has been reported on their characteristics, reactivity, hydration mechanisms, microstructural development, interactions with other SCMs and impact on overall binder performance. The underlying reasons for the strength improvement have not been addressed, particularly on how the physical, chemical and mineralogical

characteristics of alum sludge affects the properties of cement mixtures. The first step towards this is a better understanding of the characteristics of the raw sludge, how these properties can be modified by heat treatment and the variation in cementitious reactivity. These properties are conducive to assessing the impact of reactive sludge on the hydration, microstructure development and engineering properties of blended cements. As shown later in Chapter 4, the chemical composition of the alum sludge sample collected for this work varies significantly from samples presented in literature. The significantly more alumina content of the alum sludge in this work is conducive to assessing the reactivity of the synthetic aluminates added during water treatment. An understanding of sludge characteristics and the underlying factors describing its interaction in blended cement systems provide a means for predicting performance and finding solutions to problems of low strength, durability and poor mixture workability that are commonly associated with the use of pozzolans as SCMs. Furthermore, published data show potential benefits from the interactions between reactive aluminates and carbonates in limestone powder. However, the potential synergy between limestone and alum sludge remains largely unexplored.

The key questions in this study are therefore:

- What are the physical, chemical and mineralogical characteristics of raw and calcined sludges?
- What is the effect of calcination temperature on the reactivity of alum sludge?
- What is the impact of calcined sludge on the hydration of clinker?
- What is the impact of physical characteristics of calcined sludge on the workability of blended cement mortars?
- Is there an interaction between calcined sludge and other SCMs such as slag and limestone? If so, then what does it depend on?
- What are types and amounts of hydrates formed (phase assemblage) in blended cements incorporating calcined sludge?
- How does matrix densification progress in the presence of calcined sludge?
- What are the key factors affecting strength and permeability in in blended systems containing calcined sludge?

CHAPTER III: Materials and Methods

3.1 Raw Materials

The CEM I 52.5R used in this study was supplied by Italcementi and is of the same batch used in a previous study [211]. The cement had no additional limestone in order to avoid complications in calculating the reacted $CaCO_3$ in blended limestone cement systems. The GGBS selected was supplied by Hanson cement. The limestone used was supplied by Heidelberg Cement and is of the same batch as used in a previous study [212]. The cementitious materials along with their BET surface areas and specific densities are shown in Table 3-1. The chemical analysis of the materials determined by XRF are shown Table 3-2. It is important to note that the slag small used has a calcium carbonate content of 3.23 wt.%. Table 3-3 provides the phase composition of CEM I as calculated by Bogue calculation. Particle size distributions, as measured by laser granulometry, are shown in Figure 3-1.

The alum water treatment sludge investigated was collected from Elvington water treatment works located in York, United Kingdom. The sludge was black in colour and had an inoffensive odour. The sludge had been dewatered by mechanical means prior and had the consistency of damp soil. Detailed characterization of alum sludge is provided in chapter 4.

The fine aggregate used to produce mortar samples was natural sand sieved to a maximum size of 2mm in accordance with BS EN 196-1 [213]. The particle size distribution of aggregates used for preparing mortars are shown in Figure 3-2.

Tap water was used for preparing cement pastes and mortars. An aqueous solution of modified polycarboxylate-based superplasticiser (Sika Viscocrete 25MP) was used at constant dosages to offset the loss in workability upon incorporating alum sludge in cement mixtures. It has a specific gravity of 1.065 kg/l. A stock aqueous solution was prepared and then used in mixing cement pastes and mortars.

Table 3- 1: BET surface area and densities of cementitious materials

Property	CEM I 52.5R	GGBS	Limestone powder
BET Surface area (m^2/g)	1.01	1.56	1.03
Density (g/cm^3)	3.17	2.94	2.72

Table 3- 2: Oxide compositions of cementitious materials (wt. %)

Composition	Cement (%)	GGBS (%)	Limestone (%)
SiO_2	20.50	34.51	2.00
Al_2O_3	4.60	11.20	0.80
Fe_2O_3	2.40	0.35	0.32
CaO	63.40	43.07	53.13
MgO	2.00	7.64	0.64
SO_3	3.60	1.76	0.07
Na_2O	0.13	0.14	-
P_2O_5	0.30	-	-
MnO	0.00	0.17	-
TiO_2	0.30	0.74	-
K_2O	0.74	0.48	-

Table 3- 3: Mineralogical composition of CEM I 52.5R (wt. %)

Phase	C_3S	C_2S	C_3A	C_4AF
CEM I 52.5R	68	10	9	4

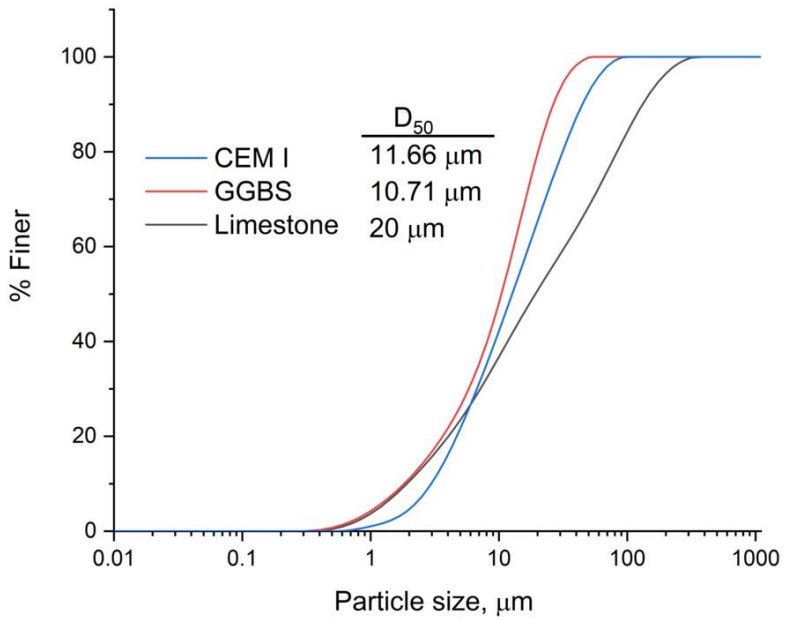

Figure 3- 1: Particle size analysis of cementitious materials determined by laser granulometry

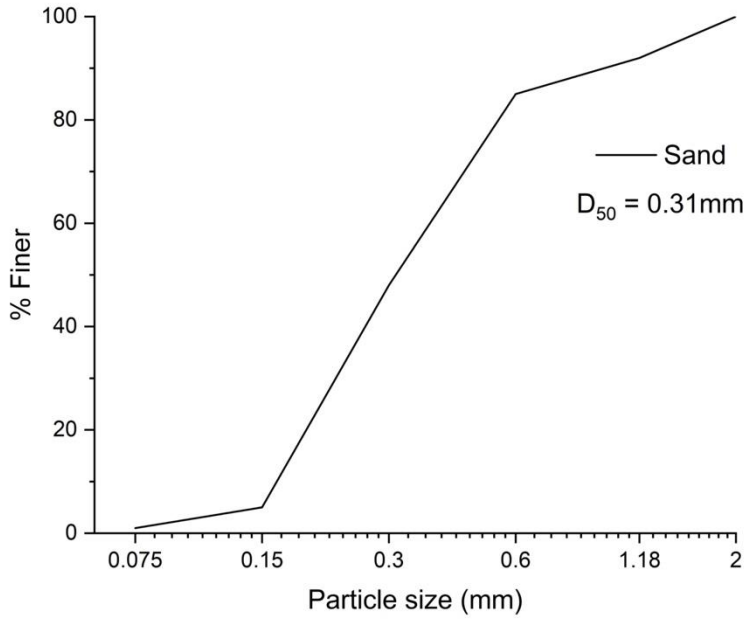

Figure 3- 2: Particle size analysis of fine aggregate (sand) determined by sieve analysis.

3.2 Methods

3.2.1 Calcining alum sludge

The as-received alum sludge had a moisture content of 402%. It was dried in an oven at 105^{o}C to constant mass, which took several weeks. The dried alum sludge was crushed manually using a pestle and mortar to about 2mm particle size then sieved through a 10mm sieve to check for any coarse or foreign particles. The dried sludge was placed in an electric furnace (Carbolite, UK), raising the temperature at a heating rate of 10^{o}C/min followed by a holding time of 2 hours at target temperature. As soon as the fixed dwell time was up, sample were removed from the furnace and allowed to cool at room temperature.

3.2.2 Grinding alum sludge

The raw sludge (i.e. dried and ground uncalcined sample) and calcined sludge samples were ground in a RETSCH vibratory disc mill RS 200 at 1300rpm for 5 minutes. These milling conditions were selected because laser diffraction analysis showed that further grinding did not result in considerable reduction in particle size.

3.2.3 Preparation of cement paste samples

Paste samples were prepared with a stock solution of SP and water, w/b of 0.55 and an SP dose of 1 wt% of binder. For each sample, 80g of powder was manually mixed with fluid in a 200 ml plastic cup for 3 minutes. The pastes were then poured in 8ml plastic vials in stages and vibrated at each stage to remove air pockets. The lids of the plastic containers were sealed with paraffin sheets and placed on a sample rotator at 9 rpm for approximately 24 hours to prevent bleeding. Thereafter, the samples were vacuum-sealed in plastic bags and placed in water baths to cure at 20^{o}C until test age.

XRD, FTIR and TG analyses were conducted on powder samples while disc samples were used for microstructural analysis. Meanwhile isothermal calorimetry and in-situ FTIR were performed on fresh cement pastes.

Before testing, pastes were hydration stopped by solvent exchange with isopropanol followed by washing with diethyl-ether [112,214]. The hydration-stopping regime was used on two sample sizes: 1.5mm discs and powder samples ground to ~1mm using a pestle and mortar. The powdered samples were immersed in isopropanol for 2 hours before filtering. The residue was subsequently washed in diethyl ether before drying at about 40^{o}C to ensure the complete removal of the diethyl ether. Similarly, 1.5mm discs were sliced from cured cement pastes using an Isomet precision cutter. The discs were immersed in isopropanol for 24 hours and subsequently rinsed with diethyl-ether and dried at about 40^{o}C. The hydration stopped samples were stored in plastic bags and stored in a vacuum desiccator over silica gel. All hydration stopped samples were tested within 24 hours.

For SEM analysis, 1.5mm discs were impregnated in epoxy-resin under vacuum. The face containing the cement disc was ground and polished with silicon carbide paper with #600, #1200 and #2500 grit sizes on a Struers Rotopol polisher. Fine polishing was subsequently conducted using diamond paste and cloths from 6 µm down to 0.25 µm. Polished samples were coated with ~10nm layer of carbon prior to SEM analysis.

3.2.4 Preparation of mortar samples

Mortar samples were prepared with a stock solution of SP and water, w/b of 0.55 and an SP dose of 1 wt% of binder. Mixing of mortars was carried out for 4

minutes using a Controls Automix automatic programmable mixer duration in accordance with BS EN 196-1 [213]. For compressive strength and sorptivity tests, the fresh mortars were cast in cubic 50mm moulds. For gas permeability test, the mortars were cast in cylindrical moulds with a height of 40mm and diameter 50 mm. The freshly cast samples were kept in moulds to harden for 24 hours at ambient laboratory temperature (20^{o}C). Following demoulding, samples were placed in a curing room at 95% relative humidity and 20^{o}C until test age.

3.2.5 Methods for characterization of raw materials and cement pastes

3.2.5.1 Particle size distribution by Laser diffraction

A Malvern Mastersizer 2000 was used for particle size analysis of all raw materials. The equipment uses laser diffraction to calculate and analyse the particle sizes of suspended solids. When particles are dispersed in a liquid, incident laser beams are scattered based on the refractive index of the particles. The software can be used to detect this fingerprint and calculate the particle size distribution of the particles. The suspended particles are dispersed by high frequency stirring at 3000rpm. Obscuration was kept at 8-10% with 10 measurements taken per sample and a pause time of 5 seconds between repeat measurements. These settings are as recommended elsewhere [20] and were maintained for consistency.

3.2.5.2 Density measurement

The alum sludge samples underwent mechanical and heat treatment, affecting their reactivity. Understanding the density of mineral additions is important in designing mortar and concrete mixtures. Material density was determined by gas pycnometry. In this method, the powder sample is place in a sample chamber of known internal volume and nitrogen gas is purged to pressurize the chamber. When equilibrium is reached, the nitrogen is released to a second chamber of known internal volume. Again, pressure equilibrium is reached in the system consisting of two chambers and a channel linking them. The internal volumes of the two chambers and equilibrium pressures enable the determination of the volume of the powder sample according to Lowell et al. [215]:

$$V = V_1 + \frac{V_2}{1 - \frac{P_1}{P_2}}$$

where V is the is the volume of the sample, V_1 and V_2 are the internal volumes of the empty first and second chambers respectively. P_1 and P_2 are the first and second equilibrium pressures reached respectively. The density of the sample can then be determined as the ratio of mass to volume.

3.2.5.3 Specific surface area and pore characteristics (BET method)

SCM particle fineness impacts the microstructural development of cement pastes. Although the air permeability method (Blaine) is commonly used to measure the specific surface area of cementitious materials, the method is inaccurate for porous materials like aluminas, pumice and zeolites which have large surface areas [216,217]. Thus, the surface area and porosity data of all raw materials were measured by the BET method [218] using a Micromeritics TriStar 3000 surface are and porosity analyser. The principle of the method is based on measuring the amount of adsorptive gas required to cover external and accessible internal pores of solid with a complete monolayer of adsorbate.

3.2.5.4 X-ray Fluorescence

The oxide compositions of sludge samples were determined by XRF spectroscopy using a Rigaku WDXRF Spectrometer. Fused bead samples were prepared with lithium tetraborate to ensure a homogenous sample for analysis.

3.2.5.5 Determination of total carbon

Total carbon in sludge samples was determined using LECO SC-444 carbon and sulfur analyzer. The procedure [219] involved weighing samples and soaking in 10% HCl to dissolve inorganics for 24 hours. The HCl was then washed off, dried and analysed using the LECO carbon and sulfur analyser.

3.2.5.6 Thermal analysis

Thermogravimetric analysis (TGA) measures the mass change of a sample with increasing temperature. Differentiation of the TG (DTG) curve allows a better resolution and identification of successive mass changes. Since phase changes could take place without a mass loss, Differential Scanning Calorimetry (DSC) compares the variation in sample temperature with that of a reference empty crucible during analysis. The heat flow of a sample varies directly with its specific heat [220] so a comparison with a reference empty crucible can detect reactions occurring associated with variation in specific heat which cannot be spotted by mass changes on just TGA. Another method that is similar to the DSC, is DTA. During DTA the sample and an inert reference are simultaneously heated; however thermal reactions cause a difference between the temperatures of the sample and inert reference. TGA-DSC and DTA provide information about the decomposition behavior of minerals and hydrates.

Thermal analysis is relevant to cement science because minerals and cement hydrates undergo many thermal reactions including dehydration, dehydroxylation, decarbonation, phase transition and sintering. The temperature at which these processes take place are generally characteristic for a particular mineral or cement hydrate. Bhatty [221] and Collier [222] provide a comprehensive literature review showing the characteristic temperatures at which specific cementitious phases decompose.

As the sample is heated, the water-bearing phases including C-S-H, ettringite and AFm decompose first. Ettringite decomposes around 100-150^{o}C with AFm phases decomposing within this temperature range. Calcium hydroxide decomposes between 420^{o}C and 550^{o}C and decarbonation of carbonates occurs between 600 ^{o}C and 800^{o}C, releasing CO_2. The bound water content defined as the mass loss between 50^{o}C and 550^{o}C, along with the portlandite (CH) and residual carbonate (CC) contents were measured on hydration-stopped paste samples by TGA using a NETZCH STA 449 series under nitrogen atmosphere. 25-30 mg was weighed into a platinum crucible and heated from 20^{o}C to 1000^{o}C at a constant rate of 20^{o}C/min.

The CH and residual carbonate contents were determined by the tangent method (Figure 3-3). The data was normalized to the ignited mass at 550^{o}C, effectively reporting data to 100 g of anhydrous solid material. In pastes containing no additional limestone powder, a correction to the portlandite content was made to account for the

amount of carbonated CH which can be detected in the decarbonation process between 600 and 900ºC [89]. The CH, CC and W_n contents were calculated by:

$$CH = \Delta CH * \left(\frac{M_{Ca(OH)_2}}{M_{H_2O}}\right)$$

$$CH_{total} = \Delta CH * \left(\frac{M_{Ca(OH)_2}}{M_{H_2O}}\right) + \Delta CC * \left(\frac{M_{Ca(OH)_2}}{M_{CO_2}}\right)$$

$$CC = \Delta CC * \left(\frac{M_{CaCO_3}}{M_{CO_2}}\right) * 100$$

$$W_n = \frac{W_{50} - W_{550}}{w_{550^oC}} * 100$$

Where:

ΔCH - mass loss due dehydration of portlandite

ΔCC - mass loss due to decarbonation of calcite

$M_{Ca(OH)2}$ molar mass of CH, 74g/mol

M_{H_2O} – molar mass of water, 18g/mol

M_{CaCO_3} – molar mass of CC, 100g/mol

M_{CO_2} – molar mass of CO_2, 44g/mol

W_{50} – mass loss at 50ºC

W_{550} – mass loss at 550ºC

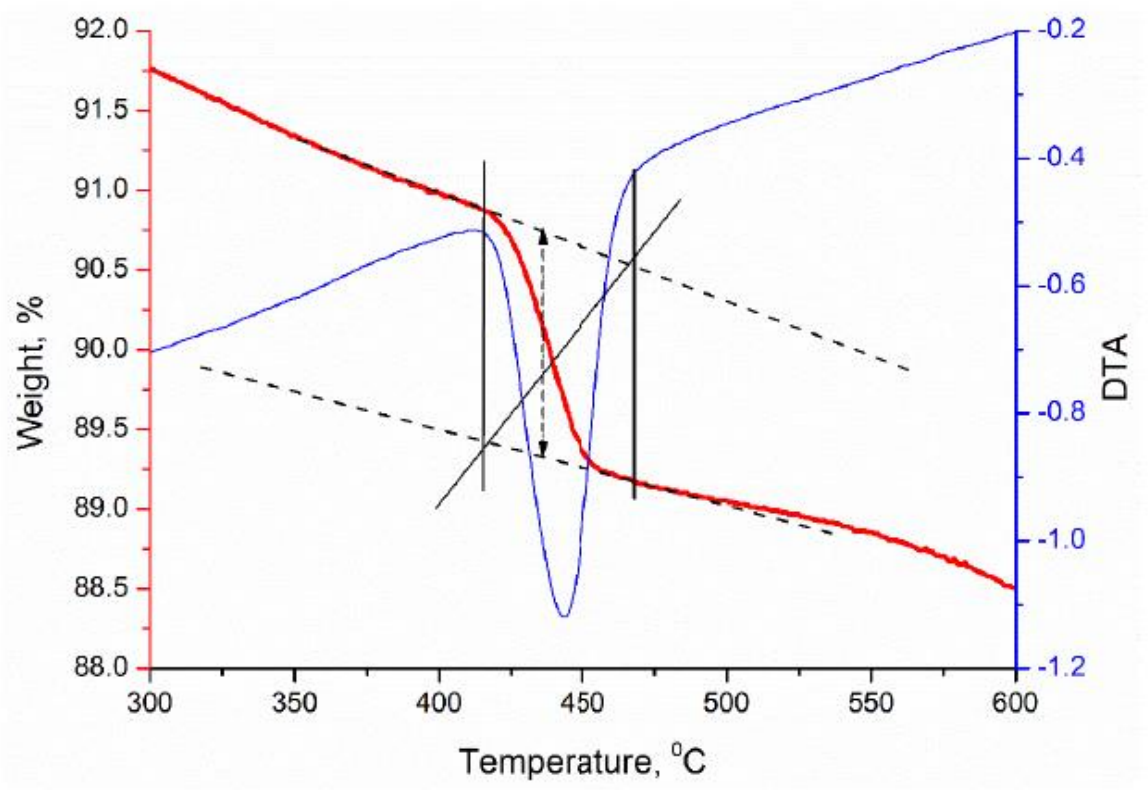

Figure 3- 3: Quantification of CH by tangent method [212].

TG-DTA analysis was also used to investigate the decomposition of dried raw alum sludge. The peaks and inflections on the curves which are indicative of thermal reactions, were used to inform the selection of calcination temperatures for further analysis. TG data can be used with other complementary techniques (XRD, FTIR) to characterize types of minerals and their relative amounts within a sample.

3.2.5.7 Scanning Electron Microscopy (SEM)

In SEM, a beam of electrons is fired at a sample which interacts with atoms in the sample, producing information about surface topography and composition. The electrons interact with atoms of a sample to produce secondary electrons, backscattered electrons or X-rays.

Secondary electrons released from the sample have a lower energy which enables the collection of a topographic image of a sample. On the other hand, backscattered electrons are reflected from the sample surface by elastic scattering and their number is controlled by the atomic mass of the sample. As atomic number

rises, more electrons are reflected producing a brighter image. This allows the phases present in a sample to be distinguished according to grey scale.

SEM characterisation was performed to understand the physical performance and the microstructure of sludge powders, as well as hydrated cement pastes, using a Carl Zeiss EVO MA15.

Morphological analysis of raw and calcined alum sludge was conducted on powder samples dispersed onto adhesive carbon pads and carbon coated prior to microscopic investigation using a secondary electron detector and a 10 keV accelerating voltage.

The hydration of slag and clinker were quantified by BSE image analysis. 1.5mm cement paste discs were prepared and analysed in backscattered electron mode. 25 BSE images were randomly collected per sample at a 800x magnification, 20KeV accelerating voltage and a working distance of ~8.5mm. Scrivener et al. [223] suggested 10-20 images were adequate for reasonable statistical accuracy. The BSE images were analysed using ImageJ software. This method involved correcting for brightness and contrast, applying a median filter, smoothening features and removal of noise [86,212]. Anhydrous cement and slag as well as porosity were segmented by applying a threshold according to the grey level histogram as shown in Figure 3-4. The slag used had a composition and density that produced a grey level matching that of CH, which does not allow the discrimination of the two phases according to grey levels. As a result, slag was segmented on the basis of their chemical signature using EDS mappings of magnesium in addition to grey level. The procedure for quantifying anhydrous slag was as published previously [212]. The slag and CH areas of the grey-level were thresholded, converted to a binary image and then inverted so that only the thresholded region was visible. This was overlaid with a Mg map to isolate the slag grains as slag contained significant amount of immobile magnesium while CH does not. This process is illustrated in Figure 3-5. The sludge grains were visible, but it was not possible to quantify the residual sludge grains because of the high proportion of fine particles which will bring more errors due to a lower limit of resolution of the EDX detector (1–2 μm). Also, isolating the unreacted sludge grains could not be done because its grey-levels overlapped with that of C-S-H.

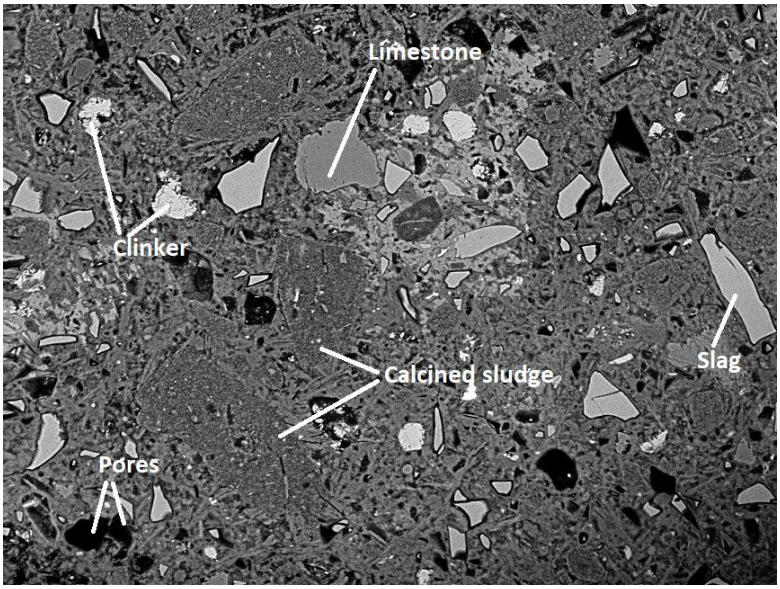

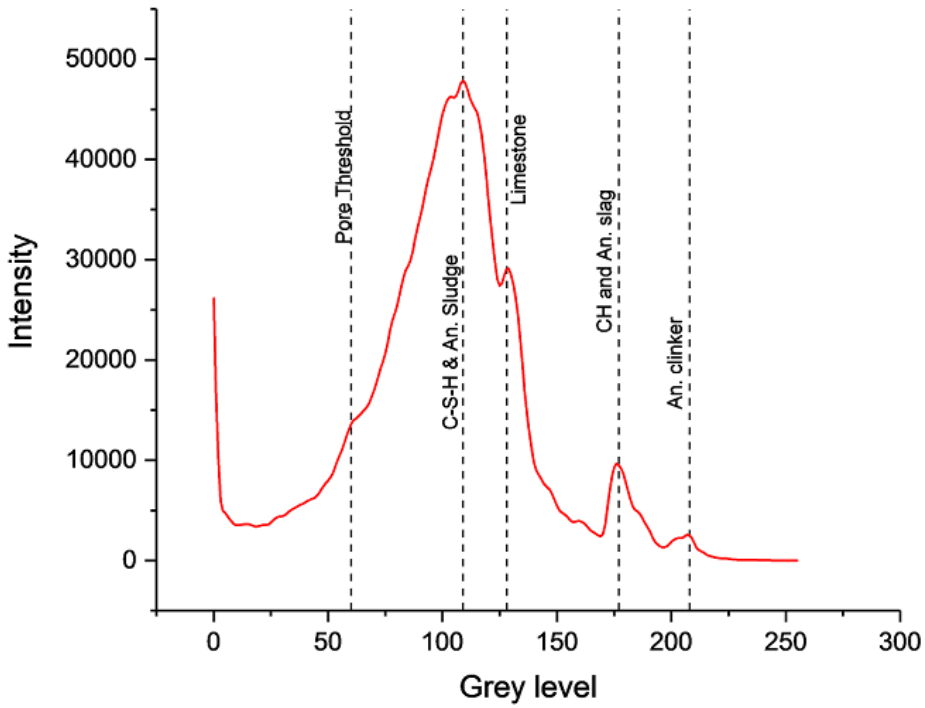

Figure 3- 4: SEM micrograph of cement-calcined sludge-slag-limestone paste at 28 days with corresponding grey level histogram

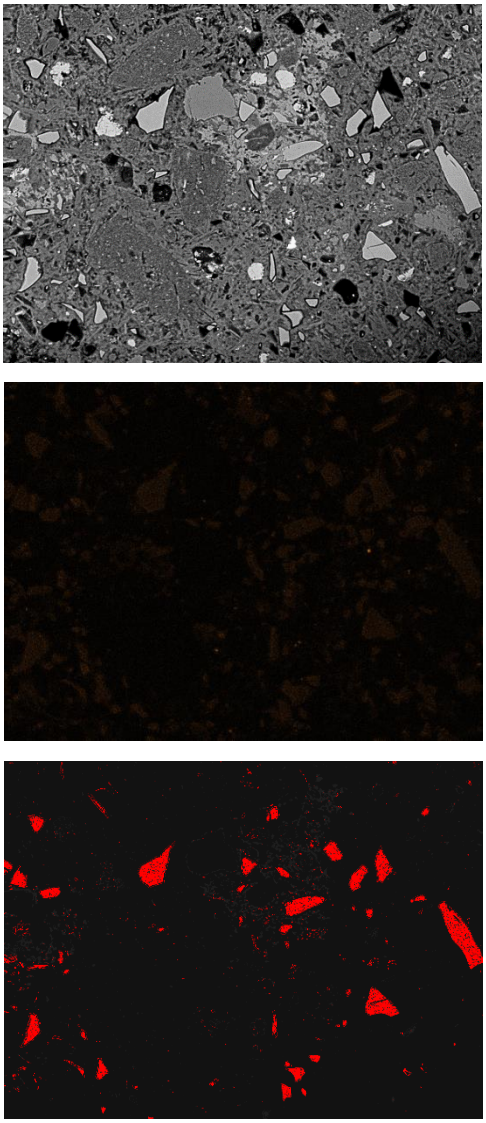

Figure 3- 5: Quantification of anhydrous slag grains using BSE image analysis combined with EDX mapping on cement-slag limestone-calcined sludge paste at 28 days.

The volume fractions of anhydrous materials (t=0) in a mix can be calculated from the densities (ρ) and mass (m) [212]:

$$V_{y,0} = \frac{\frac{m_{y,0}}{\rho_{y,0}}}{\frac{m_{CEMI,0}}{\rho_{CEM\ I,0}} + \frac{m_{slag,0}}{\rho_{slag,0}} + \frac{m_{Limestone,0}}{\rho_{limestone,0}} + \frac{m_{Sludge,0}}{\rho_{sludge,0}} + \frac{m_{water,0}}{\rho_{water,0}}}$$

Where $V_{y,0}$ is volume fraction of a constituent material y at time t = 0, $m_{y,0}$ is the mass fraction of constituent y at time t = 0, $\rho_{y,0}$ is density of constituent y at time t = 0,

Using the stereographic assumption that converts area fraction to volume fraction [86,224], the measured area fractions of anhydrous material are used to calculate the degree of hydration of slag and clinker [212]:

$$\rho^{CEM\ I} = 1 - \frac{V_{t(CEM\ I)}}{V_{y,0\ (CEM\ I)}} * 100\%$$

$$\rho^{slag} = 1 - \frac{V_{t,(slag)}}{V_{y,0\ (slag)}} * 100\%$$

Where $\rho^{CEM\ I}$ and ρ^{slag} are the degrees of hydration of CEM I and slag respectively.

A high-resolution SEM image that covers the size range of relevant features is an important prerequisite for accurate quantification by image analysis. However, the drawback of SEM-IA is its size range limitation and this could bring two difficulties [225]: Firstly, the ability to resolve the smallest features, and secondly, the size of field of view necessary for a statistically valid representation of the microstructure. Generally, the higher the pixel size, the more accurate is the boundary detection when quantifying a feature. The shape and size of small features can be more accurately resolved by simply increasing the magnification. However, it will result in a smaller field of view and hence large number of images are needed to obtain statistical significance. A small field of view will also limit the size of the features that can quantified accurately, irrespective of the number of processed images. If a high amount of small features are present, a higher resolution may be needed for accurate quantification. Thus, the selected magnification (800x) is a trade-off between resolution of the phases and the need for representative image analyses by the acquisition of fewer images. Moreover, the acquisition of EDX Mg maps for the segmentation of slag grains is time-consuming.

The probe size and electron-solid interaction volume are parameters that affect the attainable resolutions for bulk materials [226]. Monte Carlo Simulations [227] demonstrated that measurement errors due to finite pixel size are not significant for features larger the 1μm but the error is higher for smaller features and become significant (>50%) when the features are smaller than the electron probe size. Small features were also found to be mainly noise generated from image capture and segmentation. These errors can be reduced by using a size filter that excludes features smaller than 10 pixels.

Atomic number is the main factor determining the grey level contrast in BSE images [228]. Cementitious materials mainly consist of light elements so the electron -solid interaction volume is large [229]. Because interaction volume increases with electron voltage, they should both be minimised for increased resolution and also to reduce the energy of the electron beam which can damage the sample [230]. However, low voltages will mean that electrons only come from near the surface and the quality of the surface is affected by polishing defects and carbon coating. Thus, the selected accelerating voltage (20kV) is a compromise between reducing the size of the interaction volume while giving a high enough intensity of electrons [229].

Considering the above factors, the settings used (800X magnification, 20KV) represent a good compromise for obtaining a decent sampling area and high resolution to discriminate the phases of interest.

To follow changes in C-S-H composition, EDS point analysis was conducted from about 100 points per sample. The main limitation of SEM-EDS analysis is the intermixing of analysed phases. This study adopts a method similar to Deschner et al. [112] where Al/Ca and Si/Ca atomic ratios were plotted to better identify the C-S-H composition and to exclude intermixed phases. The Al/Si ratios were taken as the slope of the line drawn from the origin through the points with the lowest measured Al/Ca ratio. While Deschner et al. [112] defined the cloud of data points along this line as the range of Ca/Si ratios in a sample, this study reports the right edge of the cloud of data points as the Ca/Si, corresponding to the least intermixed C-S-H [92]. Furthermore, Deschner et al. [112] chose a beam voltage of 10kV to reduce the interaction volume and hence, the intermixing of analysed phases. In contrast, a 20kV voltage was used in this study to give enough intensity of electrons thereby discounting for defects on sample surface due to the polishing process. Because the higher voltage used will result in a larger interaction volume and intermixing of phases, the right-hand edge of the cloud of data points was used in this study to more accurately represent C-S-H composition rather than the bulk of EDS data points. The selected voltage falls within the range commonly used to study polished sections [229,230]. In addition, only inner product areas were examined in this study to minimise intermixing with other phases present in the microstructure. Similar composition could be acquired from outer product areas, but the higher intermixing of phases makes the determination of C-S-H composition less reliable.

To avoid the problem of intermixing, the high-resolution technique Transmission Electron Microscopy (TEM) is an alternative method. TEM samples are thinned to about 100-150 nm which limits the size of the interaction volume thereby limiting the intermixing of analysed phases [230]. However, this benefit is outweighed by the difficulty, time, and cost of specimen preparation.

3.2.5.8 X-ray Diffraction

X-ray diffraction is an analytical technique that allows the identification and compositional examination of the crystal structures of a material. When an X-ray beam hits a sample, the crystal structure of the sample diffracts incident X-ray beams over a range of angles with different intensities, from which the electron density of a sample can be derived and used to define their unique composition by application of the Bragg's law:

$\eta\lambda = 2d \sin \theta$

where:

η is an integer value, known as order of reflection

λ is the wavelength of the X-ray beam

d is the characteristic spacing between lattice planes

θ is the angle of incident of X-ray beam relative to the sample.

Anhydrous and hydrated cement consist of a number of crystalline or poorly crystalline phases which can be identified by XRD and used to understand hydration. However, the poorly crystalline phases appear as broad humps on an XRD pattern, with no well-defined peaks. In recent times, Rietveld refinement has gained prominence as method of quantifying phase composition and determining the amorphous content with multi-blended cement systems.

3.2.5.8.1 Principle of Rietveld Method

Rietveld refinement [231] is a method of analysing XRD data allowing phase quantification. The principle of Rietveld refinement is to iteratively compare the observed diffraction pattern obtained experimentally with a pattern simulated based on refined models of the crystal structures. Crystal parameters and equipment

parameters are refined to minimise the difference between the observed and calculated patterns by least squares. The intensity at a certain point *i* can be a combination of many Bragg reflections. The calculated intensities y_{ci} are determined from structural factor F_k by the adding the calculated contributions of the background and all neighbouring Bragg reflections. The model accounts for different factors including structure factor, profile function and preferred orientation.

$$y_{ci} = s\sum_{k} L_k \left|F_k\right|^2 \varphi(2\theta_i - 2\theta_k) P_k A - y_{bi}$$

Where:

s – scale factor

k – Miller indices for a Bragg reflection

L_k – Lorentz, polarization, and multiplicity factors,

φ – profile function

P_k – Preferred orientation function

A – absorption factor

F_k – structure factor

y_{bi} – background intensity

In this study, the cement phases present were identified using the X'Pert Highscore program with reference crystal structures collected from the Inorganic Crystal Structure Database (ICSD). The appropriate crystal structures were verified based on the attainment of good fit to the available experimental data. Phase dependent parameters that were refined are scale factors, lattice parameters and peak profile function. The refined global parameters were background function and displacement error. In complex systems such as cements, it is recommended that refinement of crystal structure parameters such as atomic positions and displacement factors should be avoided [229]. The parameters that were specifically considered in this work are discussed in the following sections.

3.2.5.8.2 Structure Factor F_k

The calculation of structure factor F_k requires knowledge of the crystal structures of all phases of interest. Accordingly, the lattice parameters which define the unit cell of each crystal structure are refined while the atomic coordinates and isotropic thermal displacement parameter were kept fixed [229]. To limit parameter

variation and avoid parameter drift, constraints were assigned on the variation intervals: for lattice parameters 1% variation from literature values was allowed.

3.2.5.8.3 Profile function

The profile function models the peak shape of the crystalline phases considering instrumental and sample effects [229]. To model the profile function to best fit the experimental data, the pseudo-Voigt function was used defined as a combination of the Lorentzian and Gaussian functions:

$$pV = hL + (1 - h)G$$

Where:
h = mixing parameter, kept constant at 0.6 [231]
L = Lorentzian term
G = Gaussian term
The width *H* of the peaks was also refined using the function described by Caglioti et al. [232]:

$$H^2 = Utan^2\theta + Vtan\theta + W$$

The refinement of the profile W parameter is adequate to model the peak profile. The simultaneous refinement of the U, W and V profile parameters usually leads to errors in the quantification of the phase of interest. As a result, the U and V parameters are kept fixed =0 and only W was refined for selected phases [229].

3.2.5.8.4 Preferred Orientation

When powder samples are loaded into a sample holder, certain phases become preferentially oriented parallel to the sample surface due to crystal morphology. This behaviour leads to a change in the intensities of the diffracted lines along crystallographic planes. This effect can be reduced through the avoidance of strong pressure on the sample during sample preparation [229]. Alite, portlandite and calcium sulfate phases are prone to preferred orientation. It is best to avoid preferred

orientation in the first place, but can partially counteracted by using the March- Dollase model [233] during refinement:

$$P_k = ({P_1}^2 cos^2 a_k + {P_1}^2 sin^2 a_k)^{-\frac{3}{2}}$$

Where:

P_1 – Refinable parameter (where a value of 1, indicates no preferred orientation)

a_k – Angle between preferred orientation direction and the normal to crystallite

3.2.5.8.5 Determination of Background

Backgrounds can either be manually fitted or modelled. In the Highscore Plus software, backgrounds can be manually fitted by either selecting points or using the Sonneveld & Visser algorithm [234] where the granularity and bending factors are adjusted as required. Modelled backgrounds using the polynomial function can also be used but do not account for the amorphous hump of C-S-H in hydrated cement samples [89,92]. In addition, Bruker D8 machines have been observed to produce patterns with artifacts and elevated backgrounds at low angles resulting from scattering from the sample mount [235]. As a result, Rietveld analysis finds it difficult to model these low angle artifacts so the lowest angle data are usually excluded from refinement [235,236].

The choice of background is illustrated in figure 3-6. To account for C-S-H contribution and reduce the effect of low angle artifacts, a manual background was adopted. A manual fitting of the background has the advantage of being flexible. However, it is recognized that a manual fitting of the background depends strongly on operator-based decisions and may lead to errors as background levels may be taken too high into the C-S-H leading to an overestimation of the C-S-H contribution to amorphous phases. Advances in XRD suggests the use of the so-called partial or no known crystal structure PONKCS method to model amorphous phases.

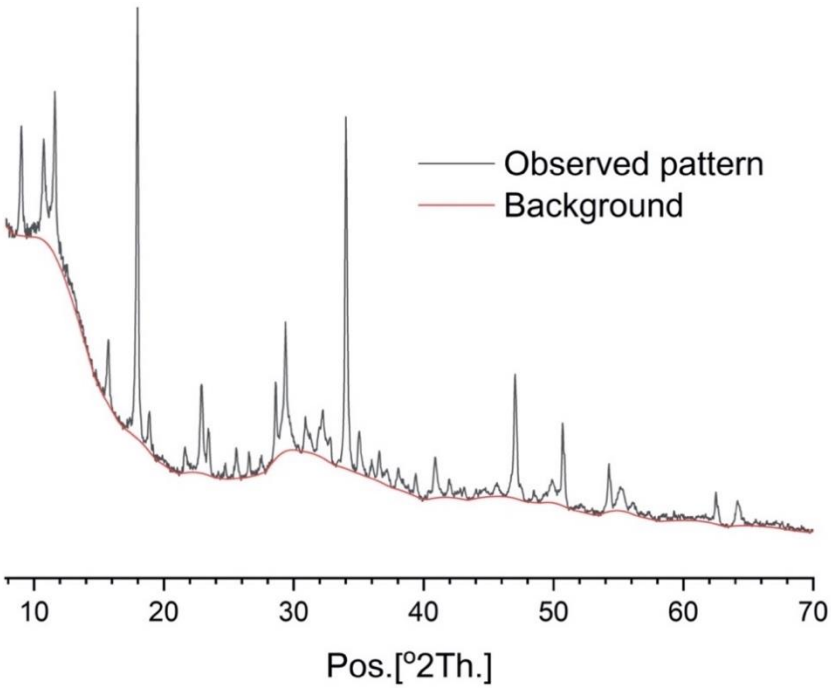

Figure 3- 6: Determination of Background in in calcined sludge cement paste containing 13.3% sludge and 6.7% limestone

3.2.5.8.6 Development of Control file

To ease refinement, the crystal structure models identified in anhydrous cement are imported or entered in a so-called control file that acts as input initial model for the Rietveld QPA. Refinement of phase dependent parameters (scale factors, unit cell parameters, peak shape parameters and preferred orientation parameters) was first conducted on the main clinker phases (C_3S, C_2S, C_3A, C_4AF) using the appropriate crystal structures selected based on the attainment of best fit to the available experimental data. To limit parameter variation and avoid parameter drift, constraints were assigned on the variation intervals: for lattice parameters 1% variation from literature values was allowed [229]. The refined clinker phases were then combined with other minor phases present in the anhydrous cement (sulfates, calcite and lime) and then refined. The experimental and calculated patterns for the anhydrous CEM I 52.5R is shown in Figure 3-7.

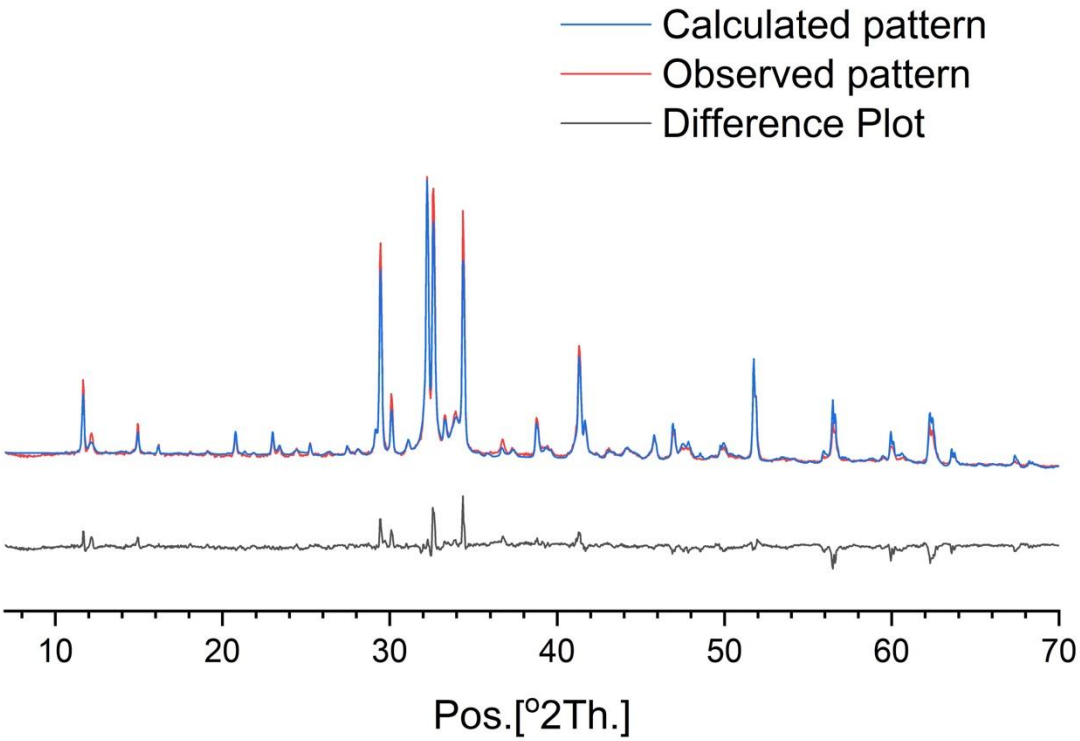

Figure 3- 7: Rietveld refinement of anhydrous CEM I 52.5R showing the experimental data, the calculated pattern and the difference plot

Table 3- 4: Summary of the main refined parameters

Phase	Crystal structure	ICSD code	S.F	Unit Cell						P.O	W
				a	b	c	α	β	γ		
Alite	Monoclinic	64759	×	×	×	×		×		×	×
Belite	Monoclinic (b)	79550	×	×	×	×		×			
Aluminate	Cubic	1841	×	×	×	×					
Aluminate	Orthorombic	1880	×	×	×	×					
Ferrite	Orthorombic	51265	×	×	×	×		×			×
Gypsum	Monoclinic	409581	×	×	×	×				×	
Calcite	Trigonal	166364	×	×	×	×					
Portlandite	Monoclinic	15471	×	×	×	×		×		×	
Lime	cubic	75786	×	×	×	×					
Ettringite	Hexagonal	155395	×	×	×	×				×	×
Monosulfoaluminate	Trigonal	100138	×	×	×	×					
Hemicarboaluminate	Trigonal	263124	×	×	×	×					
Monocarboaluminate	Triclinic	59327	×	×	×	×	×	×	×		
Hydrotalcite	Monoclinic	81963	×	×	×	×					
Calcite	Trigonal	166364	×	×	×	×				×	
Corundum	Rhombohedral	73725	×	×	×	×					

For hydrated systems, crystalline hydration products: ettringite, hemi and mono-carboaluminate, hydrotalcite and calcium hydroxide were identified and refined. Hydrotalcite is mostly amorphous which made refinement difficult. As a result, the

refinement of this phase was imperfect such that only the best visual fit was reached. Table 3-4 shows the crystal structures identified in anhydrous clinker and hydrated cement mixtures. The crystal structures were taken from the ICSD database.

3.2.5.8.7 Phase quantification

The values calculated by traditional Rietveld refinement is given as 100% of crystalline phases by weight, not accounting the amorphous phases. However, hydrated cement phases and systems incorporating amorphous SCMs require an alternative approach to account for these X-ray silent phases. The external standard method or G-factor method has been used to quantify cement systems [88,237] and has the advantage that the sample does not need to be intermixed with an internal standard, thus avoiding sample preparation and homogenisation issues. By comparing the scale factor determined for a sample to that of standard reference (corundum, α-Al_2O_3) both measured under exactly the same experimental conditions, the true contents of the crystalline phases can be calculated by the following equation:

$$C_j = S_j \frac{r_j {v_j}^2 m}{G} = \frac{S_j r_j {v_j}^2 m}{S_c \frac{r_c {v_c}^2 m_c}{C_c}}$$

Where:
S_j – scale factor of phase j
r_j – density of phase j
v_j – volume of phase j
m - mass attenuation coefficient of sample
G – calibration factor determined from the standard
S_c– scale factor of corundum
r_c – density of corundum
v_c – volume of corundum
m_c- mass attenuation coefficient of corundum
C_c – mass fraction of corundum

The mass attenuation coefficient (MAC) of a sample is calculated from the oxide composition of the raw materials as measured by XRF and is simple the sum of weighted MAC of the individual oxides. MAC values for each oxide can be found in the International Tables for Crystallography. For hydrated systems, the water content is accounted for in the MAC calculation.

3.2.5.8.8 Measuring the degree of hydration clinker

The clinker phases in cement are crystalline and their dissolution can be followed by quantifying their residual contents at different curing ages. The degree of hydration of a clinker phase can be determined by:

$$DoH_{clinker} = \left(\frac{M_{clinker,t=0} - M_{clinker,t=t}}{M_{clinker,t=0}}\right) * 100$$

$DoH_{clinker}$ – degree of hydration of the clinker

$M_{clinker,t=0}$ – Mass fraction of anhydrous clinker

$M_{clinker,t=t}$ – Mass fraction of clinker at time *t*

3.2.5.8.9 Experimental Setup

In this work, phase identification and Rietveld quantitative phase analysis (QPA) was conducted using the X'Pert Highscore Plus software. The quantification of X-ray amorphous phase content was conducted using the external standard method [238] with corundum (Al_2O_3) as the external standard. All structure models were taken from the ICSD library for Rietveld refinement. XRD data were collected using an XRD Bruker D8 phaser machine equipped with Cuk_α X-ray source and Vantec detector operating at a voltage of 40 kV and current of 40 mA. The samples were scanned in the range 5-70° 2θ at a step size of 0.0330° with a complete analysis taking 50 minutes per sample. The ground powders were backloaded manually into a standard circular 16mm diameter sample holder by gently pressing unto a frosted glass side to minimize preferred orientation.

3.2.5.9 Fourier Transform infrared spectroscopy (FTIR)

FTIR analysis is used to measure the variation in the intensities of electromagnetic radiation that is transmitted through a material. The atoms of a material absorb electromagnetic radiation at unique frequencies corresponding to the frequency of vibrations between atomic bonds. Scanning a range of wavenumbers in an infrared spectrum enables identification of functional groups within a material. FTIR generates a molecular fingerprint of samples, whether solid, liquid or gas, which makes it ideal for studying the cement systems.

In ATR (attenuated total reflection) FTIR, the infrared radiation is fired through a crystal or internal reflection element (IRE). The IR radiation interacts with the sample

through an evanescent wave that penetrates a few microns into the sample. The penetration depth of the evanescent wave is directly proportional to the wavelength, which means that lower wave numbers would have higher absorption. The IR beam interacts with the sample where light of different frequencies is absorbed depending on the molecules present in the sample and a detector records the signals. The IRE must have a higher refractive index than higher than the sample to achieve total internal reflection. A diamond IRE is ideal because it has chemical and mechanical durability, making it ideal for studying hard and alkaline cement samples.

The phase identification of sludge and cement paste samples were conducted using a Perkin Elmer ATR-FTIR spectrometer; the IR spectra were recorded over the region 400-4000 cm^{-1} with a resolution of $4cm^{-1}$. The sludges and dried cement paste powders were prepared and just enough sample was placed on the diamond crystal (IRE) to cover it. The pressure shoe was locked directly against the IRE/sample area by applying a force to the sample. Obtaining good quality spectra is dependent on maintaining good contact between the sample and the IRE. This was facilitated by ensuring the samples were ground to sufficient fineness [239]. The measured IR spectra were the average of 32 scans; a background spectrum with no sample was collected before running samples.

In-situ ATR measurements of fresh cement pastes were conducted to obtain the time resolved determination of the phase composition in hardening cement pastes. A cylindrical steel sample holder that just covers the diamond crystal and allows the pressure shoe to reach the sample was used. This is necessary because if sufficient pressure is not applied to the sample, the contact between the sample and the crystal reduces as the cement hardens. This will lead to the measurement of lower absorption, making it difficult to compare different hydration times. Immediately after mixing, spectra were collected every 2 minutes for the first hour and then every 10 minutes for another hour.

3.2.5.10 Isothermal calorimetry

The exothermic nature of cement hydration allows the kinetics of reaction to be followed by isothermal conduction calorimetry. In this technique, the heat evolution rate and the total heat released is measured alongside a reference material. The purpose of the reference is to minimise noise and drift which could arise from external

factors. Hence it is necessary that the sample and reference material have similar thermal properties [92]. As cement has a specific heat capacity of 0.75 $J.g^{-1}$. K^{-1}, quartz with a specific heat of 0.8 $J.g^{-1}.K^{-1}$ is a suitable reference material for analysis.

In this study, the heat released during cement hydration was measured using a TAM-air 8 twin channel calorimeter (Figure 3-8). 6g of binder was placed in a 20mL ampoule and mixed with 3g water and 0.06 of SP using an orbital shaker for 2 minutes. The ampoules were then placed in the sample channel with a similar quartz paste in the reference channel at 20^{o}C.

The heat contribution of calcined sludge can be distinguished from that of cement by replacing the sludge fraction in the mix with unreactive quartz. To extract the contribution of calcined sludge, the total heat was normalised to the clinker content as shown in Figure 3-9. The change in heat between the plain and quartz paste is due to the filler effect while the difference in heat between the quartz and calcined sludge pastes is attributed to the reaction of the calcined sludge.

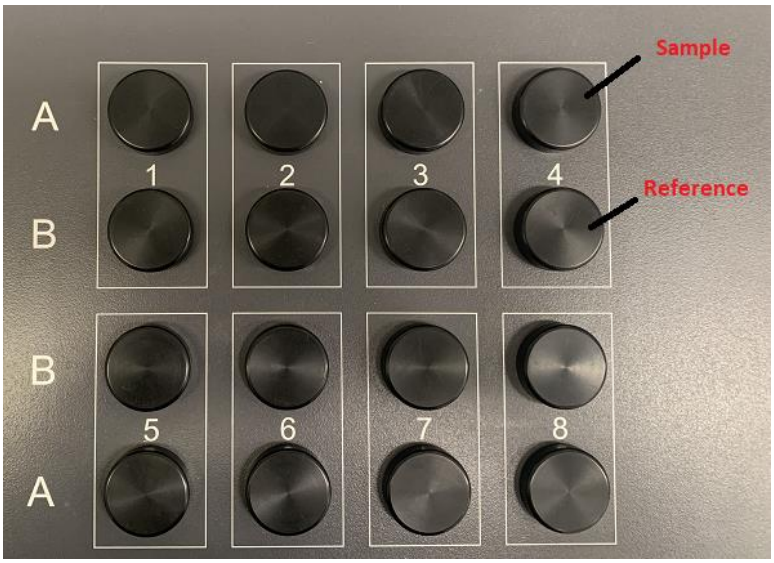

Figure 3- 8: Experimental setup for Isothermal calorimetry

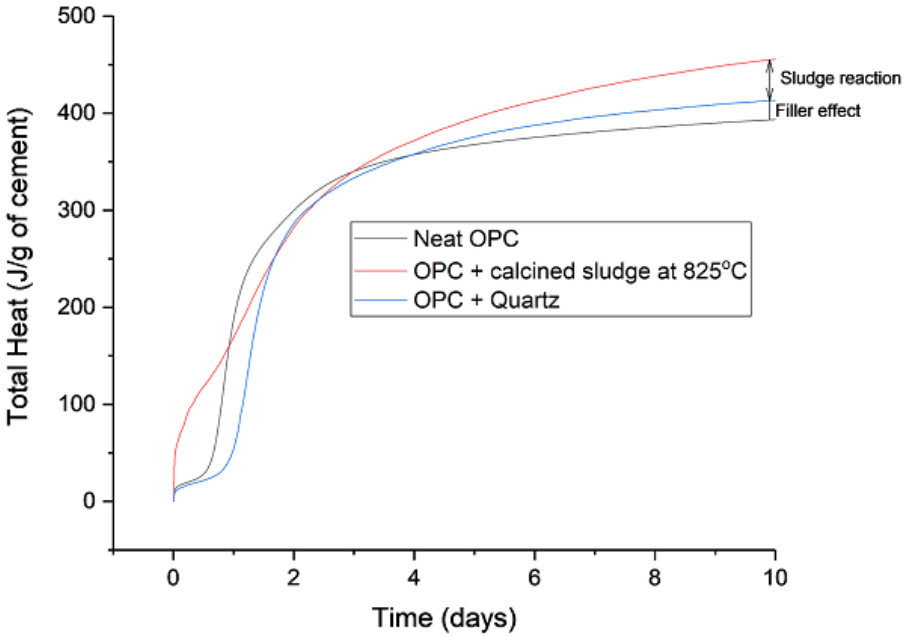

Figure 3- 9: Illustration of filler effects and hydration of calcined sludge

3.2.6 Methods for evaluating engineering performance

3.2.6.1 Workability

The workability of fresh mortar was evaluated by BS EN 1015-3 [240]. The test involves filling a conical mould of specified size with fresh mortar, removing the mould and then jolting the cone of fresh material 15 times within about 15 seconds. The spread of the mortar mix due to the drop action is measured with callipers in 3 directions and the average measurement is reported as the flow table spread in mm. Due to the high-water adsorption on the calcined sludge particles, the workability of calcined sludge-cement mixtures is far lower than neat Portland cement. To compensate for the loss in workability, a polycarboxylate superplasticiser (Sika Viscocrete 25MP) was used in cement and paste mixtures. By varying the w/c ratio and SP content, several trial cement mixes were prepared incorporating the sludge with the highest water adsorption (825^{o}C), until adequate workability was reached (similar to a standard mortar mix with a flow of 16 ± 2 cm). Based on this, the adopted parameters are a w/b of 0.55 and an SP content 1% by weight of binder. These parameters were kept constant for the preparation of all paste and mortar mixes in this study.

3.2.6.2 Compressive strength

Compressive strength of 50mm cubic specimens were determined in accordance with ASTM 109 [241] using a 3000KN ToniPACT compression machine equipped with a motorized Servicon digital control. The compressive strength values were calculated as the average of three cubes for each test age.

The strength activity indices (SAI) of all blended cements were determined according to ASTM C311 [242] to evaluate the field performance of sludge-blended cement mixtures. The calculation of SAI is as follows:

$$SAI = \frac{\mathrm{A}}{\mathrm{B}} * 100$$

Where: A is the average compressive strength of blended mortar (MPa), B is the average compressive strength of control sample (MPa).

3.2.6.3 Gas permeability

Permeability is an important durability property that controls the extent to which destructive materials such as chloride or sulfate ions or carbon dioxide migrate through cement-based materials. Several arrangements have been developed to assess the rate at which liquids and gases migrate through mortars and concretes by the application of steady pressure through a specimen in a tri-axial pressure cell with unidirectional flow [137,243–245].

Cylindrical mortar samples (50 ± 2mm in diameter and 40 ± 2mm in height) were cast in triplicate in plastic moulds, demoulded after 24 hours and then cured in a curing room at 95% relative humidity and 20^{o}C for 28 days. Samples were oven dried at 40^{o}C until constant weight, i.e when the mass change was less than 0.2 % within 2 hours [246]. Cabrera & Lynsdale [244] reported that insufficient drying results in residual water being in the pore system which can block the passage of gas thereby reducing permeability. The top and bottom surfaces of the samples were ground using silicon carbide paper to expose the internal pore structure. This ensured consistency across all samples and prevented any surface features from affecting the accuracy of results.

The gas permeability test was conducted using the Leeds permeability cell shown in Figure 3-10 [244]. The samples (S) were weighed and measured using Vernier callipers and then placed inside a rubber sleeve (A), leaving only the top and bottom sample surfaces exposed. This was then enclosed in the plastic sleeve (B);

and placed in the Leeds cell (L) with the O ring (C) placed over the sample. The Leeds cell was firmly sealed by screwing the cell lid (D). This setup ensured unidirectional gas flow through the specimen. Nitrogen gas at constant pressure was then forced through the sample and the gas flow rate was measured using a bubble flow meter. Time was allowed for the gas flow through the sample to stabilize before taking final readings. This took about 20 minutes. Three samples were tested at five pressures: 0.4, 1, 1.4, and 2.4 bar. Intrinsic permeability determined using the modified Darcy equation:

$$K = \frac{2P_{out}\upsilon L\acute{\eta}}{\mathrm{A}(P_{in}^2 - P_{out}^2)}$$

Where:

P_{in} is the inlet pressure (bar)

P_{out} is the pressure at which the flow rate is measured (atmospheric, 1.01325 bar)

υ is the flow rate, measured in cm^3/s

L is the length of the sample in meters

ή is the viscosity of nitrogen gas at ambient temperature ($1.756 * 10^{-6}$ at room temperature)

A is the cross-sectional area of the specimen in m^2

P_{in} is the inlet pressure (bar)

Due to gas slippage, it is erroneous to calculate the intrinsic permeability as the mean of the calculated values of *K* at the different inlet pressures. Therefore, a method described in literature [245] was used to correct the calculated values of permeability. Using regression analysis, the relationship between gas permeability and inverse of mean pressure ($1/P_m$ where $P_m = (P_{in} + P_{out})/2$) was determined. The coefficient b of the resultant equation $K = a\ (l/P_m) + b$ gives the correct value for gas intrinsic permeability of the sample (K_g). *b* is the y-intercept of the linear regression fit of gas permeability at different inlet pressures and inverse of mean pressure.

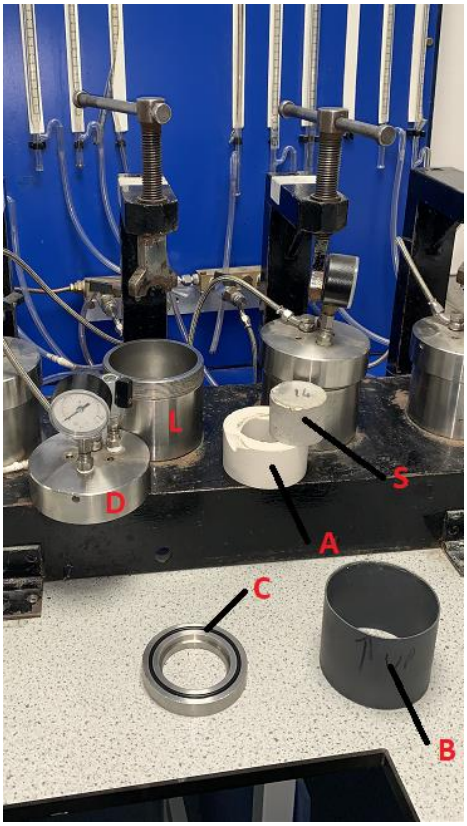

Figure 3-10: Experimental setup for gas permeability test

3.2.6.4 Sorptivity

The sorptivity of cement-based materials is a measure of their ability to absorb water by capillary action. This means that it is highly dependent on the porosity of a material. As with permeability, reliable and comparable results require that the mortar samples are well-dried to ensure that the initial degrees of saturation of all samples are equal. Hall [247] reported that samples with different initial levels of saturation will saturation showed different water absorption behaviour and a non-linear relation between mass change and $T^{0.5}$. For a given degree of saturation, the measurement of mortars and concretes sorptivity is a relatively quick and simple procedure. The method used in this study, as with many other studies [20,137,248,249], produces reliable and reproducible results by applying a simple test [247].

The sorptivity of concretes and mortars is highly influenced by a number of factors including water content, w/b content, binder type and content, curing conditions and the presence of aggregates [250]. In this study, the sorptivity of mortars composed of PC, calcined sludge and limestone were investigated. Since all mortar samples were prepared using the same binders, aggregates, water content, w/b ratio and

curing conditions, any variations in sorptivity can be related to microstructural differences brought about by differences in mix proportions.

In this study, the sorptivity was measured in cubic 50mm mortars. The specimens were cured in a curing room at 95% relative humidity and 20^{o}C for 28 days. This was followed by drying to constant weight in an oven at 40^{o}C, i.e when the mass change was less than 0.2 % within 2 hours [246]. The drying period of these specimens was 2-3 weeks. The lower sides of each specimen were carefully coated with petroleum jelly (~20mm); ensuring that no petroleum jelly was rubbed on the bottom surface. Once coated, the specimens were weighed and placed on top of a small mesh stand within a pan of potable water, kept at 5mm above the bottom of the specimen, as shown in Figure 3-11. Sample masses were measured at fixed times (1, 4, 9, 16, 25, 36, 49 and 62 min.). Before taking mass measurements, the water on the sample surface was removed by placing on a damp towel. Each measurement was completed within 30 seconds. By measuring the volume of water absorbed at different times, the sorptivity coefficient for each mix can be determined by:

$$k = \frac{\mathrm{Q}}{\mathrm{A}t^{0.5}}$$

Where:

k is the sorptivity coefficient

Q is the volume of water absorbed (m^3)

A is the specimen cross sectional area (A)

t is the time (s)

k is determined by plotting versus $t^{0.5}$; where *k* is the slope of the linear fit

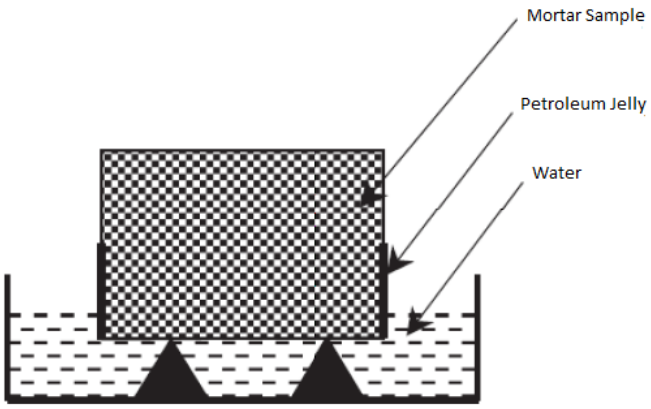

Figure 3- 11: Experimental setup for sorptivity test. Adopted from [251]

Chapter IV: Characteristics of raw and calcined alum water treatment sludge

As the properties of constituent materials affect the reactivity and performance of composite cements, this chapter focuses on the chemical composition, mineralogy and physical properties of raw and heat-treated alum sludge. Firstly, the oxide compositions and organic carbon content of the as-received sludge was determined. Simultaneous thermogravimetric analysis (STA) was performed on the raw sludge to understand how thermal treatment affects phase decomposition and to determine suitable calcination temperature(s). Based on thermal analysis data, various calcination temperatures were selected with a holding time of 2 hours to ensure complete calcination at any temperature. To understand the effect of calcination on sludge properties, the raw sludge and its calcination products were characterized by a range of experimental techniques, namely: XRF for oxide composition; TOC analysis for organic carbon content; helium pycnometry for particle density; laser diffraction for particle size analysis; BET for particle surface area and porosity; SEM for particle morphology; plus XRD and FTIR for mineralogical composition.

4.1 Chemical characterization of raw alum sludge

4.1.1 Chemical composition

The chemical compositions of the raw sludge and other cementitious materials studied in this work are shown in Table 4-1. The sources of the various elements are discussed here and are based on further characterization tests reported in later sections. The major oxide, Al_2O_3, and minor amounts of SO_3 originate mainly from $Al_2(SO_4)_3$ added as a chemical coagulant during the water treatment process. Silica is found to be the second most abundant oxide in the raw sludge. The SiO_2 and Al_2O_3 content are also influenced by the geology of water catchment area where clay minerals such as montmorillonite are concentrated into the sludge volume during the purification process. Iron is the third most abundant element in the raw sludge. It can originate not only from iron-rich minerals, like illite and chlorite, but also other clay minerals, such as montmorillonite, where iron can serve as one of octahedral layer of cations or as a lattice substitution for Si and Al atoms [1]. The iron content in raw sludge is responsible for the reddish colour after calcination at higher temperatures. Clays containing iron calcined at temperatures up to 1000^{o}C are reddish in colour due

to the occurrence of fine and dispersed grains of hematite, [252]. Details about the colour changes will be discussed later. It is important to note that the slag sample used has a calcium carbonate content of 3.23 wt. %.

Table 4- 1: Chemical compositions of raw materials

Composition	Raw alum sludge (%)	Cement (%)	GGBS (%)	Limestone (%)
SiO_2	10.28	20.50	34.51	2.00
Al_2O_3	44.23	4.60	11.20	0.80
Fe_2O_3	2.51	2.40	0.35	0.32
CaO	2.50	63.40	43.07	53.13
MgO	0.34	2.00	7.64	0.64
SO_3	1.24	3.60	1.76	0.07
Na_2O	0.15	0.13	0.14	-
P_2O_5	-	0.30	-	-
MnO	-	0.00	0.17	-
TiO_2	-	0.30	0.74	-
K_2O	0.42	0.74	0.48	-
LOI	36.4	-	-	-
Organic Carbon	9.72	-	-	-
Inorganic Carbon	0.60	-	3.23	-

Table 4- 2: Comparison of raw sludge in this study to those reported in literature

SiO_2	Al_2O_3	Fe_2O_3	CaO	MgO	Na_2O	K_2O	P_2O_5	TiO_2	LOI	Reference
54.1	28.84	9.92	3.1	0.64	0.30	0.75	-	1.28	-	[145]
64.3	21.2	10.4	2.05	1.06	0.17	0.79	-	-	8.04	[146]
52.75	20.15	6.75	0.3	-	0.872	3.69	-	-	13.45	[147]
53.6	20.9	6.6	0.3	1.9	-	-	-	-	11.9	[148]
24.68	30.39	11.59	0.16	0.17	-	0.35	-	0.90	30.67	[149]
29.63	17.57	5.18	11.85	2.15	6.09	2.85	0.94	0.56	22.70	[150]
49.2	26.3	6.6	0.8	1.0	0.6	3.2	-	-	-	[151]
40.61	27.36	6.99	2.62	1.89	1.05	1.28	-	-	-	[152]
10.28	44.23	2.51	2.50	0.34	0.15	0.42	-	-	36.4	Present study

The measurement of the organic carbon in waste materials is particularly important for reuse as SCMs, since organic carbon absorbs water and coats cement grains leading to a decrease in compressive strength [253]. Alum sludge comprises organic and inorganic substances in the solid and liquid states and whose composition

differs in terms of physical, chemical and biological properties [143]. In addition to the alum coagulant added during water treatment, organic polymers known as polyelectrolytes are also added to serve as binding agents that increase the shear strength of the newly formed flocs. The organic and inorganic carbon contents of the raw sludge were 9.72% and 0.60% respective as shown in Table 4-1.

Table 4-2 shows the composition of previously reported alum sludges for comparison with the sludge collected in this study. The variability in water quality and treatment processes is responsible for the differences in composition of the sludges. Typically, SiO_2 constitutes a major part of the sludge followed by Al_2O_3 and Fe_2O_3 while other oxides including CaO, MgO, Na_2O, K_2O, P_2O_5 and TiO_2 are present in trace amounts. However, the sludge sample investigated in this work has alumina as its most abundant oxide followed by silica and then iron. The higher alumina content compared to samples reported in literature is mainly due to a higher dose of alum coagulant applied during the water purification process. Such a composition allows the assessment of whether a reactive product can be derived from the synthetic alum content in the sludge.

Oxide analysis indicates the potential for pozzolanicity, where silica and alumina must be dominant. Otherwise, the material will not be able to react with CH and carbonates to form cement hydration products (C-S-H, CAH and carboaluminate hydrate phases). The simple criterion of $SiO_2+Al_2O_3+Fe_2O_3 > 70\%$ by mass defined by ASTM C618 [15] serves as a basic assessment in that respect. The composition of the raw sludge collected in this work falls short of this criterion. The loss on ignition (LOI) of ~36% observed in the raw sludge is due to its unburnt carbon and water content. In order to limit the unburnt carbon content in fly ash used as an SCM, BS EN 450 [254] limits the loss on ignition to a maximum of 9%. It was anticipated that heat treatment of the raw sludge would drive off water and unburnt carbon, thus raising the silica and alumina contents, potentially over the 70% threshold. In addition, the raw sludge, being a mixture of hydrated aluminium hydroxides and clay minerals, requires dehydroxylation to increase its reactivity in cement. Thus, the following sections investigate the effects of calcination on the physical, chemical and mineralogical characteristics of the raw alum sludge. These properties are conducive to assessing the reactivity and performance of alum sludge in cement in Chapters 5 and 6.

4.1.2 Thermogravimetric and mass spectroscopic analysis

In order to analyse the thermal properties and gaseous products formed during decomposition of the oven-dried raw sludge, thermogravimetry/differential thermal analysis (TG-DTA) and temperature programmed mass spectrometry (MS) was performed. Figure 4-1 presents the TG-DTA curves. The steady mass loss suggests multiple, overlapping decomposition steps, but with two main mass losses with temperature. Prior to TG analysis, the raw sludge was dried at 105^{o}C which removed most of the physically absorbed water, so the residual free or unbound water was only about 2.2%, indicated by the endothermic peak at 75^{o}C. More distinctly, there was ~19% mass loss over the temperature range 200^{o}C to 625^{o}C, attributed mainly to the dehydroxylation of $Al(OH)_3$ to various alumina phases, and the combustion of organic carbon. These changes are denoted by the strong endothermic and exothermic peaks centred at 275^{o}C and 400^{o}C respectively. Wang et al. [255] reported that gelation boehmite (γ-AlOOH) or pseudoboehmite contained more than 15wt% chemically bound water, and it is plausible that the raw sludge may contain some pseudoboehmite. The mass loss from 580^{o}C to 700^{o}C is slight compared to that from 200^{o}C to 625^{o}C. At 579^{o}C the α- to β-quartz transition was observed. β-quartz then remains stable up to 900-1000^{o}C [256]. An inflection centred at 789^{o}C in the DTA curve was accompanied by slight mass loss up to 1000^{o}C, and could be attributed to desulfurization [177,187]**.**

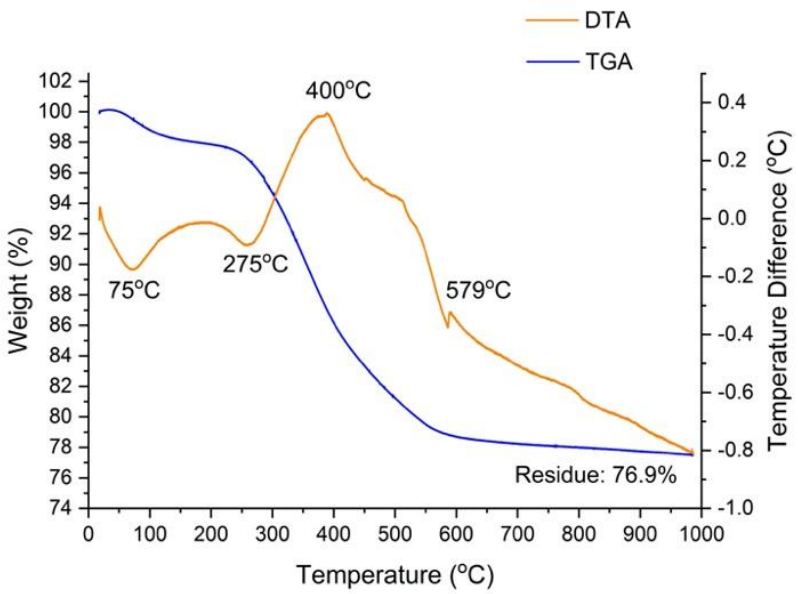

Figure 4- 1: Thermal analysis of as-received alum sludge

To confirm thermal decomposition stages, gas evolution was followed by TG-MS. The main gases evolved during heating include H_2 (*m/z* = 2), H_2O (*m/z* =18), CO (*m/z* =28), CO_2 (*m/z* =44) and SO_2 (*m/z*= 64). Gas emissions are shown as ion current versus temperature in Figure 4-2.

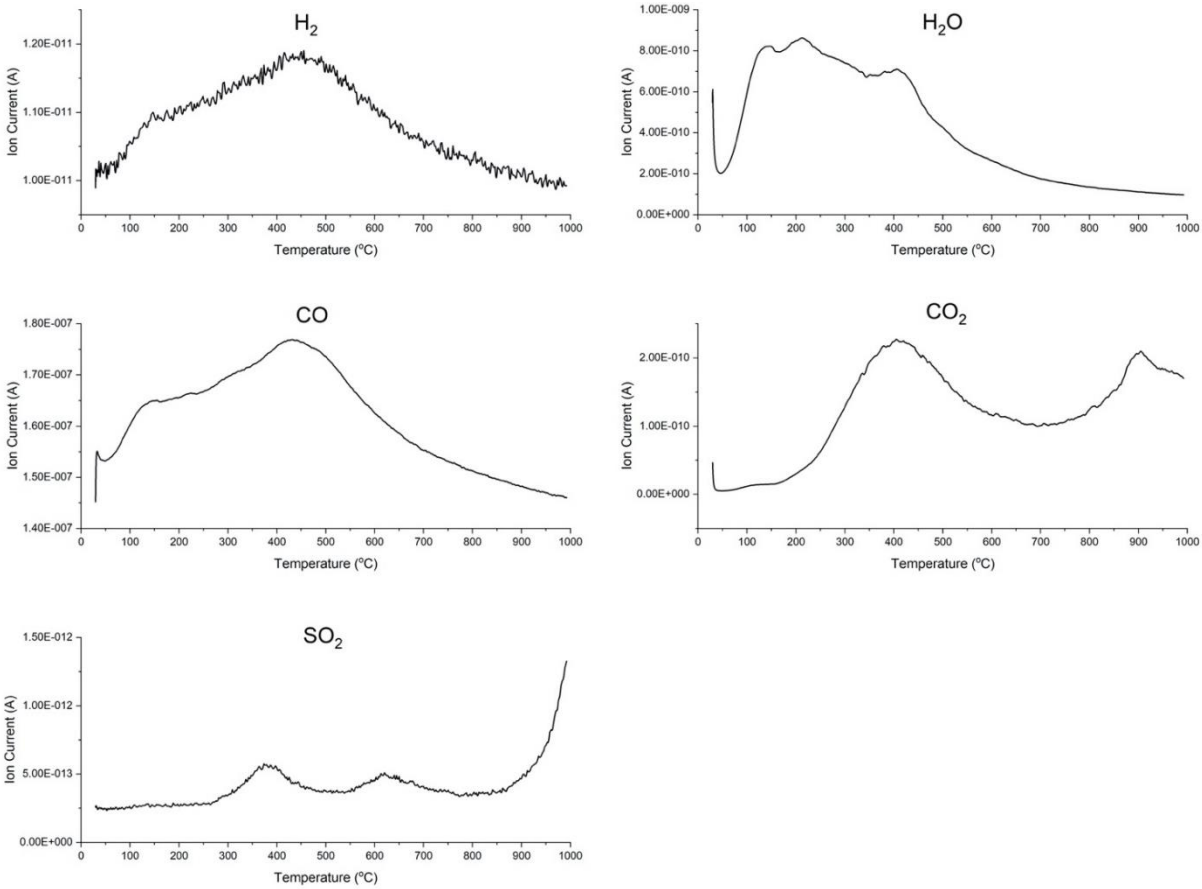

Figure 4- 2: Mass spectrometry data for as-received alum sludge

Water was released between 100 and 500 °C, attributed to the dehydration of free and chemically bound water, and consistent with the corresponding mass loss from TG curve. In the temperature range 200-500°C, carbon monoxide (CO), carbon dioxide (CO_2) and hydrogen (H_2) were the dominant products. The formation of H_2 is attributed to the dehydrogenation of volatile matter. Organic compounds are known to decompose within this temperature range to produce CO which is oxidized to CO_2. The emission peaks of H_2, CO and CO_2 at 475°C suggests that their formation follow the same pathways related to the decomposition of volatile matter and the organic fraction in the raw sludge. CO_2 was also released at about 900°C, assigned to carbonate decomposition. It is generally considered that $CaCO_3$ decomposes nominally at 898°C but in silica-rich minerals, this can occur at 500-750°C [257].

Furthermore, there was emission of SO_2 from the raw sludge at 375, 625 and increased emission in the 800-1000^oC temperature range. The results indicate that the sulfate content in the raw sludge encompasses sulfate species with different thermal stabilities. Rabee et al. [258] observed similar features at 633 and 840^oC for a two-step sulfate decomposition from sulphated zirconias. For alum sludge reported by Ren et al. [259], a release of SO_2 in the temperature range between 200 and 350^oC was attributed to the desorption of physisorbed SO_2 while SO_2 emission between 350 and 600^oC was attributed to the decomposition of sulfur radicals and/or elemental sulfur. The MS data collected is consistent with mass losses observed in TG analysis. The thermal analysis data defined the temperatures for heat-treating the raw sludge; namely 475, 625, 825, 1000 and 1100^oC. These temperatures lie between the end of combustion of organics and the beginning of the formation of α-alumina, the end product of $Al(OH)_3$ decomposition.

4.2 Influence of calcination temperature on properties of alum sludge

4.2.1 Chemical Properties

Table 4-3 shows the oxide compositions of raw sludge and sludge calcined at 825, 1000 and 1100^oC. The oxide compositions of raw and calcined sludges are clearly different. This is due to the presence of organic matter, organic carbon and physically adsorbed water in the raw sludge, which is then removed by calcination. This also leads to increased oxide contents and zero loss on ignition in the calcined sludges. As for the raw sludge, the calcined sludge comprises mainly alumina oxides from the alum coagulant added during water treatment. The enrichment of oxides due to calcination gives a total SiO_2, Al_2O_3 and Fe_2O_3 of ~92% in calcined sludges, which is greater than the 70% required for pozzolans according to ASTM C618. There was also loss of SO_3 at 1000^oC. However, there is not loss of alkalis which typically volatilise at high temperatures in cement kilns.

Table 4- 3: Oxide compositions of raw and calcined sludges

	Calcination Temperature			
Oxide	Raw sludge	825 °C	1000°C	1100°C
SiO_2	10.28	17.67	18.93	19.09
Al_2O_3	44.24	67.38	68.40	68.29
Fe_2O_3	2.51	4.75	4.83	4.74
CaO	2.50	4.55	4.72	4.79
MgO	0.34	0.53	0.46	0.49
SO_3	1.24	2.12	0.08	0.05
Na_2O	0.15	0.75	0.76	0.80
P_2O_5	0.44	0.77	0.78	0.76
MnO	0.15	0.30	0.30	0.30
TiO_2	0.16	0.34	0.31	0.24
K_2O	0.43	0.76	0.76	0.80
LOI 950°C	36.4	-	-	-
Total	98.84	99.92	100	100
Organic Carbon	9.72	0.07	-	-
Inorganic Carbon	0.59	0.20	0.11	0.02

Although previously reported calcined alum sludges constitute mainly SiO_2 followed by Al_2O_3 and Fe_2O_3 [260], the sludge in this study is predominantly composed of Al_2O_3. A ternary diagram of the main oxide contents is plotted in Figure 4-3 for 6 calcined sludge samples published in the cement literature [8,9,157–159,166], the calcined sludge in this project, plus typical contents for more established cementitious materials [214,261,262]. The calcined sludges reported in the literature have similar compositions to calcined clays, being rich in silica whilst containing alumina to a lesser degree. The significant alumina content in the sludge used here suggests the potential for different behaviour to conventional SCMs.

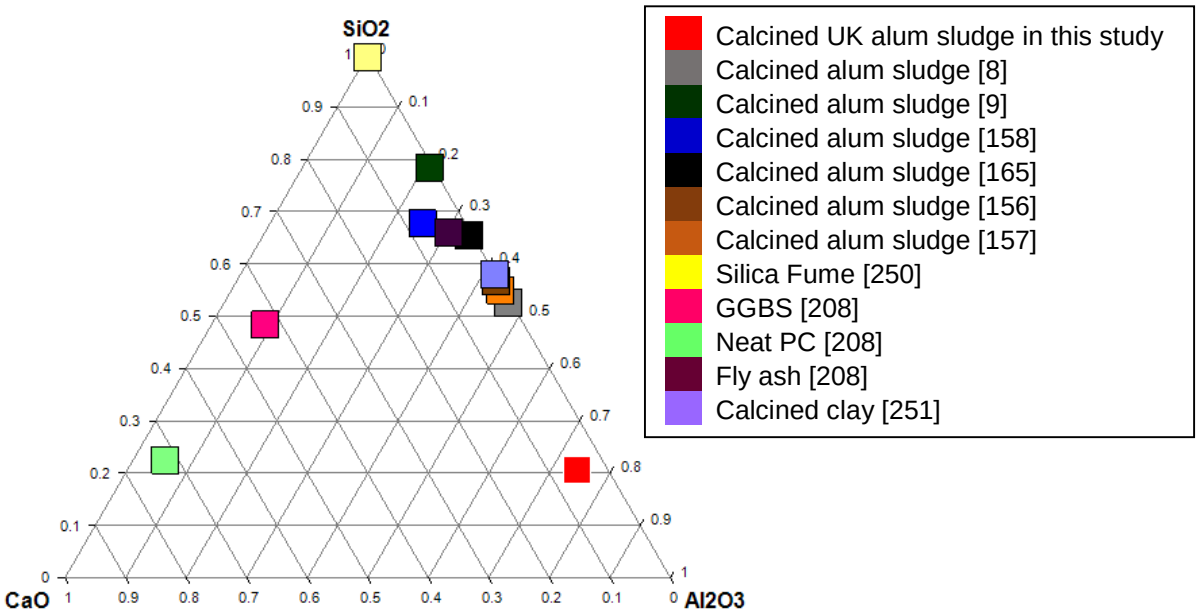

Figure 4- 3: Ternary plot of SiO_2, Al_2O_3 and CaO contents for calcined alum sludge in comparison to conventional SCM

4.2.2 Mineralogical Properties

4.2.2.1 XRD Analysis

Figure 4-4 shows the XRD patterns of the raw sludge and samples calcined up to 1100^{o}C. The raw sludge was primarily amorphous with quartz and montmorillonite the only crystalline phases detected. Although crystalline quartz is inert, calcined montmorillonite is reported to be 'fairly pozzolanic', having higher pozzolanic activity than calcined illite but lower than kaolinite [156]. Upon heating the raw sludge to 475^{o}C and then 625^{o}C there was no change in the crystalline phases detected, indicating that mass loss observed by STA was due to loss of water, organic matter and organic carbon. Only upon heating to 825^{o}C was there a noticeable change in crystallinity, with the appearance of reflections due to η-alumina (eta). Previous studies suggest that η-alumina is a transition phase produced by the thermal decomposition of poorly crystalline pseudoboehmite (AlO(OH)) or well-crystallized bayerite α-$Al(OH)_3$ [176,263]. This means that since bayerite was not detected at lower temperatures, it is possible that pseudoboehmite is present in the raw sludge.

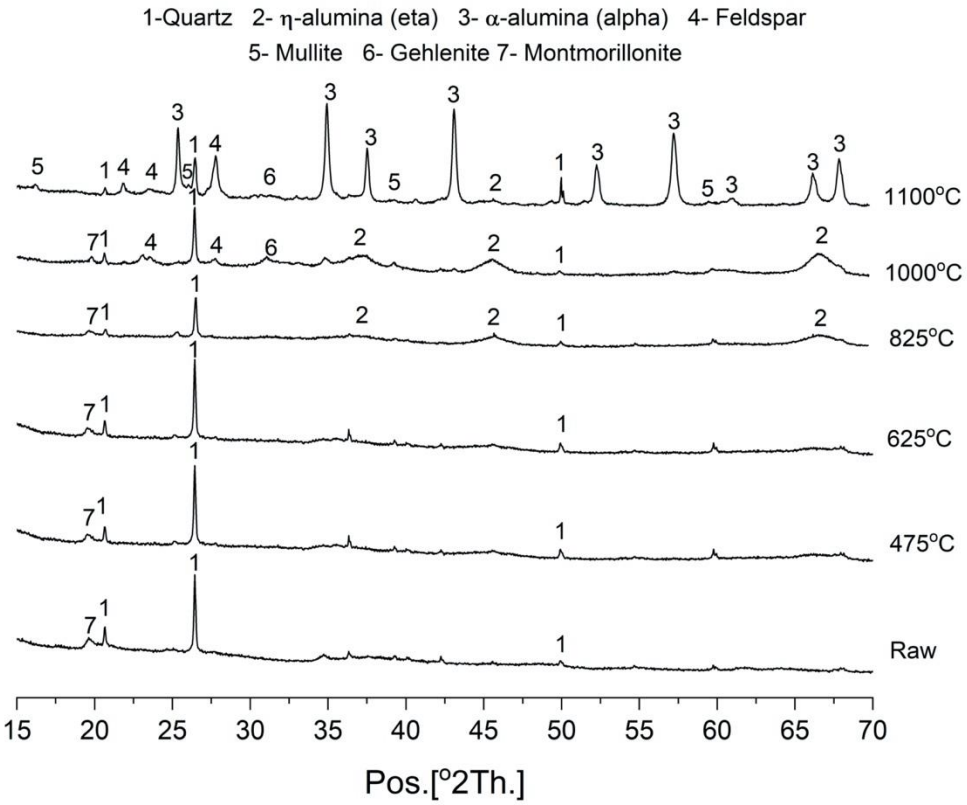

Figure 4- 4: XRD analysis of raw and calcined sludge

The diffraction patterns of η- and γ-alumina (gamma) are almost identical. Characterisation was primarily on the basis that the η-alumina has a spinel-cubic structure with a regular cubic-oxygen lattice of lattice parameter a= 0.79 nm while γ-alumina is of the spinel-tetragonal type with lattice parameters a=0.796, c=0.781 nm [177]. The observed formation of η-alumina is consistent with studies of aluminium hydroxide gels synthesized from various aluminium sulfates [177,178]**.** By 1000°C, feldspar reflections were detected, which is a useful indicator of montmorillonite decomposition [156] and the η-alumina reflections became more prevalent. Also, there was formation gehlenite, arising from the reaction between CaO and reactive Al_2O_3 and SiO_2. On further heating at 1100°C, the montmorillonite reflection disappeared while η-alumina reflections transformed to highly-crystalline α-alumina, indicating complete alumina dehydroxylation [156,264,265]. This occured with the formation of another high temperature phase, mullite, from the reaction of silica- and alumina-rich phases in the sludge, suggesting that mullite formation and α-alumina reaction occurred concurrently**.** This implies that by 1100°C, η-alumina may have reacted with silica-rich phases. Literature suggests that in spite of being a very rare mineral in

nature, mullite is a common high temperature reaction product of many aluminosilicates. Alumina and silica-rich systems such as pure clays and clay-aluminium hydroxide or clay-aluminium oxide are widely used to produce mullite ceramics [266]. The observed thermal changes are consistent with previous studies on the thermal decomposition of standard clays and aluminium hydroxides [7,196,267,268].

4.2.2.2 FTIR Analysis

FTIR Spectroscopy was used to confirm the thermal transformation of raw alum sludge, i.e. an aluminium hydroxide precipitate containing clay minerals, as indicated by XRD. Figure 4-5 shows the raw alum sludge to be a hydrated material, with intense broad bands at 1640cm^{-1} and 3340cm^{-1}, indicating the presence of molecular and free water. The band at 1640 cm^{-1} may be attributed to H-O-H bending vibrations of interlayer water, while the broad band at 3340cm^{-1} is due to OH^- bonds of structural water present in $Al(OH)_3$ [269,270]. These bands gradually decreased in intensity with increasing temperature, finally disappearing by 1100^{o}C, indicating the gradual loss of hydroxyl groups and the complete dehydroxylation. This coincides with the collapse of the montmorillonite structure, as observed by XRD.

Very weak $\upsilon 3$ carbonate stretching bands are present at 1435cm^{-1}. The bands diminished with increasing temperature; disappearing by 825^{o}C. This is in line with known behaviour of calcite and loss of inorganic carbon as observed in total organic carbon analysis (Table 4-3).

Silicate absorption bands are in the range 465-1150 cm^{-1} [271]. In the raw alum sludge, the intense Si-O stretching bands at 1030 cm^{-1} and 532 cm^{-1}, the bending band at 465 cm^{-1}, as well as the shoulder at 912 cm^{-1} are typical for smectite minerals [1,271]. The band at 912 cm^{-1} is attributed to Al-O-H deformation of the octahedral sheet in such structures. Bands at ~532 and 465 cm^{-1} are assigned to Al-O-Si and Si-O-Si deformations, the latter being characteristic of amorphous silica. The presence of quartz is also confirmed by the band at 793 cm^{-1} [150,272].

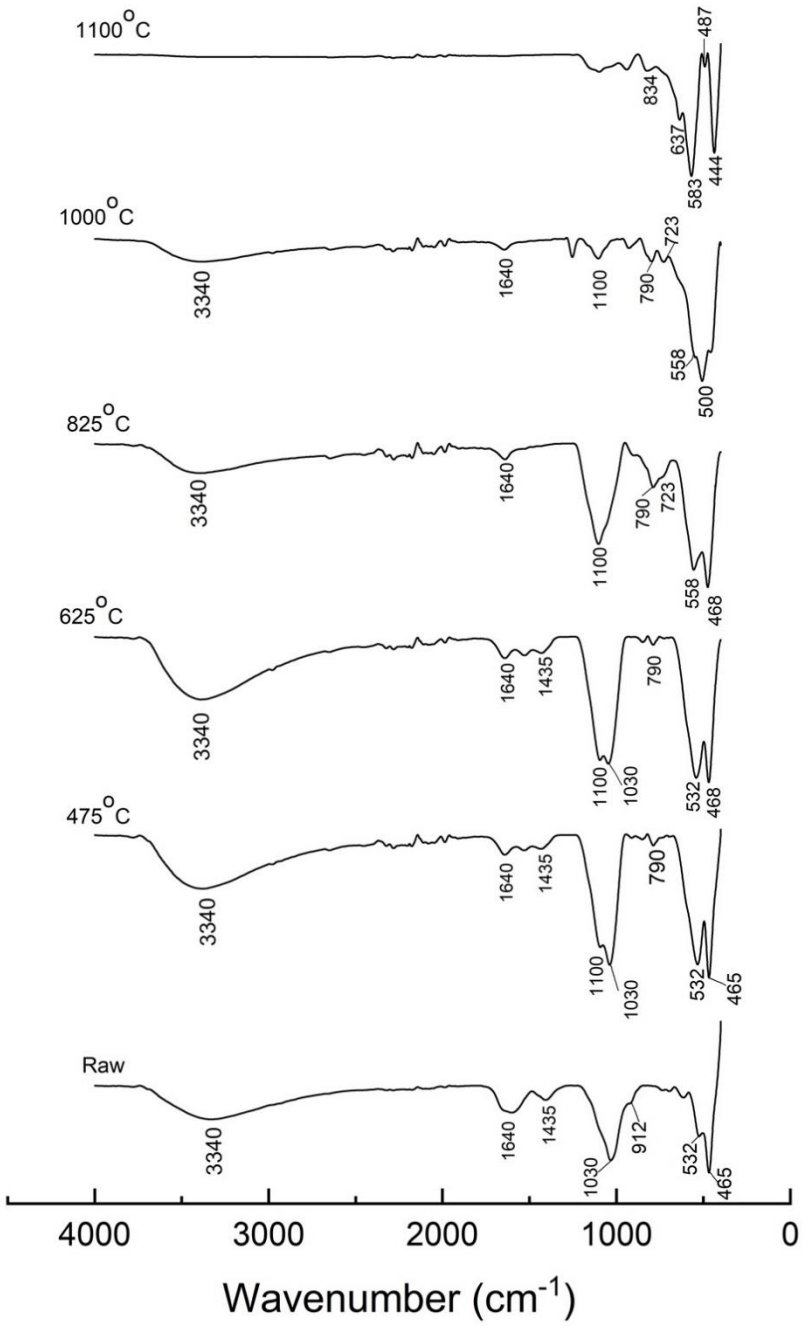

Figure 4- 5: FTIR analysis of raw and calcined sludge

Increasing calcination temperature up to 475ºC led to the disappearance of the Al-O-H band at 912 cm^{-1}, signifying the dehydroxylation of clay minerals. Within the broad band at 1030cm^{-1}, a small shoulder at around 1100cm^{-1} is observed, which can be assigned to the presence of montmorillonite [1]. With further increase in calcination temperature, possible alteration in the montmorillonite layers and distorted bonding of the bridging oxygen atoms is suggested by the gradual reduction in the intensities of

Al-O-Si and Si-O-Si deformation bands at 532 and 465 cm^{-1} [271]. With increasing temperature, the bands at 1100 cm^{-1} and 1030 cm^{-1} transformed to a single absorption at 1100 cm^{-1} characteristic of amorphous reactive silica species as reported in several studies [268,273]. Upon heating at 825^{o}C, a new band at 723cm^{-1} emerged assigned to Al-O-Al. The transformation of $Al(OH)_3$ to an oxide is seen in the steady strengthening of this band with increasing temperature [269]. After heating to 1100^{O}C, the spectrum from the calcined sludge showed sharp and distinct peaks due to corundum (α-alumina), in agreement with the XRD patterns. The corundum structure is composed of octahedral AlO_6 only and its most characteristic bands are at 444 cm^{-1}, 487 cm^{-1}, 637cm^{-1} and 583 cm^{-1} [274], all visible in the obtained spectrum. The formation of mullite at 1100^{o}C is indicated by the emergence of the broad band at 834 cm^{-1} [275], attributed to Si-O-Al linkages and indicating the presence of $Al_2O_3.SiO_2$ structure. These findings are consistent with XRD analysis.

4.2.3 Physical Properties

4.2.3.1 Particle size and Density

The pozzolanic activity of SCMs is not only influenced by their chemical composition, but also by their physical properties, which are significantly modified by thermal treatment, particularly clay and alumina particles. Alum sludge calcined at different temperatures and then subjected to the same grinding regime showed systematic variations in physical properties. Figure 4-6 show the particle size distribution (PSD) for the raw and calcined sludges. Table 4-4 show the d_{10}, d_{50} and d_{90} values of the ground raw and calcined sludges. According to Sanchez-Soto et al. [276], particle size reduction in clay minerals by dry grinding is by delamination but longer grinding times lead to particle aggregation and agglomeration. Table 4-4 and Figure 4-6 show that the mean particle size gradually coarsens with calcination temperature up to 825^{o}C. As indicated by SEM analysis, this is attributed to the agglomeration of the finest particles when calcined up to 825^{o}C while the occurrence of finer particles at higher temperatures is due to the breakdown of agglomerates. The observed agglomerated state is likely to influence mortar and concrete performance. For example, Diamond and Sahu [277] found that agglomerates of micro-silica can survive concrete mixing. As a result, the retained agglomerates in cement pastes cannot induce the filler effect commonly attributed to microsilica particles. The

densities of the sludge samples also increased with calcination temperature due to the removal of water (hydroxyl groups and a second layer of adsorbed water molecules) and their mesoporosity due to their strongly aerated state [278]. For sludge samples calcined at lower temperatures, the strong tendency to adsorb water was observed during density measurements by helium pycnometry as they were difficult to completely degas. As the dehydration/dehydroxylation process progresses with temperature and denser aluminas are formed [177], the grindability of the sludge samples increases [252]. At calcination temperatures up to 825ºC, sludge particles adhered to the surface of the grinding jar and agglomeration was evident. At higher temperatures, there was significantly lower adherence of the sludge particles to the surface of the grinding jar and the particles were finely divided.

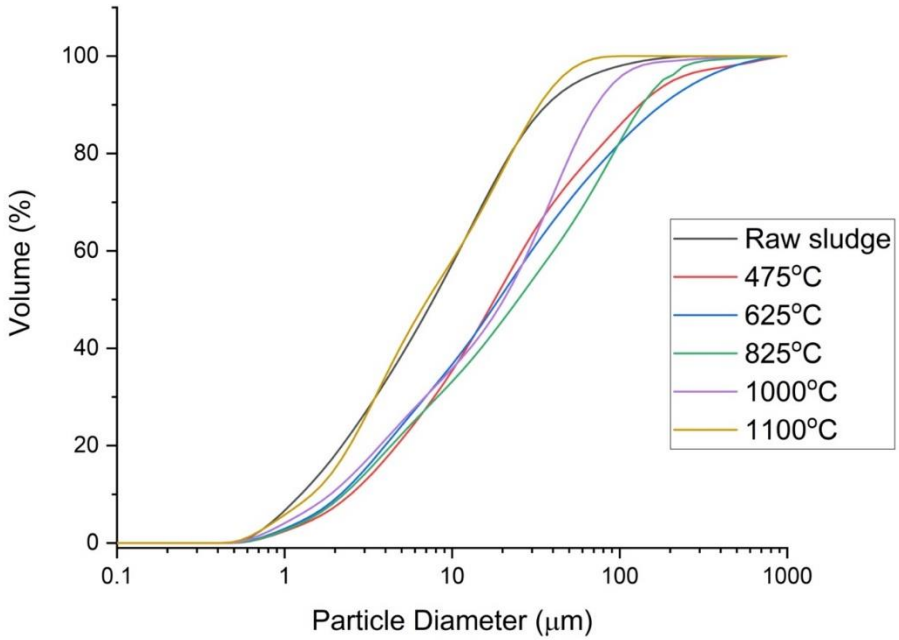

Figure 4- 6: Particle size analysis of raw and calcined sludge

Table 4- 4: Particle size parameters and densities obtained after grinding for raw and calcined sludges

Physical Property	Raw sludge	475 °C	625 °C	825 °C	1000°C	1100°C
Density (g/cm^3)	2.20	2.58	2.85	3.09	3.12	3.31
D_{10} (µ)	1.22	2.44	2.22	2.25	1.86	1.47
D_{50} (µ)	7.51	17.37	19.95	24.76	20.34	7.73
D_{90} (µ)	41.32	148.54	206.32	145.2	76.34	34.33

4.2.3.2 Specific Surface Area and Pore size Characteristics

The specific surface area (SSA) is another important parameter in studying and understanding the properties of SCMs. It is directly determined by particle size and porosity [279]. Previous studies on synthesis of aluminium oxides and hydroxides have established that heat treatment leads to the formation of alumina forms with large surface area and internal porosity. In this work, the SSA and pore volumes were determined by the BET standard method [280]. The BET analysis evaluates the specific surface area by nitrogen adsorption measured as a function of the rise in relative pressure. Table 4-5 shows the BET surface areas and pore characteristics of all materials studied.

Table 4- 5: BET surface areas and pore size data for all materials studied

	Cement	GGBS	Limestone	Raw sludge	475 °C	625 °C	825 °C	1000°C	1100°C
BET area (m^2/g)	1.01	1.56	1.03	53.77	99.41	81.68	110.18	61.43	15.14
Total Pore Volume (cm^3/g)	-	-	-	0.199	0.345	0.395	0.533	0.401	0.220
Average Pore Diameter (nm)	-	-	-	10.04	9.06	13.30	13.78	19.45	44.40

The trend in SSA and particle size distribution can be further explained by the nitrogen adsorption isotherms and pore size distributions presented in Figure 4-7 and Figure 4-8 respectively. Upon calcination, the surface area of the raw sludge increased from 53.77 m^2/g at ambient temperature to 110 m^2/g at 825°C and the corresponding

total pore volume increased from 0.199 to 0.533cm^3/g. From 825^oC the surface area started to decline, with a corresponding decrease in pore volume. When the temperature increased from 825^oC to 1100^oC, however, there was a dramatic reduction in surface area and total pore volume indicating collapse of the pore structure and crystallization of clay minerals and aluminas [281].

Pore-size distributions and pore volumes were calculated from the desorption branch of the isotherm data using the BJH equation [188], which quantifies the thickness of the adsorbed layer on the pore surface as a function of relative pressure. The shape of the isotherm and its hysteresis pattern provide useful information about the physisorption mechanism. IUPAC (International Union of Pure and Applied Chemistry) classified the adsorption isotherms into six types (Type I-VI), along with four hysteresis isotherms pattern types (H1-H4) [280]. The hysteresis patterns provide insight about pore size distribution, pore geometry and interconnectivity with the sludge particles. Figure 4-7 shows that the N_2 adsorption and desorption isotherm curves of the studied sludge samples do not overlap, resulting in hysteresis loops. The type for all sludge samples seems to be Type V isotherm with H3 hysteresis loops characteristic of mesoporous materials with plate-like particles (e.g clays) or slit-shaped pores [280]. The described pores have an excellent interconnected pore network which favor the flow of gas. The BJH pore-size distribution of the sludge samples show that particles are mainly in the mesoporous range, i.e. having pore diameters of 2-50 nm. The presence of mesoporosity is generated by the irregular shape of the sludge particles. With increasing calcination temperature, the pore diameter increases, and the pore size distribution becomes broader. The pore sizes in calcined sludges can differ due to microstructure heterogeneity i.e mineral content, volatile matters and diagenesis effects [281].

The variation in surface area and porosity of sludge samples can be summarized as: the raw sludge, an $Al(OH)_3$ gel, contains considerable amount of water including free water, adsorbed water and structure water. With increasing temperature from 0-825^oC, the dehydroxylation of $Al(OH)_3$ gel to denser alumina forms creates considerable amount of pores and internal surface area. The porosity and associated high specific surface area of alumina formed has been attributed to the rapid loss in mass without a reduction in the external dimensions of the hydroxide particles [176,282]. This explains why the calcined sludge at 825^0C has the highest surface area. Further increase in temperature results in a decrease in pore volume

indicating the partial collapse of pore walls upon removal of the hydroxyl groups [283]. In the 1000-1100^{o}C temperature range, the surface area decreased significantly indicating first signs of sintering and formation of α-alumina [165]. The observed changes in physical properties are consistent with results from synthesized aluminium hydroxides [188,283,284].

The adsorption-desorption isotherms of cement, GGBS and limestone powder show little or insignificant hysteresis and almost reversible adsorption-desorption branches. The adsorption isotherms are of Type II which are typical for non-porous solids.

Understanding the pore size distributions in calcined sludges is critical in assessing the workability as well as the filler effect in blended cements. Differences in porosity and corresponding BET surface area of the sludge samples is expected to influence their water sorption when incorporated in cement mixtures. Based on the variation in SSA, it is expected that the water demand of sludge blended cement will increase with calcination temperature up to 825^{o}C and thereafter decline.

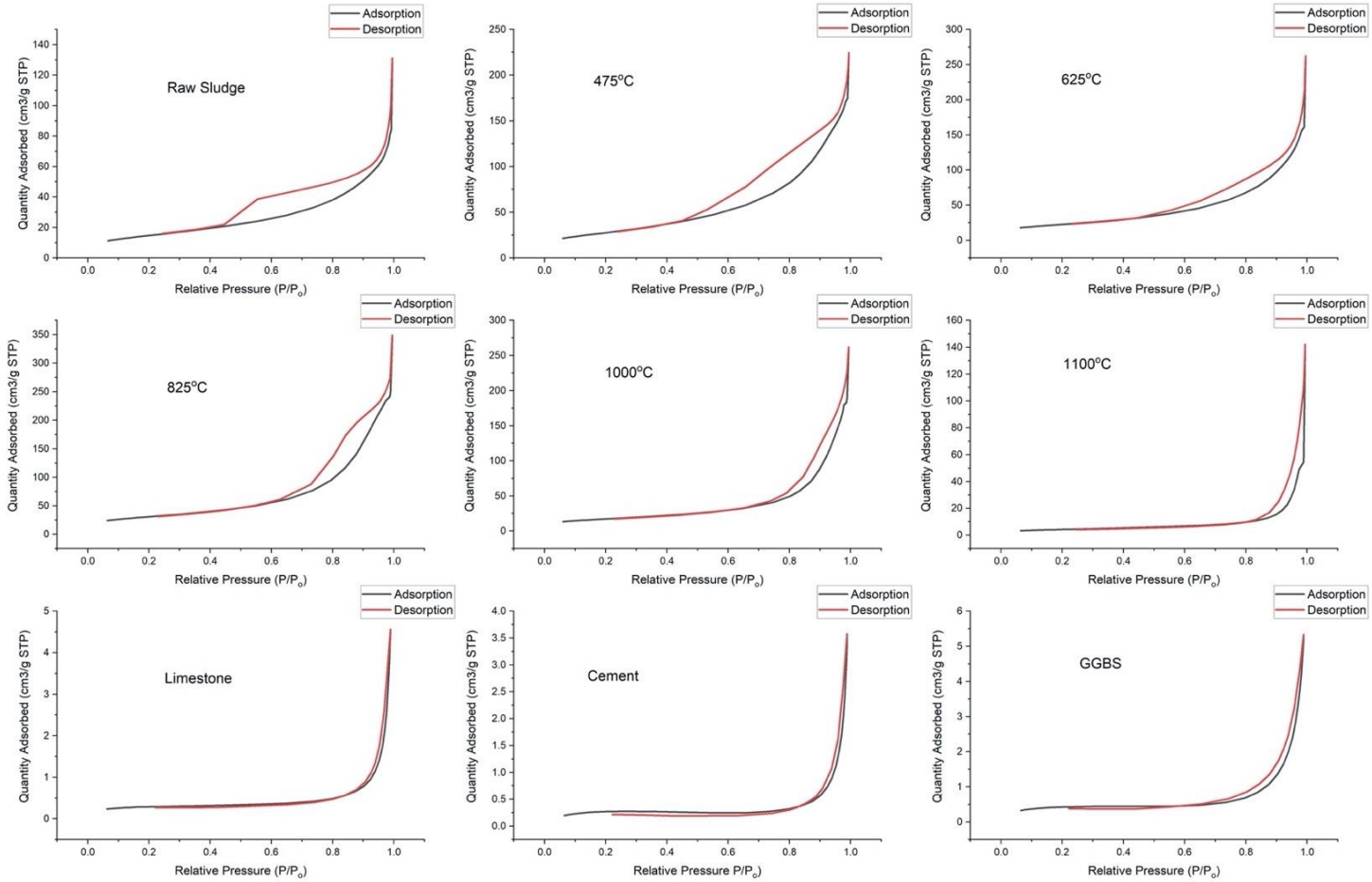

Figure 4- 7: Nitrogen adsorption and desorption isotherms for all materials studies

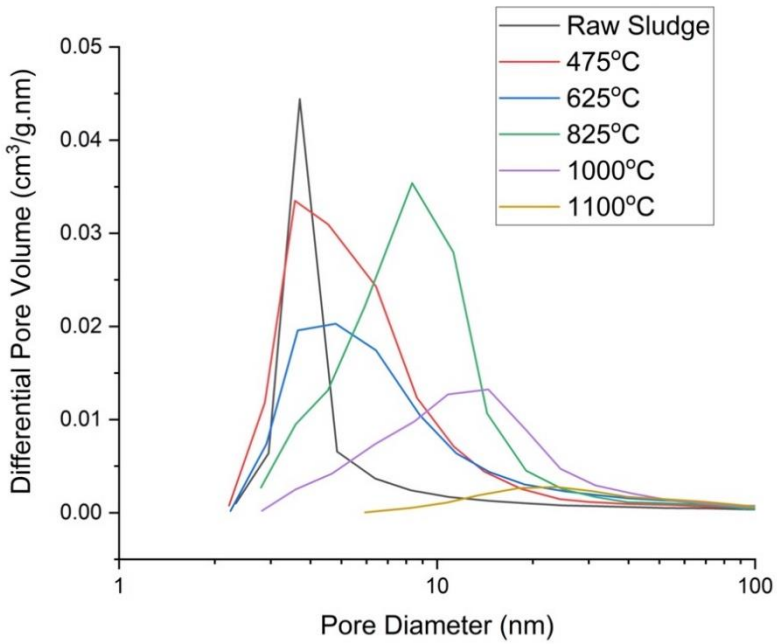

Figure 4- 8: BJH pore size distributions for all materials studied

4.2.3.3 Morphological characteristics

The particle morphology of raw and calcined sludges was examined by SEM operated in secondary electron mode. SEM images shown in Figure 4-9 (a-f) illustrate the influence of calcination temperature on particle morphology and a visual indication of previously discussed variations in particle size, BET surface area and pore characteristics (Table 4-5). At lower temperatures, particles were irregularly shaped with various sizes and rough surface textures. No significant morphological changes were observed at calcination temperatures up to 825°C, where maximum SSA and particle size was observed due to agglomeration. At 1000°C, features typical of sintering were observed as particle edges became more rounded consistent with the decreased BET surface area. At 1100°C, dehydroxylation is complete, crystalline corundum is formed with a drastic reduction in SSA and particle size. This is attributed to the collapse of pore walls as indicated by reduced pore volumes. In general, it appears from SEM images that calcination up to 825°C resulted in the agglomeration of particles. Further calcination up to 1000°C showed rounded particles with reduced surface roughness due to sintering. At 1100°C, the breakdown of particles due to collapse of pore walls produced finer particles.

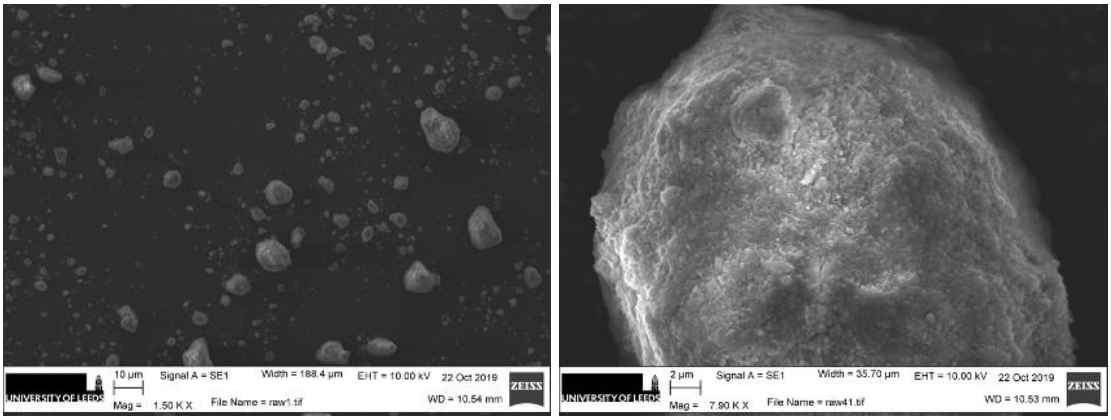

a) Raw sludge

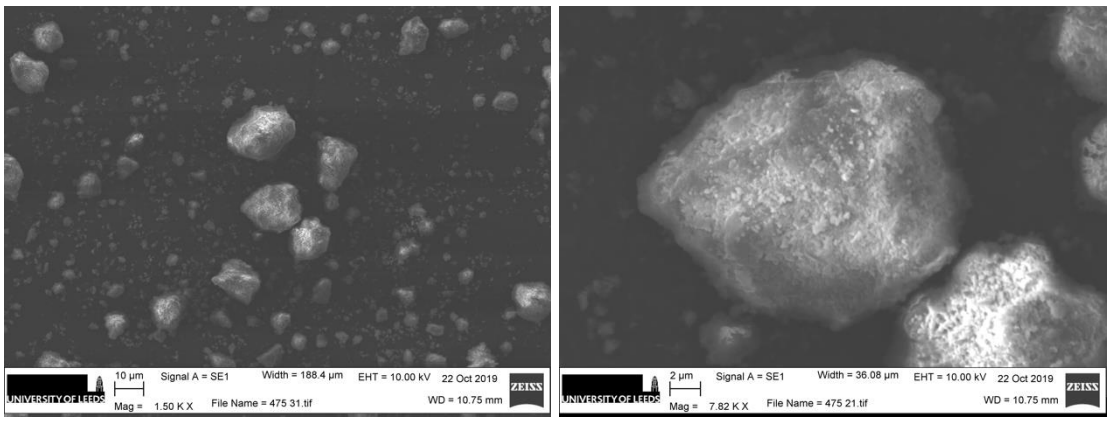

b) 475ºC

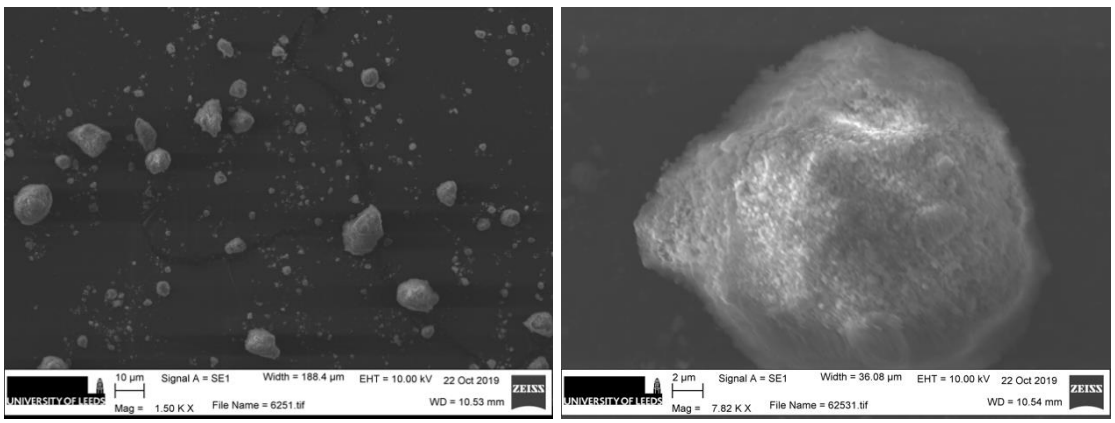

c) 625 ºC

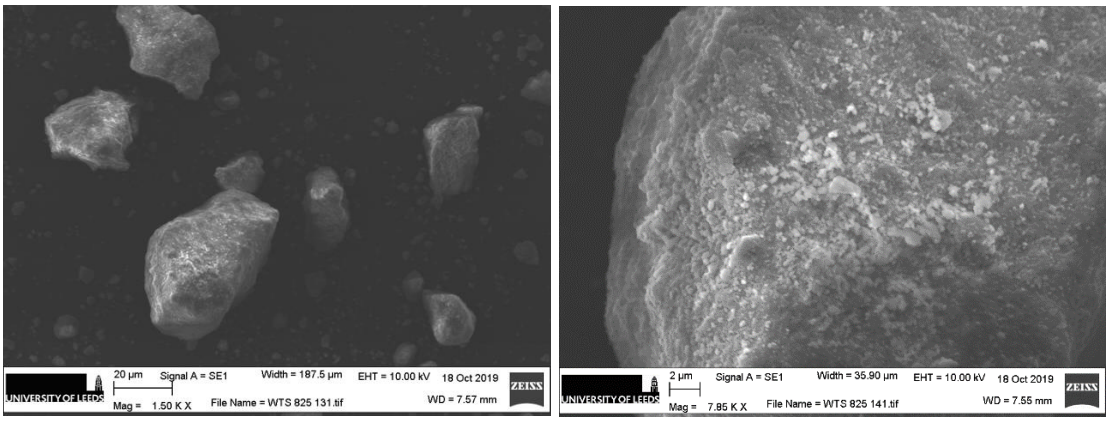

d) 825 ^{o}C

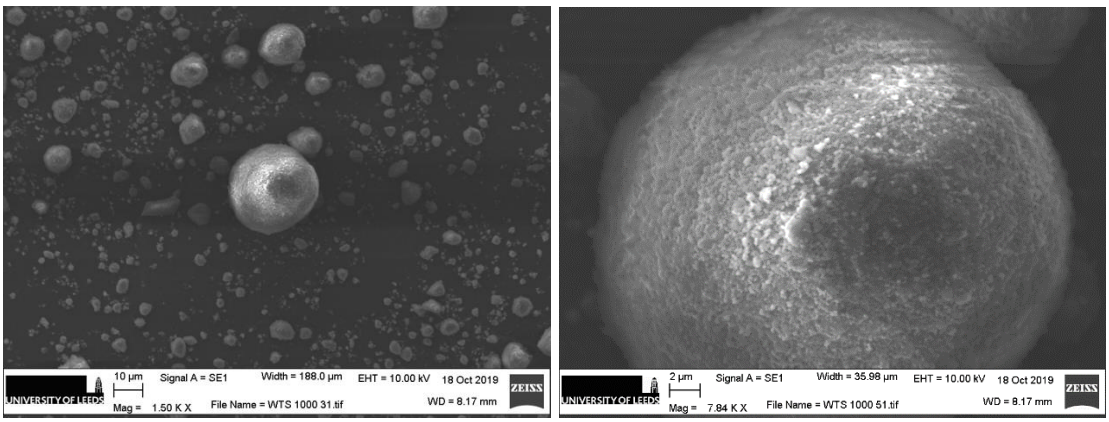

e) 1000 ^{o}C

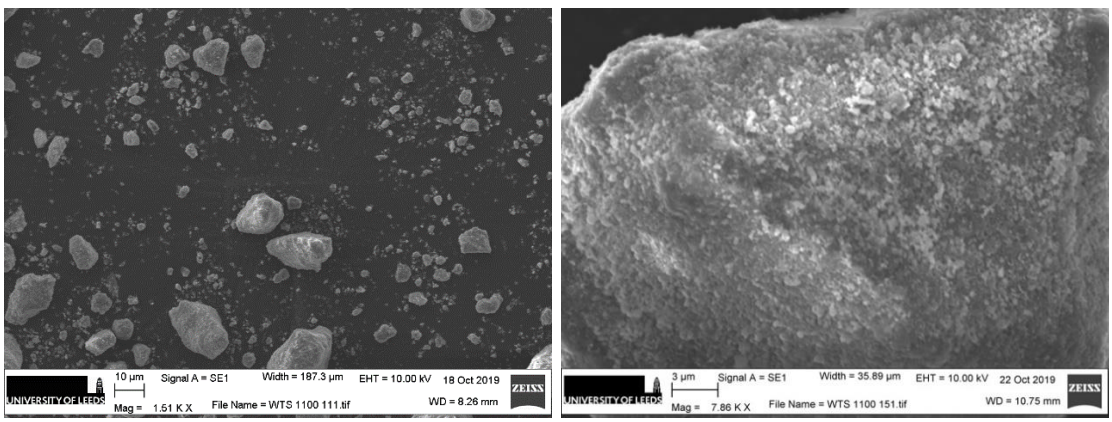

f) 1100 ^{o}C

Figure 4- 9(a-f): Secondary electron images of raw and calcined sludges captured at 1500x (field of view: 185 x 140µm) and 7850x (field of view: 37x28µm).

4.2.3.4 Physical appearance

The colour of clay wastes depends mainly on chemical composition, clay microstructure, kiln atmosphere and temperature [252]. Figure 4-10 shows the visual appearance of raw sludge and sludges calcined at 825^{o}C and 1100^{o}C. The black colour of the raw sludge is due to its significant carbon content (~9.7%). The colours of sludges calcined at 825^{o}C and 1100^{o}C are reddish and beige respectively. According to Kreimeyer [285], clays with high iron content (3-7wt%) calcined at high temperature are reddish in colour due to the presence of "free" Fe_2O_3 in the form of hematite. At higher temperatures the reddish colour turns to beige due to the incorporation of iron in specific high temperature crystalline phases such as mullite rather than as its occurrence as free Fe_2O_3 in the form of hematite. The clay microstructure could also influence the colour as stiff particles could inhibit oxidation of Fe^{2+} and the clay matrix can darken [252]. The calcination and kiln atmosphere can also influence the colour of the calcined products. The sludges in this work were calcined using electric laboratory furnace, the oxidant atmosphere gave a reddish shades at calcination temperatures up to 825^{o}C, but rotary kilns reported elsewhere [252], depending on air/fuel ratio produced brownish particles.

Figure 4- 10: Physical appearance of a) As-received sludge; Ground Calcined sludge b) 825^{o}C; c) 1100^{o}C.

4.3 Summary

Alum sludge is composed of impurities (including clay minerals) removed and precipitated from untreated water along with residues of the alum coagulant used during water treatment. The presence of silica and alumina in alum sludge makes it a potential SCM candidate for cement replacement. It is well-known that thermal treatment of siliceous and alumina-rich raw materials is usually required to enhance pozzolanic reactivity. In this chapter, an in-depth characterization of alum sludge was performed to investigate the effect of calcination on its physical, chemical and mineralogical properties within the interval 475^{o}C -1100^{o}C. These properties are conducive to assessing the reactivity of raw and calcined alum sludge in chapter 5. The main findings of this chapter are summarized as follows:

4.3.1 Thermal analysis

TG-MS analysis of oven-dried sludge suggests multiple, overlapping decomposition steps, but with two main mass losses with temperature. The first one over the temperature range 0-140^{o}C is a 2.2% mass loss due to the removal physically absorbed water. More distinctly, there was a ~19% mass loss over the temperature range 200^{o}C to 625^{o}C, attributed mainly to the dehydroxylation of $Al(OH)_3$ to aluminas (i.e. $2Al(OH)_3 \rightarrow Al_2O_3 + 3H_2O$) and the combustion of organic compounds. Within this temperature range, carbon monoxide (CO), carbon dioxide (CO_2) and hydrogen (H_2) were the dominant gaseous emission products. The formation of H_2 is attributed to the dehydrogenation of volatile matter. Organic compounds are known to decompose within this temperature range to produce CO which is oxidized to CO_2. At 579^{o}C the α- to β-quartz transition was observed. An inflection centred at 789^{o}C in the DTA curve was accompanied by slight mass loss up to 1000^{o}C and is attributed to desulfurization. MS data showed a three-step decomposition of SO_2 at 375 ^{o}C, 625 ^{o}C and increased emission within 800-1000^{o}C temperature range. This suggests the presence of sulfate species of different thermal stabilities. The thermal analysis data defined the temperatures for heat-treating the raw sludge; namely 475, 625, 825, 1000 and 1100^{o}C. These temperatures lie between the end of combustion of organics and the beginning of the formation of α-alumina, the end product of $Al(OH)_3$ decomposition.

4.3.2 Chemical composition

TOC analysis of raw sludge found organic and inorganic carbon contents of 9.72% and 0.6% respectively. Oxide analysis found that the raw sludge has Al_2O_3 as its most abundant oxide followed by SiO_2 and Fe_2O_3 with contents of 44.23%, 10.28% and 2.51% respectively. Calcination of the raw sludge at temperatures between 825-1100^oC led to an enrichment of oxides due to the removal of biodegradable organic matter, organic compounds and physically adsorbed water. The SiO_2 + Al_2O_3 + Fe_2O_3 oxides percentage in calcined sludges was approximately 92% chemically fulfilling the ASTM C618 requirement for fly ash and natural pozzolans.

4.3.3 Mineralogy

Mineralogical analysis by XRD and FTIR suggests that the raw sludge is primarily amorphous, with quartz and montmorillonite the only crystalline phases detected. Heating to 475^oC and then 625^oC revealed no change in the crystalline composition, indicating that mass loss observed in STA was due to loss of water and organic carbon. Only upon heating to 825^oC was there a noticeable change in crystallinity, with appearance of reflections due to η-alumina (eta). The formation of η-alumina is consistent with previous studies on calcined aluminium hydroxide gels synthesized from aluminium sulfates. This confirms that the significant Al_2O_3 content observed in the sludge samples is related to the alum coagulant added during water treatment. Upon calcination at 1000^oC, feldspar was detected and the η-alumina reflections become more prevalent. Also, gehlenite was formed arising from CaO plus reactive Al_2O_3 and SiO_2. On further heating at 1100^oC, the montmorillonite reflection disappeared while η-alumina transformed to alpha alumina, indicating complete dehydroxylation [264,265]. This occurs with the formation of another high temperature phase, mullite, from the reaction of silica- and alumina-rich phases in the sludge, suggesting the possible reaction of η-alumina with silica-rich phases. The phase transitions are consistent with previous studies on calcined clays and aluminium hydroxides.

4.3.4 Physical properties and morphology

Alum sludge calcined at different temperatures and then subjected to the same grinding regime showed systematic variations in particle size, specific surface area

and morphology. The raw sludge consisted of very fine and irregular particles. The mean particle size of the sludge samples increased with calcination temperature up to 825^{o}C due to agglomeration of the finest particles. The highest BET surface area was also observed in samples calcined at 825^{o}C. During the dehydration/dehydroxylation process, the rapid mass loss occurred without a reduction in external dimension of the sludge particles thereby developing internal porosity and increased BET surface area. At 1000^{o}C, typical characteristics of sintering processes were observed at the particle surfaces as the edges became rounded and smoother with a corresponding decrease in BET surface area. At 1100^{o}C, the complete removal of hydroxyl groups and formation of a-alumina led to the partial collapse of pore walls resulting in a drastic reduction in particle size and BET surface.

Chapter V: Assessment of Cementitious Activity

This chapter presents results and discussions on the hydration and performance of cement composites incorporating alum sludge. Firstly, the pozzolanic activity of raw sludge and sludge calcined within the interval 475-1100^{o}C was assessed using the Strength Activity Index (SAI) test [242]. The sludge samples that passed the prescribed 75% SAI were then blended variously with GGBS and limestone powder to investigate compressive strength in mortars and hydration in corresponding pastes. The thermal changes discussed in chapter 4 were related to performance results to understand underlying factors influencing sludge interactions in blended cement systems. Hydration of blended cement pastes was monitored to determine the influence of alum sludge calcining temperature on the hydration kinetics, phase assemblage and microstructural evolution of blended cement pastes. This enabled an understanding of how the main properties and characteristics of alum sludge influence sludge reactivity and cement hydration. By doing so, the mix design of calcined sludge cementitious matrices can be optimized, and unfavourable hydration reactions and their consequences may be avoided.

5.1 Performance of Mortars Containing Raw and Calcined alum sludge

5.1.1 Workability

The influence of alum sludge on the workability of binary blended cement mortar was investigated using the flow table test [240]. Based on the SAI test, Table 5-1 shows the mix proportions prepared using 50mm mortar cubes with a binder/sand ratio of 1:3 and a water/binder ratio of 0.55 and 1% superplasticiser. The mix descriptions CR, C475, C625, C825, C1000 and C1100 refer to 20% cement replacement of raw sludge, calcined sludge at 475, 625, 825 and 1100^{o}C respectively. Earlier discussed morphological changes occurring upon sludge calcination can be used to describe the flow behaviour of blended cement mortars. Figure 5-1 shows how the workability of binary blended cement mortars reduced with calcination temperature up to 825^{o}C and then increased at higher calcination temperatures. Figure 5-2 shows the relation between flow diameter and the sludge BET surface area. There is a linear decrease in flow diameter with increasing surface area of calcined sludge. Earlier

findings, presented in Chapter 4, suggest that the raw sludge comprises irregular shaped particles which agglomerate with increasing calcination temperature, developing internal porosity and BET surface area. The increase in surface area of sludge samples up to a calcination temperature of 825^{o}C increases the water absorption on the surface of the sludge particles which lowers the free water available for lubricating granular cement system. Similar to this study, it has been reported that nano-particles containing silica often exist in aggregated (firmly-held clusters) or agglomerated (loosely held clusters) forms with final cluster sizes ranging from nanometers to as high as 100mm due to their very high surface area [277]. Even in well-dispersed colloidal dispersions, nano particles still exist as agglomerates when incorporated in the highly alkaline environment of hydrating cement [278]. The first signs of sintering were observed when the sludge was calcined at 1000^{o}C, as the particles became smoother and rounded. This led to a corresponding decrease in surface area which increased workability in blended cement mortar. Further calcination at 1100^{o}C led to a breakdown of pore walls producing very fine sludge particles, which markedly increased the workability of blended cement mortar.

Table 5- 1: Mix Proportions for Binary Blended Cement Mortar incorporating Alum Sludge

Mix description	w/b	Water (g)	Cement (g)	Alum Sludge (g)	Sand (g)	SP (%)
C	0.55	247.5	450	-	1350	1
CR	0.55	247.5	360	90	1350	1
C475	0.55	247.5	360	90	1350	1
C625	0.55	247.5	360	90	1350	1
C825	0.55	247.5	360	90	1350	1
C1000	0.55	247.5	360	90	1350	1
C1100	0.55	247.5	360	90	1350	1

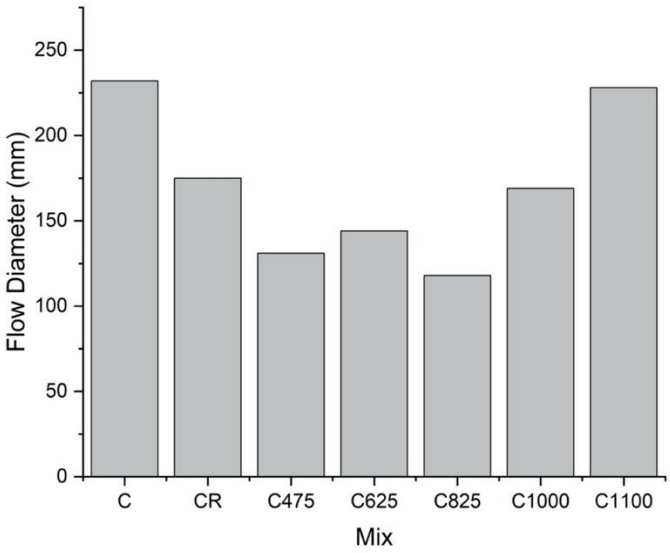

Figure 5- 1: The influence of alum sludge on the workability of binary blended cement mortar

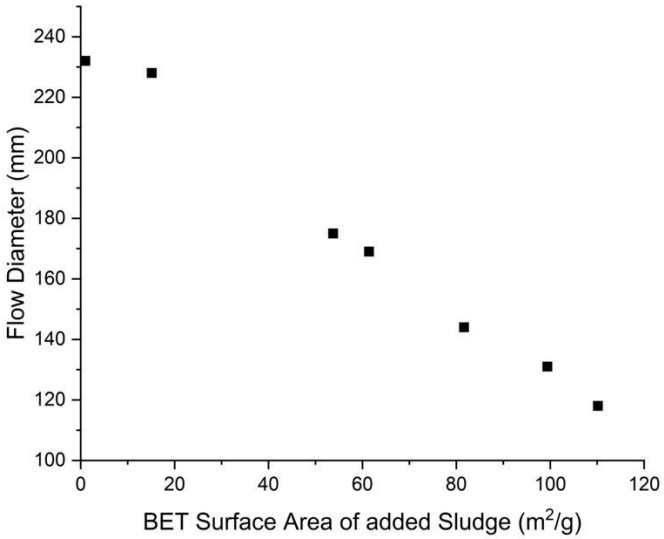

Figure 5- 2: Relationship between measured flow diameters of mortars and surface area of sludge samples

5.1.2 Strength Activity index

To evaluate the pozzolanic activity of alum sludge at different temperatures, Strength Activity Index (SAI) test was performed [242] using the mix proportions defined in Table 5-1. The SAI is defined as the ratio between strength of blended mortar (containing 20% SCM) and the strength in control mortar at 7 and 28 days of curing. Figure 5-3 shows the 7 and 28-day compressive strengths, while Figure 5-4

shows the corresponding SAI. The performance of mortars can be related to the properties of constituent materials discussed in Chapter 4. All blended cement mortars exhibit lower compressive strengths than the neat PC system (control mix). The mechanical strength of blended cement mortars increased with sludge calcination temperature. Mortar samples containing raw sludge gave zero strength at all ages tested. This could be attributed to the 9.8% organic carbon content in the raw sludge. Organic carbon is known to inhibit cement hydration by its adsorption onto hydration products, mainly C-S-H [286]. The 28-day SAI's for sludges calcined at 475^{o}C and 625^{o}C were 50.1% and 58.6% respectively. The increase in SAI could be attributed to only the removal of organic carbon as characterization of sludges at these temperatures showed that no new phases were formed. Mortar containing sludge calcined at 825^{o}C (C825) showed a significant increase in the 28-day SAI to 75.9%, which coincides with the formation of poorly-crystalline η-alumina in the incorporated sludge sample. Calcination of sludge at 1000^{o}C produced finer particles and well-crystallized η-alumina, giving an SAI of 77.1%. The increased fineness and reduced reactivity brought about by crystallization of the alumina suggests that the improvement in strength is mainly due to a filler effect. Calcining sludge at 1100^{o}C produced finer α-alumina particles, possibly increasing the filler effect and corresponding mechanical strength in blended mortar.

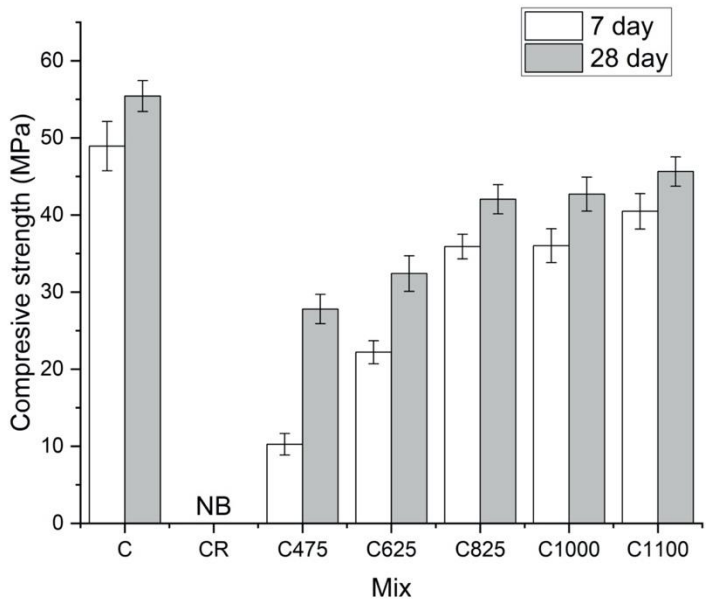

Figure 5- 3: Influence of calcination temperature of alum sludge on compressive strength of blended cement mortars. NB: non-binding

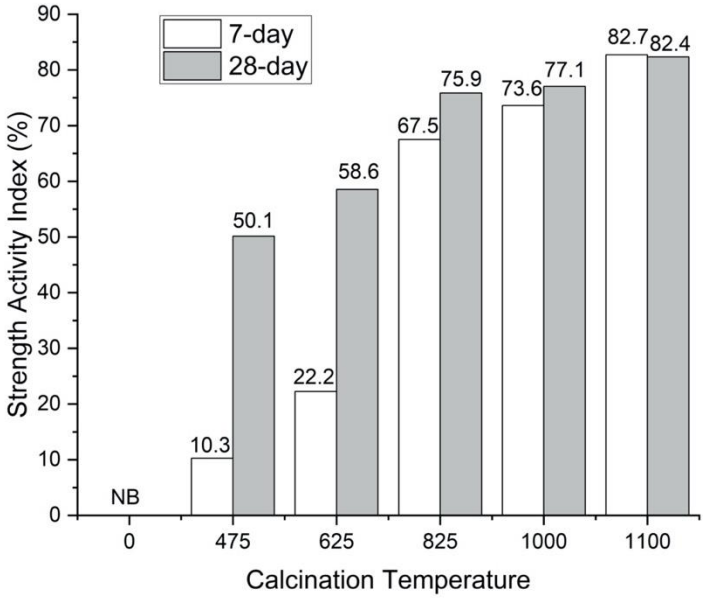

Figure 5- 4: Influence of calcination temperature on Strength Activity Index of alum sludge. NB: non-binding

The effects of alum sludge on strength can be related to the state of agglomeration and mesoporosity within the sludge particles and thus their water retention capacity. This could affect the amount water available for cement hydration. As a result, a lower degree of clinker hydration was observed in pastes containing porous mineral additions due to entrapment of some mix water [287]. On the other hand, mineral additions with lower water absorption capacity result in a higher degree of hydration in cement. In general, at any given replacement level, the workability of cement mixtures would decrease as the surface area of the sludge particles increases. It is well known that increased surface area could significantly enhance cementitious reactivity of SCMs. Nevertheless, the extent of agglomeration and porosity of particles are additional influencing factors [278]. It has been demonstrated that the C-S-H gel precipitated on agglomerated nano-silica particles produces lower mechanical properties than well-dispersed silica nano-particles. The presence of an interparticle transition zone (ITZ) between large agglomerates and the bulk paste has been reported, which acts as a weak zone that decreases the final compressive strength of mortars [278]. Based on these considerations and the fact that calcined sludge at

825ºC has the highest agglomeration state, mesoporosity and flowability, its Strength Activity Index may be adversely affected by these factors.

Furthermore, the strength development can be related to the expected hydration reactions. The dilution effect induced by the 20 w.t% cement replacement reduces the amount of cement to hydrate, which leads to lower compressive strength relative to the neat cement system. Typically, pozzolans compensate for this dilution effect mainly through the reaction between Ca^{2+} within the cement and SiO_2 in the pozzolan to form C-S-H, the main hydrate phase contributing to strength and durability [261]. As observed in chapter 4, the calcined sludges mostly contain alumina (~68%) with silica (~18%) to a lesser degree. Although, the Al_2O_3 content in pozzolans are also known to be reactive with Ca^{2+} to form C-A-H hydrates, these are not a major contributor to strength [288]. It is widely reported that carbonates in limestone can react with aluminates in alumina-rich SCMs and improve mechanical properties [98,99]. The reaction between carbonates and aluminates produces calcium monocarboaluminate and hemicarboaluminate rather than monosulfoaluminate allowing additional sulfate to produce ettringite. This synergistic reaction is not exploited in the investigated blends since the CEM I used does not contain additional limestone. Thus, the chemical and mineralogical composition of the investigated sludge samples and CEM I could explain the lower compressive strength observed in all calcined sludge-blended systems.

It is stated in ASTM C618 that a test material can be considered pozzolanic if the 28-day SAI is higher than 0.75 at the cement replacement level of 20%. Thus, the sludges calcined at 825ºC, 1000ºC and 1100ºC can be considered pozzolans as they meet the 75% SAI threshold. These calcination temperatures were selected for further work investigating the hydration and microstructure of various calcined sludge-blended systems.

5.2 Hydration and microstructure of calcined sludge composites

5.2.1 Mixes Investigated

Thirteen mixes were formulated to investigate the influence of calcined sludge on the kinetics, hydration and microstructure of blended cements. The specific objectives include:

- To determine the influence of calcined sludge on hydration of cement clinker.

- To determine the influence of calcined sludge on microstructure of hydrated cement paste, including types and amounts of hydrates formed (phase assemblage).
- To identify the main properties and characteristics that influence the reactivity of calcined sludge and further cement hydration.
- To determine the relation between microstructure and mechanical strength of calcined-sludge blended cement.

The above objectives were studied in pastes and mortars containing various combinations of CEM I, slag, limestone and sludge calcined at 825, 1000 and 1100^{o}C. Details of the mixes investigated are given in Table 5-2 and the techniques to characterise hydration and microstructure are given in Table 5-3.

Table 5- 2: Mixes for investigating the hydration and microstructure of calcined sludge-blended cements (wt. %)

						Calcined Sludge at:		
Series	Nomenclature	CEM I	GGBS	Limestone	Quartz	825^{o}C	1000^{o}C	1100^{o}C
	C	100	-	-	-	-	-	-
S1	CQ	80	-	-	20	-	-	-
	C825	80	-	-	-	20	-	-
	C1000	80	-	-	-	-	20	
	C1100	80	-	-	-	-	-	20
S2	CS	50	50	-	-	-	-	-
	CSQ	40	40	-	20	-	-	-
	CS825	40	40	-	-	20	-	-
	CS1000	40	40	-	-	-	20	
	CS1100	40	40	-	-	-	-	20
S3	CSL	50	40	10	-	-	-	-
	CSLQ	40	32	8	20	-	-	-
	CSL825	40	32	8	-	20	-	-
	CSL1000	40	32	8	-	-	20	-
	CSL1100	40	32	8	-	-	-	20

Table 5- 3: Experimental matrix for samples under investigation

		Experimental Techniques					
Series	Mix ID	QXRD	Calorimetry	SEM-IA	SEM-EDS	TGA	FTIR
	C	×	×	×	×	×	×
S1	CQ		×				
	C825	×	×	×	×	×	×
	C1000	×	×	×		×	×
	C1100	×	×	×	×	×	×
S2	CS	×	×	×		×	
	CSQ		×				
	CS825	×	×	×		×	
	CS1000	×	×	×	×	×	
	CS1100	×	×			×	
S3	CSL	×	×	×	×	×	
	CSLQ		×				
	CSL825	×	×	×	×	×	
	CSL1000	×	×	×		×	
	CSL1100	×	×	×	×	×	

Three series (S1, S2 and S3) of binary, ternary and quaternary blends incorporating calcined sludge were prepared. In each series the amount of calcined sludge substituted for Portland cement was 20% of the total binder. In each series, an additional blend was prepared with the same 20% amount of inert quartz to decouple the chemical and filler effects of adding calcined sludge. The ternary blends were prepared by replacing cement with 40-20 wt.% slag-calcined sludge. The quaternary blends were prepared by replacing cement with 32-8-20 wt.% slag-limestone-calcined sludge. Series S2 and S3 included a 50-50 wt. % cement-slag and 50-40-10wt. % cement-slag-limestone blends respectively. These mix formulations were chosen to understand the influence of calcined sludge on the hydration of cement composites.

5.2.2 Overview of Hydration

The bound water and portlandite content give a general indication of the progress of hydration but cannot be directly related to the overall degree of hydration [289]. The bound water and portlandite contents were measured for the binary blends at 2, 7 and 28 days of curing and at 7 and 28 days of curing for the other blends. The progress of hydration of Portland cements is usually followed by measuring the increase in portlandite with time. However, the values must be carefully examined to

understand reasons for the observed variations in portlandite content. This is because the presence of pozzolans modifies the ordinary course of cement hydration in different ways. The pozzolanic reaction of traditional SCMs such as slag and fly ash involves the consumption of portlandite to form C-S-H. However, it has also been reported that aluminate additions can have an inhibiting effect on the hydration of clinker but will react with calcium, carbonate and sulfate ions to form AFm and AFt phases [25,27,204,205,290]. This means that a decrease in portlandite content with time might not necessarily suggest the progress of pozzolanic reactions. Thus, the observed portlandite content depends on a number of factors including the degree of clinker hydration as well as the progress of pozzolanic reaction, the composition of hydrates and the type of pozzolan [289].

The formation of portlandite depends on clinker hydration but in blended systems, it would be consumed by the pozzolanic reaction of slag and could serve as a calcium source during the formation AFt and AFm phases [125]. Table 5-4 shows the development of portlandite content in the investigated cement pastes. In the binary calcined sludge-cement blends (series S1), the portlandite contents increased with crystallinity of the sludge but were all lower than in the neat cement system. When normalised back to the Portland cement fraction, only the C825 paste showed a lower level of portlandite compared to the neat cement system. The lower portlandite content in the C825 paste is clearly related to the amorphous alumina present in calcined sludge. In cement pastes incorporating nano-alumina, it was observed that Al^{3+} and SO_3^{2-} immediately react with Ca^{2+} ions to form ettringite [204,205]. Furthermore, it has been reported that the oversaturation of aluminium in the pore solution reduces the extent of alite dissolution [25,27,204]. The pastes containing more crystalline sludges (C1000 and C1100) showed higher portlandite contents than the neat system up 7 days of curing. The increased portlandite content in C1000 and C1100 at early age suggests more of a dilution effect where the more crystalline additions increase the effective water/cement ratio, enhancing clinker hydration. From 7 to 28 days, the CH content per unit cement in C825 and C1000 decreases as it is consumed by the pozzolanic reaction of the amorphous sludge present. Because the C1100 paste contains inert sludge, its portlandite content increases from 7 to 28 days as the pozzolanic reaction is limited.

Table 5- 4: Portlandite and bound water contents in the investigated cement pastes.

			CH Content		Bound Water Content	
Series	Paste	Age	Per 100g anhydrous binder	Per anhydrous PC content	Per 100g anhydrous binder	Per anhydrous PC
S1	C	2	17.0	17.0	20.3	20.3
		7	17.3	17.3	30.6	30.6
		28	24.1	24.1	36.7	36.7
	C825	2	13.1	16.4	24.5	30.6
		7	13.8	17.2	26.2	32.8
		28	12.6	15.8	28.9	36.1
	C1000	2	15.7	19.6	22.6	28.2
		7	18.4	23.0	24.0	30.0
		28	13.7	17.2	30.2	37.7
	C1100	2	15.9	19.8	20.9	26.1
		7	19.1	23.9	23.4	29.2
		28	20.0	25.0	25.9	32.4
S2	CS	7	11.4	22.8	23.4	46.8
		28	10.3	20.6	34.9	69.8
	CS825	7	7.02	17.6	21.6	53.9
		28	4.7	11.4	30.7	76.8
	CS1000	7	8.6	21.4	19.1	47.8
		28	6.5	16.1	26.7	66.8
	CS1100	7	10.4	25.9	18.6	46.4
		28	9.7	24.2	25.0	62.6
S3	CSL	7	10.6	21.3	24.3	48.6
		28	9.2	18.4	29.0	58.0
	CSL825	7	4.7	11.8	24.2	60.6
		28	3.8	9.6	24.7	61.8
	CSL1000	7	6.3	15.6	23.1	57.8
		28	6.4	16.0	29.4	73.4
	CSL1100	7	6.8	17.1	18.8	47.0
		28	7.9	19.7	22.9	57.3

Hydration can be further explained by bound water measurements. At 2 days, all binary systems showed greater bound water contents than the neat system. This could be interpreted as the filler effect of the sludge particles accelerates clinker hydration, causing an increase in C-S-H. At this age, the greater bound water observed in C825 as well as a lower level of portlandite compared to the neat cement system suggests increased early formation of ettringite [194,202,290]. However, at later age, the C825 paste showed lower bound water content per unit cement content

than the neat system. Li et al. [209] and Salvador et al. [200] reported that AFt and AFm phases formed from rapid aluminate reaction with gypsum blocks C_3S dissolution sites and prevents its continued reaction. The bound water content in C1100 were the lowest of those at 7 and 28 days, indicating that the dilution effect of the inert sludge does not compensate for clinker substitution.

The CS paste and all ternary blended cements (series S2) resulted in the formation of significantly lower levels of portlandite than the neat system, since portlandite is produced only by hydrating cement clinker. When normalised back to PC fraction, all blends in series S2 resulted in the higher portlandite content at 7 days. This can be interpreted as an acceleration of clinker hydration at early age due to the filler effect imparted by both slag and calcined sludge. From 7 to 28 days, normalised portlandite contents observed in CS, CS825 and CS1000 pastes decreased and were lower than the neat cement system. This can be attributed to the pozzolanic reaction of both calcined sludge and slag. In contrast, normalised portlandite content in CS1100 paste increased with curing age and was higher than the neat system and all other blends in series S2 at both 7 and 28 days. This suggests that although slag hydration may have occurred, the crystalline calcined sludge imparted a filler effect that promoted portlandite production, compensating for portlandite consumed by pozzolanic reaction of slag. Similar to the trend observed in series S1, the portlandite content observed in series S2 increased with crystallinity of the sludge addition. The observed evolution of portlandite can be further explained by bound water measurements. The bound water contents in series S2 are lower than in the neat cement system but are all greater when normalised to the Portland cement fraction. CS825 paste showed significantly higher bound water content than the neat cement system and all other pastes in series S2. The observed decrease in portlandite in the CS825 paste and the presence of more hydratable aluminates suggests that the significantly higher bound water is due to enhanced pozzolanic reaction as well as formation of AFt and AFm phases. Alumina-rich SCMs react with sulfates to form ettringite which converts to monosulfoaluminate when sulfates are depleted. AFt formation requires a source of calcium so this might explain the significantly lower portlandite in the CS825 paste. Because the sludge contained in the CS825 paste is amorphous, it is expected that it will contain higher amount of dissolved aluminates which can have the mentioned poisoning effect on alite hydration, hence the drastically reduced portlandite content.

The quaternary blends (series S3) showed significantly lower levels of portlandite than the neat cement system and all pastes in series S2 and S3. The observed decrease in portlandite when limestone powder is present indicates the formation of hydration products which consume portlandite such as hemi and/ monocarboaluminate hydrates [11,127]. The portlandite content per mass of clinker is higher in the CSL paste at both 7 and 28 days of curing due to the filler effect of slag. CSL825 paste showed the most drastic reduction in portlandite content in all pastes investigated. This is likely due to the higher dissolution of aluminates provided by the amorphous sludge which reacts with limestone to form carboaluminates, consuming portlandite in the process. Increased portlandite content was observed in CSL1000 and CSL1100 pastes likely due to higher crystallinity of the contained sludge which would have lower reactivity with limestone. The bound water per unit cement content was highest in the CSL825 at 7 days of curing indicative of sludge reaction of limestone. However, at later age, CSL1000 paste showed significantly greater amount of normalised bound water. This is likely due to the enhanced C-S-H due to the filler effect of the contained sludge. The lower bound water in CSL825 paste may also be due to the earlier mentioned poisoning effect of aluminium ions on alite hydration.

The development of bound water and portlandite contents can be interpreted by how the two properties vary as hydration progresses. Bound water increases with hydration of slag, clinker and calcined sludge. Better to say that portlandite contents can increase or decrease due to a number of factors, i.e. increase due to hydration and decrease due to inhibited hydration or consumption in pozzolanic reactions. Thus, at this point, the variation of portlandite and bound water cannot be unambiguously assigned. A deeper investigation was therefore performed to understand the interplay between hydration kinetics, phase assemblage and microstructure of the calcined sludge cement systems.

5.2.3 Early hydration of Calcined-Sludge Composites

5.2.3.1 Influence of Calcined Sludge on Hydration Kinetics

Figure 5-5 shows the calorimetric curves of neat PC and calcined sludge-cement pastes normalized to PC content. The cumulative heat curves indicate that the calcined sludges contribute both a filler and chemical effect, with more crystalline sludges, namely those calcined at 1000^{o}C (C1000) and 1100^{o}C (C1100), exhibiting a

lesser chemical effect on PC hydration. There was acceleration of the alite hydration peak likely due to the provision of additional surface area by sludge particles for the nucleation of hydrates. For the sludges calcined at 1000 and 1100^{o}C acceleration was slight, but there was clear evidence of sludge reaction, seen in the increased total heat evolution. The reaction was ever so slightly greater for the sludge heated at 1000^{o}C, likely due to the inert nature of the corundum formed at 1100^{o}C.

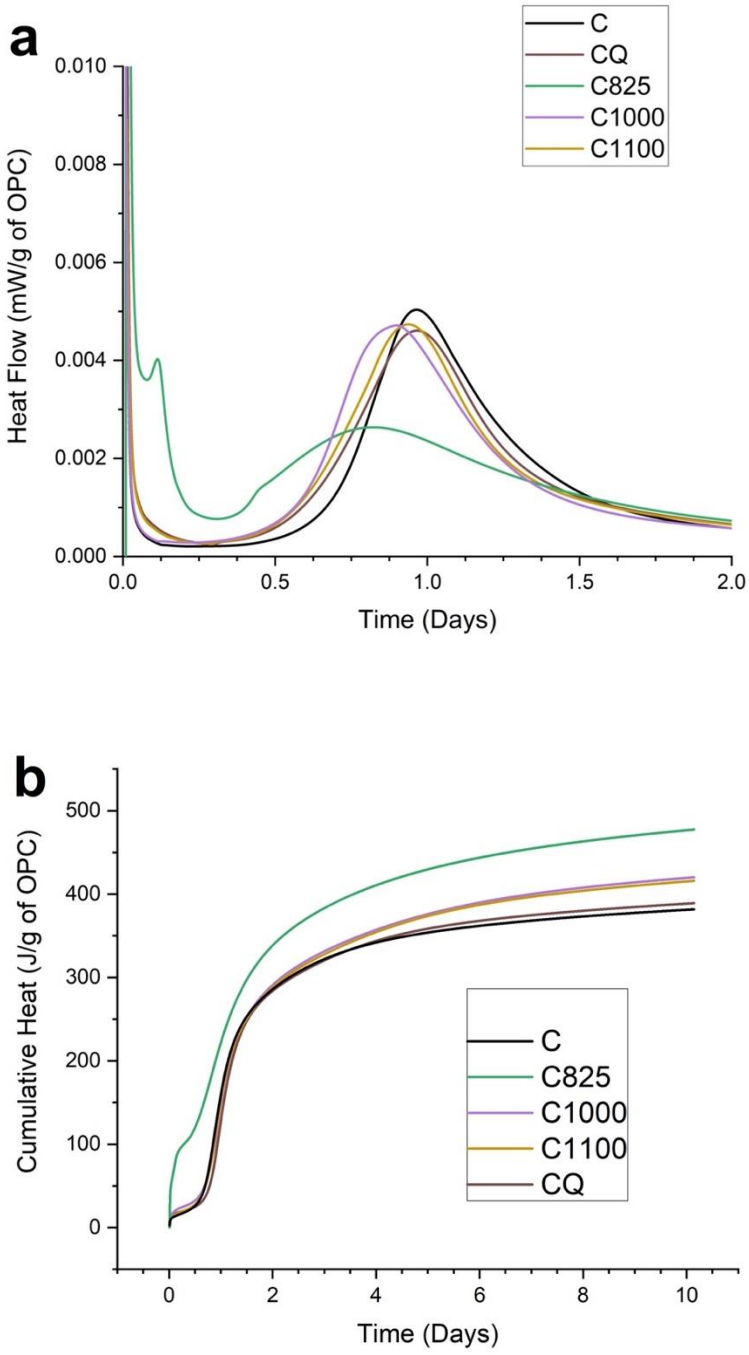

Figure 5- 5: Calorimetric curves of binary cement pastes (series S1) a) Heat Flow rate b) Cumulative heat.

The sludge calcined at 825ºC (C825) showed a marked change in hydration behaviour from pure Portland cement. C825 contains significant quantities of reactive, amorphous aluminates. These led to significant shortening of the induction period. In addition, there was a high initial exotherm and a peak preceding the main hydration peak. The first exotherm is associated with ettringite formation, which induces rapid hardening and early set of cement pastes [201,210]. This was evidenced during mixing of cement pastes where the C825 paste solidified much faster than the others. The amount of ettringite formed during these very early stages is controlled by the concentration of Al^{3+}, C_3A content and gypsum dissolution rate [200]. The rapid reaction between of $[Al(OH)_4]^-$ from the sludge and gypsum to form ettringite accelerates C_3A hydration. This rapid reaction is followed by the conversion of ettringite to monosulfoaluminate after about 3 hours [205]. Because C_3A reacts prior to the onset of silicate reaction, the C825 system is undersulfated [29,205]. Furthermore, the induction period of C825 paste is significantly shortened. This could be attributed to the rapid consumption of Ca^{2+} and SO_4^{2-} which expedites gypsum and alite dissolutions, thereby accelerating the onset of the silicate hydration peak [200,203]. In C825 paste, the main hydration peak was lower and broader. Although, the early AFt precipitation contributes to early space filling, the higher aluminate dissolution rate may have limited alite hydration as observed in a number of studies [25,27,291,292]. Suraneni & Flatt [27] and Nicoleau et al. [291] observed that C_3S doped with aluminium presents a different hydration behaviour from pure C_3S. In the presence of gypsum, aluminates react with sulfate ions, leading to the formation of ettringite. This reaction does not affect C_3S hydration negatively, which proceeds normally [29]. However, when the liquid phase does not contain sulfate ions, aluminium can adsorb on hydroxylated C_3S mainly through strong ionic interactions between aluminate and calcium ions on the surface of silicate. This blocks the reactive sites on alite surface, reducing its solubility and reactivity. Furthermore, Begarin et al. [28] found that when the aluminium pore solution concentration is above 0.005mmol/L, aluminate ions poison the first C-S-H nuclei and prevents them from growing. The heat flow curves in Figure 5-2 show similar inhibition of alite hydration, particularly in the C825 paste, which would contain higher concentrations of aluminates due to its amorphous state. Pustovgar et al. [25] and Suraneni & Flatt [27] found that the inhibiting effect of aluminium on dissolution of alite is highly dependent on pH. Above pH 13, there is very little effect of the aluminium, regardless of the concentration, and

in a pH range of 12–13, the effect depends on the aluminium concentration. At higher pH values, the binding strength of aluminates to hydroxylated C_3S decreases so that its passivating effect and retardation is reduced [25]. The alum sludge investigated in this work has a pH of 7.6. It is expected that its dissolution will lower pore solution pH and hinder alite hydration. In pastes C1000 and C1100, a properly sulfated condition exists because C_3A hydration does not occur before the onset of the silicate hydration peak [29]. The higher crystallinity of the sludges in these mixes limits the dissolution of aluminates from the sludge thereby maintaining sulfate balance. This results in longer induction periods and increased alite hydration.

The calorimetric curves of ternary cements containing slag and calcined sludge (series S2) together with reference mixes C and CS are shown in Figure 5-6. Mix CS (without calcined sludge) shows a clear influence of slag on the hydration of clinker. In the presence of slag, the induction period was slightly shortened with an acceleration of the alite hydration peak. Because slag and clinker had similar BET surface areas, the acceleration is likely due to the consumption of portlandite which enhanced alite dissolution in order to balance the Ca^{2+} concentration in the chemical equilibria [293]. This results in higher silicate ion concentration thereby promoting the nucleation process and the shortening of the induction period. The hydration behaviours of the ternary cement pastes are distinctly different depending on the crystallinity of the sludge added. In ternary paste containing slag and sludge calcined at 1100ºC (Mix CS1100), acceleration was slight and a properly sulfated condition is observed with the occurrence of a shoulder after the maximum heat flow of alite hydration is reached [29,294]. However, in ternary paste containing slag and calcined sludge at 1000ºC (Mix CS1000), C_3A hydration occurs in an undersulfated system which increases the intensity of the main hydration peak [200]. Briendl et al. [295] investigated aluminium sulfate-based accelerators and observed identical heat flow signals, where the first intense exotherm was ascribed to undersulfated C_3A reactions and the second one is the alite hydration peak. In blended cement systems containing aluminate-based accelerators and slag, Salvador et al. [296] observed a similar sharp peak between 1.5 and 3 hours assigned to undersulfated C_3A hydration. It has been suggested that the acceleration of C_3A hydration is linked to the amount of aluminium in the system [297].

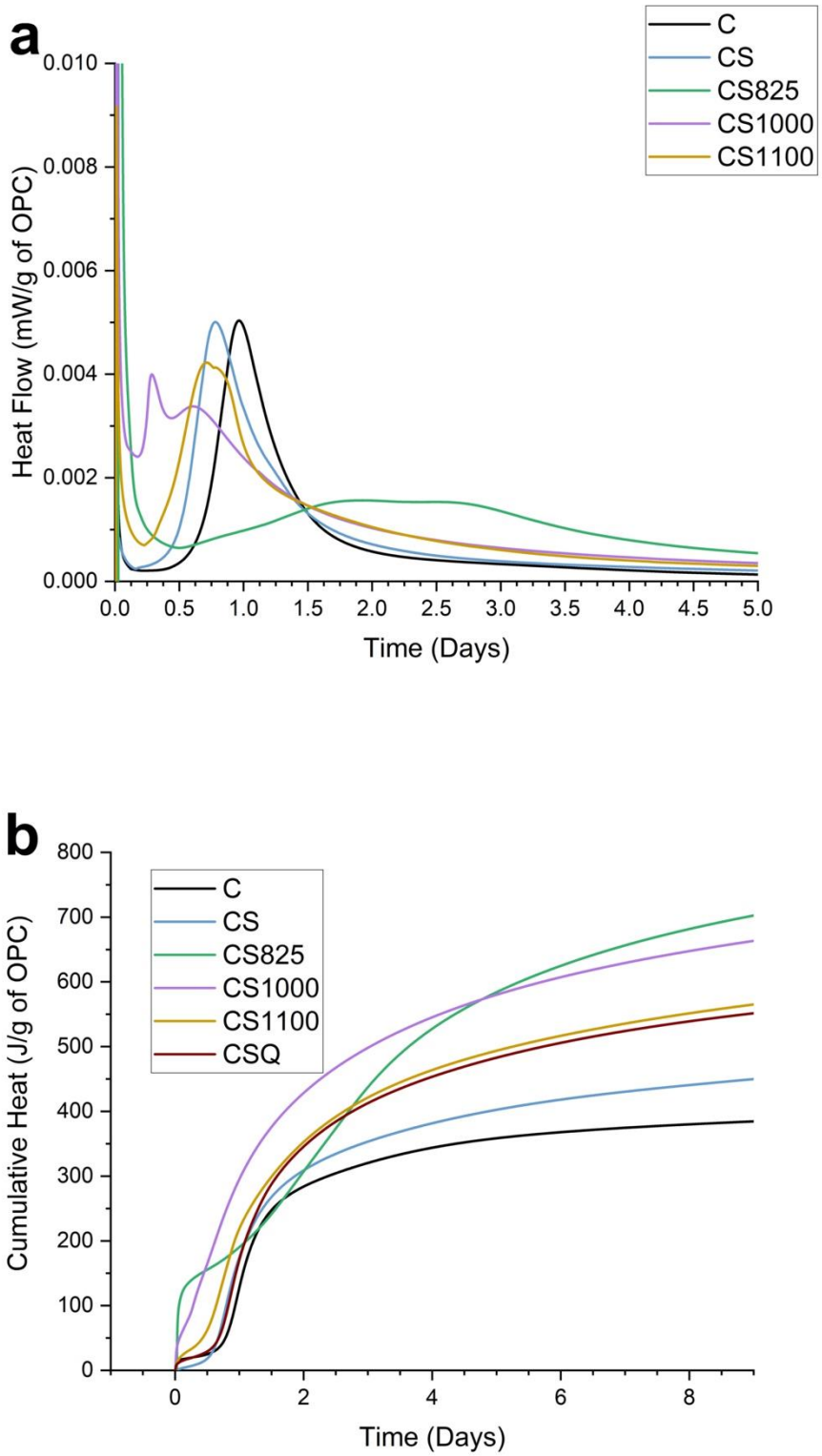

Figure 5- 6: Calorimetric curve of ternary cement pastes (series S2) a) Heat flow rate b) Cumulative heat.

In Mix CS1000, the contained calcined sludge at 1000ºC, provides another source of aluminium in addition to C_3A and slag. At very early age, the presence of aluminium consumes SO_4^{2-} which accelerates C_3A hydration. As observed in series S1, the uncontrolled reaction of C_3A can hinder the silicate reaction. By the depletion of SO_4^{2-} from the liquid phase, aluminium is incorporated in the alite structure which blocks reactive sites, reducing its solubility and reactivity. This explains drastically reduced alite peak in Mix CS1000. The properly-sulfated condition observed in Mix CS1100 is likely due to the inert nature of corundum formed at 1100ºC while the poorly crystalline eta-alumina in Mix CS1000 dissolves leading to the observed undersulfated condition. In comparison to the binary blends (series S1) discussed earlier (Figure 5-5), the presence of slag in ternary pastes may also explain the observed decreases in the overall hydration rate because slag is less reactive than clinker minerals. The replacement of cement with both slag and calcined sludge reduced the overall sulfate content in the paste thereby accelerating C_3A hydration. Since the amorphous sludge contained in Mix CS825 is more reactive, the impact of undersulfated C_3A reaction is more significant leading to a greater inhibition of alite hydration. This results in an even lower and broader main hydration peak in CS825 paste compared to earlier discussed C825 paste. An additional blend (CSQ), was prepared without calcined sludge but instead with the same amount inert quartz filler to decouple the physical and chemical effects of calcined sludge on hydration of Mix CS. The difference in cumulative heat (Figure 5-6b) between mix CS and Mix CSQ is due to the filler effect. Naturally, the difference in cumulative heat between the respective ternary calcined sludge blends (e.g CS825) and the ternary quartz blend (CSQ) is due to the hydration of the calcined sludge. The cumulative heat curves indicate that the calcined sludges contribute both a filler and chemical effect, with more crystalline sludges, namely those calcined at 1000ºC and 1100ºC, exhibiting a lesser chemical effect on hydration of Mix CS.

In Figure 5-7, the calorimetric curves of quaternary blends containing slag, limestone and calcined sludge are shown, together with reference mixes C and CSL. It can be seen that even in the presence of limestone, the mix containing calcined sludge at 1000ºC (CSL1000) still exhibits undersulfated C_3A reaction denoted by the exothermic peak at ~3 hours. Similar finding were reported by Briendl et al. [295] in pastes containing aluminium sulfate-based accelerators and limestone. The kinetics of aluminate reactions is generally more rapid with sulfates than with carbonates. This means that even in an excess of carbonates, an undersulfated condition can still occur.

The authors observed that pastes containing limestone powder still exhibited an undersulfated condition with an earlier and more intense C_3A hydration peak compared to blends without limestone.

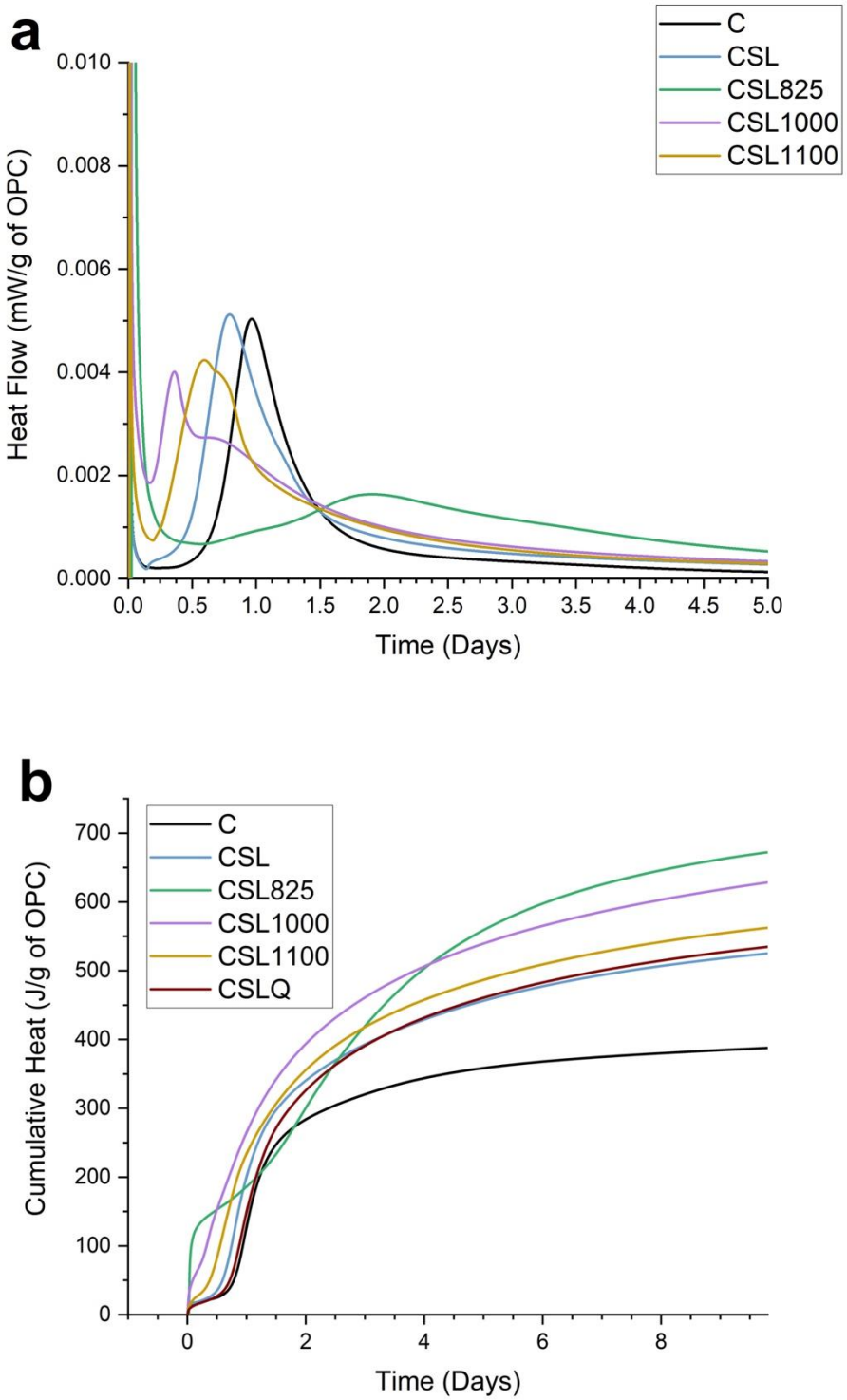

Figure 5- 7: Calorimetric heat curves of quaternary cement pastes a) Heat flow rate b) Cumulative heat.

It is suggested that at sufficient Ca^{2+} concentration (i.e. in the presence of limestone), sulfate ions are adsorbed on C-A-S-H surface and are not able to passivate C_3A surface. When sulfate reaches a critical level, C_3A starts to dissolve faster and sulfate ions desorb from C-A-S-H and react together to form ettringite or AFm phases. This means that when limestone is present, there is a higher adsorption of sulfate ions on C-A-S-H compared to neat PC systems. This leads to faster sulfate depletion and earlier C_3A reaction [53]. This explanation is also applicable in the investigated systems in this work where the undersulfated C_3A reactions occurred in CSL1000 paste even though limestone is present. The fact that a properly sulphated condition exists in CSL1100 (containing inert sludge) paste suggests that the additional aluminium provided by the sludge in CSL1000 plays a role in sulfate depletion and subsequent undersulfation. In addition, the replacement of cement with slag, calcined sludge and limestone reduced the overall sulfate content in the paste, thereby accelerating C_3A hydration. Briendl et al. [295] observed that in aluminium sulfate-based cement pastes containing 25% wt. limestone and an additional 7% wt. gypsum, proper sulfation occurs as C_3A hydration occurs after the main hydration peak; Whereas blends with 25% wt. limestone with no additional gypsum led to undersulfated C_3A reactions. In both cases, there was no difference in the extent of silicate hydration peak which suggests undersulfated C_3A reactions only hinder silicate reaction in the absence of limestone. It is inferred that a competition for Ca^{2+} ions is the reason for the lower silicate hydration peaks in the case of undersulfated C_3A reactions in the absence of limestone [295]. The limestone provides Ca^{2+} which are consumed by the aluminates provided by the sludge for the formation of calcium bearing hydration products (AFm and AFt phases). Without limestone, the additional calcium need for the formation of monosulfoaluminate has to be consumed from the pore solution which results in competition for calcium ions need for the formation of C-A-S-H phases. In addition, a drop in pH due to sludge addition favours the blocking of C_3S dissolution sites which hinders C_3S hydration. Consequently, it has been suggested that hindered silicate hydration due to competition for calcium ions can be prevented by incorporating higher doses of both limestone and gypsum [295].

An additional blend (CSLQ), was prepared without calcined sludge but instead with the same amount inert quartz filler to decouple the physical and chemical effects of calcined sludge on hydration of Mix CSL. The difference in cumulative heat (Figure 5-7b) between mix CSL and Mix CSLQ is due to the filler effect. Naturally, the

difference in cumulative heat between the respective quaternary calcined sludge blends (e.g CSL825) and the quaternary blend with quartz (CSLQ) is due to the hydration of the incorporated calcined sludge. The cumulative heat curves indicate that the calcined sludges contribute both a filler and chemical effect, with more crystalline sludges, namely those calcined at 1000^{o}C and 1100^{o}C, exhibiting a lesser chemical effect on hydration of Mix CSL.

Figure 5-8 shows a comparison of heat flow curves of C825, CS825 and CSL825 pastes to highlight the influence of sludge calcined at 825^{o}C in different pastes. As discussed earlier, the main hydration peak of all cement pastes is suppressed due to undersulfated C_3A reactions, leading to inhibition of alite hydration. As the C825 contains higher amount of silicates due to lower clinker replacement, the extent of silicate hydration is the greatest. The CS825 paste contains significant aluminates contributed by the both slag and sludge, leading to more significant inhibition of alite hydration. However, in the quaternary CSL825 mix, the extent of silicate hydration is slightly increased owing to the presence of limestone, similar to findings reported in literature [205,295]. It is likely that limestone reacts with Al^{3+} ions from the sludge to form hemi and mono-carboaluminates. In addition, limestone can compensate for sulfate depletion caused by increased dissolution of aluminates from the sludge thereby reducing the inhibiting effect of aluminates on silicate hydration [205].

The influence of calcined sludge on aluminate reaction suggests that the level of calcium sulfate addition should be re-optimized for a blended cement rather than the using the same calcium sulfate clinker ratio contained in the neat Portland cement Antoni et al. [124] found that optimization of gypsum addition could increase one day strength in a blend with clinker and limestone by more than 50% compared to just having the sulfate clinker ratio in the neat Portland cement. The observations of this section suggest a competition between silicate and aluminate reactions. C_3A reaction is significantly affected by calcined sludge, particularly the more amorphous sludge at 825^{o}C which contains higher hydratable Al^{3+} concentration. The composition of the calcined sludge is expected to have an effect on AFt and AFm formation, and clinker hydration. This will affect mechanical strength development.

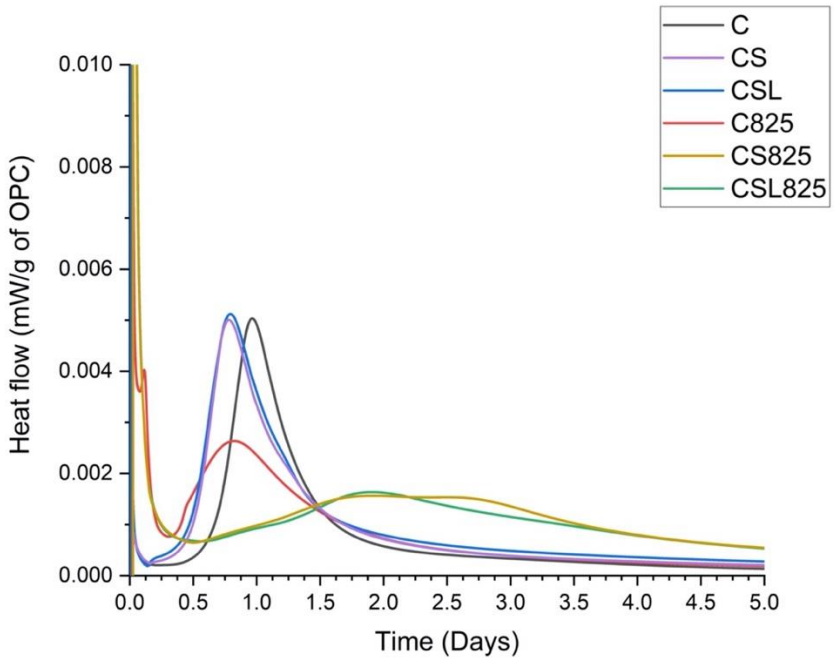

Figure 5- 8: Calorimetric heat curves of composite cement pastes containing calcined sludge.

5.2.3.2 FTIR Analysis

To corroborate calorimetry results on early formation of AFt in the presence of calcined sludge, Figure 5-9 presents the FTIR spectrum of binary calcined sludge cement pastes at approximately 12 hours. Prominent absorption bands appear at about 3640cm^{-1} and 3397cm^{-1} assigned to the stretching vibration of O-H in portlandite and symmetrical stretching υ2H_2O of capillary water [298]. The absorption band at 1109cm^{-1} represents the υ3SO_4^{2-} in ettringite or gypsum. The peak at approximately 872cm^{-1} is assigned to Al-O-H bending vibrations in AFt [299,300] and has the highest intensity in the C825 paste, which indicates that the most amount of ettringite has been formed due to reaction of the amorphous aluminium phase in the calcined sludge. This increased formation of ettringite identified by FTIR confirms calorimetry results that amorphous alumina in the 825^{o}C consumes gypsum to form AFt at very early age.
Other major bands at wavenumbers 450cm^{-1} assigned to bending vibrations of Si-O-Si and O-Si-O due to inert quartz in the calcined sludge additions; 1655 cm^{-1} is assigned to υ2H_2O; the band at 1410 cm^{-1} is related to calcium carbonate [301] due to carbonation during sample preparation and testing.

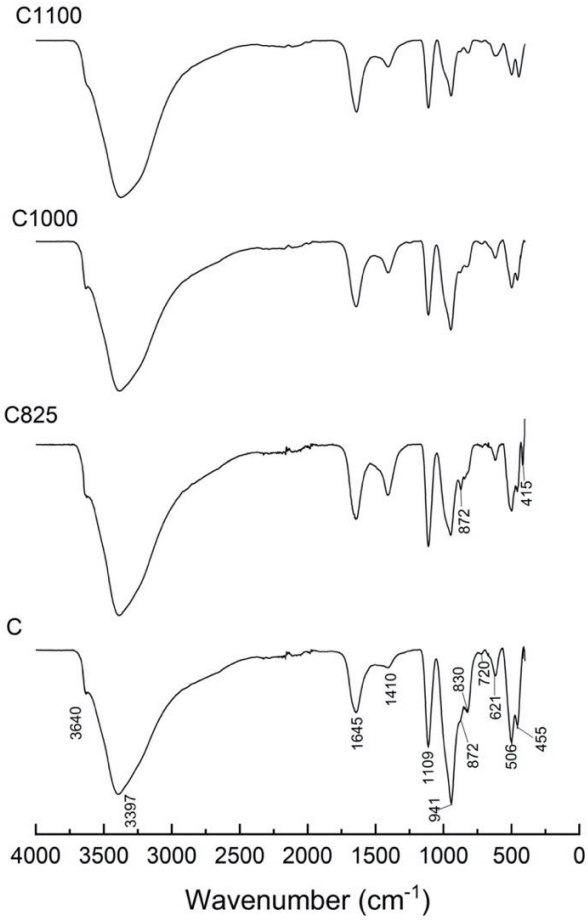

Figure 5- 9: FTIR Spectra of binary cement pastes at 12 hours of hydration.

5.2.4 Degree of Hydration of Clinker in Composite Cements

Hydration of the main clinker phases in cement pastes was followed by XRD-Rietveld refinement (Table 5-5). From this data the degree of clinker reaction was determined as described in section 3.2.5.8.8. The phase contents of major clinker phases in anhydrous cement: C_3S, C_2S, C_3A and C_4AF were 58, 20, 2.8 and 9.8% respectively, giving a total of ~90.6%. Gypsum content was 5.1%.

The small initial C_3A content led to its complete reaction within 7 days of curing in all systems. Ferrite hydration was modest, with about 80 to 90% reacted after 28 days. The trends indicated accelerated aluminate and ferrite reaction in blended systems. These effects are consistent with earlier discussed calorimetry plots where undersulfated C_3A reactions were observed. However, the content of aluminate and ferrite phases in the pastes are rather low and their relative error will be large, rendering interpretation of these results difficult.

Table 5- 5: Evolution of clinker phases in all investigated systems relative to anhydrous content in wt %

		Time (d)	C_3S	C_2S	C_3A	C_4AF	DoH PC (XRD)	DoH PC (SEM-IA)	DoH Slag (SEM-IA)
	C	0	58	20	2.8	9.8			
		2	10	17.4	0.8	5.9	62.3		
		7	6	15.1	0	5.2	70.9		
		28	3.2	12.1	0	2.2	80.7	88.7	
Series S1	C825	0	46.4	16	2.2	7.8			
		2	16.5	15.4	0	5.1	48.8		
		7	10.4	11.5	0	3.7	64.6		
		28	8.5	9.2	0	1.2	73.9	80.4	
	C1000	0	46.4	16	2.2	7.8			
		2	13.4	15.2	0.4	5.6	52.2		
		7	9.2	13.3	0	4.1	63.2		
		28	5.1	8.2	0	1.1	80.1	88.0	
	C1100	0	46.4	16	2.2	7.8			
		2	8	14.9	0.7	4.5	61.2		
		7	5.1	12.1	0	1.9	73.6		
		28	0.7	9.2	0	0.7	85.3	88.9	
Series S2	CS	0	29	10	1.4	4.9			
		7	2.9	8.1	0	3.1	68.9		
		28	0.5	6.9	0	1.1	81.2	85.4	49.3
	CS825	0	23.2	8.0	1.12	3.92			
		7	11.0	7.6	0	1.4	44.8		
		28	3.6	5.6	0	0.4	74.6	78.3	23.4
	CS1000	0	23.2	8.0	1.12	3.92			
		7	6.8	7.0	0	1.1	58.8		
		28	3.4	5.1	0	0.5	75.1	72.3	32.1
	CS1100	0	23.2	8.0	1.12	3.92			
		7	4.4	6.1	0	0	71.0		
		28	1.2	4.4	0	2.1	84.5		
Series S3	CSL	0	29	10	1.4	4.9			
		7	3.0	7.9	0.4	1.1	72.6		
		28	0.7	7.1	0	0	82.8	90.2	57.2
	CSL825	0	23.2	8.0	1.12	3.92			
		7	7.1	7.3	0	0.28	60.2		
		28	2	6.1	0	0	77.6	79.4	45.3
	CSL1000	0	23.2	8.0	1.12	3.92			
		7	5.5	7.3	0	0.8	62.4		
		28	3.1	6.3	0	0	74.1	77.3	52.5
	CSL1100	0	23.2	8.0	1.12	3.92			
		28	0.2	4.9	0	0.6	84.2	89.0	53.1

The effect of SCMs on the hydration degree of clinker can be split between early and late regime at 7 and 28 days respectively. In the binary systems, at early age, the degree of clinker reaction (series S1) was higher in the C1100 paste than in the neat system, likely due to the filler effect of the contained inert sludge. However, C825 and C1000 pastes exhibited lower clinker hydration, likely related to their amorphous aluminium content. At 28 days of curing, the same trend was observed where the C1100 paste exhibited higher clinker hydration than the neat system. However, comparable degrees of clinker hydration were observed in the neat system, C1000 and C1100 pastes with 80.7, 80.1 and 85.3% respectively while the C825 paste maintained a significantly lower clinker hydration of 73.9% at 28 days.

For mixes in series S2, the clinker hydration at early age was exceptionally low in CS825 and CS1000 pastes with 44.8 and 58.8% respectively. However, clinker reaction in Mix CS1100 (71.0%) surpassed both reference mixes C (70.9%) and CS (68.9%). At 28 days of curing, the degrees of clinker hydration were C (80.7%), CS (81.2%), CS825 (74.6%), CS1000 (75.1%) and CS1100 (84.5%). A consistent trend can be observed where the extent of clinker hydration increases with crystallinity of the sludge addition. This suggests that the dissolution of aluminates play a significant role in the observed inhibition of clinker hydration. From 7 to 28 days, mixes CS825 and CS1000, exhibited a tremendous increase in clinker hydration. This difference can be explained by the pH sensitive inhibition of alite reaction by aluminium ions [25,27,291]. In freshly mixed cement paste, Al^{3+} ions from calcined sludge are converted into $[Al(OH)_4]^-$ which leads to a drop in initial pH [200]. Pustovgar et al. [25] and Nicoleau et al. [291] established that aluminates adsorb on the C_3S surface mainly through ionic interactions of aluminium and calcium ions on the surface of silicate. With the progress of hydration, higher pH and calcium concentrations are achieved and the binding strength of aluminates to the C_3S surface decreases so that its passivating effect, and retardation, is reduced.

For mixes in series S3, the addition of limestone led to enhanced clinker hydration, particularly in the CSL825 paste. It is argued that the earlier described inhibition of C_3S hydration in the absence of limestone is due competition for Ca^{2+} ions [295]. In the absence of limestone, the additional calcium needed for the formation of AFm phases has to be consumed from the pore solution which results in competition for calcium ions needed for the formation of C-A-S-H phases. When limestone is present, the aluminates from the sludge react to form AFm phases. As a result, the

adsorption on aluminium ions on the silicate surface is reduced and higher degrees of hydration are achieved.

The degree of hydration clinker at 28 days of curing was also determined by SEM-IA (Table 5-5). Compared to the results from XRD-Rietveld analysis, SEM-IA slightly overestimates the degree of hydration of clinker, probably due to the exclusion of small anhydrous particles not identified by SEM-IA [223]. Overall, there is reasonable agreement between the two methods. The quantification results are consistent with earlier discussed portlandite contents and calorimetric heat. Generally, the findings suggest decreased reaction of clinker in the presence of amorphous sludge.

5.2.5 Hydration of Slag in Composite Cements

The degrees of hydration (DoH) for slag are presented in Table 5-5, determined by SEM-IA at 28 days' hydration. The degree of reaction for reference mix CS was 49.3%, similar to values reported elsewhere for a similar composition [88]. The pastes CS825 and CS1000 showed significantly lower slag reaction, with 23.4 and 32.1% respectively. Slag reactivity is dependent on several factors including slag loading, composition, fineness, w/b ratio and solution pH [73]. Because these factors are constant in the calcined-sludge blends in each series, this suggests that the composition of the calcined sludge has a major influence on slag reaction. The retardation of slag hydration in CS825 and CS1000 may be related to the low portlandite content in the blends (Table 5-4), and consequently a lower solution pH. Generally, the solubility of amorphous silica in SCMs is very sensitive to increases in pH between 12 and 14 [73]. The SCM replacement level in the calcined sludge-slag blends is high (60%), implying that pH will drop, reducing the solubility of the amorphous silicates and thus slowing the rate of reaction. The higher the pH, the faster the rate of reaction. As earlier mentioned, the amorphous aluminates (eta alumina) present in the CS825 and CS1000 consumes hydroxyl ions in solution leading to a drop in pH. This hinders C_3S reaction and consequently pozzolanic reaction of slag. Furthermore, slag hydration in limestone-containing (series S3) cements were greater. It is well established that a synergistic reaction occurs between carbonates in limestone and alumina in slag to form hemi- and mono- carboaluminates [237]. In the composites studied, limestone enhances slag hydration by raising solution pH for slag

dissolution, promoting formation of portlandite for pozzolanic reaction and synergic reaction with aluminates for carboaluminate formation.

5.2.6 Limestone reaction in Composite Cements

The results presented thus far suggest limestone plays a reactive role in the composite cements. Carbonate-AFm phases are more stable than sulfate-AFm and prevent the decomposition of ettringite to monosulfoaluminate after sulfate depletion. As a result, it is favourable to increase the limestone content in blended cements. The amount of limestone that can react in a given matrix is determined by the availability of aluminium and calcium. The calcium carbonate contents in the studied pastes were measured by TGA. The consumed carbonate was calculated by subtracting the residual calcium carbonate from the initial content. There is a small amount of calcium carbonate in the slag sample (3.23 wt. %) and this was accounted for when calculating the total amount of carbonate consumed in the blends.

As shown in Figure 5-10, the degree of reaction of limestone after 7 days was 16.26% in Mix CSL and significantly higher in the composite systems with 64.1%, 32.6% and 18.4% reacted in CSL825, CSL1000 and CSL1100 respectively. This means that more calcite was consumed in the presence of calcined sludge, and increasingly so with amount of amorphous aluminate present. The higher reactive alumina contents in the various sludge blends alters the reaction pathway and leads to increased formation of carboaluminates instead of monosulfoaluminates, thereby stabilizing ettringite. After 28 days, the amount of reacted carbonate was only slightly increased with a consumption of 21.4%, 69%, 38.9 and 25.3% in CSL, CSL825, CSL1000 and CSL1100 respectively. The higher dissolution of calcite at early age is related to the lower pH induced by calcined sludge compared to neat cement [96,302]. Calcite dissolution is enhanced in order to balance the Ca^{2+} concentration in the chemical equilibria. It is important to note that this could raise pH to levels where calcite dissolution may be inhibited. However, such effects are most likely counteracted by the additional aluminates provided by calcined sludge [290]. Furthermore, the accelerated rate of calcite reaction at early age, particularly in CSL825 paste, may be related the faster rate of sulfate depletion induced by the incorporated sludge. Bizzozero & Scrivener [100] observed that when there is excess sulfate (i.e. above 50 mol% in pore solution) in respect to aluminate, ettringite is more stable than carbonate AFm therefore limestone is not consumed. The tremendous

calcite reaction in the presence of calcined sludge is however contrary to the limited reactivity widely reported in literature [96,100,303,304]. Puerta-Falla et al. [305] investigated the role aluminous source on the reactivity of limestone in blended cement systems. The authors found that calcium aluminate cements, despite their significant aluminium content, show very little, if any, reactivity with limestone. This suggests a significant role of aluminium source (i.e. not just aluminium content) in enhancing limestone reaction in cement systems. Of all aluminous agents studied including metakaolin, the authors found that an amorphous 'hydratable alumina' is the most reactive in enhancing limestone reaction. They defined hydratable alumina as "a finely divided, amorphous substance produced via a calcination process." This description compares well with the alum sludge calcined at 825^{o}C, showing similar increased reactivity with limestone compared to conventional SCMs.

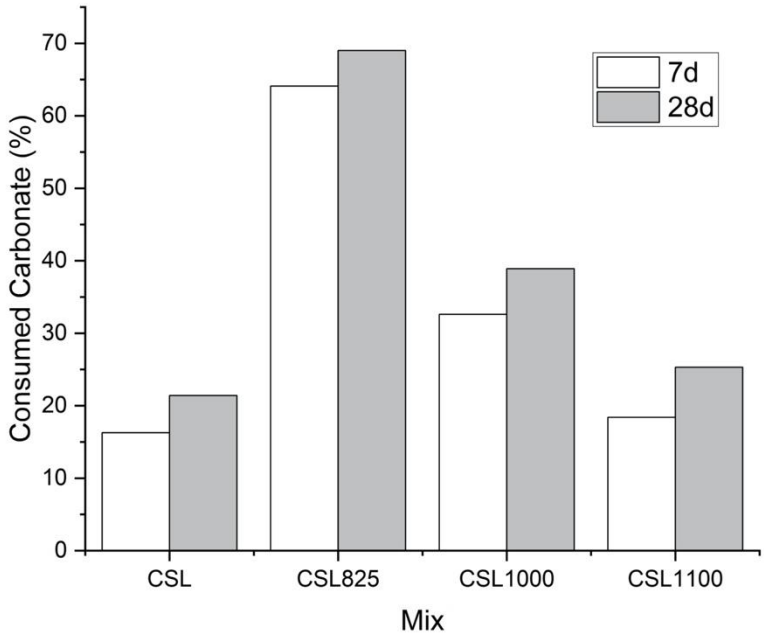

Figure 5- 10: Degree of limestone reaction in composites cements

5.2.7 Phase assemblage of composite cements

5.2.7.1 Experimental evidence from TGA and XRD

An indication of the hydrated phases formed was obtained from the TGA and XRD data presented in Figures 5-11 through to 5-16. The DTG plots show that the main hydrated phases were C-S-H, ettringite and portlandite, identified by peaks at

around 100-200ºC, 100ºC and 450ºC respectively. A shoulder at the right-hand side of the peak at 100ºC indicates the formation of AFm phases [290]. The peaks above 600ºC are due to decarbonation of calcite, indicative of residual calcite in limestone-blended cements or slight carbonation of portlandite in all systems. The evolution of AFt and AFm phases, as determined by XRD Rietveld analysis, is shown in Table 5-6. The observed humps in the XRD patterns are the low angle artefacts described in section 3.2.5.8.5.

Table 5- 6: Evolution of AFt and AFm phases in investigated blends.

Series	Mix ID	Time (d)	Ms	AFt	Hc	Mc
	C	2	0.3	7.3	0	0
		7	1.3	8.2	0.7	0
		28	1.7	12	1.2	0
Series S1	C825	2	1.1	10.2	1.1	0.7
		7	9.9	5.0	0	0
		28	16.8	2.9	0	0
	C1000	2	0.47	9.6	1.2	0.6
		7	9.8	6.8	0.7	0
		28	11.0	4.6	0.5	0
	C1100	2	0.06	9.5	0.8	0
		7	1.9	7.0	0.4	0
		28	8.2	3.8	0.5	0.5
Series S2	CS	7	0.3	4.9	5.0	3.7
		28	0.3	8.5	5.4	4.0
	CS825	7	1.1	3.2	4	6.9
		28	1.4	2.7	7.1	6.6
	CS1000	7	1.2	3.4	6.4	4.5
		28	0.6	3.7	5.5	4.0
	CS1100	7	0.1	8	6.5	1.7
		28	0.3	5.7	1.7	4.7
Series S3	CSL	7	0.2	4.8	2.72	4
		28	0	6.6	3.6	4.7
	CSL825	7	0.3	12.6	16.0	10.5
		28	0	8.8	11.0	11.5
	CSL1000	7	0.1	7.5	8.2	5.3
		28	0	7.8	6.1	9.8
	CSL1100	28	0	4.1	1.0	7.7

Figure 5-11 shows the DTG curve for binary blended cement pastes. The main differences between the binary-blended cements and the neat system are the more intense AFm peaks and reduced portlandite contents in the calcined sludge blends, particularly in Mix C825. As discussed earlier in the calorimetry results, mix C825, which contains significant quantities of reactive, amorphous aluminates, rapidly reacts with gypsum to form ettringite at very early age. The depletion of gypsum accelerates C_3A hydration which leads consumption of ettringite to form monosulfoaluminate as early as 3hrs. This early formation monosulfoaluminate explains the more intense AFm peak in the DTG curve. The more crystalline sludges had a lesser accelerating effect on C_3A hydration, hence the lower intensities of the AFm peaks. Furthermore, it was earlier shown that undersulfated condition induced by amorphous sludge led to inhibited C_3S hydration which explains the lower portlandite content. The XRD patterns (Figure 5-12) and quantification results (Table 5-6) confirms the influences of calcined sludge on phase assemblage. At 28 days of curing, ettringite is virtually consumed in the Mix C825 paste and a significant amount of monosulfoaluminate is observed. Conversely, the neat system contains increased ettringite due to a more controlled C_3A reaction in the absence of calcined sludge.

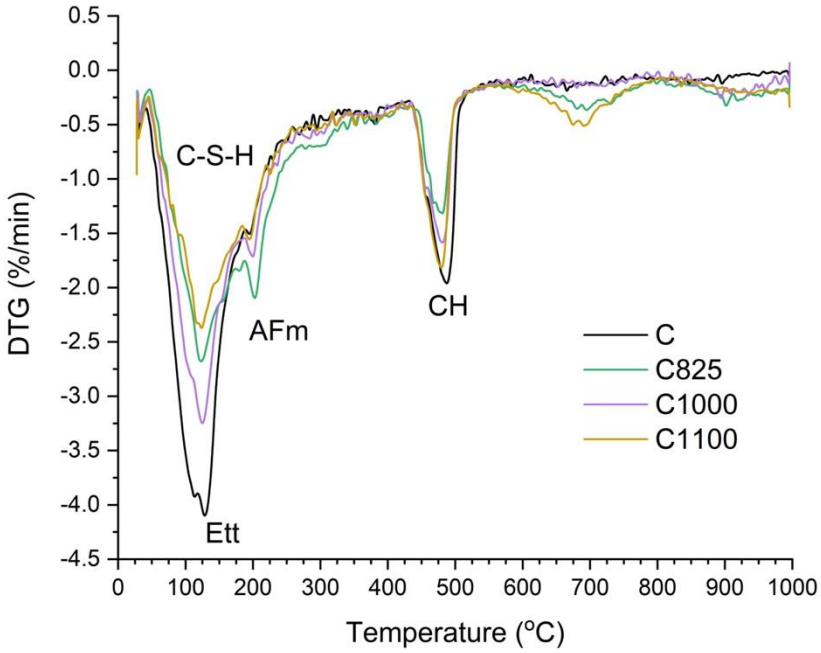

Figure 5- 11: DTG curves of binary blended composites studied hydrated for 28 days.

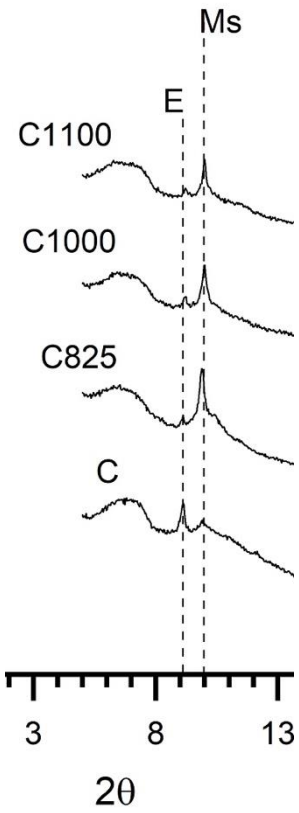

Figure 5- 12: XRD pattern for binary blended pastes hydrated for 28 days

Figure 5-13 shows the DTG curve for ternary blended cement pastes consisting of cement, slag and calcined sludge. Similar to the binary blends, the ternary blends show more prominent AFm peaks and lower portlandite contents than the neat system. The XRD patterns (Figure 5-14) indicate that the AFm phases formed are hemi- and mono-carboaluminates. This may have resulted in significant consumption of portlandite as the formation of carboaluminate phases consumes portlandite. The presence of calcium carbonate in the slag sample reduces ettringite dissolution when sulfate is depleted. Generally, aluminates will react with carbonates to form the AFm phases monocarboaluminate and hemicarboaluminate instead of consuming ettringite to form monosulfoaluminate. However, the calcium carbonate content in the slag sample used is small (3.23 wt.%), so it is possible that the carboaluminate hydrates formed are also a result of carbonation of C-A-H phases [306,307]. Therefore, the AFm peak in the DTG curves was most intense in the paste containing sludge calcined at 825^{o}C suggesting higher carboaluminate formation. Quantitative analysis of ettringite and carboaluminate phases (Table 5-6) confirms differences in the aluminate bearing phase assemblages. The ettringite content of reference mix CS was the

highest. On the other hand, the ettringite content, particularly in the CS825 and CS1000 pastes, were low even with carboaluminate formation. It is not clear why, but this could be related to the higher aluminate content contained in the sludges. Because calcium carbonate content in slag is small (3.23 wt.%), the significant unreacted aluminates in the sludge may have expedited C_3A reaction leading to the consumption of ettringite. It is important to note that AFm phases are sensitive to hydration stopping and often lose their crystallinity. Therefore, XRD analysis of them is difficult and not too quantitative [308].

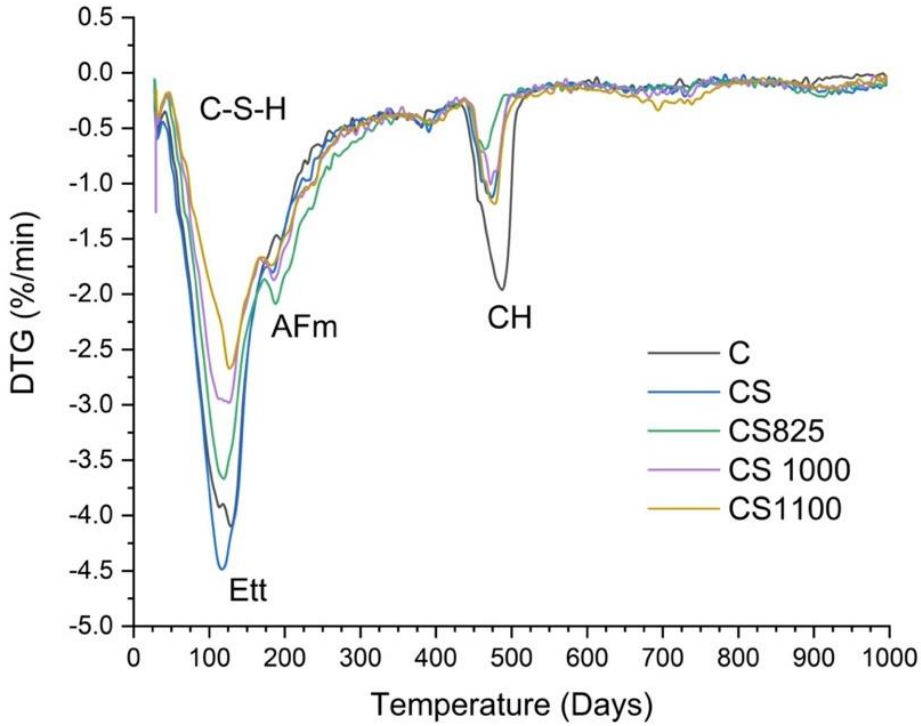

Figure 5- 13: DTG curves of ternary blended composites hydrated for 28 days.

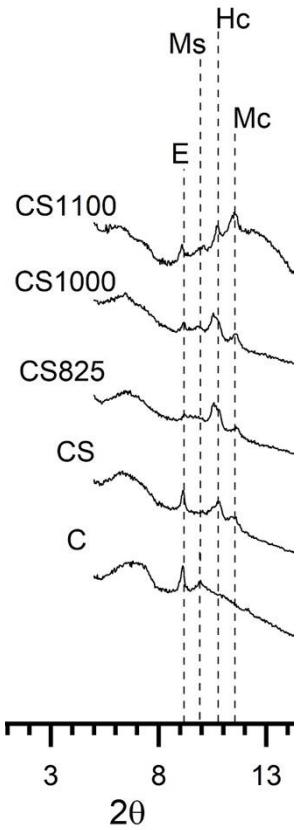

Figure 5- 14: XRD pattern for ternary blended pastes hydrated for 28 days.

Figure 5-15 shows the DTG curve for quaternary blended cement pastes consisting of cement, slag, calcined sludge and limestone. The intense AFm peak in the CSL825 paste suggests significant reactivity of limestone in the presence of amorphous sludge. The AFm peak was smaller in pastes containing more crystalline sludge additions, suggesting reduced carboaluminate formation. This is consistent with XRD results (Table 5-6 and Figure 5-16). The reactivity of limestone is evident from the carboaluminate evolution, and the controlling mechanism can be deduced. It is speculated that in the presence of sludge calcined at 825^{o}C, the formation of hemicarboaluminates may be a consequence of the larger supply of aluminate [$Al(OH)_4^-$] species, which serves in a charge balancing role, and therefore suppresses CO_3^{2-} abundances in solution ensuring the precipitation of hemicarboaluminates at the expense of monocarboaluminate. Substantial quantities of [$Al(OH)_4^-$] are ensured by the high pH of the pore solution and the amorphous nature of the sludge calcined at 825^{o}C, which renders it amenable to dissolution [305]. As hydration progresses, hemicarboaluminate transforms to monocarboaluminate given the higher stability of the latter. Thus, the high consumption of limestone suggests that amorphous sludge is most efficient in provoking carboaluminate formation. This supports the idea that,

unlike slag-blended systems where the pozzolanic reaction is also a major contributor to strength, when amorphous sludge is added, its reactivity is mainly controlled by the presence of limestone.

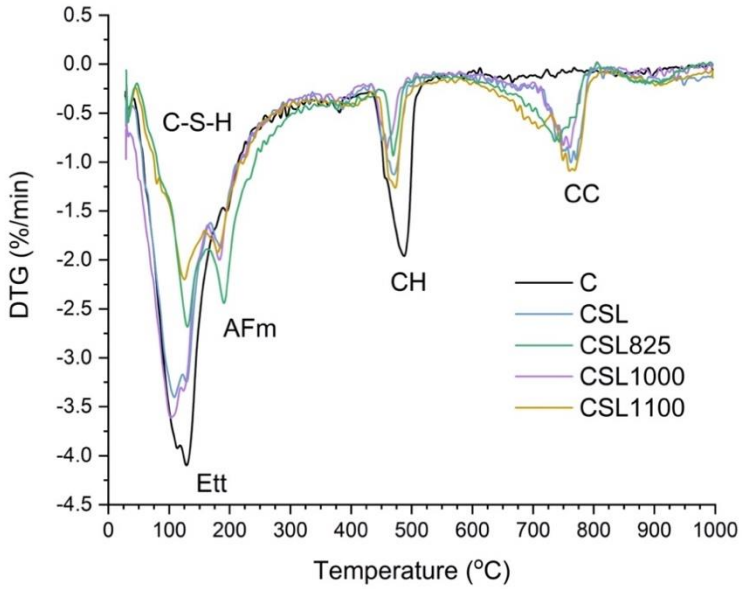

Figure 5- 15: DTG curves of quaternary blended composites hydrated for 28 days

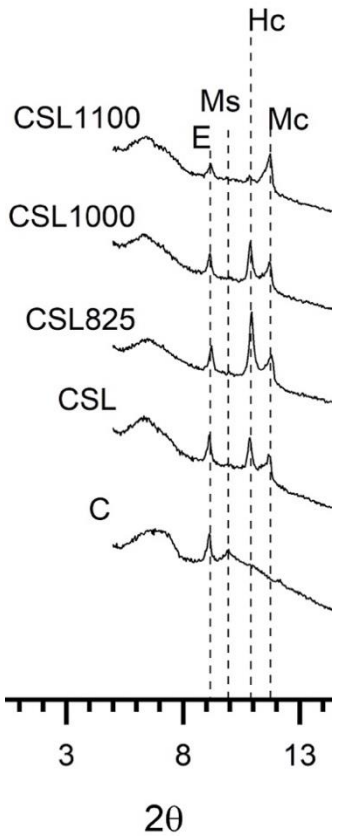

Figure 5- 16: XRD patterns of quaternary cement pastes hydrated for 28days.

5.2.7.2 C-S-H Composition by SEM-EDS

SEM-EDS analysis was used to determine the elemental composition of the C-S-H. Figure 5-17 through to Figure 5-23 compares the Al/Ca and Si/Ca atomic ratios for selected cement pastes. As explained in Section 3.2.5.7, the Al/Si ratio of C-S-H is defined by the slope of a line drawn through the points with lowest Al/Ca ratio; while the Ca/Si ratio is taken as the point along this line at the high Si/Ca edge of the cloud of data points. To minimise intermixing, only inner-product C-S-H was analysed.

Table 5-7 summarizes the Ca/Si and Al/Si atomic ratios. The Ca/Si and Al/Si ratios of the neat PC system were ~1.88 and 0.06 respectively. Similar Ca/Si have been reported elsewhere [88,309]. Clinker replacement resulted in changes in C-S-H composition. In the case of C825, the Ca/Si ratio decreased to 1.83 while the Al/Si ratio increased to 0.10. In the C1100 which contains virtually inert sludge the C-S-H composition was closer to the neat system with Ca/Si ratio and Al/Ca ratios of 1.85 and 0.06. This suggests that the incorporation of sludge calcined at 825^{o}C causes a more significant shift in C-S-H composition due to the higher reactivity and amorphous content present. The distinct change is due to significant number of aluminates contributed by sludge in the pore solution. Previous reports have shown that alumina incorporation in C-S-H is strongly influenced by the alumina availability rather than Ca/Si ratio of C-S-H [48,64,310]. In addition, the decrease in Ca/Si ratio in the C825 paste could also be influenced by the earlier observed inhibition of alite. This limits portlandite formation thereby limiting calcium concentration in the pore solution. However, the results show that there is no significant difference in Ca/Si ratio in the binary blends. The differences are generally small and are likely due to experimental error. As explained in section 3.2.5.7, SEM analysis results in a larger interaction volume which results in intermixing of analysed phases leading to inaccurate representation of C-S-H. Richardson and Groves [50] observed that although microanalysis using an Electron microprobe analyzer (EMPA), a method that works like an SEM, gives Ca/Si ratio consistent with those found with TEM, it was impossible to obtain EMPA analyses of single-phase C-S-H without intermixing of phases. Thus, it can be inferred that the slight differences in Ca/Si ratio particularly in the binary blends are not likely to be statistically significant.

The addition of both slag and calcined sludge in ternary cement (CS1000) showed a marked reduction in Ca/Si ratio to 1.63 and an increase in Al/Si ratio to 0.11. As the incorporated sludge is mainly crystalline, the observed variation is attributed to the alumina in slag. These values are similar to those reported in literature; where the effect of slag on C-S-H composition is well documented [88,91]. The higher alumina contributions (by slag and sludge) would affect the buffering capacity of pastes where the long-term portlandite content may be virtually zero. The resulting pH set by C-S-H will be lower and also the Ca/Si ratio of the gel and this affect the corrosion of steel in the paste [91].

The samples containing limestone showed a decrease in Ca/Si ratio compared to the neat system as reported elsewhere [311]. The Ca/Si and Al/Si ratios of Mix CSL was 1.54 and 0.06 respectively. Mix CSL1100 had a similar composition with Ca/Si and Al/Si ratios of 1.51 and 0.07 likely due to inert nature of the sludge addition. In the case of CSL825, Ca/Si was 1.55, similar to other limestone blends but as expected Al/Si ratio increased considerably to 0.14 likely due to amorphous sludge present. The decrease in Ca/Si, even in the presence of limestone, demonstrates that the calcium content in C-S-H depends not on calcium availability but on the aluminium and silica content in that phase. This is supported by Richardson & Groves [50] who demonstrated that the amount of cations such as calcium ions in C-S-H decreases with increasing aluminium which replaces the silicon. For the incorporation of additional aluminium in C-S-H, more silicon is needed. These alterations are accompanied by increasing polymerization of aluminosilicate chains and charge balancing by additional interlayer calcium ions.

The observed changes in the chemistry of C-A-S-H is likely to have an effect on the development of microstructure and in turn durability of cementitious systems. As discussed earlier in the calorimetry results, the acceleration of clinker hydration by sludge calcined at 825^{o}C will lead to the formation of low Ca/Si C-A-S-H that progressively fills pore spaces with hydrates. In addition, the low packing density of C-A-S-H with low Ca/Si ratio will increase the densification of pore spaces [310]. This characteristic will have an impact on transport properties, which depend on the nature and packing of hydrates in the pore spaces. Furthermore, recent investigations on the mechanisms of sulfate attack have indicated that aluminium is mobilized from C-A-S-H phases in hardened paste made with PC/fly ash and contributes to the formation of ettringite [66,67].

Table 5- 7: Ca/Si and Al/Si atomic ratios of inner product C-S-H Phase obtained by SEM-EDS

Mix	Ca/Si	Al/Si
C	1.88	0.06
C825	1.83	0.10
C1100	1.85	0.06
CS1000	1.63	0.11
CSL	1.54	0.06
CSL825	1.55	0.14
CSL1100	1.51	0.07

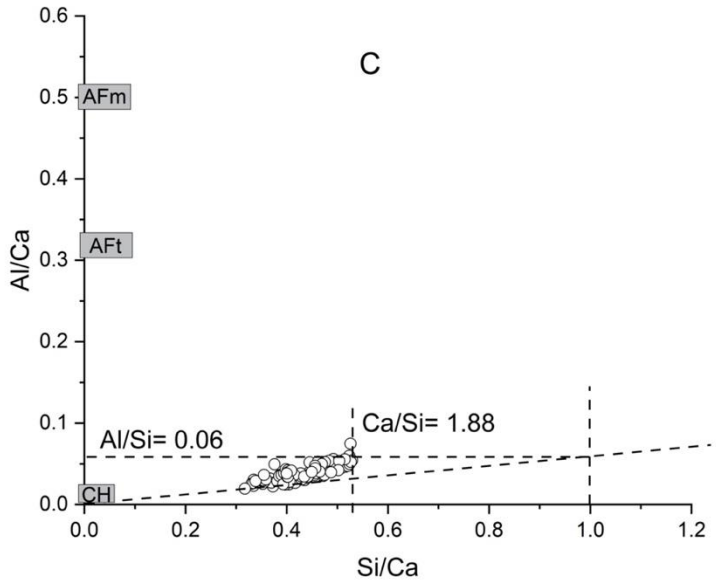

Figure 5- 17: Al/Ca v Si/Ca for neat cement cured for 28 Days.

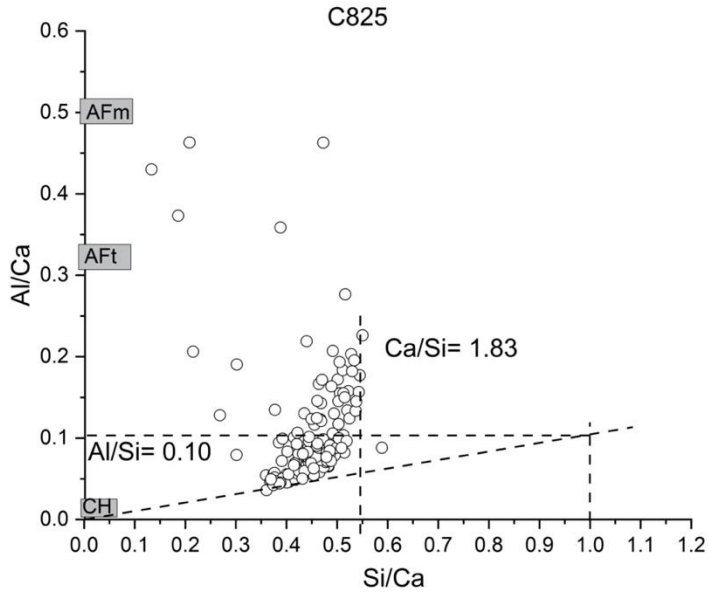

Figure 5- 18: Al/Ca v Si/Ca for C825 cured for 28 Days.

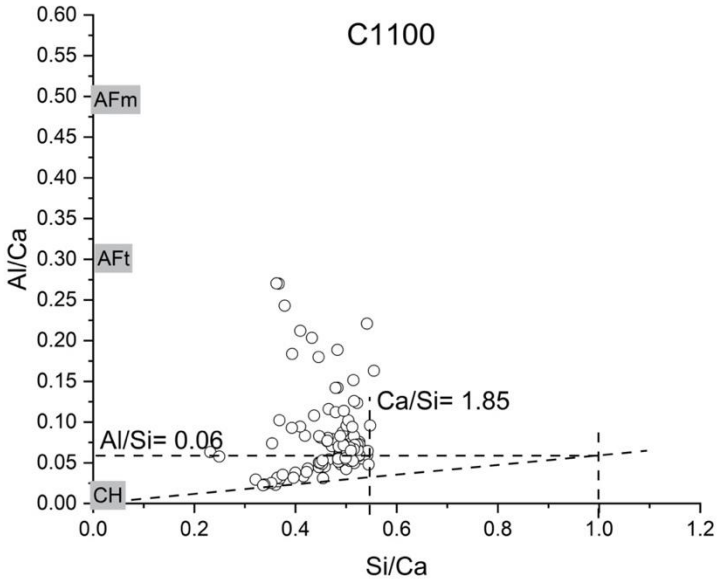

Figure 5- 19: Al/Ca v Si/Ca for C1100 cured for 28 Days.

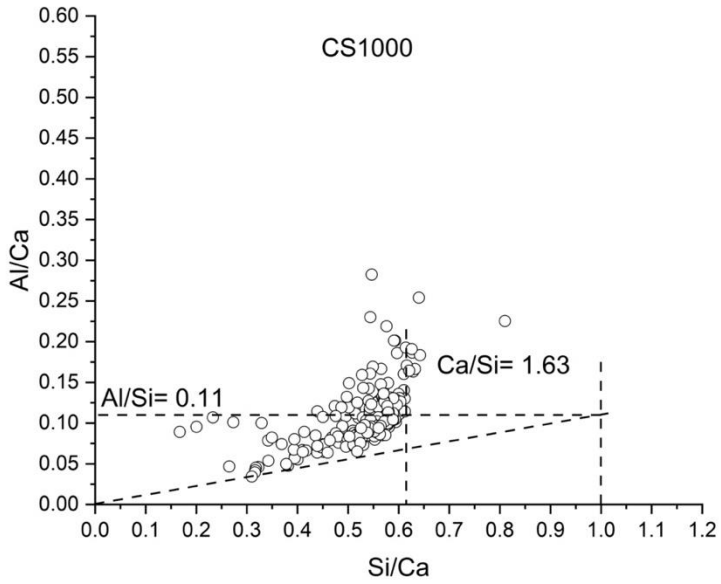

Figure 5- 20: Al/Ca v Si/Ca for CS1000 cured for 28 Days.

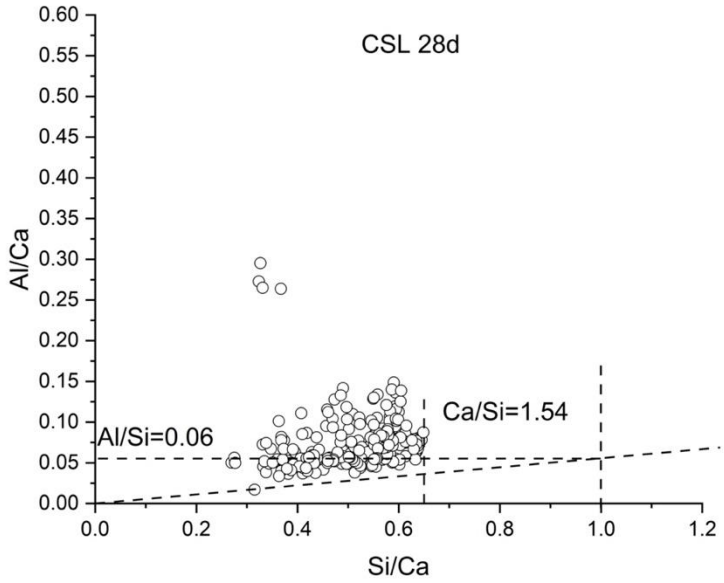

Figure 5- 21: Al/Ca v Si/Ca for CSL cured for 28 Days.

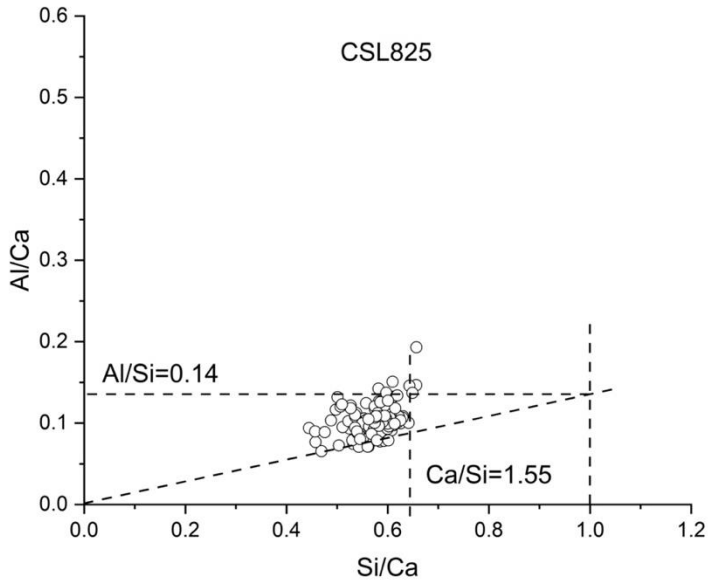

Figure 5- 22: Al/Ca v Si/Ca for CSL825 cured for 28 Days.

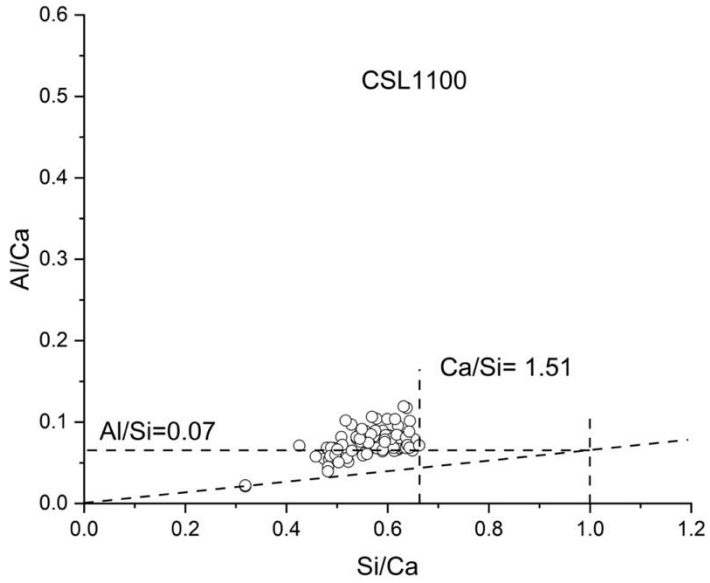

Figure 5- 23: Al/Ca v Si/Ca for CSL1100 cured for 28 Days.

5.2.7.3 Microstructure of blended cements

An important factor affecting the strength and durability of cementitious systems are the microstructural characteristics, comprising anhydrous phases, hydrated phases and capillary pores. Backscattered electron (BSE) images taken at 800x magnification were used to qualitatively assess microstructural variations in blended cement pastes cured for 28 days.

Figure 5-24 shows BSE images of the neat cement pastes together with binary blended pastes (series S1). The images show the presence of partially hydrated cement particles, C-S-H, portlandite and pores. Ettringite is characterized by a lot of small cracks. This is due to the the presence of a vacuum during sample preparation and imaging, which removes water from this phase thereby causing shrinkage and cracking [100]. The visibly higher degree of clinker hydration in the neat system is consistent with SEM-IA, XRD and TG results. Portlandite is abundant in the neat system and clusters from small to large can be observed. The high w/b ratio (0.55 and 1% SP) used increases the capillary pores because initial dispersion of cement grains by water leads to the divergence of hydrated phases in the pore spaces to produce a porous cement matrix. Consistent with earlier findings, C825 and C1000 pastes show a lower extent of clinker hydration with the presence of large portions of anhydrous cement grains and large number of discrete pores. There is significantly less portlandite in the C825 paste with rather large clusters forming. In addition to the degree of hydration of cement, the physical characteristics of SCMs such as particle size, shape and density) will also influence the compactness of the cement matrix. These physical properties are even more relevant where less reactive materials are incorporated in cement. Image analysis of BSE images was used to determine the coarse porosity of cement pastes at 7 and 28 days and the results are presented in Figure 5-25. From 7 to 28 days, the coarse porosity of all cement pastes decreased as hydration progressed. After 28 days, Mix C825 showed a higher porosity than the neat cement paste, indicating that increased AFm formation does not compensate for the reduced degree of hydration. As shown in Chapter 4, sludge calcined at 825^{o}C is irregularly shaped so the filling effect will be slight. Incorporation of sludge calcined at 1000^{o}C reduced porosity more than that calcined at 825^{o}C, due to its smooth and rounded shape which enables better dispersion and space filling of the matrix. The addition of sludge calcined at 1100^{o}C further decreased porosity owing to the finer

particle size. Because its particle was finer than the cement particles, its addition filled voids between cement particles, increasing the packing density.

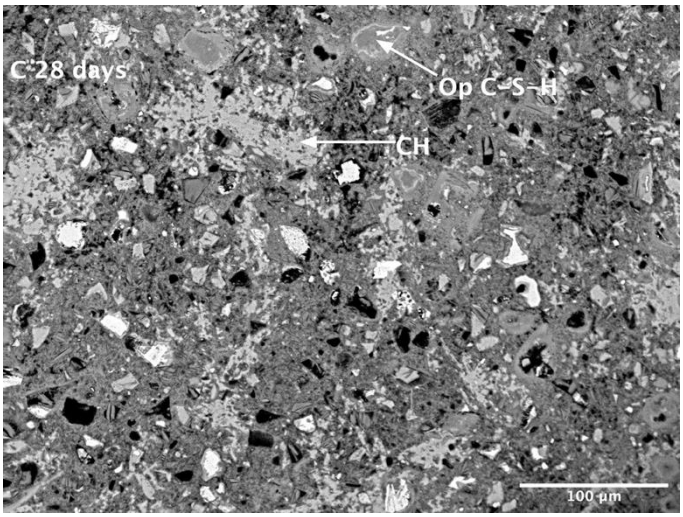

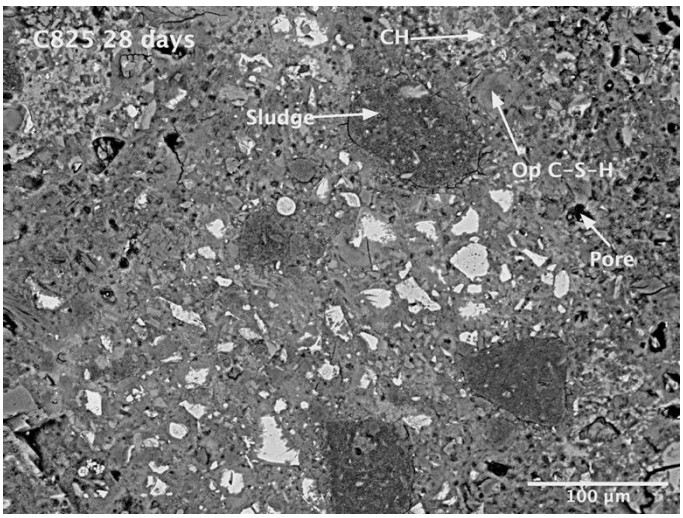

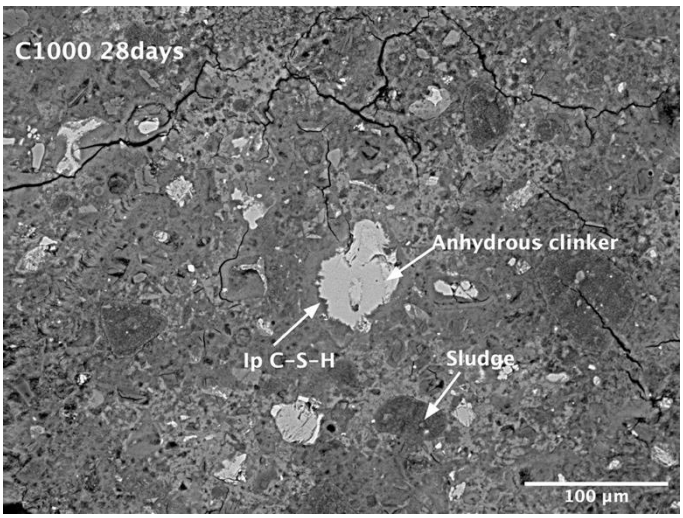

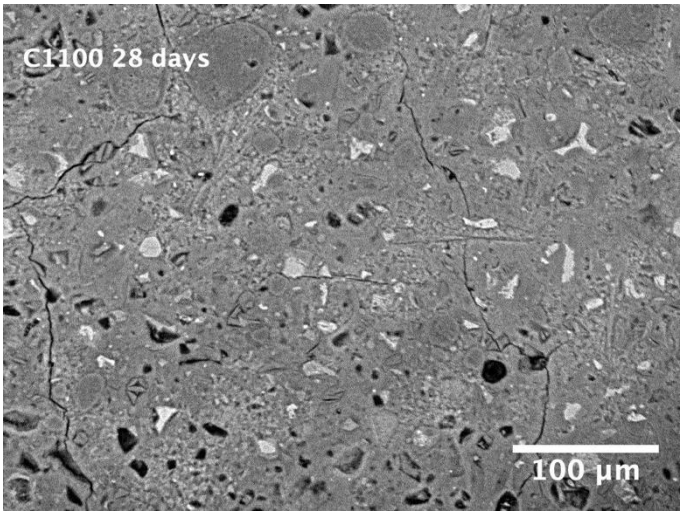

Figure 5- 24: SEM-BSE images of C, C825, C1000 and C1100 pastes hydrated for 28 days (images captured at 800x, field of view is approximately 450 x 340µm).

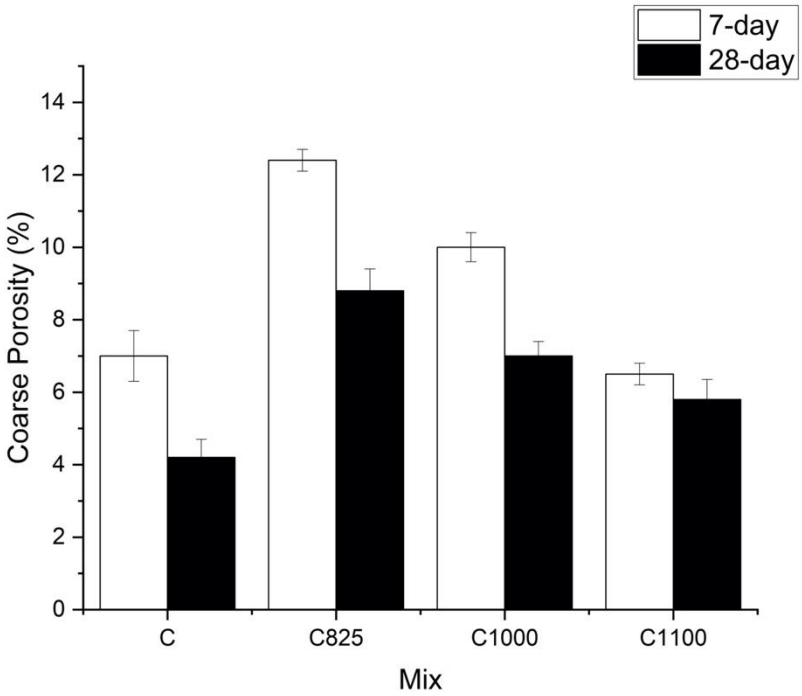

Figure 5- 25: Coarse porosity of calcined sludge-blended cement pastes at 7 and 28 days.

Figure 5-26 shows the BSE images of the slag-blended cement pastes (series S2 and S3) hydrated for 28 days. The variation in coarse porosity of these pastes is presented in Figure 5-27. The microstructure of Mix CS showed the presence of increased outer-product C-S-H and less portlandite than the neat cement system due to the pozzolanic reaction of slag. Because fineness of slag is similar to that of cement,

the higher extent of clinker hydration is likely due to the dilution effect induced by the slow reacting slag particles. This slow reactivity and the high w/b ratio used led to increased porosity. At later ages, as slag reaction progressed, increased filling of pores was expected to reduce porosity. Due to the earlier mentioned inhibition alite hydration in the presence of excess aluminium, C-S-H and portlandite were only present in small amounts in CS825 and CS 1000 which resulted in increased porosity. The addition of limestone promoted the hydration of clinker as increased clusters of C-S-H and portlandite can be observed in the limestone blends. Porosity was particularly lower in the CSL825 likely due to increased reactivity of limestone in the presence of amorphous sludge which leads to formation of carboaluminate phases. In contrast, Mixes CSL1000 and CSL1100 showed large clusters of unreacted limestone powder indicative of the lower reactivity of aluminates in the sludge additions.

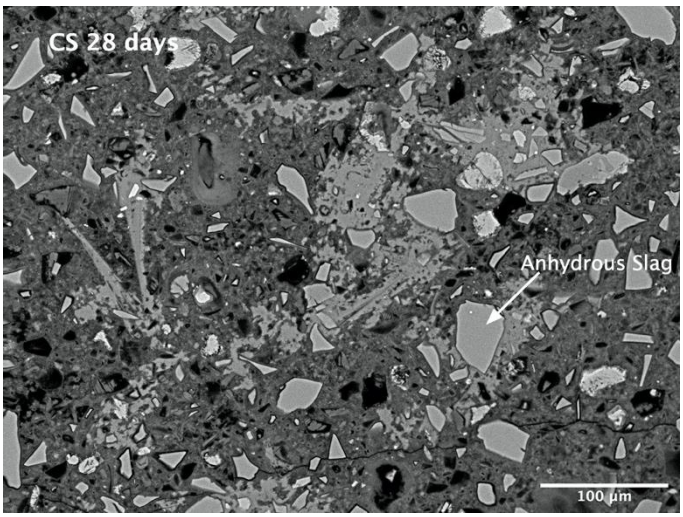

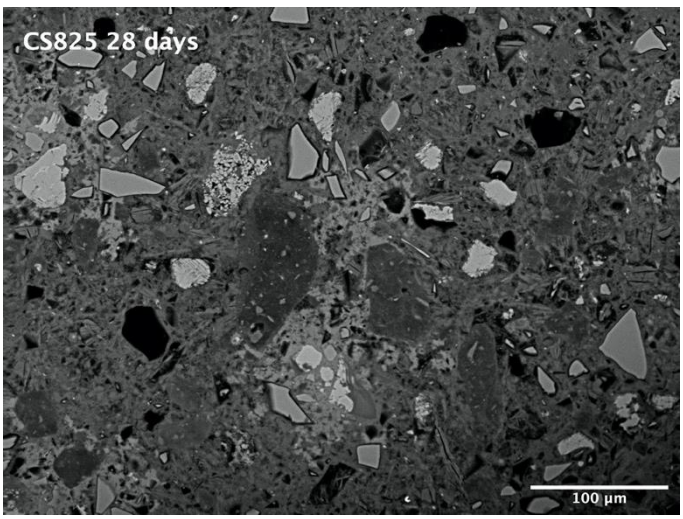

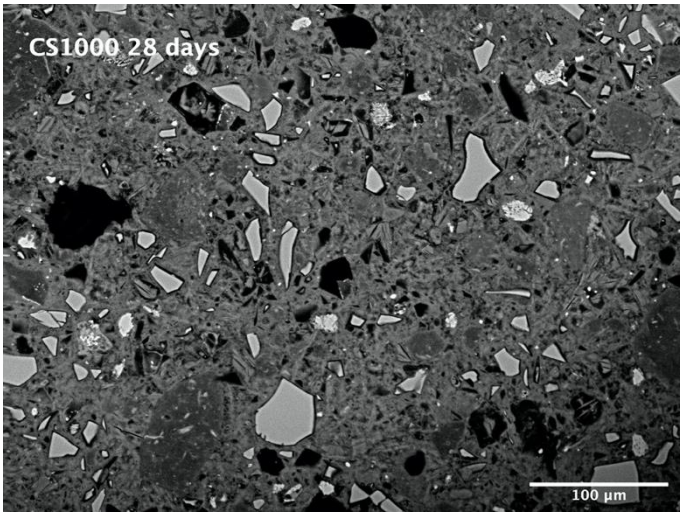
CS1000 28 days
100 µm

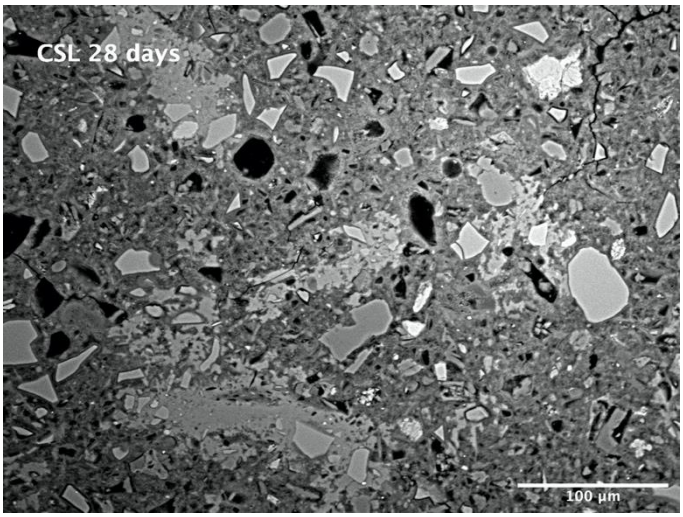
CSL 28 days
100 µm

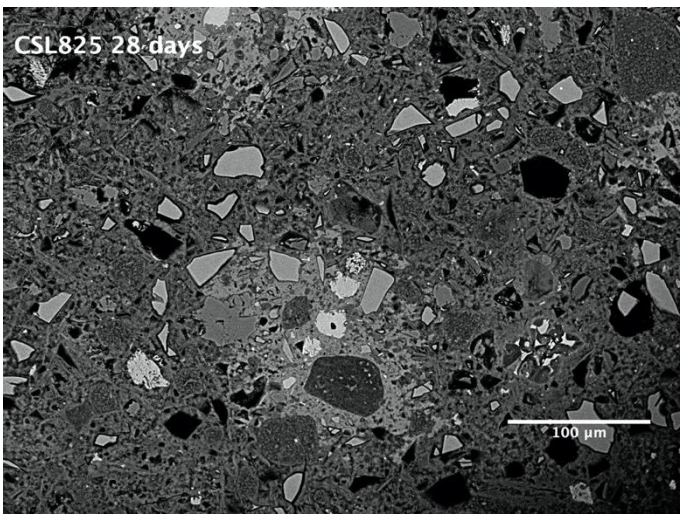
CSL825 28 days
100 µm

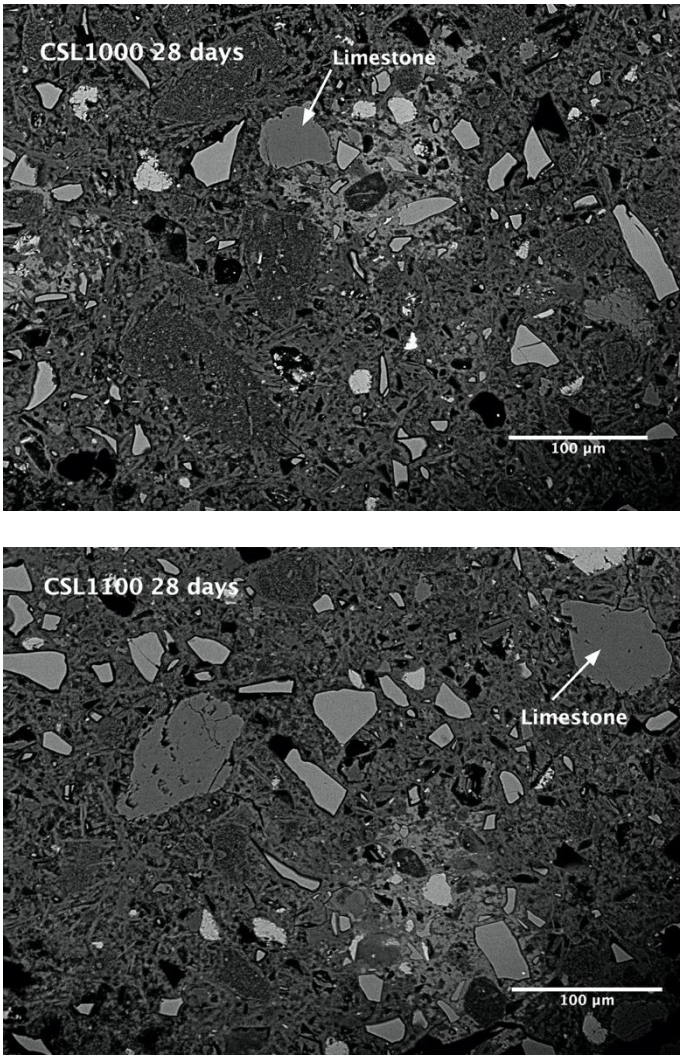

Figure 5- 26: SEM-BSE images of slag-blended cement pastes hydrated for 28 days (images captured at 800x, field of view is approximately 450 x 340μm).

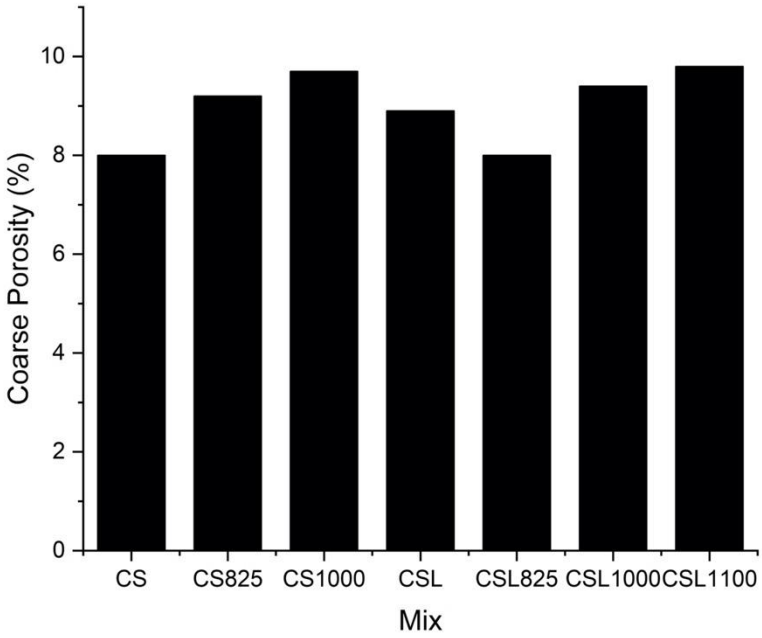

Figure 5- 27: Coarse porosity of ternary and quaternary cement pastes cured for 28 days.

5.2.8 Compressive Strength

Figure 5-28 shows the compressive strengths of binary calcined sludge-cement mortars cured for 7 and 28 days. The strength of blended cement mortars increased with calcining temperature of alum sludge within the range 825^{o}C and 1100^{o}C. However, compressive strengths of blended cement mortars were lower than the neat system at all curing ages. These differences can be explained based on the characteristics of the sludge additions and how they influence cement hydration, as observed by calorimetry, TGA, XRD and SEM.

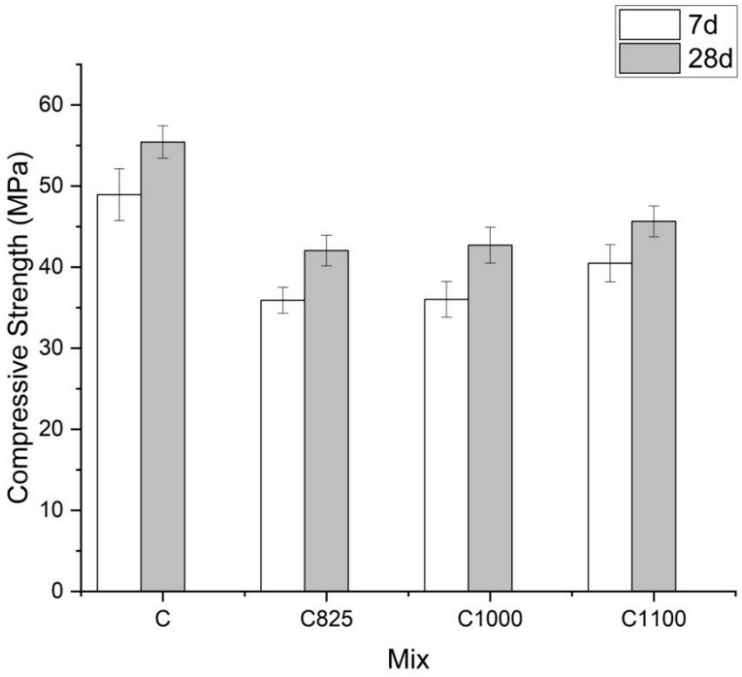

Figure 5- 28: Compressive strength of mortars with binary blends at 7 and 28 days curing.

The sludge calcined at 825^{o}C contains poorly crystalline η-alumina (eta) which was found to rapidly deplete sulfates to form ettringite, resulting to an undersulfated condition. This accelerates C_3A hydration which consumes ettringite to monosulfoaluminate. In the absence of sulfate, aluminium is incorporated into the alite structure [25,27,205] which hinders C_3S hydration. This results in reduction in the rate of mechanical strength development in the C825. At higher calcination temperatures, i.e. 1000^{o}C and 1100^{o}C, where more crystalline η-alumina (eta) and inert corundum are formed, the lower dissolution of aluminates avoids an undersulfated condition and alite hydration is enhanced. However, compressive strength is still considerably lower than the neat system. This is likely due to the low silica content in the sludges (~18%) which limits the pozzolanic reaction with portlandite to form additional C-S-H. The trend in strength in the calcined sludge mixtures can also be explained by the filling effect of the sludge particles brought about by their characteristic shapes and sizes. Alumina minerals may act as super fine aggregates and fill porous interfacial zone [197]. The SEM images illustrate denser and more compact paste microstructures with increasing sludge calcination temperatures. This can be explained by the morphological changes that occur in the sludge particles with calcination temperature

leading to differences in space filling effect. The sludge particles calcined at 825^{o}C consist of agglomerated irregular particles which become more rounded at 1000^{o}C due to sintering processes. Further calcination at 1100^{o}C led to a breakdown of agglomerates producing very fine particles. These changes enabled better space filling which translated to higher strength.

Figure 5-29 shows the compressive strengths of blended cement mortars incorporating calcined sludge and slag (series S2) cured for 7 and 28 days. For reference Mix CS, calorimetry and portlandite measurements showed a clear enhancement of clinker hydration by slag. However, compressive strength in this mix was lower than the neat system but was slightly higher than the ternary blends containing both slag and calcined sludge. SEM images showed a porous microstructure likely due to the high-water cement ratio used coupled with the slow reactivity of slag relative to cement. For CS1100, declined strength was due to high clinker replacement which reduced portlandite available for slag reaction. In CS825 and CS1100, strength was further reduced due to hindering effect of excess aluminates on clinker hydration which also limited slag reaction.

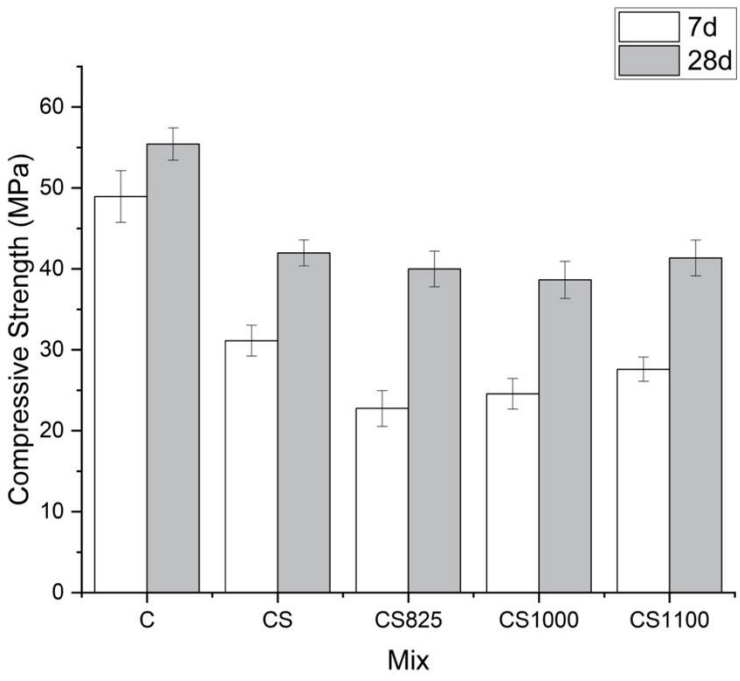

Figure 5- 29: Compressive strength of mortars with ternary blends at 7 and 28 days curing.

It has been reported that additional reactive alumina from SCMs such as slag and fly ash react with limestone powder to form carboaluminate phases that lead to

higher mechanical strength [125,304]. To exploit this synergy, mixes were prepared with the addition of limestone (Figure 5-30). In quaternary PC-slag-limestone-calcined sludge blends, the sludge at 825ºC (CSL825) produced better mechanical strength than more commonly used PC-slag-limestone (CSL). Lower mechanical strength was observed for slag-limestone blends incorporating sludges calcined at 1000ºC (CSL1000) and 1100ºC (CSL1100). In the CSL825, TG and XRD analysis showed increased limestone reaction and thus greater formation of hemi and mono-carboaluminates thereby stabilizing ettringite. The higher volume of hydrates translated to enhanced strength. Compressive strengths in mortars prepared with sludge calcined at 1000ºC (CSL1000) and 1100ºC (CSL1100) were lowest due to the crystallization of alumina which limited limestone reaction.

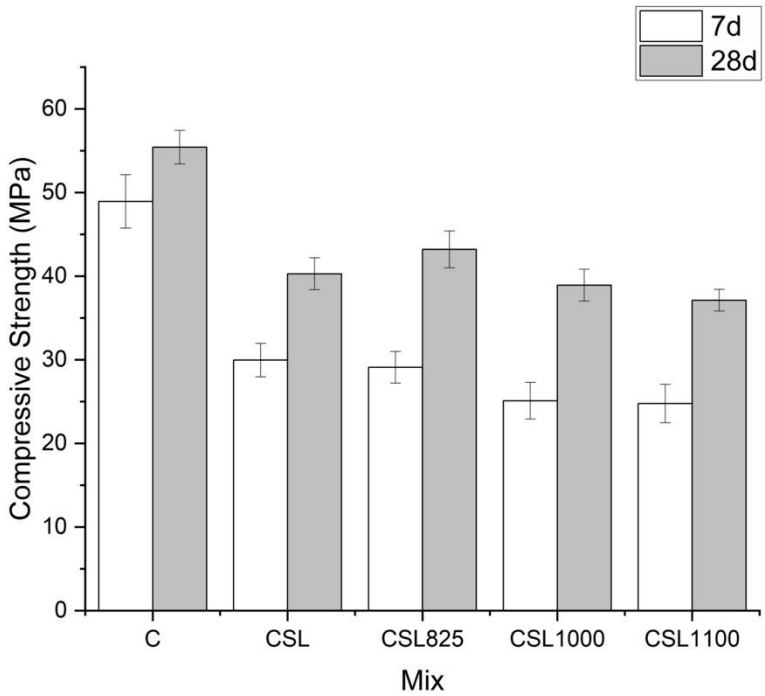

Figure 5- 30: Compressive strength of mortars with quaternary blends at 7 and 28 days curing.

The relationship between compressive strength and coarse porosity for all mixes tested after 28 days is presented in Fig. 5-30. The plot shows a clear negative correlation between porosity and compressive strength. This suggests that the coarse porosity dominates the compressive strength, independent of the mix designs, which is in agreement with the previous observations [11,312].The presence of either

limestone, slag or calcined sludge does not alter the relation between coarse porosity and compressive strength.

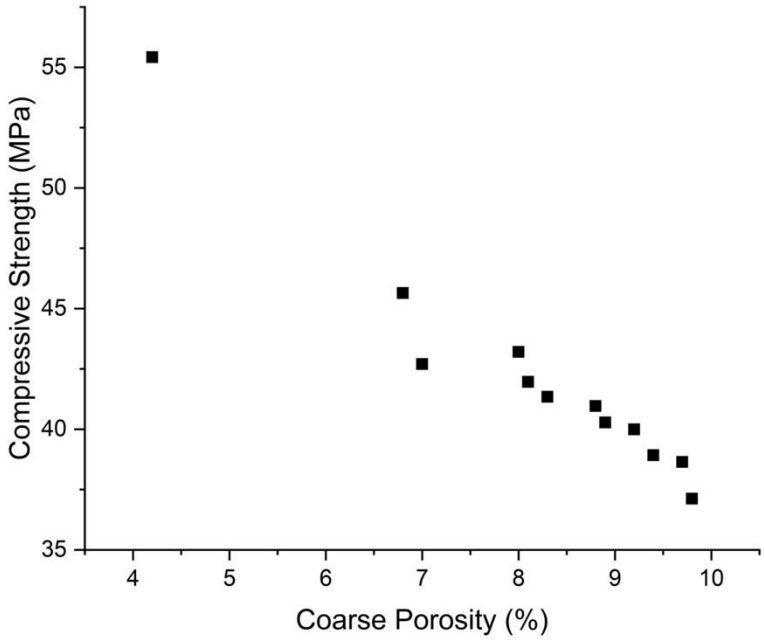

Figure 5- 31: Relationship between compressive strength and coarse porosity

5.2.9 Summary

Chapter 5 presented the characterization of the hydration behaviour and performance of different cement composites containing raw and heat-treated alum sludge. The experimental results are summarized as follows:

- The workability of fresh mortars varied consistently with changes in morphology and BET specific surface area (SSA) of incorporated sludge. Within the interval 0-1100^{o}C, a clear negative correlation was observed between SSA of calcined sludges and the workability of corresponding cement mortars. Higher surface area meant more water was adsorbed by the sludge particles which resulted in reduced workability. Thus, workability of blended cement mortars decreased by calcining alum sludge at temperatures up to 825^{o}C, and then increases with further increase in temperature.
- The pozzolanic activity of raw and calcined sludge was assessed using the performance-based Strength Activity Index (SAI) test. Accordingly, the sludges calcined at 825, 1000 and 1100^{o}C can be considered pozzolans. Characterization of cement pastes incorporating sludges at these three

temperatures showed that calcining alum sludge at 825ºC gives the best reactivity due to the formation of poorly crystallized η-alumina. With increasing calcination temperature to 1100ºC, the reactivity decreased due to crystallization of alumina phases present. The calcined products derived at 1000ºC and 1100ºC showed a greater filler effect, and so led to greater strength development.

- Under alkaline conditions of cement paste, Al^{3+} ions dissolved from sludge calcined at 825ºC are converted to $[Al(OH)_4]^-$ which are very reactive with Ca^{2+} and SO_4^{2-} ions, resulting in the early formation of ettringite. This reaction rapidly depletes gypsum and undersulfated C_3A reactions occur prior to alite hydration. C_3A consumes ettringite to form monosulfoaluminate after 3 hours. The rapid consumption of Ca^{2+} during the early formation of ettringite accelerates the onset of the silicate hydration peak. However, results suggest that the higher dissolution of η-alumina in C825 paste is related to the limited alite hydration which contributed to lower degrees of clinker hydration at later ages. This led to lower mortar compressive strengths in blends containing sludge calcined at 825ºC. Studies in literature suggest that the ensued undersulfated condition leads to the adsorption of aluminium on silicate surface thereby hindering its further dissolution. This decreases the rate and extent of alite hydration, resulting in lower compressive strength at later ages.

- For ternary blends consisting of cement, slag and calcined sludge, the addition of sludge calcined at 825ºC showed similar undersulfated condition due to increased Al^{3+} concentration in solution contributed by both slag and sludge which leads to a significantly suppressed alite hydration. As a consequence, slag hydration is also hindered. In CS1100 paste, the rate of gypsum depletion is lower due to the crystallinity of the sludge addition and enough sulfate remains for controlling C_3A hydration thereby enhancing alite hydration. In general, the degree of hydration of blended cement pastes are reduced in the presence of amorphous sludge and slag. Such a reduction is more evident when sludge calcined at 825ºC is used, because of the high level of clinker replacement (and lower gypsum content) which lead to very rapid undersulfated reactions that inhibit alite hydration and strength development. Analysing the

XRD patterns, small amounts of hemi and mono-carboaluminates are formed due to small amount of calcite contained in slag.

- Isothermal calorimetry showed that in the presence of limestone, undersulfated C_3A hydrations still occur with a more intense peak prior to silicate reaction. However, there was a slight indication of improved silicate reaction compared to the blends without limestone (i.e. ternary blends). It is inferred that in the presence of sufficient calcium ions contributed by the limestone, sulfates are adsorbed on C-A-S-H surface and therefore they are not able to passivate the C_3A surface leading to an earlier sulfate depletion. In addition, the drop in pH induced by aluminium ions is counteracted by calcium ions provided by limestone which reduces the binding strength of Al^{3+} on alite which leads to the observed enhancement in clinker hydration [25]. Furthermore, the limestone provides Ca^{2+} and CO_3^{2-} ions for the formation of hemi- and mono-carboaluminate, as shown by XRD and TG data. In quaternary PC-slag-limestone-calcined sludge blends, the sludge at 825^{o}C (CSL825) produced better mechanical strength than more commonly used PC-slag-limestone (CSL). Compressive strengths in mortars prepared with sludge calcined at 1000^{o}C (CSL1000) and 1100^{o}C (CSL1100) were lowest due to the crystallization of alumina which limited limestone reaction.
- The results of this chapter suggest that clinker hydration and mechanical strength are strongly influenced by aluminate-sulfate ratio in the calcined sludge-blended cements. For enhancement of compressive strength, it is proposed that higher doses of gypsum and limestone powder should be used to control the accelerator effect of 825^{o}C sludge on C_3A hydration. In this way, the higher reactivity of the 825^{o}C sludge can be better utilized for improved performance. Chapter 4 and 5 of this thesis provides a fundamental base and a promising direction for further work on proper utilization UK alum sludge as an SCM.

Chapter VI: Hydration and Microstructure of Ternary Cements Containing Calcined Sludge and Limestone

The previous chapter showed that calcining alum sludge at 825^{o}C produced the most reactive material. Higher strength was observed in the quaternary CSL825 blend due to increased limestone reaction and greater formation of carboaluminates compared to reference mix CSL and equivalent blends containing less reactive calcined sludges (CSL1000 and CSL1100). Based on this finding, this chapter aims to investigate the interaction between limestone powder and calcined alum sludge (at 825^{o}C) in ternary composite cements. Potential synergistic effects are explored with respect to their contribution to clinker hydration, formation of hydration products as well as development of mechanical strength and transport properties. Hydration and microstructure of blended cement pastes was followed by isothermal calorimetry, XRD, TGA, FTIR and SEM analysis. The mechanical and transport properties were assessed by measurements of compressive strength, sorptivity and gas permeability of corresponding mortars.

6.1 Mixes Investigated

Chapter 5 showed that calcining alum sludge at 825^{o}C produced the most reactive material, so this was adopted for the preparation of composite limestone blends. Six mixes were formulated to investigate the influence of calcined sludge on the kinetics, hydration and microstructure of blended cements. Details of the mixes investigated are given in Table 6-1. The binders were formulated by replacing cement with 20% calcined sludge and limestone at ratios of 1:2, 1:1 and 2:1. The rationale behind the selection of mixes was:

- To determine the influence of calcined sludge and limestone on the hydration of clinker.
- To determine the influence calcined sludge and limestone on the types and amounts of hydrates formed.
- To identify compositional effects of the studied mixes on the microstructure and mechanical properties.

Table 6- 1: Mix proportions for investigating limestone ternary blends.

Mix description C-S-L	Cement (C), grams	Calcined Sludge (S), grams	Limestone (L), grams	Sand, grams	W/B	SP, %
100-0-0	450	-	-	1350	0.55	1%
80-20-0	360	90	-	1350	0.55	1%
80-0-20	360	-	90	1350	0.55	1%
80-6.7-13.3	360	30	60	1350	0.55	1%
80-10-10	360	45	45	1350	0.55	1%
80-13.3-6.7	360	60	30	1350	0.55	1%

6.2 Overview of Hydration

The effect of limestone and calcined sludge on the CH and bound water contents was determined by TG analyses (Table 6-2). The CH contents were all lower in the composite cements compared to the neat cement system, when expressed per total binder mass. However, when normalised back to the mass of PC, all blends resulted in similar or higher CH content at 7 days. This can be interpreted as an acceleration of clinker hydration at early age due to the filler effect imparted by the mineral additions. At 7 days of curing, replacing cement with 20% limestone (Mix 80-0-20) produced the highest CH content per unit mass of PC. Limestone addition increases the effective water to PC ratio and provides additional surface for hydration products to precipitate on thereby stimulating PC reaction [98]. However, the bound water per unit mass of PC is less than all other investigated systems, indicating that the filler effect does not compensate for the replacement of PC. Limestone shows very limited reactivity in cement, but it enhances clinker hydration mainly by imparting filler and dilution effects. The higher amount of limestone in the 80-0-20 blend led to reduced amount of reactive constituents and hence the lower bound water content.

In the ternary cements incorporating both limestone and calcined sludge, higher bound water per unit mass of PC was observed at all ages compared to the other investigated blends. Nucleation effects of limestone on clinker hydration as well as carboaluminate formation and the stabilisation of ettringite is attributed for the higher bound water content in the ternary cements [12]. This is supported by the lower CH content observed in ternary blends compared to other investigated systems, which

Table 6- 2: Portlandite and bound water contents in the investigated cement pastes.

		CH Content		Bound Water Content	
Paste	Age	Per 100g anhydrous binder	Per unit mass anhydrous PC	Per 100g anhydrous binder	Per unit mass anhydrous PC
100-0-0	7	17.3	17.3	30.6	30.6
	28	24.1	24.1	36.7	36.7
	56	24.6	24.6	36.9	36.9
80-20-0	7	13.8	17.2	26.2	32.8
	28	12.6	15.8	28.9	36.1
80-0-20	7	15.5	19.4	22.2	27.8
	28	18.1	22.7	32.0	40.0
	56	17.7	22.1	28.8	36.0
80-6.7-13.3	7	14.2	17.8	26.0	32.9
	28	16.3	20.3	35.0	43.7
	56	15.8	19.7	34.7	43.5
80-10-10	7	14.4	18.0	27.1	33.9
	28	14.9	18.7	32.9	41.1
	56	14.6	18.2	35.3	44.1
80-13.3-6.7	7	13.1	16.4	26.7	33.5
	28	15.2	19.0	36.1	45.1
	56	14.7	18.4	35.8	44.7

Indicates the formation of hydration products which consume CH e.g. calcium hemi- and mono- carboaluminate hydrates and ettringite. At early age (7 days), the formation of hemicarboaluminates hydrate consumes CH and this might explain the observed decrease in CH per unit mass of PC. At later ages, increasing levels of limestone powder led to greater levels of CH per unit mass of PC. Possible explanations for this are: firstly, at higher substitution levels the filler and dilution effects are higher and the more CH is formed by enhanced clinker reaction than is consumed by the formation of hermicarboaluminate; secondly, monocarboaluminate, which does not consume CH, might have formed rather than hemicarboaluminate due to higher limestone addition and lower calcined sludge content. Also, the ternary calcined sludge-limestone cements showed limited change in the CH content with curing age possibly

due to the limited portlandite-consuming reactions i.e. pozzolanic reactions, as silica content in calcined sludge is low (18%).

Furthermore, as observed in the previous chapter, the binary cement-sludge paste (80-20-0) contains very low CH content. The oversaturation of aluminium in the pore solution leads to undersulfated C_3A reactions and the sorption of aluminium on silicate surface which reduces the extent of alite dissolution [25,27,204]. Table 6-2 confirms that the addition of limestone enhances calcium silicate reaction as shown by the higher CH content in the ternary blends compared to Mix 80-20-0. It has been reported that limestone compensates for fast sulfate depletion and at lower aluminium concentration, accelerated and undersulfated C_3A reactions can be avoided [205]. As a result, alite hydration proceeds normally and higher degrees of clinker hydration is achieved.

The development of bound water and portlandite contents can be interpreted by how the two properties vary as hydration progresses. Bound water increases with hydration of clinker, limestone and calcined sludge. In blends incorporating calcined sludge, there is an indication that the addition of limestone leads to enhanced silicate hydration. The considerably higher bound water observed in ternary blends containing both limestone and calcined sludge may suggest formation of carboaluminate hydrates. The results of this section suggest the effect of limestone in the calcined-sludge composites is clearly distinct from a filler effect.

6.3 Early age Hydration Kinetics

The early hydration of calcined sludge composites was monitored using isothermal calorimetry (Figure 6-1), with significant impacts of calcined sludge on hydration kinetics observed. All of the calcined sludge blends showed acceleration of the alite hydration peak. The calcined sludge contains significant quantities of reactive, amorphous aluminates. In the alkaline environment of freshly mixed cement paste, Al^{3+} ions are converted into $[Al(OH)_4]^-$ which rapidly react with Ca^{2+} and SO_4^{2-} ions to form ettringite which induces rapid hardening and early set of cement pastes [201,210]. In the 80-20-0 paste, the rapid reaction of calcined sludge with gypsum to form ettringite was confirmed by the higher initial heat, as shown in the cumulative heat curve (Figure 6-1b) compared to the limestone blends. This results in significant shortening of the of the induction period as alite dissolution was enhanced to balance

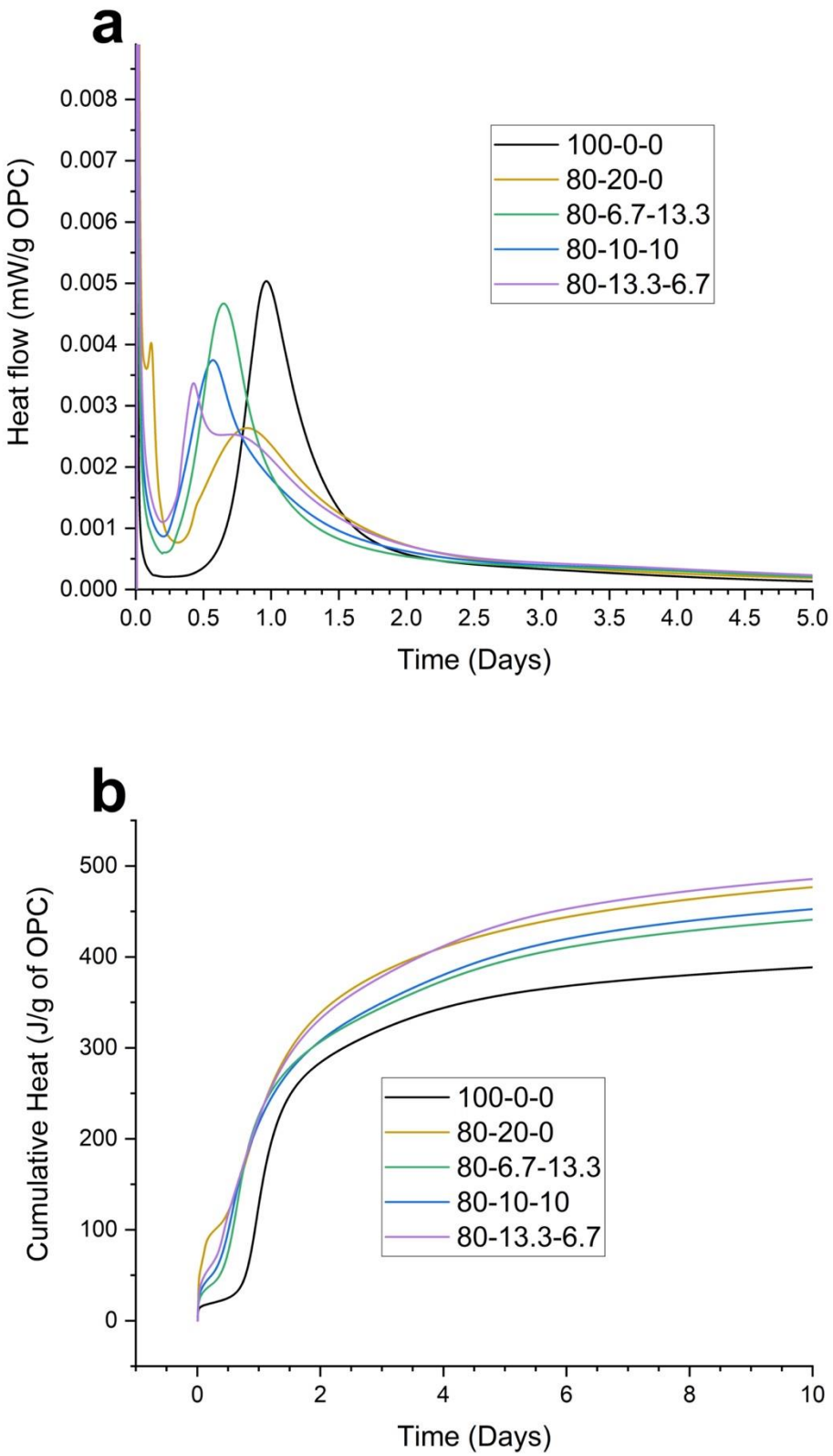

Figure 6- 1: Calorimetric curves of calcined sludge composite pastes a) Heat flow rate b) Cumulative heat.

the Ca^{2+} concentration in the chemical equilibria. In the 80-20-0 blend, the depletion of gypsum accelerated C_3A reaction, which led to the consumption of ettringite to form AFm, monosulfoaluminate. The onset of AFm formation corresponds to the exothermic peak in 80-20-0 paste at about 3 hours [205]. Because C_3A reacts prior to the onset of silicate reaction, the 80-20-0 system is undersulfated [29,205]. When the liquid phase does not contain sulfate ions, the lower pH of the pore solution at higher levels of substitution facilitates aluminium incorporation on the alite surface, reducing its solubility and reactivity. Hence, the significantly lower extent of alite hydration at in Mix 80-20-0.

In the calcined sludge-limestone pastes, a more significant shortening of the induction periods is observed compared to the sludge blend without limestone (80-20-0). This suggests that calcium and sulfate ions are consumed at a faster rate, favouring gypsum and alite dissolutions which then accelerates the onset of the main hydration peak [200]. Briendl et al. [295] reported that in the presence of limestone, more sulfate ions are adsorbed by C-S-H and the depletion of gypsum is reached earlier in time during the hydration process compared to neat cement containing no limestone. At a higher calcined sludge: limestone ratio of 2:1, an intense and earlier aluminate peak can be observed corresponding to sulfate depletion [10,295]. In the neat cement system and the blends containing lower sludge: limestone ratios (1:1 and 1:2) the aluminate peak is absent likely indicating a later sulfate depletion. Nevertheless, blends with higher calcined sludge content i.e. 80-20-0 and 80-13.3-6.7, exhibit an undersulfated condition where an intense aluminate peak occurs prior to the alite hydration peak. It can be inferred that higher levels of calcined sludge content facilitate aluminium incorporation on alite surface which hinder its solubility and reactivity.

Considering the cumulative heat curves in Figure 6-1b, the higher initial heat in the 80-20-0 is attributed to the rapid reaction between sludge and gypsum to form ettringite at very early age. Despite, the lower sludge content in the 80-13.3-6.7 blend, the cumulative heat output is higher than the 80-20-0 after 10 days hydration. It is well established that limestone will only react with aluminate ions after sulfate depletion [100,313]. Since an earlier sulfate depletion occurred in the 80-13.3-6.7 blend, the higher cumulative heat output in this blend is likely due to increased formation hemi and/or monocarboaluminates compared to other blends. In addition, a higher calcined sludge addition (and aluminium dosage) favours limestone dissolution thereby enhancing sludge reaction whereas sludge reaction is limited by gypsum dissolution

in the 80-20-0 paste. Accordingly, lower total heat release is observed in samples incorporating lower calcined sludge- limestone ratios.

6.4 Degree of Hydration of Clinker

With calorimetry results indicating differences in alite and aluminate reaction, quantitative XRD was used to determine the degree of reaction of clinker. The focus here was on the effects of calcined sludge and/ limestone. The results are shown in Table 6-3.

The small initial C_3A content led to its virtually complete reaction within 7 days in all systems. Ferrite hydration was modest, with about 80 to 90% reacted after 28 days. The trends indicated accelerated aluminate and ferrite reaction in blended systems, with most of these phases reacted within 7 days. However, the content of aluminate and ferrite phases in the pastes are rather low and their relative error will be large rendering the interpretation of these results difficult.

The trends in degree of clinker hydration are mainly due to differences in the degree of alite hydration, with the amount of anhydrous belite being similar in all investigated blends. The degree of clinker hydration is higher for 80-0-20 than the neat cement and all calcined sludge blended systems at all ages. This is due to the filler and dilution effects of limestone powder. As the C_3A content of cement is small, only a limited amount of limestone reacts. Therefore, presence of the high amount of limestone in 80-0-20 blend decreases the content of cement clinker and hydration products. For a specific w/b ratio, since limestone shows limited reactivity, its substitution with cement increases the effective water to PC ratio which results in higher degree of cement. The degree of clinker reaction in the 80-20-0 blend is lower than all investigated blends at 7 and 28 days of curing. This is likely due to the observed undersulfated C_3A reactions which leads to hindered alite hydration. At 7 days of curing, the presence of limestone in the ternary blends produced higher degree of clinker hydration compared to the blend without limestone (80-20-0). Limestone may have compensated for the fast sulfate depletion caused by high calcined sludge dosages as well as reacted with sludge to control accelerated C_3A reactions, leading to higher degrees of clinker hydration [205]. From 7 to 56 days, the degree of clinker hydration in the ternary blends decreases with calcined sludge content.

The degree of hydration of clinker at 28 days of curing was also determined by SEM-IA (Table 6-3). Compared to the results from XRD-Rietveld analysis, SEM-IA

slightly overestimates the degree of hydration of clinker, probably due to the exclusion of small anhydrous particles not identified by SEM-IA. Overall, there is reasonable agreement between the two methods.

Table 6- 3: Evolution of clinker phases in all investigated systems relative to anhydrous content wt. %

Mix ID C-S-L	Time (d)	C_3S	C_2S	C_3A	C_4AF	DoH PC (XRD)	DoH PC (SEM-IA)
100-0-0	0	58	20	2.8	9.8		
	7	6	15.1	0	5.2	70.9	
	28	3.2	12.1	0	2.2	80.7	88.7
80-20-0	0	46.4	16	2.2	7.8		
	7	10.4	11.5	0	3.7	64.6	
	28	8.5	9.2	0	1.2	73.9	80.4
80-0-20	0	46.4	16	2.2	7.8		
	7	3.2	12.2	0.4	3.6	73.2	
	28	1.1	10.8	0	1.4	81.6	85.4
	56	0.9	9.2	0	1.2	84.3	
80-6-13	0	46.4	16	2.2	7.8		
	7	5.9	11.3	0.7	1.1	73.7	
	28	2.9	11.1	0	0	80.7	85.3
	56	1.2	9.3	0	0	85.4	
80-10-10	0	46.4	16	2.2	7.8		
	7	6.1	12.2	0.1	0.8	73.4	
	28	5.3	11.4	0	0	76.9	79.4
	56	3.1	10.2	0	0	81.6	
80-13-6	0	46.4	16	2.2	7.8		
	7	8.2	12.9	0	1.1	69.3	
	28	6.9	12.2	0	0	73.6	81.3
	56	5.1	11.3	0	0	77.3	

6.5 Limestone Reaction in Composite Cements

Quantification of the amount of reacted carbonates is important to establish the reactivity of limestone in cementitious systems and determine the optimal mix proportions for maximum performance. Figure 6-2 shows the degree of reaction of limestone in the studied ternary blends after 7, 28 and 56 days. After 7 days, 10.9% of the limestone had reacted in the binary 80-0-20 system, with higher degrees of reaction in the ternary systems with 25.0, 31.4 and 40.0% in cements containing calcined sludge-limestone ratios of 1:2, 1:1 and 2:1 respectively. This means that more

calcite is consumed in the presence of calcined sludge. The reactivity of limestone is dependent on the content of alumina available from C_3A C_4AF and as well as SCMs. With regards to the 80-0-20 blend, the aluminate content of clinker is small, so the chemical reactivity of limestone is limited. The addition of calcined sludge contributes a considerable amount of reactive aluminates, which expedites limestone reaction. The higher reactive alumina content in the sludge blends alters the reaction pathway and leads to increased formation of carboaluminates instead of monosulfoaluminates thereby stabilizing ettringite. The higher dissolution of calcite at early age is related to the lower pH induced by calcined sludge compared to neat cement [96,302]. Calcite dissolution is enhanced in order to balance the Ca^{2+} concentration in the chemical equilibria. It is important to note that this could raise pH to levels where calcite dissolution may be inhibited. However, such effects are most likely counteracted by the additional aluminates provided by calcined sludge [290] which would further enhance dissolution of limestone. In addition, the formation of calcium bearing hydration products (AFt and AFm) will also enhance limestone reaction. At 56 days of curing, the degree of limestone reaction in the 80-0-20 blend had only increased slightly, to 13.8%, but in ternary blends, the degree of limestone reaction was much greater with 33.0, 43.8 and 44.0% reacted in blends having calcined sludge-limestone ratio of 1:2, 1:1 and 2:1 respectively. In summary, the degree of reaction of calcite in the ternary blends ranged between 33% and 44%. This translates to 2.2g, 4.4g and 5.9g in mixes containing 6.7%, 10% and 13.3% limestone respectively. With increase in the amount calcined sludge, the chemically reactive portion of limestone at each age increases. This is consistent with the investigations of Zajac et al. [313] which reported that the dissolution rate of calcite is dependent on alumina available for the formation of hemicarboaluminates and monocarboaluminates. Furthermore, the accelerated rate of calcite reaction at early age, particularly with higher levels of calcined sludge may be related the faster rate sulfate depletion induced by the calcined sludge. Bizzozero & Scrivener [100] observed that when there is excess sulfate (i.e. above 50 mol% in pore solution) in respect to aluminate, ettringite is more stable than carbonate AFm therefore limestone is not consumed. The observed results are consistent with limited reaction of limestone reported elsewhere [100,303].

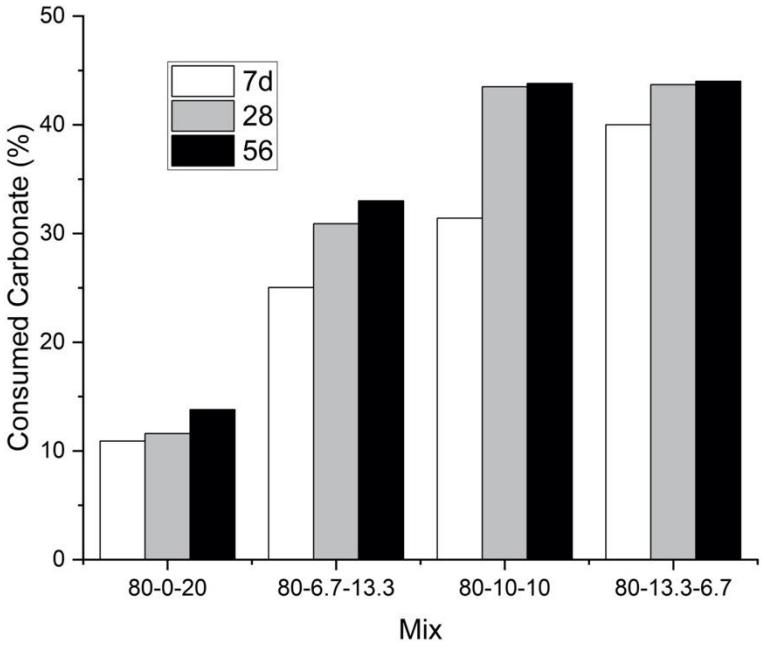

Figure 6- 2: Degree of limestone reaction in ternary limestone cements

6.6 Phase Assemblage of Composite Cements

6.6.1 Experimental evidence from TGA, XRD and FTIR

The hydrated phases were identified by TGA and XRD (Figures 6-3 and 6-4). Table 6-4 shows the quantitative phase analysis of the AFt and AFm phases. The DTG plots show that the main hydrated phases present are C-S-H, ettringite and portlandite, identified by peaks at around 100-200^{o}C, 100^{o}C and 450^{o}C respectively. A shoulder at the right-hand side of the peak at 100^{o}C indicates the formation of AFm phases. The peaks above 600^{o}C are due to decarbonation of calcite indicative of unreacted calcite.

The hydrated phase assemblage is dependent on the interactions of the constituent materials in a given cement system. The DTG curves presented in Figure 6-3 show a greatly reduced peak at about 100^{o}C, due to the decomposition of C-S-H and ettringite, in the binary 80-20-0 blend. This supports the earlier findings of hindered alite hydration by calcined sludge in the 80-20-0 blend. Upon mixing with Portland cement, the calcined sludge rapidly reacts with gypsum to form ettringite and accelerates C_3A reaction, consuming ettringite to form monosulfoaluminate. XRD analysis shows increased precipitation of monosulfoaluminate as ettringite is

Table 6- 4: Evolution of AFt and AFm phases in investigated blends relative to anhydrous content wt. %.

Mix ID C-S-L		AFt	Hc	Mc
100-0-0	7	8.2	0.7	0
	28	12	1.2	0
80-20-0	7	5.0	0	0
	28	2.9	0	0
80-0-20	7	4.3	1.0	0.5
	28	9.5	1.4	2.0
	56	11.1	1.3	4.1
80-6-13	7	8.5	1.9	3.3
	28	10.6	2.2	6.0
	56	13.1	2.1	10.0
80-10-10	7	7.9	2.6	5.4
	28	11.1	2.4	7.4
	56	14.3	2.7	14.3
80-13-6	7	5.8	3.7	5.2
	28	12.0	4.3	8.4
	56	15.9	6.0	12.6

consumed. The formation of monosulfoaluminate is marked by an intense peak in on the DTG curve at ~180^{o}C. In the neat Portland cement system, XRD shows that the amount of monosulfoaluminate also grows with time but at a lesser rate and extent compared with the 80-20-0. This confirms that that calcined sludge accelerates C_3A reaction in the absence of limestone.

The coupled use of limestone and calcined sludge is expected to preserve the ettringite and further, produce additional hydrates hemi- (Hc) and mono-carboaluminates (Mc) [10]. The DTG curves of ternary composites show the beneficial effect of limestone with an increased C-S-H/ettringite peak. The distinct peak at around 180^{o}C corresponds to the presence of carboaluminate hydrates, as confirmed by XRD. The presence of limestone compensates for the fast depleting calcium sulfate, where C_3A reacts with carbonates to form Hc and Mc instead of consuming ettringite to form monosulfoaluminate. The formation of carboaluminate hydrates starts only after

sulfate depletion, as shown previously [100,314]. Despite the higher initial sulfate content in the neat cement system, similar ettringite contents are present in the ternary blends at later age. Also, the ettringite content does not vary significantly with calcined sludge content, as it is related to initial sulfate content, which is constant. The XRD patterns show that the hemicarboaluminate is present in limestone blends at 2 days of curing. This phase progressively transforms to monocarboaluminate with curing age. At 7 days, Hc and Mc coexist in the ternary blends. Monocarboaluminate was formed earlier in the ternary blends and the contents were significantly greater than in the binary limestone blend (80-0-20). The phase transformation occurs because monocarboaluminate is slightly more stable thermodynamically, although the rate of formation is quicker for hemicarboaluminate [314]. However, increasing dosages of calcined sludge provide additional aluminates which seem to favour the formation of hemicarboaluminate instead of monocarboaluminate [302,314].

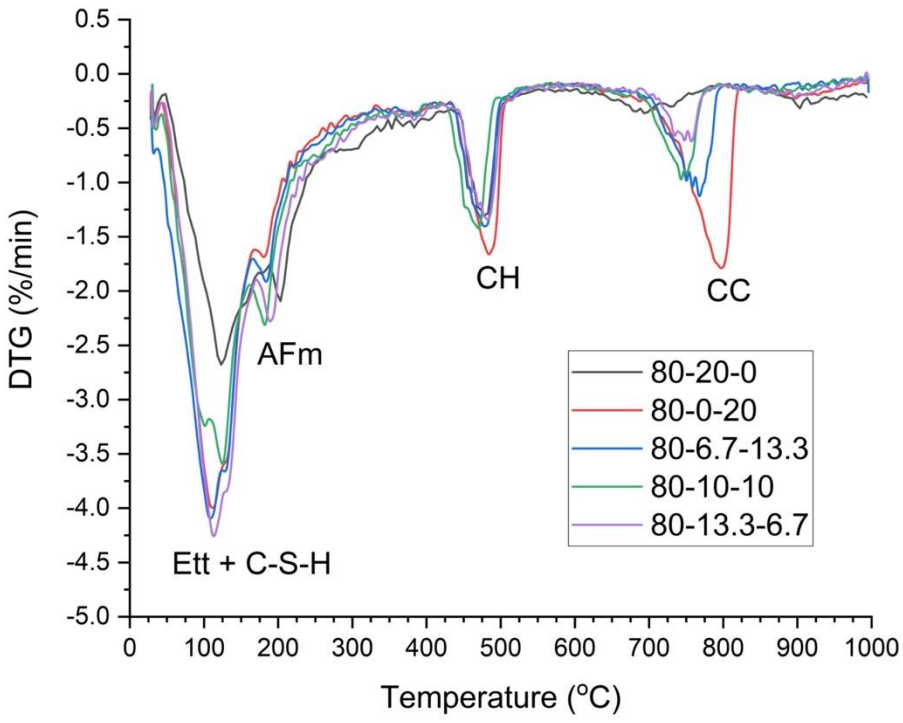

Figure 6- 3: DTG curves of calcined sludge blended systems hydrated for 28 days.

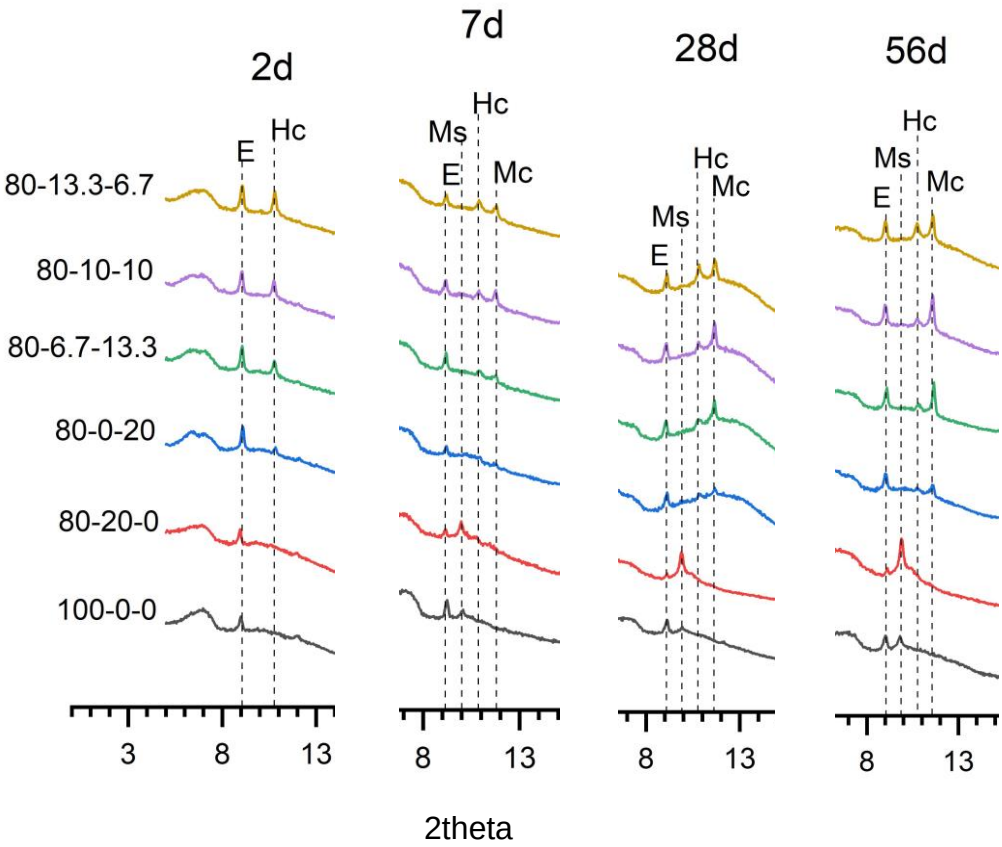

Figure 6- 4: XRD patterns of ternary limestone cements hydrated for 2, 7, 28 and 56 days.

The phases present in samples hydrated for 28 days were identified by FTIR (Figure 6-5). The O-H stretching vibration at 3640cm^{-1} marks the presence of portlandite [315]. The broad peak at 3410cm^{-1} is due to the vibration of H_2O in hydrating cement. Ettringite is stable if there are sufficient sulfate ions present in the system. In the pure CEM I paste, the characteristic peak due to the vibration υ3-SO_4^{2-} at 1120cm^{-1} indicates the presence of ettringite. This is supported by the presence of υ2-H_2O at 1675cm^{-1} assigned to the deformation of water in ettringite [298,316]. In the binary 80-20-0 blend, additional aluminates contributed by the sludge ash convert ettringite to monosulfoaluminate as indicated by the disappearance of the ettringite and the emergence of the sharp Al-O peak at 575cm^{-1} and peak at 1120cm^{-1} respectively [315]. In the pastes containing limestone powder, the monosulfoaluminate almost disappears and the ettringite peak at 1120cm^{-1} is reinforced. In the absence of gypsum, aluminates react with $CaCO_3$ to form monocarboaluminate and/or the lower carbonate content phase hemicarboaluminate. Monocarboaluminate is a more stable

phase due to its insolubility at ambient temperature and this may be the reason why it is the observed in all limestone blends. The spectra of carboaluminates can be assigned on the basis of the carbonate ion being a planar tetra-atomic species with trigonal-D3h symmetry [298]. Monocarboaluminates are indicated by the υ3-CO_3^{2-} (1416cm^{-1}) together with υ2-CO_3^{2-} (875cm^{-1}) and υ4-CO_3^{2-} (712cm^{-1}) [298]. Assignments of the spectra are consistent with TGA and XRD analysis.

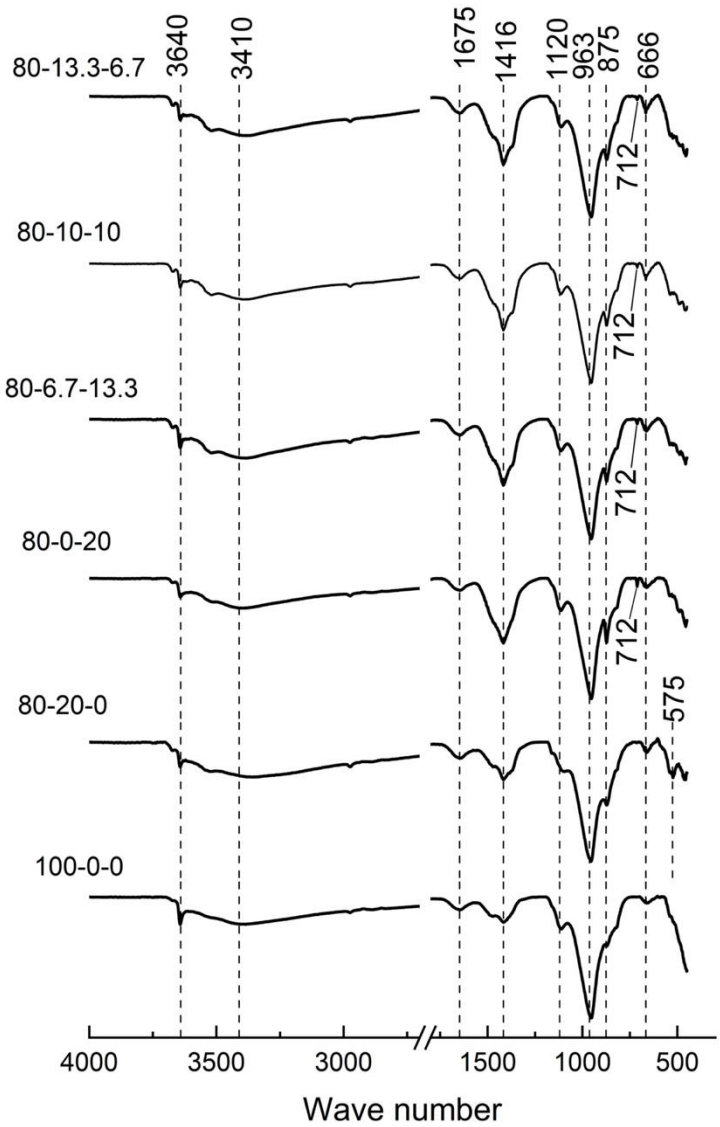

Figure 6- 5: ATR-FTIR spectra in the range of 500–4000 cm^{-1} of blended pastes cured for 28 days.

6.6.2 C-S-H Composition by SEM-EDS

SEM-EDS was used to characterise the C-A-S-H gel formed since it cannot be characterised by XRD due to its amorphous nature. The incorporation of alumina in C-S-H is dependent on different factors including alumina content of SCMs, available alkali content and Ca/Si ratio of C-S-H gel [64,317]. Table 6-5 shows the incorporation of silicon and aluminium in C-A-S-H due to calcined sludge reaction at 28 days. The use of calcined sludge led to increased Al/Si ratios, consistent with the literature [64]. The aluminium incorporation in C-A-S-H is higher in the calcined sludge blends, while Ca/Si ratio remained roughly constant. It seems there is a practical limit for the amount of alumina that can be taken up into C-A-S-H as aluminium incorporation is quite small even for higher dosages of calcined sludge. The increased AFt and AFm precipitation in the ternary blends would influence the alumina concentration in the pore solution [99] and consequently incorporation into C-S-H. There is only so much aluminium which can be incorporated in the C-S-H and the remainder precipitates in AFm phases. It has been suggested that aluminium incorporation into C-S-H is confined to bridging sites of dreierkette-based silicate chains [48,73]. Furthermore, It has been reported that Ca/Si ratio is increased with gypsum and limestone dosage [311]. Thus, the presence of limestone can explain the sustained Ca/Si ratio even at higher doses of calcined sludge.

The results show that there is no significant difference in Ca/Si ratio between the studied samples of different sludge contents. The differences are generally small and are likely due to experimental error. As explained in section 3.2.5.7, SEM analysis results in a larger interaction volume which results in intermixing of analysed phases leading to inaccurate representation of C-S-H. On the other hand, the high-resolution technique of TEM limits the size of the interaction volume thereby limiting intermixing of analysed phases. However, it should be noted that there is considerable local variation in gel composition. This was confirmed by Richardson and Groves [50,91] who observed significant variation of Ca/Si ratio (1.2 and 1.45) for two distant gel areas within the same sample. Like this study, the results were derived from a large data set. This shows data collected from localised areas even if they are large data sets cannot be used to establish compositional trends. Furthermore, the authors observed that although microanalysis using an Electron microprobe analyzer (EMPA), a method that works like an SEM, gives Ca/Si ratio consistent with those found with TEM, it was

impossible to obtain EMPA analyses of single-phase C-S-H without intermixing of phases. Thus, it can be assumed that the slight variations in Ca/Si ratio amongst calcined sludge pastes are not likely to be statistically significant.

Table 6- 5: Ca/Si and Al/Si atomic ratios of inner product C-S-H obtained by SEM-EDS

Mix	Ca/Si	Al/Si
100-0-0	1.88	0.06
80-20-0	1.83	0.10
80-0-20	1.89	0.06
80-6.7-13.3	1.85	0.06
80-13.3-6.7	1.85	0.10

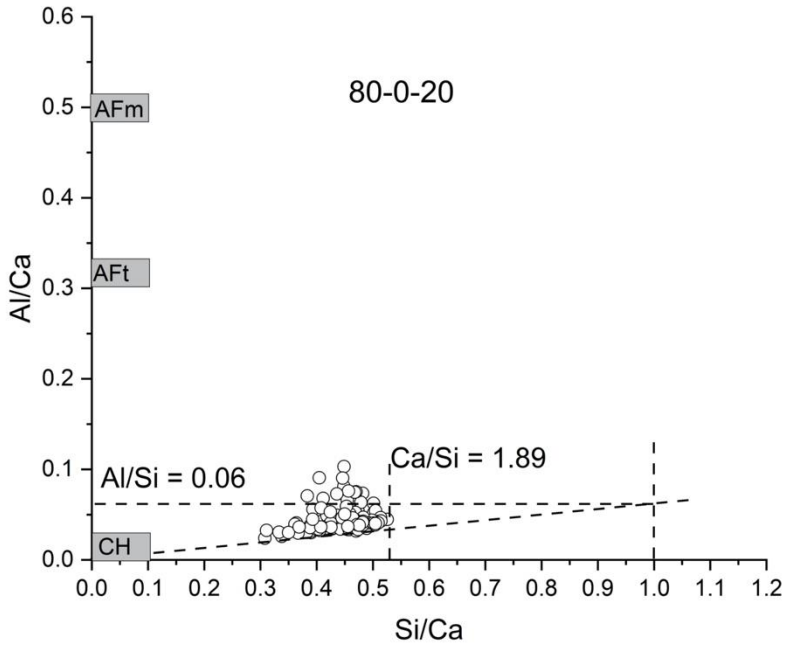

Figure 6- 6: Al/Ca v Si/Ca for 80-0-20 cured for 28 days

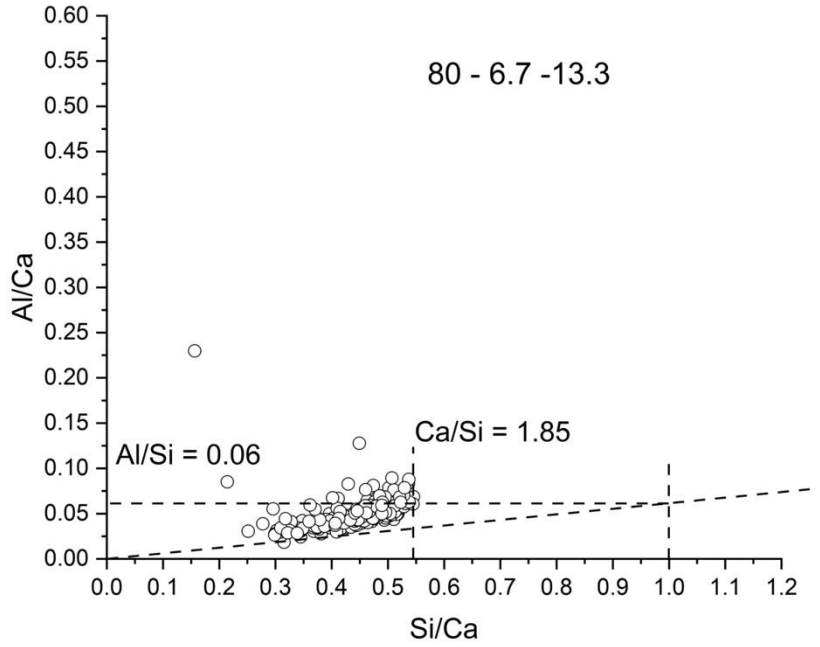

Figure 6- 7: Al/Ca v Si/Ca for 80-6.7-13.3 cured for 28 days

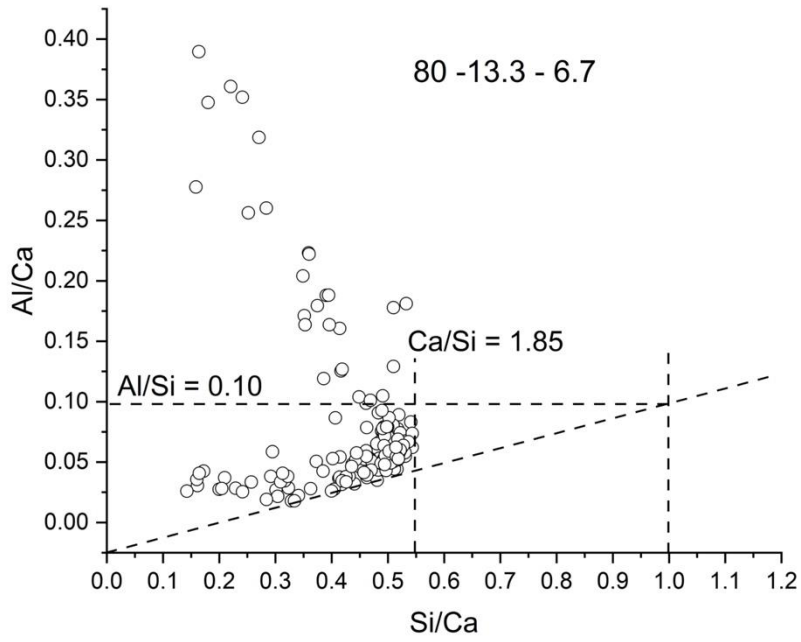

Figure 6- 8: Al/Ca v Si/Ca for 80-13.3-6.7 cured for 28 Days

6.6.3 Microstructure Development of Blended Cement Pastes

Backscattered electron (BSE) images taken at 800x magnification were used to qualitatively assess microstructural variations in blended cement pastes cured for 28 days (Figure 6-9 to 6-14). Image analysis of BSE images was used to determine the coarse porosity of cement pastes at 28 days and the results are presented in Figure 6-15.

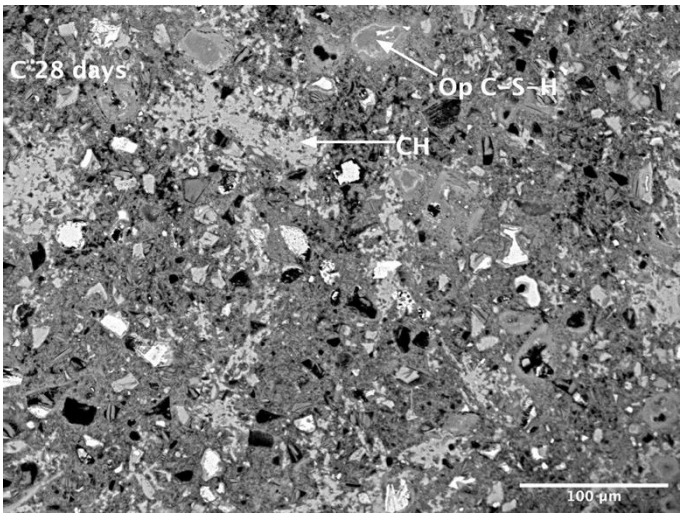

Figure 6- 9: SEM-BSE image of 100-0-0 paste hydrated for 28 days (image captured at 800x, field of view is approximately 450 x 340μm).

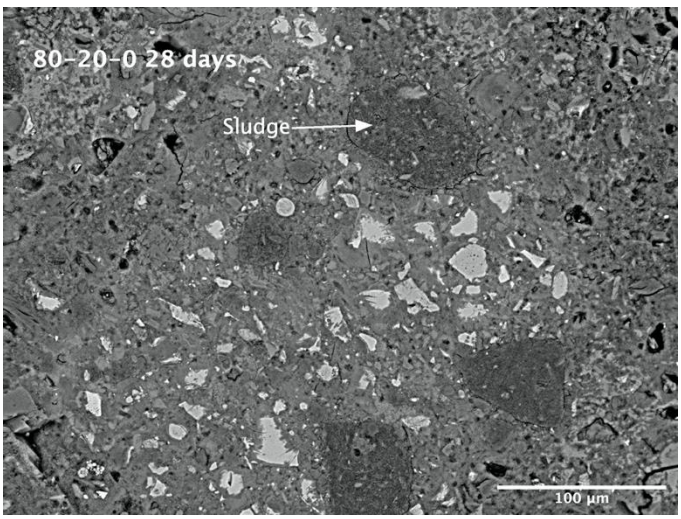

Figure 6- 10: SEM-BSE image of 80-20-0 paste hydrated for 28 days (image captured at 800x, field of view is approximately 450 x 340μm).

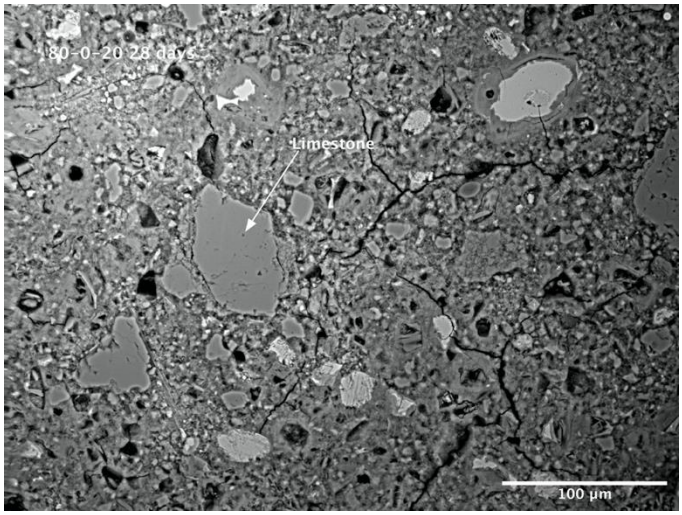

Figure 6- 11: SEM-BSE image of 80-0-20 paste hydrated for 28 days (image captured at 800x, field of view is approximately 450 x 340μm).

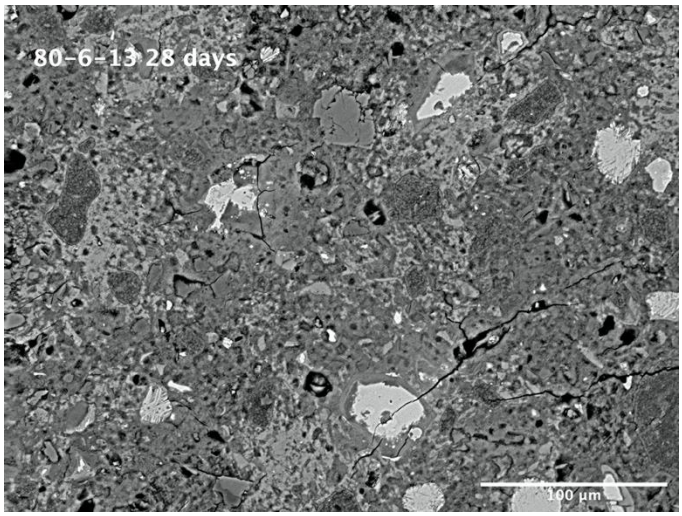

Figure 6- 12: SEM-BSE image of 80-6.7-13.3 paste hydrated for 28 days (image captured at 800x, field of view is approximately 450 x 340μm).

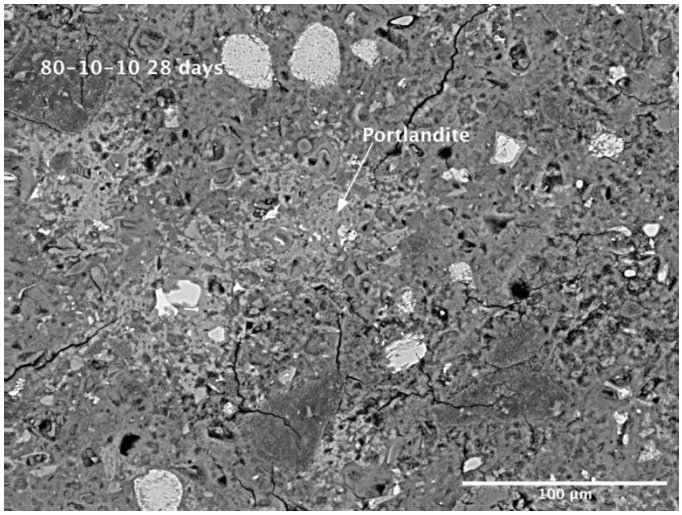

Figure 6- 13: SEM-BSE image of 80-10-10 paste hydrated for 28 days (image captured at 800x, field of view is approximately 450 x 340μm).

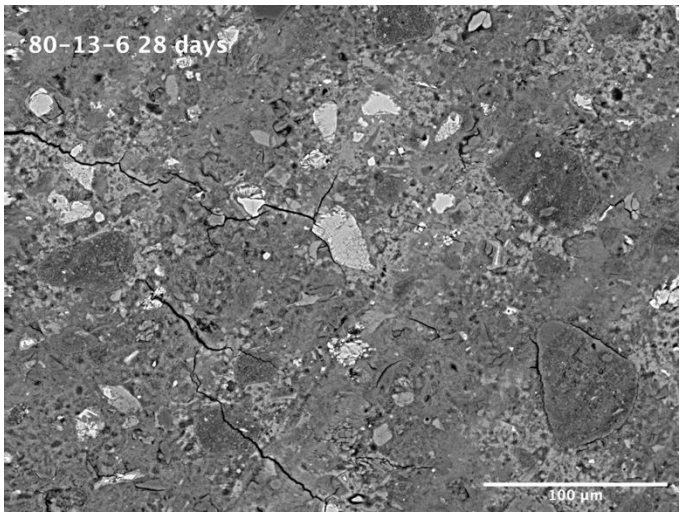

Figure 6- 14: SEM-BSE image of 80-13.3-6.7 paste hydrated for 28 days (image captured at 800x, field of view is approximately 450 x 340μm).

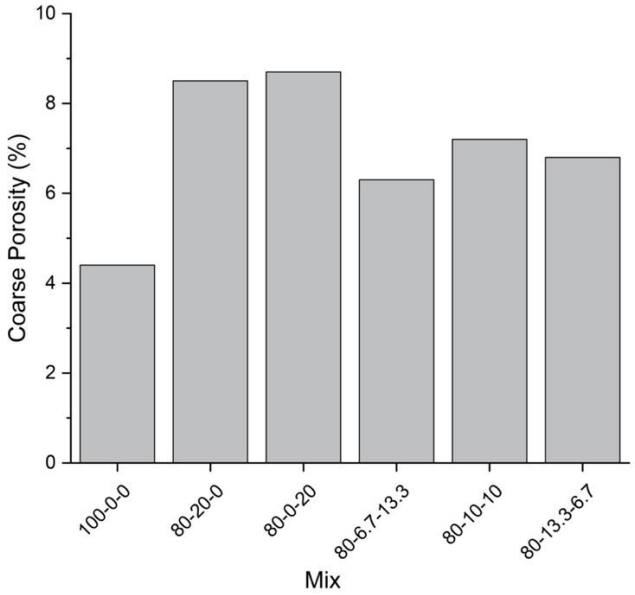

Figure 6- 15: Coarse porosity of ternary limestone cement pastes cured for 28 days.

The images show the presence of partially hydrated cement particles, C-S-H, portlandite and pores. The micrographs are characterized by lots of small cracks. The bound water content of ettringite is higher than in other hydrates. Thus, the small cracks are due sample exposure to vacuums during sample preparation and SEM analysis [100]. The visibly higher degree of clinker hydration in the neat system is consistent with SEM-IA, XRD and TG results. Portlandite is abundant in the neat system and clusters from small to large can be observed. The high w/b ratio (0.55 and 1% SP) used increases the capillary pores because initial dispersion of cement grains by water leads to the divergence of hydrated phases in the pore spaces to produce a porous cement matrix. However, the neat cement system has lower porosity than all other mixtures (Figure 6-15). Consistent with earlier findings, 80-20-0 shows a lower extent of clinker hydration, with considerable amounts of anhydrous cement and discrete pores. In the binary 80-0-20 blend, large clusters of anhydrous limestone grains and large sized pores were observed. This is consistent with findings elsewhere [99,137,245]. The largely unreactive limestone imparts a dilution effect on cement which increases the effective w/b ratio leading to higher clinker hydration. However, this dilution effect does not compensate for the reduction in cement leading to lower volume of hydrates than required to fill pore spaces. The ternary blends showed a lower porosity than the binary blends. The formation of carboaluminates and stabilization of ettringite in the presence of limestone leads to an increase in the total

volume of solid phases, as ettringite has low density and thus relatively large volume per formula unit [99]. In summary, porosity is higher in the blended systems. However, there is a refinement of the pore microstructure by the coupled addition of calcined sludge and limestone.

6.7 Strength Development

The compressive strength results of cement mortars are presented in Figure 6-16. In order to assess the contribution of pozzolanic materials on the compressive strength, the Strength Activity Indices (SAI) were determined, as presented in Figure 6-17. According to the ASTM C618 specification, the blended mixture should provide 75 % of the strength of the control at 7 or 28 days of curing.

At 2 days, the strengths were relatively similar in the blended systems and lower than the neat cement system. At this age, strength is mainly controlled by clinker hydration and the differences can be attributed to differences in the degree of alite hydration, which is influenced by the chemical inhibition and filler effects of calcined sludge and limestone respectively (as shown by isothermal calorimetry). At 7 days, there was clear evidence of the synergistic interaction of calcined sludge and limestone on strength. The 7-day SAIs of the binary blends containing either calcined or limestone were 67.5 and 70.4% respectively. At 7 days, coupled substitutions of cement with calcined sludge and limestone in the ratio 1:2, 1:1 and 2:1 led to a dramatic increase in SAI to 90.1, 97.7 and 97.0% respectively. At later ages, clinker hydration dominates, and much higher strength was observed in the neat system. As a result, the SAI values of the ternary blends fell within the range 87-91% at 28 and 56 days. The results demonstrate the effectiveness of ternary systems both at early and late ages because the SAI values were higher than the single additions.

As shown by TG, calorimetry and XRD, the calcined sludge content has an effect on the degree of limestone reaction, which leads to the formation of hemicarboaluminates (Hc) and monocarboaluminates (Mc). In addition, this reaction mostly occurs at early age, depending on the calcined sludge content, i.e. higher degree of limestone reaction with higher calcined sludge content. This confirms that Hc and Mc precipitation is responsible for the strength increase at early age. This agrees with previous studies that establish that aluminate content is the main parameter controlling the hydration and strength of limestone blended cements [297,318].

The relationship between compressive strength and coarse porosity for all mixes tested after 28 days is presented in Fig. 6-18. The plot shows a clear negative correlation between porosity and compressive strength. This suggests that the coarse porosity dominates the compressive strength, independent of the mix designs, which is in agreement with the previous observations [11,312].The presence of either limestone and calcined sludge does not alter the relation between coarse porosity and compressive strength.

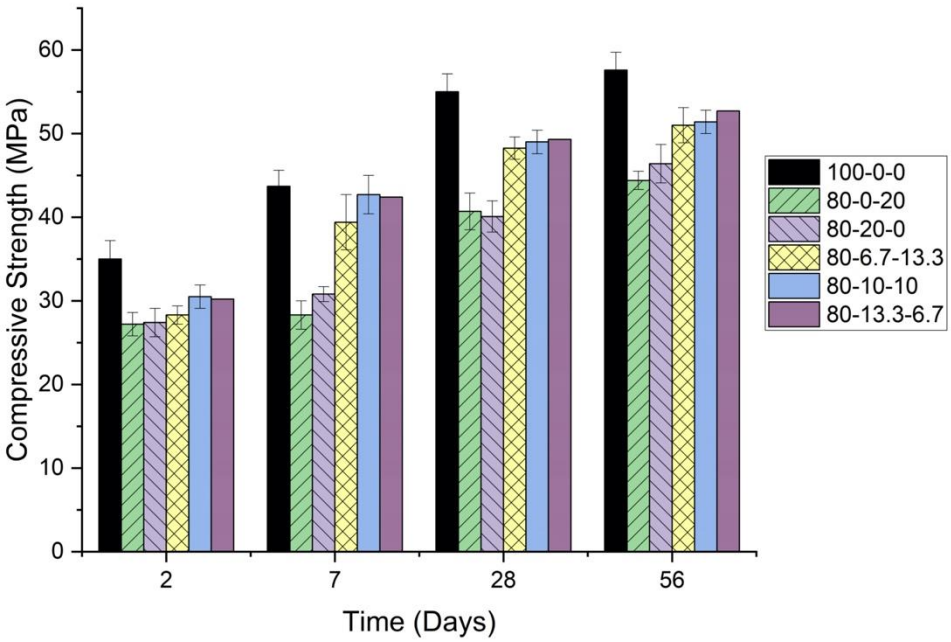

Figure 6- 16: Compressive strength of mortars cured for 2,7,28 and 56 days.

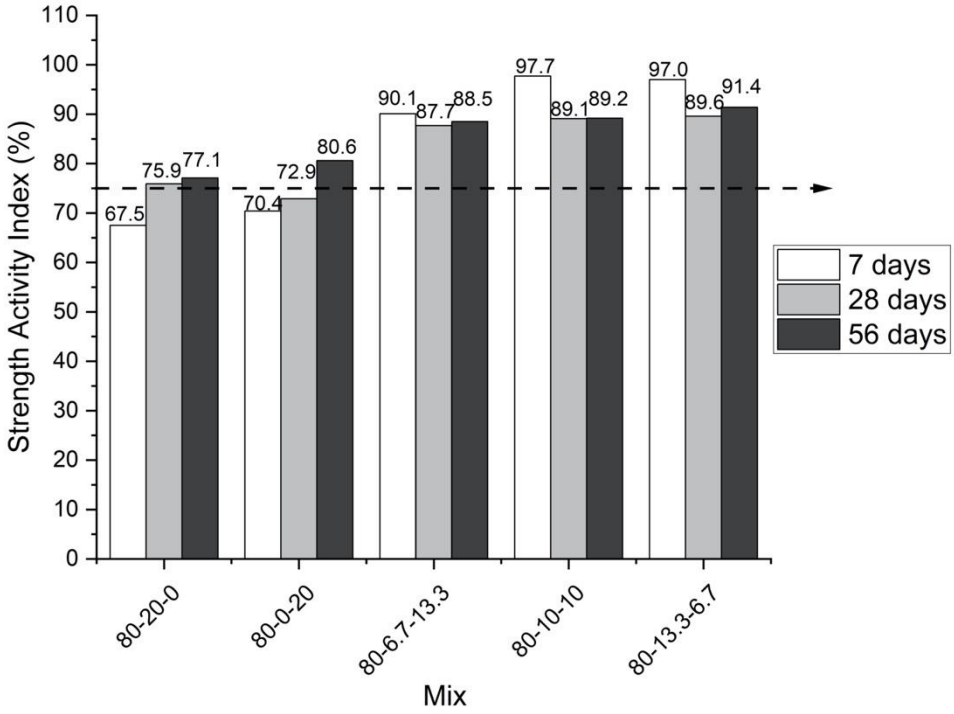

Figure 6- 17: Strength activity indices of blended cement mortars

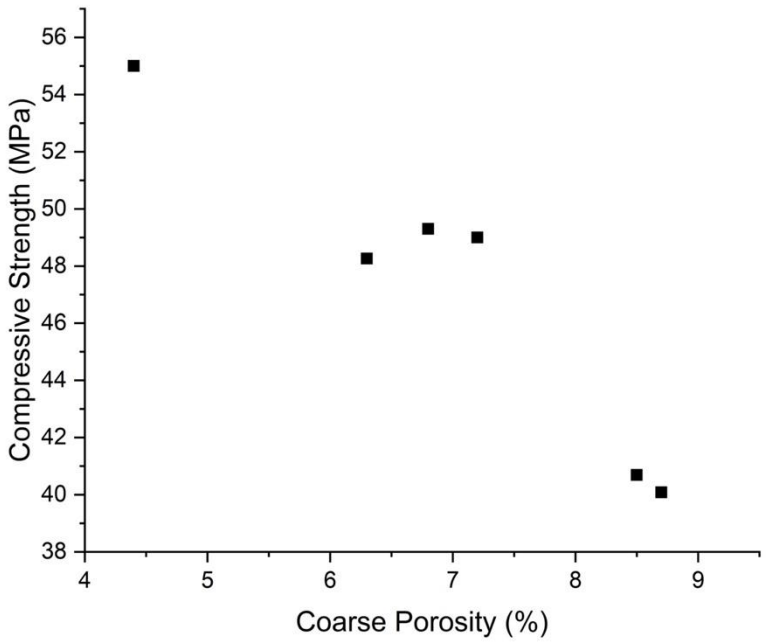

Figure 6- 18: Relationship between compressive strength and coarse porosity in studied systems.

6.8 Transport Properties

Table 6-6 presents the sorptivity and gas permeability coefficients of blended cement mortars cured for 28 days. The relationships between these parameters and compressive strength are presented in Figures 6-19 and 6-20 respectively.

Table 6- 6: Gas permeability and Sorptivity coefficients of tested samples.

Mix	Gas permeability coefficient (*10^{-16} m^2)	Sorptivity Coefficient (*10^{-6} $g/mm^2/min^{0.5}$)
100-0-0	1.40	5.81
80-20-0	4.36	18.9
80-0-20	5.92	8.29
80-6.7-13.3	1.25	14.0
80-10-10	2.28	9.83
80-13.3-6.7	1.64	28.4

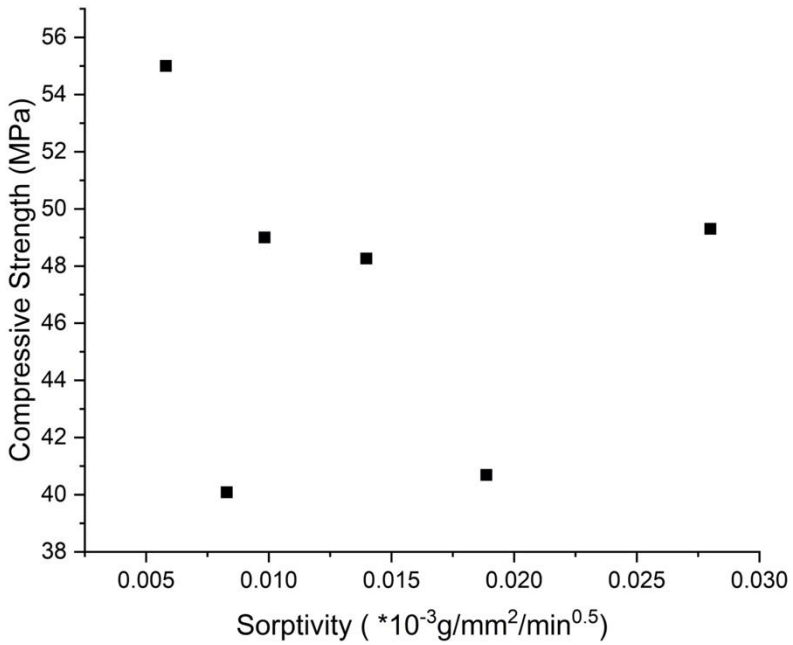

Figure 6- 19: 28-day cube strength against sorptivity coefficient.

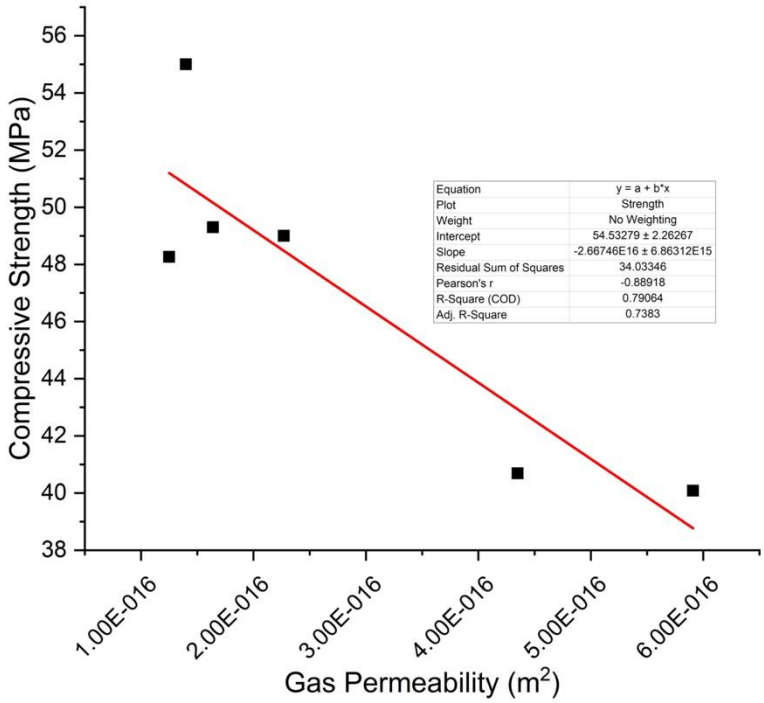

Figure 6- 20: 28-day cube strength against gas permeability coefficient

The sorptivity can be determined by measuring the capillary rise absorption rate for a reasonably homogeneous material. It is a material property that characterizes the tendency of a porous material to absorb and transmit water through capillary action. Generally, it can be seen that the sorptivity values increased with calcined sludge content with or without limestone.

Previous studies incorporating ashes have suggested that pores can be induced by the high specific surface area and particle size of unreacted ashes in concrete [319]. The higher particle size and surface area of the calcined sludge particles created pores on the surface the blended cement mortar which allowed greater ingress of water. Another possible reason for the increase in sorptivity in calcined sludge mortars is the water absorption of the sludge particles itself. Chapter 5 showed that the calcined sludge particles are highly porous with a significantly greater BET surface areas compared to cement and limestone. These porous particles have the tendency to absorb water as indicated by workability measurements in Chapter 5. The neat cement system and 80-0-20 had significantly lower fineness which produced mortar cubes with less porous surfaces which limited the ingress of

water. The sorptivity values are consistent with those reported by Owaid et al. [168] who also observed increase in sorptivity with higher replacement levels of calcined sludge. Furthermore, the sorptivity coefficients and the 28 -day mortar cube compressive strengths are plotted in Figure 6-19. Although weakly correlated, there is an inverse relationship between sorptivity and strength. This in line with the generally accepted idea that porosity is detrimental to strength. In mortars with calcined sludge, the average particle size of the mineral admixture is higher compared to the cement and limestone blends, and the pores in bulk paste and interfaces are not filled completely. Thus, calcined sludge mortars have larger capillary pores, and lower compressive strength as a result of the higher capillary sorption.

Table 6-6 shows that the neat cement system showed lower gas permeability than the blended cement mortars. Contrary to the sorptivity results, the ternary mixes exhibited lower gas permeability than the binary cement blends. The coupled substitution limestone and calcined sludge increased the contents of ettringite, Hc and Mc. The increased volume of hydrates refined the pore structure and reduced connectivity of pores resulting in lower rate of gas flow through the specimens. Furthermore, the gas permeability coefficients and the 28 -day mortar cube compressive strengths are plotted in Figure 6-19. A strong inverse correlation can be observed between the two parameters which suggests that interconnectivity of pores is a major determinant of strength.

The above results show that calcined sludge and limestone affect sorptivity differently to gas permeability. The permeability of concrete is not a simple function of its porosity, but depends also on the size, distribution, shape, tortuosity, and continuity of the pores [137]. In addition, the particle size distribution of constituent materials affects concrete permeability [33]. In the case of binary limestone cement (80-0-20), the factors that affect the pore system are the filler and dilution effects of limestone. These factors influence the total volume of hydrates and the size distribution of the pores which will finally affect the mortar permeability. Our results show that gas permeability, which is dependent on interconnectivity of pores, is closely related to compressive strength. The formation of Hc and Mc in ternary blends reduced the interconnectivity pore spaces thereby reducing gas permeability. On the other hand, sorptivity seems to be affected by size of pores and adsorptive tendency of unreacted sludge particles. In any case, further investigation is needed.

6.9 Summary

In this chapter, potential synergies between calcined sludge and limestone were explored with respect to their contribution to clinker hydration, formation of hydration products and development of mechanical strength and transport properties. The results are summarized as follows:

- The key observation is confirmation of the synergistic interaction between limestone powder and calcined sludge and its persistence over time. Calcined sludge can provide additional aluminates which will lower the sulphate/aluminate ratio and enhance limestone reaction. This reaction leads to the formation of mono- or hemicarboaluminate hydrates instead of monosulfoaluminate hydrate and stabilizes ettringite. This leads to an increase in the volume of hydrates, a subsequent decrease in porosity and an increase in strength.
- In binary 80-20-0 blend, calcined sludge rapidly reacts with gypsum to form ettringite. Isothermal calorimetry showed that calcined sludge reacted faster in the systems with limestone than the binary calcined sludge-PC blend. For higher levels of calcined sludge, the systems appear undersulfated, with sulfate depletion occurring before the maximum of the peak of the main silicate reaction. This resulted in lower degrees of alite hydration at later ages. It is inferred that the undersulfated condition and lower solution pH induced by higher levels of sludge addition facilitates aluminium incorporation on alite surface which reduces its reactivity [25,292]. This highlights the importance of optimizing aluminate-sulfate ratio for enhanced clinker hydration, particularly where high volumes of calcined sludge are used. Nevertheless, the reactivity of calcined sludge is enhanced in the presence of limestone whereas it is limited by gypsum dissolution in binary calcined sludge-PC pastes.
- Mortars made with coupled substitutions of calcined sludge and limestone show comparable strength to PC particularly at early ages and significantly better strength than binary 80-0-20 and 80-20-0 at all ages. At 7 days of curing, the ternary cements gave SAIs within the range of 90-97%. At 28 and 56 days of curing, the SAIs were within the range 87-91%. The results demonstrate the effectiveness of ternary systems both at early and late ages because the SAI values were significantly higher than the single additions. In addition, the results

suggest that calcined sludge content is the main parameter controlling strength in ternary cements.

- Gas permeability results, which are dependent on interconnectivity of pores, showed a strong inverse correlation with compressive strength. The performance against gas permeability suggests that ternary cements give comparable performance with neat PC and better performance than binary 80-0-20 and 80-20-0. On the other hand, sorptivity was weakly correlated with strength and seemed to increase with calcined sludge content. This may mean that sorptivity is influenced by the size of pores of the hardened cement matrix as well as water adsorption by unreacted sludge particles.

Chapter VII: Summary Discussions, Conclusions and Further work

This research examines UK alum sludge and its calcination products to assess their suitability as SCMs. Physical, chemical and mineralogical properties were extensively characterized, and correlated with differences observed in behaviour in blended cement mixtures. This enabled an understanding of factors controlling reactivity and performance of sludge-blended cements. Using this knowledge, unfavourable hydration reactions and their consequences were avoided by the formulation of ternary limestone cements.

A critical difference between previous research into alum sludge and the research presented in this thesis is that here, the performance of calcined sludge was correlated back to the characteristics and hydration behaviour of the respective sludges in different cement systems. Finding such relationships is important for understanding the underlying factors controlling calcined sludge interaction in different cement systems, a lot of which is not established in literature. The wide temperature range adopted for calcination was also helpful in drawing conclusions on the differences in reactivity and performance. As such, optimum mix composition was uncovered which mitigated the problems of low strength obtained in binary calcined sludge cement mixtures. Most importantly, this study confirmed a synergistic interaction exists between calcined sludge and limestone powder in ternary cements leading to comparable strength to neat PC.

7.1 Effect of Calcination Temperature on Properties of Alum Sludge

The raw sludge comprises primarily Al, Si and Fe containing 44.23%, 10.28% and 2.51% as oxide equivalents respectively. Analysis of the raw sludge found organic and inorganic carbon contents of 9.72% and 0.6% respectively. Calcination of the raw sludge at temperatures between 825-1100^{o}C led to an enrichment of oxides due to the removal of biodegradable organic matter, organic compounds and physically adsorbed water. The SiO_2 + Al_2O_3 + Fe_2O_3 oxides percentage in calcined sludges was approximately 92%, chemically fulfilling the ASTM C618 requirement for fly ash and natural pozzolans.

Mineralogical Analysis showed that the raw sludge is primarily an amorphous aluminium hydroxide precipitate with minor amounts of crystalline quartz and montmorillonite. In the temperature range 200-625^{o}C, there was no change in

crystalline composition but significant mass loss was observed due to the dehydroxylation of $Al(OH)_3$ gel and the combustion of organic carbon. The formation of poorly-crystallized η-alumina (eta) occurs by 825ºC and crystallinity increased with temperature up to 1000ºC. At 1100ºC, the η-alumina transforms to highly-crystalline α-alumina, along with the formation other high temperature phases mullite and gehlenite.

The above phase transitions were accompanied with morphological changes. The raw sludge consisted of very fine, irregular particles which agglomerated upon calcination at temperatures up to 825ºC, developing internal porosity and increased surface area. At 1000ºC, sintering occured resulting in smooth, rounded particles with decreased BET surface area. At 1100ºC, the complete removal of hydroxyl groups and formation of α-alumina led to the partial collapse of pore walls resulting in a drastic reduction in particle size and BET surface area. The workability of fresh mortars varied consistently with changes in morphology and BET specific surface area. Higher surface area meant more water was adsorbed by the sludge particles which resulted in reduced workability. Thus, workability of corresponding mortars decreased with calcination temperature up to 825ºC and then increased with further increase in temperature.

7.2 Hydration of Calcined Sludge-Blended Cement Pastes

For binary cement pastes containing sludges calcined between 825ºC to 1100ºC, there was an acceleration of the alite hydration. Calorimetric heat curves indicate that the calcined sludges contribute both a filler and chemical effect, with more crystalline sludges, namely those calcined at 1000ºC and 1100ºC, exhibiting a lesser chemical effect on PC hydration. The sludge calcined at 825ºC (C825) greatly influenced hydration behaviour of pure Portland cement. C825 contains significant quantities of reactive, amorphous aluminates which rapidly react with gypsum to form ettringite. This leads to an accelerated C_3A hydration which results in the formation of the AFm phase, monosulfoaluminate before the acceleration period of silicate phases. Because the C_3A reaction occurs before the onset of alite hydration, the system is undersulfated. In undersulfated systems, aluminium can adsorb on hydroxylated C_3S, mainly through strong ionic interactions between aluminate and calcium ions on the surface of silicate phases [25,27,291]. This blocks the reactive sites present on the

alite surface, reducing its solubility and reactivity. This process is facilitated by the drop in pH induced by dissolved aluminium. As a result, lower degrees of alite hydration are observed at later ages. In pastes containing more crystalline sludges, C1000 and C1100, a properly sulfated condition exists. The lower aluminate-sulfate ratio appears to better control C_3A hydration without affecting much the alite hydration leading to higher degrees of alite hydration at later ages. Thus, it can be inferred that if enough sulfates remain present at early age, the renewed aluminate reaction would occur after the onset of silicate acceleration period and alite hydration is therefore not inhibited.

All cement pastes containing slag and calcined sludge present faster hydration kinetics than neat PC paste. In paste containing the most amorphous sludge (CS825), the alite hydration peak is significantly lower and broader likely related to the mentioned inhibition of alite hydration by aluminium ions contributed by both slag and sludge. As a consequence, slag hydration is also hindered due to limited CH for pozzolanic reaction. In paste containing more crystalline sludge addition at 1000^{o}C (CS1000), hydration also occurs in an undersulfated system. C_3A hydration is enhanced and results in a highly exothermic peak taking place prior to the silicate hydration peak. However, in paste containing the inert sludge (CS1100) a properly-sulfated condition exists because the sludge addition is inert which lowers the aluminate-sulfate ratio. As a result, hydration progresses normally with enhanced clinker and slag hydration at later ages.

The presence of limestone in the studied quaternary blends still led to undersulfated C_3A reaction with a more intense peak occurring prior to silicate hydration peak. However, there was a slight indication of improved silicate reaction compared to the limestone-free blends. It is inferred that in the presence of sufficient calcium ions contributed by the limestone, sulfates are adsorbed on C-A-S-H surface and therefore they are not able to passivate the C_3A surface, leading to an earlier sulfate depletion. In addition, the drop in pH induced by aluminium ions is counteracted by calcium ions provided by limestone which reduces the binding strength of Al^{3+} on alite which leads to the observed enhancement in clinker hydration [25].

The aforementioned findings informed the formulation of ternary cement pastes containing the most reactive calcined sludge (at 825^{o}C) and limestone. Significant shortening of the induction periods is observed compared to the sludge blend without limestone (80-20-0). This suggests that calcium and sulfate ions are consumed at a faster rate, favouring gypsum and alite dissolutions which then accelerates the onset

of the main hydration peak [200]. Briendl et al. [295] reported that in the presence of limestone, more sulfate ions are adsorbed by C-S-H and the depletion of gypsum is reached earlier in time during the hydration process compared to neat cement containing no limestone. At a higher calcined sludge:limestone ratio of 2:1, an intense and earlier aluminate peak can be observed corresponding to sulfate depletion [10,295]. In the neat cement system and the blends containing lower sludge:limestone ratios (1:1 and 1:2) the aluminate peak is absent likely indicating a later sulfate depletion. It is well established that limestone will only react with aluminate ions after sulfate depletion [100,313]. An earlier sulfate depletion occurring in the 80-13.3-6.7 blend coincides with the higher cumulative heat output in this blend compared to all other blends. This higher heat output is attributed to increased formation of Hc and Mc. A higher calcined sludge addition (and aluminium dosage) favours limestone dissolution thereby enhancing sludge reaction whereas sludge reaction is limited by gypsum dissolution in the binary PC -sludge blend (80-20-0). Furthermore, in the presence of limestone, higher degree of clinker hydration is observed compared to the blend without limestone (80-20-0). It is argued that the earlier described inhibition of C_3S hydration in the absence of limestone is due competition for Ca^{2+} ions [295]. In the absence of limestone, the additional calcium needed for the formation of AFm phases has to be consumed from the pore solution which results in competition for calcium ions needed for the formation of C-A-S-H phases. When limestone is present, the aluminates from the sludge react to form AFm phases. In addition, the drop in pH induced by aluminium ions is counteracted by calcium ions provided by limestone which reduces the binding strength of Al^{3+} on alite and leads to an enhancement in clinker hydration [25].

7.3 Microstructure and Phase Assemblage of Calcined Sludge-Blended Cement Pastes

7.3.1 C-S-H Composition

The Ca/Si ratio in C-S-H of hydrated cement was found to be higher in neat PC than all slag cements and binary cements containing calcined sludge. The incorporation of aluminium in C-S-H was a function of crystallinity of the added sludge. The blends containing more crystalline sludges showed slightly lower aluminium contents and slightly increased Ca/Si ratios. Thus, the amorphous content of the

calcined sludge led to an increase in the dissolved aluminium concentration in pore solution, and so an increased Al/Si ratio [64]. The lower Ca/Si ratio in blended pastes is due to the additional Si, contributed by calcined sludge dissolution and/ or slag dissolution, [64,112]. Similar findings are well reported in the literature, where alumina-rich SCMs produce C-S-H with a lower Ca/Si and higher Al/Si ratios [64,112].

In ternary limestone cements containing sludge calcined at 825^{o}C and limestone, there was aluminium incorporation in C-S-H while the Ca/Si remained unchanged. It seems there is a practical limit for the amount of alumina that can be taken up into C-A-S-H as aluminium incorporation is quite small even for higher doses of calcined sludge. The increased AFt and AFm precipitation in the ternary blends would influence the alumina concentration in the pore solution [99] and consequently incorporation into C-S-H. However, there is only so much aluminium which can be incorporated in the C-S-H and the remainder precipitates in AFm phases. Furthermore, It has been reported that Ca/Si ratio is increased with gypsum and limestone dosage [311]. Thus, the presence of limestone might explain the sustained Ca/Si ratio even at higher doses of calcined sludge.

7.3.2 CH Formation

The measured CH in the studied systems is influenced by the alumina contributions of calcined sludge and/or slag, as well as pozzolanic reaction of slag. In particular, the presence of amorphous sludge (at 825^{o}C) led to significant reduction in the measured CH content. Higher aluminium concentrations in the pore solution retard silicate dissolution as the sorption on the surface sites of silicates slows down dissolution. Consequently, coupled additions of slag and amorphous sludge led to drastic reduction in measured CH per PC content. In pastes incorporating more crystalline sludges, increased CH was observed likely due to reduced solubility of aluminates in the sludges. The sludge calcined at 1100^{o}C is inert, so its addition had a dilution effect leading to enhanced clinker hydration and higher CH formation relative to the corresponding reference mixes. Furthermore, the addition of limestone leads to higher degree of clinker hydration compared to the corresponding blend without limestone. However, there was a more drastic decrease in the CH content due to the formation of calcium bearing hydration products such as hemi and/ moncarboaluminate hydrates [11,127]. Dissolved aluminates provided by the mineral

additions react with limestone to form carboaluminates, consuming portlandite in the process.

7.3.3 Hc and Mc Formation

The addition of sludge calcined at 825^{o}C contributes a considerable amount of reactive aluminates, which enhances the limestone reaction. At higher doses of calcined sludge, the reaction of calcined sludge seems to be enhanced in the system with limestone over that in the binary sludge-PC blend. Also, the limestone reacts faster in the system with calcined sludge than in the binary limestone-PC blend. These results point to strong synergistic effects with coupled substitutions of this type. XRD results show that coupled substitutions of calcined sludge and limestone alter the reaction pathway and lead to increased formation of carboaluminates over monosulfoaluminates, thereby stabilizing ettringite. Higher dissolution of calcite was observed at early age, likely related to the lower pH induced by calcined sludge compared to neat cement [96,302]. In ternary limestone cements containing calcined sludge (at 825^{o}C), the formation of carboaluminates, and their amounts depend on the availability of alumina to react with limestone. The XRD results show that limestone reacts with aluminates in calcined sludge, forming significant amounts of Hc from as early as 2 days. At 7 days of curing, Hc and Mc coexist but the latter formed to a greater extent. Also, Mc was formed earlier in the ternary blends and the contents were significantly greater than the binary limestone-PC blend. From 7days onwards, Hc progressively transforms to Mc as Mc is slightly more stable thermodynamically but the rate of formation is quicker for Hc [314]. However, increasing dosages of calcined sludge provides additional aluminates which seem to favour the formation of hemicarboaluminate instead of monocarboaluminate [302,314].

7.3.4 Ettringite formation

The amount of ettringite formed depends on the aluminate-sulfate ratio of the system. Upon mixing, aluminates from calcined sludge rapidly react with calcium sulfates to form ettringite. Sulfate depletion accelerates C_3A reaction which consumes ettringite to form monosulfoaluminate (Ms). The addition of limestone leads to the formation Hc and Mc rather than Ms leading to the stabilisation of ettringite. In ternary calcined sludge-limestone cements, the ettringite contents were similar to neat PC at later age despite the higher initial sulfate content in the neat system. However, the

ettringite content in ternary cements does not significantly vary with calcined sludge content as it is related to initial sulfate content which is constant.

7.3.5 Porosity

The coarse porosity of cement pastes was assessed by SEM-IA. In addition to the degree of hydration, the physical characteristics of SCMs such as particle size, shape and density are even more relevant where less reactive materials are incorporated in cement. In binary pastes containing sludge calcined between 825 - 1100^{o}C, the coarse porosity of all cement pastes decreased as hydration progressed. After 28 days, paste C825 showed a higher porosity than the CEM I paste, indicating that increased AFm (Ms) formation does not compensate for the reduced degree of hydration in this blend. Sludge calcined at 825^{o}C is irregularly shaped, so the filling effect is slight. Incorporation of sludge calcined at 1000^{o}C reduced porosity more than that calcined at 825^{o}C, due to its smooth and rounded shape which enables better dispersion and space filling of the matrix. The addition of sludge calcined at 1100^{o}C further decreased porosity owing to the finer particle size. Because its particles are finer than the cement particles, its addition filled voids between cement particles, increasing the packing density. The coarse porosity of cements containing both slag and calcined sludge were similar and higher than the binary pastes. The higher aluminium concentration due to coupled addition of calcined sludge and slag retards silicate dissolution. Consequently, slag hydration is limited as little portlandite is formed. This results in lower volume of hydrates and increased porosity.

Ternary calcined sludge-limestone blends showed lower coarse porosity than the binary PC-calcined sludge (80-20-0) and PC-limestone (80-0-20) blends. Reaction synergies between limestone and calcined sludge produces Hc and Mc, stabilizing ettringite in the process. The increase in the volume of hydrates leads to better space filling and a reduction in porosity.

7.4 Relationship between Sludge reactivity, Microstructure and Compressive Strength of Blended Systems.

The preceding sections discussed variations in the hydration behaviour and the ensuing microstructures for the cements studied. With increasing calcining temperatures between 0-625^{o}C, the SAI of binary calcined sludge-PC mortars

increased with temperature due to the removal of organic carbon from the sludge samples but fell below the 75% SAI prescribed by the ASTM C618 [169]. Between 825^{o}C-1100^{o}C, the SAI test suggests that calcined sludge can be considered a pozzolan [169] and reactivity of the resulting sludge particles is controlled by phase transitions that occur by heat treatment. Alum sludge calcined at 825^{o}C showed the best reactivity due to the formation of poorly crystallized η-alumina. However, the degree of clinker hydration, ettringite and portlandite contents were higher in the neat PC paste and consequently had higher hydrate volume and lower porosity. Cement replacement with calcined sludge at 825^{o}C led to lower silicate reaction likely due to higher concentrations of aluminium in solution. Also, the dissolution of aluminium ions from calcined sludge rapidly depletes gypsum leading to accelerated C_3A reactions which consume ettringite to form Ms. This led to lower mechanical strength than the neat system and other binary calcined sludge cement pastes. With increasing calcination temperature to 1100^{o}C, the reactivity of the sludge decreased due to crystallization of alumina phases present. The higher crystallinity of the sludges prevents the rapid consumption of $CaSO_4$ which delays C_3A hydration. The reduced dissolution of aluminates from the calcined sludges prevents the rapid sulfate depletion and silicate hydration progresses normally leading to higher mechanical strength.

Coupled substitution of cement with slag and calcined sludge led to higher aluminium concentration and thus lower silicate and slag hydration. These explain the higher compressive strength at all ages in neat PC compared to composite calcined sludge-slag cements. The addition of limestone led to the synergistic reaction with alumina contained in calcined sludge leading to enhanced formation of Hc and Mc. Hc and Mc precipitate in pores left behind by clinker hydration. The clusters of carboaluminates are intermixed with the surrounding C-A-S-H matrix, effectively contributing to porosity refinement and strength development. As a result, in quaternary PC-slag-limestone-calcined sludge blends, the sludge at 825^{o}C (CSL825) produced better mechanical strength than more commonly used PC-slag-limestone (CSL) blends. In addition, although the strengths were lower in the quaternary blends than the neat cement, they were higher than the equivalent ternary PC-slag-calcined sludge blends.

The synergistic effects of calcined sludge (at 825^{o}C) and limestone powder were more obvious in ternary cement pastes. The 7-day SAIs of the binary blends

containing either calcined sludge or limestone were 67.5 and 70.4% respectively while coupled substitutions of cement with calcined sludge and limestone in the ratio 1:2, 1:1 and 2:1 led to a dramatic increase in SAI to 90.1, 97.7 and 97.0% respectively. At later ages, clinker hydration dominates, and much higher strength was observed in the neat system. As a result, the SAI values of the ternary blends fell within the range 87-91% at 28 and 56 days. The results demonstrate the effectiveness of ternary systems both at early and late ages because the SAI values were higher than the single additions. The XRD and TG results show that calcium carbonate reacts with the aluminates in the calcined sludge, forming significant amounts of hemicarboaluminate and to a lesser extent monocarboaluminate from as early as 2 days. TGA shows that the reactions of calcined sludge and limestone consume calcium hydroxide, which may be completely absent at later ages in blends with high levels of calcined sludge. It was shown that even in the presence of limestone, higher levels of calcined sludge (at 825^{o}C) produced a stronger and earlier aluminate peak corresponding to sulfate depletion before the peak of the main silicate reaction. Consequently, decreased silicate hydration likely due to adsorption of aluminium ions was observed with increasing levels of calcined sludge [25,27].

The relationship between compressive strength and coarse porosity for all mixes tested after 28 days show a clear negative correlation. This suggests that the porosity dominates the compressive strength, independent of the mix designs, which is in agreement with the previous observations [11,312]. In ternary calcined sludge-limestone cement pastes, compressive strength and transport properties are also inversely correlated. The performance against gas permeability suggests that ternary cements give comparable performance with neat OPC and better performance than binary PC-calcined sludge and PC-limestone cements. The sorptivity index values increased with calcined sludge content likely due to the large surface area and thus higher water adsorption of unreacted sludge particles.

7.5 Final Comments

This work has demonstrated that calcining UK alum sludge at 825^{o}C produces reactive aluminates that can be used as an SCM. UK production of WTS in 2013 was approximately 131,000 tonnes dry solids, 44% of which is alum sludge [172,173].

Following the calcination process, this translates to 44,960 tonnes/annum of SCM that can be derived from this waste stream.

Earlier discussions in this chapter have highlighted that calcined sludge-blended cements present significant differences in terms of hydration kinetics and phase assemblage compared to neat cement systems. Particularly, the dissolution of aluminates from calcined sludge consumes calcium sulfates which accelerates C_3A reaction. Thus, it can be inferred that the chemical and mineralogical composition and the initial sulfate content in the mix are parameters that contribute to differences in hydration kinetics and might lead to an uncontrolled C_3A reaction. The undersulfated condition favours the adsorption of aluminium ions on the surface of silicates leading to its inhibited reaction. This process limits the rate and extent alite dissolution and further hydration.

The aluminate-sulfate balance in the mix may be a good indication to predict the C_3A reaction in the mixes containing calcined sludge. The incorporation of the more amorphous sludge calcined at 825^{o}C contributes hydratable aluminates which raise the aluminate-sulfate ratio of the system leading to the fast and highly exothermic C_3A reaction before or almost simultaneously with silicate hydration. Lower aluminate-sulfate ratio as in the blends containing more crystalline sludges do not have such a dramatic impact on silicate hydration. The addition of gypsum would be needed to control the aluminate reaction sufficiently in time for silicate hydration to progress normally as in “properly sulfated” systems. The adequate addition of gypsum to the matrix composition may provide a valid and inexpensive extra source of sulfates to change the aluminate-sulfate ratio towards an optimum compatibility with the calcined sludge. Thus, a compromise should be found which results in controlled C_3A hydration and enhanced silicate hydration to ensure a higher rate of strength gain at later ages.

The reactivity of calcined sludge (at 825^{o}C) is limited by gypsum availability in binary PC-calcined sludge pastes. On the other hand, the addition of limestone improves the reactivity of calcined sludge. Calcium carbonate reacts with Al^{3+} from calcined sludge (at 825^{o}C) forming hemi and monocarboaluminate. Previous reports have suggested that the level of sulfate in neat cement paste can be replaced by up to 25% calcium carbonate without modification of the properties of the system [96]. This suggests that to a certain degree, limestone can compensate for the fast sulfate depletion caused by elevated levels of calcined sludge (at 825^{o}C). Finding the optimum compatibility of gypsum and limestone in calcined sludge blended cements

is therefore paramount in order to maximize compressive strength. In this way, adequate sulfation is achieved while exploiting reaction synergies between calcined sludge and limestone powder leading to enhanced silicate hydration and improved strength.

7.6 Further Work

With respect to the work presented in this thesis, the following suggestions are recommended for future research:

- An assessment of the overall viability and carbon emissions associated with SCM production from alum sludge.
- Alum sludge is of variable composition from one water treatment plant to another and even for a specific plant over time. Therefore, there is need to study the effect of sludge variability on hydration behaviour and performance.
- An investigation into the influence of gypsum and limestone content on the hydration and mechanical properties of cement blends incorporating calcined sludge. The incorporation of limestone will produce changes in the optimum gypsum content due to the reaction with calcined sludge to form AFt and AFm phases. This means that limestone addition may affect the quantity of gypsum required to optimize reactivity of calcined sludge and mechanical properties of blended cements in the short and long term.
- The phase evolution of cement pastes containing calcined sludge should be characterized by in-situ X-ray powder diffraction. By using this technique, how the Al^{3+} concentration in calcined sludge and C_3A content in cements containing gypsum (resulting in different Al_2O_3/SO_3 ratios) influence the mechanisms and kinetics of hydration can be determined.
- This work makes use of the traditional XRD-Rietveld method which is limited to the quantification of crystalline phases and total amorphous content. Advances in XRD suggests the use of a ‘partial or no known crystal structure’ (PONCKS) method for the quantification of distinct amorphous phases. Thus, this method allows the degree of hydration of calcined sludge to be determined.
- The change in pore solution chemistry (i.e. ionic concentration and pH) caused by calcined sludge should be analyzed in order to understand the influence on the dissolution of slag, limestone and silicate phases.

- The characterization of the pore size distribution of calcined sludge blended cements by mercury intrusion porosimetry (MIP) may provide valuable information about the compaction and consolidation of the matrix containing calcined sludge. This evaluation may help further understand how the rapid reactivity of calcined sludge affects compressive strength.
- The durability of cementitious matrices containing calcined sludge to external sulfate attack should be evaluated. As the ettringite formed by calcined sludge and further C_3A hydration depend on the sulfate balance of the matrix, the deleterious expansion reactions caused by the external sulfate attack may have different damaging effects depending on concentration of calcined sludge used.
- It is well-known that the chloride binding capacity of cement can be improved by adding alumina-rich materials [320,321]. The higher the quality of alumina in cementitious materials, the higher chloride binding capacity of cement paste. Metakaolin and slag has shown an improvement of chloride binding capacity compared to pure Portland cement. It acts as an additional alumina source which facilitates to the formation of Friedel's and Kuzel's salts which enhance the chemical binding of the chloride ion [320]. In this sense, an investigation into the chloride binding capacity of calcined sludge blended cements is promising.

References

[1] T. Danner, G. Norden, H. Justnes, Characterisation of calcined raw clays suitable as supplementary cementitious materials, Appl. Clay Sci. 162 (2018) 391–402. https://doi.org/10.1016/j.clay.2018.06.030.

[2] J.S. Damtoft, J. Lukasik, D. Herfort, D. Sorrentino, E.M. Gartner, Sustainable development and climate change initiatives, Cem. Concr. Res. 38 (2008) 115–127. https://doi.org/10.1016/j.cemconres.2007.09.008.

[3] L.D. Hart, E. Lense, Alumina chemicals : science and technology handbook, American Ceramic Society, 1990. https://www.wiley.com/en-us/Alumina+Chemicals%3A+Science+and+Technology+Handbook-p-9780916094331 (accessed November 24, 2018).

[4] C. Binnie, M. Kimber, 13: Waterworks wastes and sludge, in: Basic Water Treat., Thomas Telford Publishing, 2009: pp. 232–245. https://doi.org/doi:10.1680/bwt.36086.0013.

[5] U.S. EPA, Drinking Water Treatment Plant Residuals. Management Technical Report. Summary of residuals generation, treatment and disposal at large community water systems., (2011) 378.

[6] B.C. O'Kelly, M.E. Quille, Shear strength properties of water treatment residues, Proc. ICE - Geotech. Eng. 163 (2010) 23–35. https://doi.org/10.1680/geng.2010.163.1.23.

[7] R. Fernandez, F. Martirena, K.L. Scrivener, The origin of the pozzolanic activity of calcined clay minerals: A comparison between kaolinite, illite and montmorillonite, Cem. Concr. Res. 41 (2011) 113–122. https://doi.org/10.1016/J.CEMCONRES.2010.09.013.

[8] H.M. Owaid, R. Hamid, M.R. Taha, Influence of thermally activated alum sludge ash on the engineering properties of multiple-blended binders concretes, Constr. Build. Mater. 61 (2014) 216–229. https://doi.org/10.1016/j.conbuildmat.2014.03.014.

[9] A.L.G. Gastaldini, M.F. Hengen, M.C.C. Gastaldini, F.D. do Amaral, M.B. Antolini, T. Coletto, The use of water treatment plant sludge ash as a mineral addition, Constr. Build. Mater. 94 (2015) 513–520. https://doi.org/10.1016/j.conbuildmat.2015.07.038.

[10] M. Antoni, J. Rossen, F. Martirena, K. Scrivener, Cement substitution by a combination of metakaolin and limestone, Cem. Concr. Res. 42 (2012) 1579–1589. https://doi.org/10.1016/j.cemconres.2012.09.006.

[11] K. De Weerdt, M. Ben Haha, G. Le Saout, K.O. Kjellsen, H. Justnes, B. Lothenbach, Hydration mechanisms of ternary Portland cements containing limestone powder and fly ash, Cem. Concr. Res. 41 (2011) 279–291. https://doi.org/10.1016/j.cemconres.2010.11.014.

[12] K. De Weerdt, K.O. Kjellsen, E. Sellevold, H. Justnes, Synergy between fly ash and limestone powder in ternary cements, Cem. Concr. Compos. 33 (2011) 30–38. https://doi.org/10.1016/J.CEMCONCOMP.2010.09.006.

[13] D. Wang, C. Shi, N. Farzadnia, Z. Shi, H. Jia, A review on effects of limestone powder on the properties of concrete, Constr. Build. Mater. 192 (2018) 153–166. https://doi.org/10.1016/j.conbuildmat.2018.10.119.

[14] M. Záleská, M. Pavlíková, Z. Pavlík, O. Jankovsk, J. Pokorn, V. Tydlitát, P. Svora, R.Č. Ern, Physical and chemical characterization of technogenic

pozzolans for the application in blended cements, Constr. Build. Mater. 160 (2018) 106–116. https://doi.org/10.1016/j.conbuildmat.2017.11.021.
[15] ASTM C618, Standard specification for coal fly ash and raw or calcined natural pozzolan for use in concrete, (n.d.).
[16] W. Lerch, " The Influence of Gypsum on the Hydration and Properties of Portland Cement Pastes ", Proc. Am. Soc. Test. Mater. 46 (1946) 1–48.
[17] P.C. Hewlett, Cement Components and Their Phase Relations, in: Lea´s Chem. Cem. Concrete (4th Ed.), Elsevier Ltd., 1998: pp. 95–129. https://doi.org/10.1016/B978-075066256-7/50015-1.
[18] P.C. Hewlett, Portland Cement: Classification and Manufacture, in: Lea´s Chem. Cem. Concret (4th Ed.), Elsevier Ltd., 1998: pp. 25–94. https://doi.org/10.1016/B978-075066256-7/50014-X.
[19] I. Odler, Hydration, Setting and Hardening of Portland Cement, in: Lea's Chem. Cem. Concr., 4th ed., Elsevier Ltd., 2003: pp. 241–297. https://doi.org/10.1016/B978-075066256-7/50018-7.
[20] J.D. Hawthorne, Cementitious Grouts for ILW Encapsulation – Composition, Hydration and Performance, University of Leeds, 2016.
[21] I.G. Richardson, Nature of the hydration products in hardened cement pastes, Cem. Concr. Compos. 22 (2000) 97–113. https://doi.org/10.1016/S0958-9465(99)00036-0.
[22] G.C. Bye, Portland cement: Composition, Production and Properties, 2nd editio, Thomas Telford Publishing, 1999. https://doi.org/10.1680/pccpap.27664.
[23] S. Mindess, J.F. Young, D. Darwin, Concrete, Prentice Hall, 2003.
[24] D. Stephan, S.N. Dikoundou, G. Raudaschl-Sieber, Hydration characteristics and hydration products of tricalcium silicate doped with a combination of MgO, Al_2O_3 and Fe_2O_3, Thermochim. Acta. 472 (2008) 64–73. https://doi.org/10.1016/j.tca.2008.03.013.
[25] E. Pustovgar, R.K. Mishra, M. Palacios, J.B. d'Espinose de Lacaillerie, T. Matschei, A.S. Andreev, H. Heinz, R. Verel, R.J. Flatt, Influence of aluminates on the hydration kinetics of tricalcium silicate, Cem. Concr. Res. 100 (2017) 245–262. https://doi.org/10.1016/j.cemconres.2017.06.006.
[26] G.L. Valenti, V. Sabatelli, B. Marchese, Hydration kinetics of tricalcium silicate solid solutions at early ages, Cem. Concr. Res. 8 (1978) 61–72. https://doi.org/10.1016/0008-8846(78)90058-3.
[27] P. Suraneni, R.J. Flatt, Use of micro-reactors to obtain new insights into the factors influencing tricalcium silicate dissolution, Cem. Concr. Res. 78 (2015) 208–215. https://doi.org/10.1016/j.cemconres.2015.07.011.
[28] F. Begarin, S. Garrault, A. Nonat, L. Nicoleau, Hydration of alite containing aluminium, in: Adv. Appl. Ceram., 2011: pp. 127–130. https://doi.org/10.1179/1743676110Y.0000000007.
[29] A. Quennoz, K.L. Scrivener, Interactions between alite and C_3A-gypsum hydrations in model cements, Cem. Concr. Res. 44 (2013) 46–54. https://doi.org/10.1016/j.cemconres.2012.10.018.
[30] R. Taylor, I.G. Richardson, R.M.D. Brydson, Composition and microstructure of 20-year-old ordinary Portland cement-ground granulated blast-furnace slag blends containing 0 to 100% slag, Cem. Concr. Res. 40 (2010) 971–983. https://doi.org/10.1016/j.cemconres.2010.02.012.
[31] J.W. Bullard, H.M. Jennings, R.A. Livingston, A. Nonat, G.W. Scherer, J.S. Schweitzer, K.L. Scrivener, J.J. Thomas, Mechanisms of cement hydration,

Cem. Concr. Res. 41 (2011) 1208–1223. https://doi.org/10.1016/j.cemconres.2010.09.011.
[32] L. Nicoleau, A. Nonat, D. Perrey, The di- and tricalcium silicate dissolutions, Cem. Concr. Res. 47 (2013) 14–30. https://doi.org/10.1016/j.cemconres.2013.01.017.
[33] A.M. Neville, Properties of concrete, Pearson, 2011.
[34] H. Minard, Etude intégrée des processus d'hydratation, de coagulation, de rigidification et de prise pour un système C_3S-C_3A - sulfates - alcalins, Université de Bourgogne, 2003.
[35] E. Breval, C_3A hydration, Cem. Concr. Res. 6 (1976) 129–137. https://doi.org/10.1016/0008-8846(76)90057-0.
[36] A. Quennoz, Hydration of C_3A with Calcium Sulfate Alone and in the Presence of Calcium Silicate, Ecole Polytechnique Federale De Lausanne, 2011. https://doi.org/10.5075/epfl-thesis-5035.
[37] P. Meredith, A.M. Donald, N. Meller, C. Hall, Tricalcium aluminate hydration: Microstructural observations by in-situ electron microscopy, in: J. Mater. Sci., 2004: pp. 997–1005. https://doi.org/10.1023/B:JMSC.0000012933.74548.36.
[38] H.N. Stein, Some characteristics of the hydration of $3CaO.Al_2O_3$ in the presence of $CaSO_4.2\ H_2O$, Recl. Des Trav. Chim. Des Pays-Bas. 81 (1962) 881–889. https://doi.org/10.1002/recl.19620811008.
[39] M. Collepardi, G. Baldini, M. Pauri, M. Corradi, Tricalcium aluminate hydration in the presence of lime, gypsum or sodium sulfate, Cem. Concr. Res. 8 (1978) 571–580. https://doi.org/10.1016/0008-8846(78)90040-6.
[40] W.A. Corstanje, H.N. Stein, J.M. Stevels, Hydration reactions in pastes $C_3S+C_3A+CaSO_4.2aq$+water at 25°C. II, Cem. Concr. Res. 4 (1974) 193–202. https://doi.org/10.1016/0008-8846(74)90132-X.
[41] P.W. Brown, L.O. Liberman, G. Frohnsdorff, Kinetics of the Early Hydration of Tricalcium Aluminate in Solutions Containing Calcium Sulfate, J. Am. Ceram. Soc. 67 (1984) 793–795. https://doi.org/10.1111/j.1151-2916.1984.tb19702.x.
[42] K.L. Scrivener, The Development of Microstructure During The Hydration of Portland Cement, Imperial College London, 1984.
[43] R.F. Feldman, V.S. Ramachandran, The influence of $CaSO_4.2H_2O$ upon the hydration character of $3CaO.Al_2O_3$, Mag. Concr. Res. 18 (1966) 185–196. https://doi.org/10.1680/macr.1966.18.57.185.
[44] J. Skalny, M.E. Tadros, Retardation of Tricalcium Aluminate Hydration by Sulfates, J. Am. Ceram. Soc. 60 (1977) 174–175. https://doi.org/10.1111/j.1151-2916.1977.tb15503.x.
[45] J.J. Beaudoin, V.S. Ramachandran, A new perspective on the hydration characteristics of cement phases, Cem. Concr. Res. 22 (1992) 689–694. https://doi.org/10.1016/0008-8846(92)90021-M.
[46] C. Plowman, J.G. Cabrera, Mechanism and kinetics of hydration of C_3A and C_4AF. Extracted from cement, Cem. Concr. Res. 14 (1984) 238–248. https://doi.org/10.1016/0008-8846(84)90110-8.
[47] P. Juilland, E. Gallucci, R. Flatt, K. Scrivener, Dissolution theory applied to the induction period in alite hydration, Cem. Concr. Res. 40 (2010) 831–844. https://doi.org/10.1016/j.cemconres.2010.01.012.
[48] I.G. Richardson, Nature of C-S-H in hardened cements, Cem. Concr. Res. 29 (1999) 1131–1147. https://doi.org/10.1016/S0008-8846(99)00168-4.
[49] K.L. Scrivener, T. Füllmann, E. Gallucci, G. Walenta, E. Bermejo, Quantitative study of Portland cement hydration by X-ray diffraction/Rietveld analysis and

independent methods, Cem. Concr. Res. 34 (2004) 1541–1547. https://doi.org/10.1016/j.cemconres.2004.04.014.
[50] I.G. Richardson, G.W. Groves, Microstructure and microanalysis of hardened ordinary Portland cement pastes, J. Mater. Sci. 27 (1992) 6204–6212. https://doi.org/10.1007/BF00349061.
[51] B.D. Barnes, S. Diamond, W.L. Dolch, The contact zone between portland cement paste and glass “aggregate” surfaces, Cem. Concr. Res. 8 (1978) 233–243. https://doi.org/10.1016/0008-8846(78)90012-1.
[52] P. Juilland, Early Hydration of Cementitious Systems, Ecole Polytechnique Federale De Lausanne, 2009.
[53] E.M.J. Berodier, Impact of the Supplementary Cementitious Materials on the kinetics and microstructural development of cement hydration, Lausanne, EPFL, 2015. https://doi.org/10.5075/EPFL-THESIS-6417.
[54] K.L. Scrivener, Backscattered electron imaging of cementitious microstructures: Understanding and quantification, Cem. Concr. Compos. 26 (2004) 935–945. https://doi.org/10.1016/j.cemconcomp.2004.02.029.
[55] M.M.C. Fernandez, Effect of Particle Size on the Hydration Kinetics and Microstructural Development of Tricalcium Silicate, Techniques. 4102 (2008) 99–114. https://doi.org/10.5075/epfl-thesis-4102.
[56] P. Juilland, A. Kumar, E. Gallucci, R.J. Flatt, K.L. Scrivener, Effect of mixing on the early hydration of alite and OPC systems, Cem. Concr. Res. 42 (2012) 1175–1188. https://doi.org/10.1016/j.cemconres.2011.06.011.
[57] E. Gallucci, X. Zhang, K.L. Scrivener, Effect of temperature on the microstructure of calcium silicate hydrate (C-S-H), Cem. Concr. Res. 53 (2013) 185–195. https://doi.org/10.1016/j.cemconres.2013.06.008.
[58] K.O. Kjellsen, R.J. Detwiler, Reaction kinetics of portland cement mortars hydrated at different temperatures, Cem. Concr. Res. 22 (1992) 112–120. https://doi.org/10.1016/0008-8846(92)90141-H.
[59] J. Cheung, A. Jeknavorian, L. Roberts, D. Silva, Impact of admixtures on the hydration kinetics of Portland cement, Cem. Concr. Res. 41 (2011) 1289–1309. https://doi.org/10.1016/j.cemconres.2011.03.005.
[60] F. Ridi, L. Dei, E. Fratini, S.H. Chen, P. Baglioni, Hydration kinetics of tri-calcium silicate in the presence of superplasticizers, J. Phys. Chem. B. 107 (2003) 1056–1061. https://doi.org/10.1021/jp027346b.
[61] J. Rieger, J. Thieme, C. Schmidt, Study of precipitation reactions by X-ray microscopy: $CaCO_3$ precipitation and the effect of polycarboxylates, Langmuir. 16 (2000) 8300–8305. https://doi.org/10.1021/la0004193.
[62] B. Lothenbach, K. Scrivener, R.D. Hooton, Supplementary cementitious materials, (2011). https://doi.org/10.1016/j.cemconres.2010.12.001.
[63] I.G. Richardson, G.W. Groves, The incorporation of minor and trace elements into calcium silicate hydrate (CSH) gel in hardened cement pastes, Cem. Concr. Res. 23 (1993) 131–138. https://doi.org/10.1016/0008-8846(93)90143-W.
[64] E. L’Hôpital, B. Lothenbach, G. Le Saout, D. Kulik, K. Scrivener, Incorporation of aluminium in calcium-silicate-hydrates, Cem. Concr. Res. 75 (2015) 91–103. https://doi.org/10.1016/j.cemconres.2015.04.007.
[65] J.J. Chen, The nanostructure of calcium silicate hydrate., Northwestern University, 2003.
[66] W. Müllauer, R.E. Beddoe, D. Heinz, Sulfate attack expansion mechanisms, Cem. Concr. Res. 52 (2013) 208–215.

https://doi.org/10.1016/j.cemconres.2013.07.005.
[67] W. Müllauer, Mechanisms of sulfate attack for plain and fly ash cements at different storage temperatures and sulphate concentrations, Technische Universität München, 2013. https://mediatum.ub.tum.de/1115224 (accessed January 11, 2020).
[68] Q. Ding, J. Yang, D. Hou, G. Zhang, Insight on the mechanism of sulfate attacking on the cement paste with granulated blast furnace slag: An experimental and molecular dynamics study, Constr. Build. Mater. 169 (2018) 601–611. https://doi.org/10.1016/j.conbuildmat.2018.02.148.
[69] E. Berodier, K. Scrivener, Understanding the Filler Effect on the Nucleation and Growth of C-S-H, J. Am. Ceram. Soc. 97 (2014) 3764–3773. https://doi.org/10.1111/jace.13177.
[70] F. Zunino, K. Scrivener, The influence of the filler effect on the sulfate requirement of blended cements, Cem. Concr. Res. 126 (2019). https://doi.org/10.1016/j.cemconres.2019.105918.
[71] F. Roelofs, W. Vogelsberger, Dissolution kinetics of nanodispersed γ-alumina in aqueous solution at different pH: Unusual kinetic size effect and formation of a new phase, J. Colloid Interface Sci. 303 (2006) 450–459. https://doi.org/10.1016/j.jcis.2006.08.016.
[72] J. Zhou, K. Zheng, Z. Liu, F. He, Chemical effect of nano-alumina on early-age hydration of Portland cement, Cem. Concr. Res. 116 (2019) 159–167. https://doi.org/10.1016/j.cemconres.2018.11.007.
[73] B. Lothenbach, K. Scrivener, R.D. Hooton, Supplementary cementitious materials, Cem. Concr. Res. 41 (2011) 1244–1256. https://doi.org/10.1016/J.CEMCONRES.2010.12.001.
[74] G. Le Saoût, E. Lécolier, A. Rivereau, H. Zanni, Chemical structure of cement aged at normal and elevated temperatures and pressures, Part II: Low permeability class G oilwell cement, Cem. Concr. Res. 36 (2006) 428–433. https://doi.org/10.1016/j.cemconres.2005.11.005.
[75] J.O. Ukpata, P.A.M. Basheer, L. Black, Performance of plain and slag-blended cements and mortars exposed to combined chloride–sulfate solution, Adv. Cem. Res. (2017) 1–16. https://doi.org/10.1680/jadcr.17.00121.
[76] European Committee for Standardization., British Standards Institution., Cement. Part 1, Composition, specifications and conformity criteria for common cements., (2007) 47. https://shop.bsigroup.com/ProductDetail/?pid=000000000030159150 (accessed September 23, 2019).
[77] P.C. Hewlett, Cements Made From Blast Furnace Slag, in: Lea´s Chem. Cem. Concret (4th Ed., Elsevier Ltd., 1998: pp. 633–674. https://doi.org/10.1016/B978-0-7506-6256-7.50023-0.
[78] M. Öner, K. Erdogdu, A. Günlü, Effect of components fineness on strength of blast furnace slag cement, Cem. Concr. Res. 33 (2003) 463–469. https://doi.org/10.1016/S0008-8846(02)00713-5.
[79] J. Bensted, P. Barnes, Structure and Performance of cements, Second Edi, Taylor & Francis, 2002.
[80] O.R. Ogirigbo, Influence of Slag Composition and Temperature on the Hydration and Performance of Slag Blends in Chloride Environments, University of Leeds, 2015. https://doi.org/doi:10.1201/b18972-71\r10.1201/b18972-71.
[81] S. Kucharczyk, J. Deja, M. Zajac, Effect of Slag Reactivity Influenced by

Alumina Content on Hydration of Composite Cements, J. Adv. Concr. Technol. 14 (2016) 535–547. https://doi.org/10.3151/jact.14.535.
[82] P.Z. Wang, R. Trettin, V. Rudert, T. Spaniol, Influence of Al_2O_3 content on hydraulic reactivity of granulated blast-furnace slag, and the interaction between Al_2O_3 and CaO, Adv. Cem. Res. 16 (2004) 1–7. https://www.icevirtuallibrary.com/doi/pdf/10.1680/adcr.2004.16.1.1 (accessed June 25, 2018).
[83] T. Matschei, B. Lothenbach, F.P. Glasser, The AFm phase in Portland cement, Cem. Concr. Res. 37 (2007) 118–130. https://doi.org/10.1016/j.cemconres.2006.10.010.
[84] J.S. Lumley, R.S. Gollop, G.K. Moir, H.F.W. Taylor, Degrees of reaction of the slag in some blends with Portland cements, Cem. Concr. Res. 26 (1996) 139–151. https://doi.org/10.1016/0008-8846(95)00190-5.
[85] J.I. Escalante, L.Y. Gómez, K.K. Johal, G. Mendoza, H. Mancha, J. Méndez, Reactivity of blast-furnace slag in Portland cement blends hydrated under different conditions, Cem. Concr. Res. 31 (2001) 1403–1409. https://doi.org/10.1016/S0008-8846(01)00587-7.
[86] V. Kocaba, E. Gallucci, K.L. Scrivener, Methods for determination of degree of reaction of slag in blended cement pastes, Cem. Concr. Res. 42 (2012) 511–525. https://doi.org/10.1016/j.cemconres.2011.11.010.
[87] M. Whittaker, M. Zajac, M. Ben Haha, F. Bullerjahn, L. Black, The role of the alumina content of slag, plus the presence of additional sulfate on the hydration and microstructure of Portland cement-slag blends, Cem. Concr. Res. 66 (2014) 91–101. https://doi.org/10.1016/j.cemconres.2014.07.018.
[88] M. Whittaker, M. Zajac, M. Ben Haha, F. Bullerjahn, L. Black, The role of the alumina content of slag, plus the presence of additional sulfate on the hydration and microstructure of Portland cement-slag blends, Cem. Concr. Res. 66 (2014) 91–101. https://doi.org/10.1016/j.cemconres.2014.07.018.
[89] V. Kocaba, Development and evaluation of methods to follow microstructural development of cementitious systems including slags, Ecole Polytechnique Federale De Lausanne, 2009. https://doi.org/10.5075/epfl-thesis-4523.
[90] K. Luke, F.P. Glasser, Internal chemical evolution of the constitution of blended cements, Cem. Concr. Res. 18 (1988) 495–502. https://doi.org/10.1016/0008-8846(88)90042-7.
[91] I.G. Richardson, G.W. Groves, Microstructure and microanalysis of hardened cement pastes involving ground granulated blast-furnace slag, J. Mater. Sci. 27 (1992) 6204–6212. https://doi.org/10.1007/BF01133772.
[92] M.J. Whittaker, The Impact of Slag Composition on the Microstructure of Composite Slag Cements Exposed to Sulfate Attack, University of Leeds, 2014. http://etheses.whiterose.ac.uk/id/eprint/9307.
[93] X. Wu, D.M. Roy, C.A. Langton, Early stage hydration of slag-cement, Cem. Concr. Res. 13 (1983) 277–286. https://doi.org/10.1016/0008-8846(83)90111-4.
[94] C. Çetin, S.T. Erdołan, M. Tokyay, Effect of particle size and slag content on the early hydration of interground blended cements, Cem. Concr. Compos. 67 (2016) 39–49. https://doi.org/10.1016/j.cemconcomp.2015.12.001.
[95] V.. Bonavetti, V.. Rahhal, E.. Irassar, Studies on the carboaluminate formation in limestone filler-blended cements, Cem. Concr. Res. 31 (2001) 853–859. https://doi.org/10.1016/S0008-8846(01)00491-4.
[96] B. Lothenbach, G. Le Saout, E. Gallucci, K. Scrivener, Influence of limestone

on the hydration of Portland cements, Cem. Concr. Res. 38 (2008) 848–860. https://doi.org/10.1016/j.cemconres.2008.01.002.
[97] M. Heikal, H. El-Didamony, M.S. Morsy, Limestone-filled pozzolanic cement, Cem. Concr. Res. 30 (2000) 1827–1834. https://doi.org/10.1016/S0008-8846(00)00402-6.
[98] D. Wang, C. Shi, N. Farzadnia, Z. Shi, H. Jia, Z. Ou, A review on use of limestone powder in cement-based materials: Mechanism, hydration and microstructures, Constr. Build. Mater. 181 (2018) 659–672. https://doi.org/10.1016/j.conbuildmat.2018.06.075.
[99] B. Lothenbach, G. Le Saout, E. Gallucci, K. Scrivener, Influence of limestone on the hydration of Portland cements, Cem. Concr. Res. 38 (2008) 848–860. https://doi.org/10.1016/J.CEMCONRES.2008.01.002.
[100] J. Bizzozero, K.L. Scrivener, Limestone reaction in calcium aluminate cement–calcium sulfate systems, Cem. Concr. Res. 76 (2015) 159–169. https://doi.org/10.1016/J.CEMCONRES.2015.05.019.
[101] M. Cyr, P. Lawrence, E. Ringot, Efficiency of mineral admixtures in mortars: Quantification of the physical and chemical effects of fine admixtures in relation with compressive strength, Cem. Concr. Res. 36 (2006) 264–277. https://doi.org/10.1016/j.cemconres.2005.07.001.
[102] W. Li, Z. Huang, T. Zu, C. Shi, W.H. Duan, S.P. Shah, Influence of Nanolimestone on the Hydration, Mechanical Strength, and Autogenous Shrinkage of Ultrahigh-Performance Concrete, J. Mater. Civ. Eng. 28 (2016) 04015068. https://doi.org/10.1061/(ASCE)MT.1943-5533.0001327.
[103] I. Soroka, N. Setter, The effect of fillers on strength of cement mortars, Cem. Concr. Res. 7 (1977) 449–456. https://doi.org/10.1016/0008-8846(77)90073-4.
[104] E.F. Irassar, Sulfate attack on cementitious materials containing limestone filler - A review, Cem. Concr. Res. 39 (2009) 241–254. https://doi.org/10.1016/j.cemconres.2008.11.007.
[105] B. Craeye, G. De Schutter, B. Desmet, J. Vantomme, G. Heirman, L. Vandewalle, Ö. Cizer, S. Aggoun, E.H. Kadri, Effect of mineral filler type on autogenous shrinkage of self-compacting concrete, Cem. Concr. Res. 40 (2010) 908–913. https://doi.org/10.1016/j.cemconres.2010.01.014.
[106] K. Vance, M. Aguayo, T. Oey, G. Sant, N. Neithalath, Hydration and strength development in ternary portland cement blends containing limestone and fly ash or metakaolin, Cem. Concr. Compos. 39 (2013) 93–103. https://doi.org/10.1016/j.cemconcomp.2013.03.028.
[107] A.M. Poppe, G. De Schutter, Cement hydration in the presence of high filler contents, Cem. Concr. Res. 35 (2005) 2290–2299. https://doi.org/10.1016/j.cemconres.2005.03.008.
[108] V. Bonavetti, H. Donza, V. Rahhal, E. Irassar, Influence of initial curing on the properties of concrete containing limestone blended cement, Cem. Concr. Res. 30 (2000) 703–708. https://doi.org/10.1016/S0008-8846(00)00217-9.
[109] M. Nehdi, S. Mindess, P.C. Aïtcin, Optimization of high strength limestone filler cement mortars, Cem. Concr. Res. 26 (1996) 883–893. https://doi.org/10.1016/0008-8846(96)00071-3.
[110] S. Rode, N. Oyabu, K. Kobayashi, H. Yamada, A. Kühnle, True atomic-resolution imaging of (1014) calcite in aqueous solution by frequency modulation atomic force microscopy, Langmuir. 25 (2009) 2850–2853. https://doi.org/10.1021/la803448v.
[111] Y. Araki, K. Tsukamoto, N. Oyabu, K. Kobayashi, H. Yamada, Atomic-

resolution imaging of aragonite (001) surface in water by frequency modulation atomic force microscopy, Jpn. J. Appl. Phys. 51 (2012). https://doi.org/10.1143/JJAP.51.08KB09.
[112] F. Deschner, F. Winnefeld, B. Lothenbach, S. Seufert, P. Schwesig, S. Dittrich, F. Goetz-Neunhoeffer, J. Neubauer, Hydration of Portland cement with high replacement by siliceous fly ash, Cem. Concr. Res. 42 (2012) 1389–1400. https://doi.org/10.1016/j.cemconres.2012.06.009.
[113] P. Thongsanitgarn, W. Wongkeo, A. Chaipanich, C.S. Poon, Heat of hydration of Portland high-calcium fly ash cement incorporating limestone powder: Effect of limestone particle size, Constr. Build. Mater. 66 (2014) 410–417. https://doi.org/10.1016/j.conbuildmat.2014.05.060.
[114] H.J. Kuzel, Initial hydration reactions and mechanisms of delayed ettringite formation in Portland cements, Cem. Concr. Compos. 18 (1996) 195–203. https://doi.org/10.1016/0958-9465(96)00016-9.
[115] L.G. Baquerizo, T. Matschei, K.L. Scrivener, M. Saeidpour, L. Wadsö, Hydration states of AFm cement phases, Cem. Concr. Res. 73 (2015) 143–157. https://doi.org/10.1016/j.cemconres.2015.02.011.
[116] A. Barker, H.P. Cory, The early hydration of limestone-filled cements Cem. Constr. Pap. Present. Int. Conf. Univ. Sheffield, UK, 9-12 Sept. 1991. (1991).
[117] K. Ingram, M. Poslusny, K. Daugherty, W. Rowe, Carboaluminate reactions as influenced by limestone additions, in: ASTM Spec. Tech. Publ., Publ by ASTM, 1990: pp. 14–23. https://doi.org/10.1520/stp23467s.
[118] J. Bensted, Some hydration investigation involving Portland cement- Effect of calcium carbonate substitution with gypsum, World Cem. Technol. 11 (1980).
[119] T. Schmidt, B. Lothenbach, M. Romer, J. Neuenschwander, K. Scrivener, Physical and microstructural aspects of sulfate attack on ordinary and limestone blended Portland cements, Cem. Concr. Res. 39 (2009) 1111–1121. https://doi.org/10.1016/j.cemconres.2009.08.005.
[120] J. Bizzozero, K.L. Scrivener, Limestone reaction in calcium aluminate cement-calcium sulfate systems, (2015). https://doi.org/10.1016/j.cemconres.2015.05.019.
[121] W.A. Klemm, L.D. Adams, Investigation of the formation of carboaluminates, in: ASTM Spec. Tech. Publ., Publ by ASTM, 1990: pp. 60–72. https://doi.org/10.1520/stp23472s.
[122] T. Matschei, B. Lothenbach, F.P. Glasser, The role of calcium carbonate in cement hydration, Cem. Concr. Res. 37 (2007) 551–558. https://doi.org/10.1016/j.cemconres.2006.10.013.
[123] D.P. Bentz, Modeling the influence of limestone filler on cement hydration using CEMHYD3D, Cem. Concr. Compos. 28 (2006) 124–129. https://doi.org/10.1016/j.cemconcomp.2005.10.006.
[124] M. Antoni, J. Rossen, F. Martirena, K. Scrivener, Cement substitution by a combination of metakaolin and limestone, Cem. Concr. Res. 42 (2012) 1579–1589. https://doi.org/10.1016/j.cemconres.2012.09.006.
[125] K. De Weerdt, M. Ben Haha, G. Le Saout, K.O. Kjellsen, H. Justnes, B. Lothenbach, Hydration mechanisms of ternary Portland cements containing limestone powder and fly ash, Cem. Concr. Res. 41 (2011) 279–291. https://doi.org/10.1016/J.CEMCONRES.2010.11.014.
[126] N. Voglis, G. Kakali, E. Chaniotakis, S. Tsivilis, Portland-limestone cements. Their properties and hydration compared to those of other composite cements, Cem. Concr. Compos. 27 (2005) 191–196.

https://doi.org/10.1016/j.cemconcomp.2004.02.006.
[127] K. De Weerdt, K.O. Kjellsen, E. Sellevold, H. Justnes, Synergy between fly ash and limestone powder in ternary cements, Cem. Concr. Compos. 33 (2011) 30–38. https://doi.org/10.1016/J.CEMCONCOMP.2010.09.006.
[128] D. Damidot, B. Lothenbach, D. Herfort, F.P. Glasser, Thermodynamics and cement science, Cem. Concr. Res. 41 (2011) 679–695. https://doi.org/10.1016/j.cemconres.2011.03.018.
[129] P. Mounanga, M.I.A. Khokhar, R. El Hachem, A. Loukili, Improvement of the early-age reactivity of fly ash and blast furnace slag cementitious systems using limestone filler, Mater. Struct. Constr. 44 (2011) 437–453. https://doi.org/10.1617/s11527-010-9637-1.
[130] Z. Yong, Y. Guang, Effect of limestone powder on microstructure of ternary cementitious system, in: Sustain. Constr. Mater. 2012 - Proc. 2nd Int. Conf. Sustain. Constr. Mater. - Des. Performance, Appl., 2013: pp. 224–233. https://doi.org/10.1061/9780784412671.0020.
[131] D.P. Bentz, E.J. Garboczi, Percolation of phases in a three-dimensional cement paste microstructural model, Cem. Concr. Res. 21 (1991) 325–344. https://doi.org/10.1016/0008-8846(91)90014-9.
[132] P.K. Mehta, P.J.M. Monteiro, Concrete: Microstructure, Properties, and Materials, Third, McGraw-Hill, New York, 2005.
[133] D.P. Bentz, E.F. Irassar, E. Bucher, W.J. Weiss, Limestone Fillers Conserve Cement Part 2: Durability issues and the effects of limestone fineness on mixtures, Concr. Int. (2009).
[134] M. González, V.F. Rahhal, V.L. Bonavetti, H. Donza, E.F. Irassar, Effect of curing on early chloride diffusion of filler cement concrete, Mater. Sci. (1999).
[135] A.A. Ramezanianpour, E. Ghiasvand, I. Nickseresht, M. Mahdikhani, F. Moodi, Influence of various amounts of limestone powder on performance of Portland limestone cement concretes, Cem. Concr. Compos. 31 (2009) 715–720. https://doi.org/10.1016/j.cemconcomp.2009.08.003.
[136] R.K. Dhir, M.C. Limbachiya, M.J. McCarthy, A. Chaipanich, Evaluation of Portland limestone cements for use in concrete construction, Mater. Struct. Constr. 40 (2007) 459–473. https://doi.org/10.1617/s11527-006-9143-7.
[137] S. Tsivilis, J. Tsantilas, G. Kakali, E. Chaniotakis, A. Sakellariou, The permeability of Portland limestone cement concrete, Cem. Concr. Res. 33 (2003) 1465–1471. https://doi.org/10.1016/S0008-8846(03)00092-9.
[138] P. Pipilikaki, M. Beazi-Katsioti, The assessment of porosity and pore size distribution of limestone Portland cement pastes, Constr. Build. Mater. 23 (2009) 1966–1970. https://doi.org/10.1016/j.conbuildmat.2008.08.028.
[139] E.I. Nadelman, Hydration and Microstructural Development of Portland Limestone Cement-Based Materials Hydration and Microstructural Development of Portland Limestone Cement-Based Materials, Georgia Institute of Technology, 2016.
[140] J.C. Crittenden, R.R. Trussell, D.W. Hand, K.J. Howe, G. Tchobanoglous, MWH's Water Treatment: Principles and Design: Third Edition, John Wiley and Sons, 2012. https://doi.org/10.1002/9781118131473.
[141] B. Gersten, An engineering assessment of domestic water treatment residuals to remove phosphorus from wastewater, Cardiff University, 2017.
[142] J.A. Ippolito, K.A. Barbarick, H.A. Elliott, Drinking water treatment residuals: A review of recent uses, J. Environ. Qual. 40 (2011) 1–12. https://doi.org/10.2134/jeq2010.0242.

[143] T. Ahmad, K. Ahmad, M. Alam, Sustainable management of water treatment sludge through 3'R' concept, J. Clean. Prod. 124 (2016) 1–13. https://doi.org/10.1016/j.jclepro.2016.02.073.
[144] K.-Y. Chiang, P.-H. Chou, C.-R. Hua, K.-L. Chien, C. Cheeseman, Lightweight bricks manufactured from water treatment sludge and rice husks, J. Hazard. Mater. 171 (2009) 76–82. https://doi.org/10.1016/J.JHAZMAT.2009.05.144.
[145] H. El-Didamony, K.A. Khalil, M. Heikal, Physico-chemical and surface characteristics of some granulated slag–fired drinking water sludge composite cement pastes, HBRC J. 10 (2014) 73–81. https://doi.org/10.1016/J.HBRCJ.2013.09.004.
[146] C.H. Huang, S.Y. Wang, Application of water treatment sludge in the manufacturing of lightweight aggregate, Constr. Build. Mater. 43 (2013) 174–183. https://doi.org/10.1016/j.conbuildmat.2013.02.016.
[147] C. Huang, J.R. Pan, Y. Liu, Mixing Water Treatment Residual with Excavation Waste Soil in Brick and Artificial Aggregate Making, J. Environ. Eng. 131 (2005) 272–277. https://doi.org/10.1061/(ASCE)0733-9372(2005)131:2(272).
[148] C.-F. Lin, C.-H. Wu, H.-M. Ho, Recovery of municipal waste incineration bottom ash and water treatment sludge to water permeable pavement materials, Waste Manag. 26 (2006) 970–978. https://doi.org/10.1016/J.WASMAN.2005.09.014.
[149] S.N. Monteiro, J. Alexandre, J.I. Margem, R. Sánchez, C.M.F. Vieira, Incorporation of sludge waste from water treatment plant into red ceramic, Constr. Build. Mater. 22 (2008) 1281–1287. https://doi.org/10.1016/J.CONBUILDMAT.2007.01.013.
[150] N.H. Rodríguez, S.M. Ramírez, M.T.B. Varela, M. Guillem, J. Puig, E. Larrotcha, J. Flores, Re-use of drinking water treatment plant (DWTP) sludge: Characterization and technological behaviour of cement mortars with atomized sludge additions, Cem. Concr. Res. 40 (2010) 778–786. https://doi.org/10.1016/j.cemconres.2009.11.012.
[151] C.-L. Yen, D.-H. Tseng, T.-T. Lin, Characterization of eco-cement paste produced from waste sludges, Chemosphere. 84 (2011) 220–226. https://doi.org/10.1016/J.CHEMOSPHERE.2011.04.050.
[152] J.L. Zou, G.R. Xu, G.B. Li, Ceramsite obtained from water and wastewater sludge and its characteristics affected by Fe_2O_3, CaO, and MgO, J. Hazard. Mater. 165 (2009) 995–1001. https://doi.org/10.1016/J.JHAZMAT.2008.10.113.
[153] A. Benlalla, M. Elmoussaouiti, M. Dahhou, M. Assafi, Utilization of water treatment plant sludge in structural ceramics bricks, Appl. Clay Sci. 118 (2015) 171–177. https://doi.org/10.1016/j.clay.2015.09.012.
[154] C. Huang, J.R. Pan, K.D. Sun, C.T. Liaw, Reuse of water treatment plant sludge and dam sediment in brick-making., Water Sci. Technol. 44 (2001) 273–7. http://www.ncbi.nlm.nih.gov/pubmed/11794666 (accessed October 9, 2017).
[155] A. Babatunde, Y.Q. Zhao, Constructive approaches toward water treatment works sludge management: An international review of beneficial reuses, Crit. Rev. Environ. Sci. Technol. 37 (2007) 129–164. https://doi.org/10.1080/10643380600776239.
[156] R. Fernandez, F. Martirena, K.L. Scrivener, The origin of the pozzolanic activity of calcined clay minerals: A comparison between kaolinite, illite and montmorillonite, Cem. Concr. Res. 41 (2011) 113–122.

https://doi.org/10.1016/J.CEMCONRES.2010.09.013.
[157] S.E. Hagemann, A.L.G. Gastaldini, M. Cocco, S.L. Jahn, L.M. Terra, Synergic effects of the substitution of Portland cement for water treatment plant sludge ash and ground limestone: Technical and economic evaluation, J. Clean. Prod. 214 (2019) 916–926. https://doi.org/10.1016/j.jclepro.2018.12.324.
[158] M. Frías, R. Vigil de la Villa, I. de Soto, R. García, T.A. Baloa, Influence of activated drinking-water treatment waste on binary cement-based composite behavior: Characterization and properties, Compos. Part B Eng. 60 (2014) 14–20. https://doi.org/10.1016/J.COMPOSITESB.2013.12.020.
[159] M.A. Tantawy, Characterization and pozzolanic properties of calcined alum sludge, Mater. Res. Bull. 61 (2015) 415–421. https://doi.org/10.1016/j.materresbull.2014.10.042.
[160] B. O'Kelly, Characterisation and undrained strength of amorphous clay, Proc. Inst. Civ. Eng. (2014) 311–320. https://doi.org/10.1680/geng.11.00025.
[161] N.H. Rodríguez, S.M. Ramírez, M.T.B. Varela, M. Guillem, J. Puig, E. Larrotcha, J. Flores, Re-use of drinking water treatment plant (DWTP) sludge: Characterization and technological behaviour of cement mortars with atomized sludge additions, Cem. Concr. Res. 40 (2010) 778–786. https://doi.org/10.1016/j.cemconres.2009.11.012.
[162] R. Fernandez, F. Martirena, K.L. Scrivener, The origin of the pozzolanic activity of calcined clay minerals: A comparison between kaolinite, illite and montmorillonite, Cem. Concr. Res. 41 (2010) 113–122. https://doi.org/10.1016/j.cemconres.2010.09.013.
[163] M.J. McCarthy, N. Strompinis, L.J. Csetenyi, G.M.S. Islam, Influence of Portland cement characteristics on air-entrainment in fly ash concrete, Mag. Concr. Res. 67 (2015) 786–797. https://doi.org/10.1680/macr.14.00279.
[164] A.D.V. Souza, C.C. Arruda, L. Fernandes, M.L.P. Antunes, P.K. Kiyohara, R. Salomão, Characterization of aluminum hydroxide (Al(OH)3) for use as a porogenic agent in castable ceramics, J. Eur. Ceram. Soc. 35 (2015) 803–812. https://doi.org/10.1016/j.jeurceramsoc.2014.09.010.
[165] A.D.V. Souza, R. Salomão, Evaluation of the porogenic behavior of aluminum hydroxide particles of different size distributions in castable high-alumina structures, J. Eur. Ceram. Soc. 36 (2016) 885–897. https://doi.org/10.1016/J.JEURCERAMSOC.2015.11.019.
[166] L.G.G. de Gabriel, A.B. Rohden, M.R. Garcez, E.B. da Costa, S. Da Dalt, J.J. de O. Andrade, Valorization of water treatment sludge waste by application as supplementary cementitious material, Constr. Build. Mater. 223 (2019) 939–950. https://doi.org/10.1016/j.conbuildmat.2019.07.333.
[167] T. Ahmad, K. Ahmad, M. Alam, Investigating calcined filter backwash solids as supplementary cementitious material for recycling in construction practices, Constr. Build. Mater. 175 (2018) 664–671. https://doi.org/10.1016/j.conbuildmat.2018.04.227.
[168] H.M. Owaid, R. Hamid, M.R. Taha, Durability properties of multiple-blended binder concretes incorporating thermally activated alum sludge ash, Constr. Build. Mater. 200 (2019) 591–603. https://doi.org/10.1016/j.conbuildmat.2018.12.149.
[169] ASTM C618 - Standard Specification for Coal Fly Ash and Raw or Calcined Natural Pozzolan for Use in Concrete, n.d. https://www.astm.org/Standards/C618.htm (accessed October 26, 2019).
[170] K. Scrivener, F. Martirena, S. Bishnoi, S. Maity, Calcined clay limestone

cements (LC3), Cem. Concr. Res. 114 (2018). https://doi.org/10.1016/j.cemconres.2017.08.017.
[171] UK Government. Department of Business Energy & Industrial Strategy (2017), Fly ash and Blast Furnace Slag for Cement Manfacturing, BEIS Res. Pap. 19. (n.d.).
[172] Y. Zhao, R. Liu, O.W. Awe, Y. Yang, C. Shen, Acceptability of land application of alum-based water treatment residuals – An explicit and comprehensive review, Chem. Eng. J. 353 (2018) 717–726. https://doi.org/10.1016/j.cej.2018.07.143.
[173] N. Finlay, Using Water Treatment Residual to immobilise lead for in-situ remediation of contaminated soil, Durham University, 2015.
[174] M. Shamaki, S. Adu-amankwah, L. Black, Reuse of UK alum water treatment sludge in cement-based materials, Constr. Build. Mater. 275 (2021) 122047. https://doi.org/10.1016/j.conbuildmat.2020.122047.
[175] L.K. Hudson, C. Misra, A.J. Perrotta, K. Wefers, F.S. Williams, Aluminum Oxide, in: Ullmann's Encycl. Ind. Chem., Wiley-VCH Verlag GmbH & Co. KGaA, Weinheim, Germany, 2000. https://doi.org/10.1002/14356007.a01_557.
[176] K. Wefers, C. Misra, Oxides and Hydroxides of Aluminum, Alcoa Technical Paper No. 19, 1987. http://epsc511.wustl.edu/Aluminum_Oxides_Alcoa1987.pdf (accessed October 16, 2018).
[177] J.K. Pradhan, I.N. Bhattacharya, S.C. Das, R.P. Das, R.K. Panda, Characterisation of fine polycrystals of metastable η-alumina obtained through a wet chemical precursor synthesis, Mater. Sci. Eng. B Solid-State Mater. Adv. Technol. 77 (2000) 185–192. https://doi.org/10.1016/S0921-5107(00)00486-4.
[178] I.N. Bhattacharya, P.K. Gochhayat, P.S. Mukherjee, S. Paul, P.K. Mitra, Thermal decomposition of precipitated low bulk density basic aluminium sulfate, Mater. Chem. Phys. 88 (2004) 32–40. https://doi.org/10.1016/j.matchemphys.2004.04.024.
[179] G. Castruita, Y.A. Perera-Mercado, E.M. Saucedo-Salazar, Sol-Gel Aluminum Hydroxides and Their Thermal Transformation Studies for the Production of α-Alumina, J. Inorg. Organomet. Polym. Mater. 23 (2013) 1145–1152. https://doi.org/10.1007/s10904-013-9905-y.
[180] C.J. Serna, J.L. White, S.L. Hem, Anion-Aluminum Hydroxide Gel Interactions, Soil Sci. Soc. Am. J. 41 (1977) 1009–1013. https://doi.org/10.2136/sssaj1977.03615995004100050041x.
[181] T. Sato, K. Sato, Preparation of Gelatinous Aluminium Hydroxide from Aqueous Solutions of Aluminium Salts Containing Sulphate Group with Alkali, 1996.
[182] L. Rajabi, A.A. Derakhshan, Room temperature synthesis of boehmite and crystallization of nanoparticles: Effect of concentration and ultrasound, Sci. Adv. Mater. 2 (2010) 163–172. https://doi.org/10.1166/sam.2010.1063.
[183] S.M. Bradley, R.A. Kydd, R.F. Howe, The Structure of Al Gels Formed through the Base Hydrolysis of Al3+ Aqueous Solutions, J. Colloid Interface Sci. 159 (1993) 405–412. https://doi.org/10.1006/JCIS.1993.1340.
[184] S.M. Kim, Y.J. Lee, K.W. Jun, J.Y. Park, H.S. Potdar, Synthesis of thermo-stable high surface area alumina powder from sol-gel derived boehmite, Mater. Chem. Phys. 104 (2007) 56–61. https://doi.org/10.1016/j.matchemphys.2007.02.044.
[185] H.C. Stumpf, A.S. Russell, J.W. Newsome, C.M. Tucker, Thermal

Transformations of Aluminas and Alumina Hydrates - Reaction with 44% Technical Acid., Ind. Eng. Chem. 42 (1950) 1398–1403. https://doi.org/10.1021/ie50487a039.
[186] R. Sarkar, S.K. Das, G. Banerjee, Calcination effect on magnesium hydroxide and aluminum hydroxide for the development of magnesium aluminate spinel, Ceram. Int. 26 (2000) 25–28. https://doi.org/10.1016/S0272-8842(99)00014-0.
[187] B.R. Das, B. Dash, B.C. Tripathy, I.N. Bhattacharya, S.C. Das, Production of g -alumina from waste aluminium dross, 20 (2007) 252–258. https://doi.org/10.1016/j.mineng.2006.09.002.
[188] Z.-X. Sun, T.-T. Zheng, Q.-B. Bo, M. Du, W. Forsling, Effects of calcination temperature on the pore size and wall crystalline structure of mesoporous alumina, J. Colloid Interface Sci. 319 (2008) 247–251. https://doi.org/10.1016/J.JCIS.2007.11.023.
[189] M. Amin, K. Abu El-Hassan, Effect of using different types of nano materials on mechanical properties of high strength concrete, Constr. Build. Mater. 80 (2015) 116–124. https://doi.org/10.1016/j.conbuildmat.2014.12.075.
[190] M. Berra, F. Carassiti, T. Mangialardi, A.E. Paolini, M. Sebastiani, Effects of nanosilica addition on workability and compressive strength of Portland cement pastes, Constr. Build. Mater. 35 (2012) 666–675. https://doi.org/10.1016/j.conbuildmat.2012.04.132.
[191] H. Li, H. gang Xiao, J. ping Ou, A study on mechanical and pressure-sensitive properties of cement mortar with nanophase materials, Cem. Concr. Res. 34 (2004) 435–438. https://doi.org/10.1016/j.cemconres.2003.08.025.
[192] M.C. Valero, P. Raybaud, P. Sautet, Influence of the hydroxylation of γ-Al_2O_3 surfaces on the stability and diffusion of single Pd atoms: A DFT study, J. Phys. Chem. B. 110 (2006) 1759–1767. https://doi.org/10.1021/jp0554240.
[193] B.J. Zhan, D.X. Xuan, C.S. Poon, The effect of nanoalumina on early hydration and mechanical properties of cement pastes, Constr. Build. Mater. 202 (2019) 169–176. https://doi.org/10.1016/j.conbuildmat.2019.01.022.
[194] Q. Shao, K. Zheng, X. Zhou, J. Zhou, X. Zeng, Enhancement of nano-alumina on long-term strength of Portland cement and the relation to its influences on compositional and microstructural aspects, Cem. Concr. Compos. 98 (2019) 39–48. https://doi.org/10.1016/j.cemconcomp.2019.01.016.
[195] J. Chen, C. Liang, B. Li, E. Wang, G. Li, X. Hou, The effect of nano-γAl_2O_3 additive on early hydration of calcium aluminate cement, Constr. Build. Mater. 158 (2018) 755–760. https://doi.org/10.1016/J.CONBUILDMAT.2017.10.071.
[196] S.C. Vieira, A.S. Ramos, M.T. Vieira, Mullitization kinetics from silica-and alumina-rich wastes, (2005). https://doi.org/10.1016/j.ceramint.2005.07.015.
[197] N. Farzadnia, A.A. Abang Ali, R. Demirboga, Characterization of high strength mortars with nano alumina at elevated temperatures, Cem. Concr. Res. 54 (2013) 43–54. https://doi.org/10.1016/j.cemconres.2013.08.003.
[198] Z. Li, H. Wang, S. He, Y. Lu, M. Wang, Investigations on the preparation and mechanical properties of the nano-alumina reinforced cement composite, Mater. Lett. 60 (2006) 356–359. https://doi.org/10.1016/J.MATLET.2005.08.061.
[199] N. De Belie, C.U. Grosse, J. Kurz, H.W. Reinhardt, Ultrasound monitoring of the influence of different accelerating admixtures and cement types for shotcrete on setting and hardening behaviour, Cem. Concr. Res. 35 (2005) 2087–2094. https://doi.org/10.1016/j.cemconres.2005.03.011.
[200] R.P. Salvador, S.H.P. Cavalaro, I. Segura, A.D. Figueiredo, J. Pérez, Early

age hydration of cement pastes with alkaline and alkali-free accelerators for sprayed concrete, Constr. Build. Mater. 111 (2016) 386–398. https://doi.org/10.1016/j.conbuildmat.2016.02.101.
[201] R. Yang, T. He, M. Guan, X. Guo, Y. Xu, R. Xu, Y. Da, Preparation and accelerating mechanism of aluminum sulfate-based alkali-free accelerating additive for sprayed concrete, Constr. Build. Mater. 234 (2020). https://doi.org/10.1016/j.conbuildmat.2019.117334.
[202] C. Paglia, F. Wombacher, H. Böhni, The influence of alkali-free and alkaline shotcrete accelerators within cement systems - I. Characterization of the setting behavior, Cem. Concr. Res. 31 (2001) 913–918. https://doi.org/10.1016/S0008-8846(01)00509-9.
[203] H. Tan, M. Li, J. Ren, X. Deng, X. Zhang, K. Nie, J. Zhang, Z. Yu, Effect of aluminum sulfate on the hydration of tricalcium silicate, Constr. Build. Mater. 205 (2019) 414–424. https://doi.org/10.1016/j.conbuildmat.2019.02.011.
[204] J. Han, K. Wang, Y. Wang, J. Shi, Study of aluminum sulfate and anhydrite on cement hydration process, Mater. Struct. Constr. 49 (2016) 1105–1114. https://doi.org/10.1617/s11527-015-0561-2.
[205] R.P. Salvador, S.H.P. Cavalaro, M.A. Cincotto, A.D. d. Figueiredo, Parameters controlling early age hydration of cement pastes containing accelerators for sprayed concrete, Cem. Concr. Res. 89 (2016) 230–248. https://doi.org/10.1016/j.cemconres.2016.09.002.
[206] A. Quennoz, K.L. Scrivener, Hydration of C 3 A-gypsum systems, Cem. Concr. Res. 42 (2012) 1032–1041. https://doi.org/10.1016/j.cemconres.2012.04.005.
[207] Q. Xu, J. Stark, Early hydration of ordinary Portland cement with an alkaline shotcrete accelerator, Adv. Cem. Res. 17 (2005) 1–8.
[208] C. Herrera-Mesen, R.P. Salvador, S.H.P. Cavalaro, A. Aguado, Effect of gypsum content in sprayed cementitious matrices: Early age hydration and mechanical properties, Cem. Concr. Compos. 95 (2019) 81–91. https://doi.org/10.1016/j.cemconcomp.2018.10.015.
[209] G. Li, J. Zhang, M. Niu, Z. Song, The mechanism of alkali-free liquid accelerator on the hydration of cement pastes, Constr. Build. Mater. 233 (2020). https://doi.org/10.1016/j.conbuildmat.2019.117296.
[210] C. Maltese, C. Pistolesi, A. Bravo, F. Cella, T. Cerulli, D. Salvioni, Effects of setting regulators on the efficiency of an inorganic acid based alkali-free accelerator reacting with a Portland cement, Cem. Concr. Res. 37 (2007) 528–536. https://doi.org/10.1016/j.cemconres.2007.01.002.
[211] J. Herterich, Microstructure and Phase Assemblage of Low-Clinker Cements during Early Stages of Carbonation, University of Leeds, 2017.
[212] S. Adu-Amankwah, Relationship between Microstructure, Durability and Performance of CEM X Composite Cements, University of Leeds, 2016.
[213] BSI, BS EN 196-1:2016, Methods of Testing Cement - Determination of Strength, BSI Standards Limited, 2016. https://doi.org/10.3403/30291447U.
[214] A. Schöler, B. Lothenbach, F. Winnefeld, M. Zajac, Hydration of quaternary Portland cement blends containing blast-furnace slag, siliceous fly ash and limestone powder, Cem. Concr. Compos. 55 (2015) 374–382. https://doi.org/10.1016/j.cemconcomp.2014.10.001.
[215] S. Lowell, Characterization of porous solids and powders : surface area, pore size, and density, Kluwer Academic Publishers, 2004.
[216] P.. Saamiya Seraj, Evaluating Natural Pozzolans for Use as Alternative Supplementary Cementitious Materials in Concrete, The University of Texas at

Austin, 2014.
[217] T. Horiuchi, T. Osaki, T. Sugiyama, K. Suzuki, T. Mori, Maintenance of large surface area of alumina heated at elevated temperatures above 1300 °C by preparing silica-containing pseudoboehmite aerogel, J. Non. Cryst. Solids. 291 (2001) 187–198. www.elsevier.com/locate/jnoncrysol (accessed November 12, 2018).
[218] BSI Standards Publication Determination of the specific surface area of solids by gas adsorption — BET method, (2010).
[219] Index of methods for the examination of waters and associated materials 1976-1992., H.M.S.O, 1992.
[220] M.J. O'Neill, Measurement of Specific Heat Functions by Differential Scanning Calorimetry., Anal. Chem. 38 (1966) 1331–1336. https://doi.org/10.1021/ac60242a011.
[221] J.I. Bhatty, A review of the application of thermal analysis to cement-admixture systems, Thermochim. Acta. 189 (1991) 313–350. https://doi.org/10.1016/0040-6031(91)87128-J.
[222] C.N.C, Transition and decomposition temperatures of cement phases-a collection of thermal analysis data, Ceramics-Silikáty. 60 (2016) 338–343. https://doi.org/10.13168/cs.2016.0050.
[223] K.L. Scrivener, B. Lothenbach, N. De Belie, E. Gruyaert, J. Skibsted, R. Snellings, A. Vollpracht, TC 238-SCM: hydration and microstructure of concrete with SCMs State of the art on methods to determine degree of reaction of SCMs, Mater. Struct. 48 (2015) 835–862. https://doi.org/10.1617/s11527-015-0527-4.
[224] M. Ben Haha, K. De Weerdt, B. Lothenbach, Quantification of the degree of reaction of fly ash, Cem. Concr. Res. 40 (2010) 1620–1629. https://doi.org/10.1016/j.cemconres.2010.07.004.
[225] H.S. Wong, Quantifying the pore structure of cement- based materials using backscattered electron, Imperial College London, 2006.
[226] Q. Xing, Information or resolution: Which is required from an SEM to study bulk inorganic materials?, Scanning. 38 (2016) 864–879. https://doi.org/10.1002/sca.21336.
[227] H.S. Wong, N.R. Buenfeld, M.K. Head, Estimating transport properties of mortars using image analysis on backscattered electron images, Cem. Concr. Res. 36 (2006) 1556–1566. https://doi.org/10.1016/j.cemconres.2006.05.002.
[228] C. Famy, K.L. Scrivener, A.K. Crumbie, What causes differences of C-S-H gel grey levels in backscattered electron images?, Cem. Concr. Res. 32 (2002) 1465–1471. https://doi.org/10.1016/S0008-8846(02)00808-6.
[229] K. Scrivener, R. Snellings, B. Lothenbach, A Practical Guide to Microstructural Analysis of Cementitious Materials, 2016. https://doi.org/10.7693/wl20150205.
[230] J.E. Rossen, K.L. Scrivener, Materials Characterization Optimization of SEM-EDS to determine the C – A – S – H composition in matured cement paste samples, Mater. Charact. 123 (2017) 294–306. https://doi.org/10.1016/j.matchar.2016.11.041.
[231] G. Le Saoût, V. Kocaba, K. Scrivener, Application of the Rietveld method to the analysis of anhydrous cement, Cem. Concr. Res. 41 (2011) 133–148. https://doi.org/10.1016/J.CEMCONRES.2010.10.003.
[232] G. Caglioti, A. Paoletti, F.. Ricci, Choice of Collimators For a Crystal Spectrometer For Neutron Diffraction, Nucl. Instruments. 3 (1958) 223–228.
[233] W.A. Dollase, Correction of Intensities for Preferred Orientation in Powder

Diffractometry : Application of the March Model, J. Appl. Crystallogr. 19 (1986) 267–272.
[234] E. Sonneveld, J.W. Visser, Automatic Collection of Powder Data from Photographs, J. Appl. Crystallogr. 8 (1975) 1–7.
[235] S.J. Chipera, D.L. Bish, Fitting Full X-Ray Diffraction Patterns for Quantitative Analysis: A Method for Readily Quantifying Crystalline and Disordered Phases, Adv. Mater. Phys. Chem. 03 (2013) 47–53. https://doi.org/10.4236/ampc.2013.31a007.
[236] S.J. Chipera, D.L. Bish, FULLPAT: A full-pattern quantitative analysis program for X-ray powder diffraction using measured and calculated patterns, J. Appl. Crystallogr. 35 (2002) 744–749. https://doi.org/10.1107/S0021889802017405.
[237] S. Adu-Amankwah, M. Zajac, C. Stabler, B. Lothenbach, L. Black, Influence of limestone on the hydration of ternary slag cements, Cem. Concr. Res. 100 (2018) 96–109. https://doi.org/10.1016/j.cemconres.2017.05.013.
[238] D. Jansen, F. Goetz-Neunhoeffer, C. Stabler, J. Neubauer, A remastered external standard method applied to the quantification of early OPC hydration, Cem. Concr. Res. 41 (2011) 602–608. https://doi.org/10.1016/j.cemconres.2011.03.004.
[239] R. Ylmén, L. Wadsö, I. Panas, Insights into early hydration of Portland limestone cement from infrared spectroscopy and isothermal calorimetry, Cem. Concr. Res. 40 (2010) 1541–1546. https://doi.org/10.1016/j.cemconres.2010.06.008.
[240] British Standards Institution, Methods of test for masonry. Part 3, Determination of consistence of fresh mortar (by flow table), n.d.
[241] ASTM International, ASTM Standard C109, 1999,"Standard Test Method for Compressive Strength of Hydraulic Cement Mortars", ASTM Stand. B. 04 (1999) 1–6. https://doi.org/10.1520/C0109_C0109M-16A.
[242] ASTM C311-04, ASTM C311/2013 - Standard Test Methods for Sampling and Testing Fly Ash or Natural Pozzolans for Use in Portland-Cement Concrete., Annu. B. ASTM Stand. 04.02 (2005) 204–212. https://doi.org/10.1520/C0311-13.2.
[243] C.S. Poon, A.I. Clark, R. Perry, A.P. Barker, P. Barnes, Permeability study on the cement based solidification process for the disposal of hazardous wastes, Cem. Concr. Res. 16 (1986) 161–172. https://doi.org/10.1016/0008-8846(86)90132-8.
[244] J.G. Cabrera, C.J. Lynsdale, A new gas permeameter for measuring the permeability of mortar and concrete, Mag. Concr. Res. 40 (1988) 177–182.
[245] S. Tsivilis, E. Chaniotakis, G. Batis, C. Meletiou, V. Kasselouri, G. Kakali, A. Sakellariou, G. Pavlakis, C. Psimadas, The effect of clinker and limestone quality on the gas permeability, water absorption and pore structure of limestone cement concrete, Cem. Concr. Compos. 21 (1999) 139–146. https://doi.org/10.1016/S0958-9465(98)00037-7.
[246] British Standard Institute, BS EN 13057:2002, in: BSI, 2002. https://bsol.bsigroup.com/Bibliographic/BibliographicInfoData/000000000030058207 (accessed February 20, 2020).
[247] C. Hall, Water sorptivity of mortars and concretes: a review, Mag. Concr. Res. 41 (1989) 51–61. https://doi.org/10.1680/macr.1989.41.147.51.
[248] T. James, A. Lord, Re-Use and Volume Reduction of Scabbled Contaminated Concrete Arising from Nuclear Decommissioning, University of Leeds, 2018.
[249] M.M. Hossain, M.R. Karim, M. Hasan, M.K. Hossain, M.F.M. Zain, Durability of

mortar and concrete made up of pozzolans as a partial replacement of cement: A review, Constr. Build. Mater. 116 (2016) 128–140. https://doi.org/10.1016/J.CONBUILDMAT.2016.04.147.
[250] H.S. Wong, M. Zobel, N.R. Buenfeld, R.W. Zimmerman, Influence of the interfacial transition zone and microcracking on the diffusivity, permeability and sorptivity of cement-based materials after drying, Mag. Concr. Res. 61 (2009) 571–589. https://doi.org/10.1680/macr.2008.61.8.571.
[251] C. Tasdemir, Combined effects of mineral admixtures and curing conditions on the sorptivity coefficient of concrete, Cem. Concr. Res. 33 (2003) 1637–1642. https://doi.org/10.1016/S0008-8846(03)00112-1.
[252] E.F. Irassar, V.L. Bonavetti, C.C. Castellano, M.A. Trezza, V.F. Rahhal, G. Cordoba, R. Lemma, Calcined illite-chlorite shale as supplementary cementing material: Thermal treatment, grinding, color and pozzolanic activity, Appl. Clay Sci. 179 (2019) 105143. https://doi.org/10.1016/j.clay.2019.105143.
[253] T.T. Lim, J. Chu, M.H. Goi, Effects of cement on redistribution of trace metals and dissolution of organics in sewage sludge and its inorganic waste-amended products, Waste Manag. 26 (2006) 1294–1304. https://doi.org/10.1016/j.wasman.2005.11.001.
[254] BSI, BS En 450-1 Fly ash for concrete. Definition, specifications and conformity criteria, British Standard Institution, UK., (2012) 34. http://shop.bsigroup.com/en/ProductDetail/?pid=000000000030216589 (accessed October 26, 2019).
[255] L.Y. Wang, D.S. Tong, L.Z. Zhao, F.G. Liu, N. An, W.H. Yu, C.H. Zhou, Utilization of alum sludge for producing aluminum hydroxide and layered double hydroxide, Ceram. Int. 40 (2014) 15503–15514. https://doi.org/10.1016/J.CERAMINT.2014.07.012.
[256] M.A. Chikouche, E. Ghorbel, M. Bibi, The possibility of using dredging sludge in manufacturing cements: Optimization of heat treatment cycle and ratio replacement, Constr. Build. Mater. 106 (2016) 330–341. https://doi.org/10.1016/j.conbuildmat.2015.12.128.
[257] H. Cheng, J. Yang, Q. Liu, J. He, R.L. Frost, Thermogravimetric analysisâ€“mass spectrometry (TGâ€“MS) of selected Chinese kaolinites, Thermochim. Acta. 507–508 (2010) 106–114. https://doi.org/10.1016/j.tca.2010.05.007.
[258] A.I.M. Rabee, G.A.H. Mekhemer, M.I. Zaki, Spectro-thermal characterization of the nature of sulfate groups immobilized on tetragonal zirconium oxide : Consequences of doping the oxide with Al or Mg cations, Thermochim. Acta. 674 (2019) 1–9. https://doi.org/10.1016/j.tca.2019.01.029.
[259] B. Ren, N. Lyczko, Y. Zhao, A. Nzihou, Chemosphere Alum sludge as an ef fi cient sorbent for hydrogen sul fi de removal : Experimental , mechanisms and modeling studies, Chemosphere. 248 (2020) 126010. https://doi.org/10.1016/j.chemosphere.2020.126010.
[260] S. De Carvalho Gomes, J.L. Zhou, W. Li, G. Long, Progress in manufacture and properties of construction materials incorporating water treatment sludge: A review, Resour. Conserv. Recycl. 145 (2019) 148–159. https://doi.org/10.1016/j.resconrec.2019.02.032.
[261] J.E. Rossen, B. Lothenbach, K.L. Scrivener, Composition of C-S-H in pastes with increasing levels of silica fume addition, Cem. Concr. Res. 75 (2015) 14–22. https://doi.org/10.1016/j.cemconres.2015.04.016.
[262] S. Krishnan, A.C. Emmanuel, S. Bishnoi, Hydration and phase assemblage of

ternary cements with calcined clay and limestone, Constr. Build. Mater. 222 (2019) 64–72. https://doi.org/10.1016/j.conbuildmat.2019.06.123.
[263] D.B. Tilley, R.A. Eggleton, The Natural Occurence of eta (η-Al_2O_3) in Bauxite, Clays Clay Miner. 44 (1996) 658–664.
[264] L. Radonjić, V. Srdić, L. Nikolić, Relationship between the microstructure of boehmite gels and their transformation to alpha-alumina, Mater. Chem. Phys. 33 (1993) 298–306. https://doi.org/10.1016/0254-0584(93)90078-Z.
[265] B.D. Aldcroft, G.C. Bye, A. Hughes, Crystallisation Processes in Aluminium Hydroxide Gels. IV. Factors Influencing the Formation of the Crystalline Trihydroxides, J. Appl. Chem. 19 (1969) 167–172. https://doi.org/10.1111/j.1464-410X.2012.11540.x.
[266] S.C. Vieira, A.S. Ramos, M.T. Vieira, Mullitization kinetics from silica-and alumina-rich wastes, (2005). https://doi.org/10.1016/j.ceramint.2005.07.015.
[267] J. Temuujin, T. Jadambaa, K.J.D. Mackenzie, P. Angerer, F. Porte, F. Riley, Thermal formation of corundum from aluminium hydroxides prepared from various aluminium salts, Bull. Mater. Sci. 23 (2000) 301–304. https://doi.org/10.1007/BF02720086.
[268] A. Tironi, M.A. Trezza, A.N. Scian, E.F. Irassar, Assessment of pozzolanic activity of different calcined clays, (2013). https://doi.org/10.1016/j.cemconcomp.2013.01.002.
[269] S. Sembiring, W. Simanjuntak, P. Manurung, D. Asmi, I.M. Low, Synthesis and characterisation of gel-derived mullite precursors from rice husk silica, Ceram. Int. 40 (2014) 7067–7072. https://doi.org/10.1016/j.ceramint.2013.12.038.
[270] N. Zhang, X. Liu, H. Sun, L. Li, Evaluation of blends bauxite-calcination-method red mud with other industrial wastes as a cementitious material: Properties and hydration characteristics, J. Hazard. Mater. 185 (2011) 329–335. https://doi.org/10.1016/j.jhazmat.2010.09.038.
[271] J. Madejová, FTIR techniques in clay mineral studies, Vib. Spectrosc. 31 (2003) 1–10. https://doi.org/10.1016/S0924-2031(02)00065-6.
[272] B. Ilić, V. Radonjanin, M. Malešev, M. Zdujić, A. Mitrović, Effects of mechanical and thermal activation on pozzolanic activity of kaolin containing mica, Appl. Clay Sci. 123 (2016) 173–181. https://doi.org/10.1016/j.clay.2016.01.029.
[273] A. Chakchouk, L. Trifi, B. Samet, S. Bouaziz, Formulation of blended cement: Effect of process variables on clay pozzolanic activity, Constr. Build. Mater. 23 (2009) 1365–1373. https://doi.org/10.1016/J.CONBUILDMAT.2008.07.015.
[274] C.K. Kumara, W.J. Ng, A. Bandara, R. Weerasooriya, Nanogibbsite: Synthesis and characterization, J. Colloid Interface Sci. 352 (2010) 252–258. https://doi.org/10.1016/J.JCIS.2010.08.083.
[275] R.L. Oréfice, W.L. Vasconcelos, Sol-Gel transition and structural evolution on multicomponent gels derived from the alumina-silica system, J. Sol-Gel Sci. Technol. 9 (1997) 239–249. https://doi.org/10.1007/BF02437187.
[276] P.J. Sanchez-Soto, A. Justo, J.L. Perez-Rodriguez, Grinding effect on kaolinite-pyrophyllite-illite natural mixtures and its influence on mullite formation, J. Mater. Sci. 29 (1994) 1276–1283.
[277] S. Diamond, S. Sahu, Densified silica fume : particle sizes and dispersion in concrete, Mater. Struct. 39 (2006) 849–859. https://doi.org/10.1617/s11527-006-9087-y.
[278] G. Quercia, A. Lazaro, J.W. Geus, H.J.H. Brouwers, Characterization of morphology and texture of several amorphous nano-silica particles used in concrete, Cem. Concr. Compos. 44 (2013) 77–92.

https://doi.org/10.1016/j.cemconcomp.2013.05.006.
[279] D. Zhou, Developing Supplementary Cementitious Materials From Waste London Clay, Imperial College London, 2016. https://spiral.imperial.ac.uk/handle/10044/1/44528.
[280] BS ISO 9277:2010 - Determination of the specific surface area of solids by gas adsorption. BET method, (n.d.). https://shop.bsigroup.com/ProductDetail/?pid=000000000030180119 (accessed October 25, 2019).
[281] A. Boruah, A. Rasheed, V.A. Mendhe, S. Ganapathi, Specific surface area and pore size distribution in gas shales of Raniganj Basin, India, J. Pet. Explor. Prod. Technol. 9 (2019) 1041–1050. https://doi.org/10.1007/s13202-018-0583-8.
[282] P. Alphonse, M. Courty, Structure and thermal behavior of nanocrystalline boehmite, Thermochim. Acta. 425 (2005) 75–89. https://doi.org/10.1016/J.TCA.2004.06.009.
[283] S.O. Kazantsev, A.S. Lozhkomoev, E.A. Glazkova, I. Gotman, E.Y. Gutmanas, M.I. Lerner, S.G. Psakhie, Preparation of aluminum hydroxide and oxide nanostructures with controllable morphology by wet oxidation of AlN/Al nanoparticles, Mater. Res. Bull. 104 (2018) 97–103. https://doi.org/10.1016/j.materresbull.2018.04.011.
[284] F.G.E. Nogueira, Y.J.O. Asencios, C.B. Rodella, A.L.M. Porto, E.M. Assaf, Alternative route for the synthesis of high surface-area η-Al_2O_3/Nb_2O_5 catalyst from aluminum waste, Mater. Chem. Phys. 184 (2016) 23–30. https://doi.org/10.1016/j.matchemphys.2016.08.032.
[285] R. Kreimeyer, Some Notes on the Firing Colour of Clay Bricks, Appl. Clay Sci. 2 (1987) 175–183.
[286] W. Carlton, A review of solidification/stabilization interferences, J. Hazard. Mater. 14 (1987) 5–21. https://doi.org/10.1016/0956-053X(94)90134-1.
[287] H. Madani, A. Bagheri, T. Parhizkar, The pozzolanic reactivity of monodispersed nanosilica hydrosols and their influence on the hydration characteristics of Portland cement, Cem. Concr. Res. 42 (2012) 1563–1570. https://doi.org/10.1016/j.cemconres.2012.09.004.
[288] N.B. Winter, Understanding cement : an introduction to cement production, cement hydration and deleterious processes in concrete, WHD Microanalysis Consultants, 2012.
[289] F. Massazza, Pozzolana and Pozzolanic Cements, in: Lea's Chem. Cem. Concr., Elsevier Ltd., 1998: pp. 471–635. https://doi.org/10.1016/B978-0-7506-6256-7.50022-9.
[290] J. Zhou, K. Zheng, Z. Liu, F. He, Chemical effect of nano-alumina on early-age hydration of Portland cement, Cem. Concr. Res. 116 (2019) 159–167. https://doi.org/10.1016/j.cemconres.2018.11.007.
[291] L. Nicoleau, E. Schreiner, A. Nonat, Ion-specific effects influencing the dissolution of tricalcium silicate, Cem. Concr. Res. 59 (2014) 118–138. https://doi.org/10.1016/j.cemconres.2014.02.006.
[292] T. Chappex, K.L. Scrivener, The influence of aluminium on the dissolution of amorphous silica and its relation to alkali silica reaction, Cem. Concr. Res. 42 (2012) 1645–1649. https://doi.org/10.1016/j.cemconres.2012.09.009.
[293] B. Kolani, L. Buffo-lacarrière, A. Sellier, G. Escadeillas, L. Boutillon, L. Linger, Hydration of slag-blended cements, Cem. Concr. Compos. 34 (2012) 1009–1018. https://doi.org/10.1016/j.cemconcomp.2012.05.007.

[294] R.P. Salvador, Accelerated cementitious matrices: hydration, microstructure and mechanical strength, Universitat Politècnica de Catalunya, 2016.
[295] L.G. Briendl, F. Mittermayr, A. Baldermann, F.R. Steindl, M. Sakoparnig, I. Letofsky-Papst, I. Galan, Early hydration of cementitious systems accelerated by aluminium sulphate: Effect of fine limestone, Cem. Concr. Res. 134 (2020) 106069. https://doi.org/10.1016/j.cemconres.2020.106069.
[296] R.P. Salvador, D.A.S. Rambo, R.M. Bueno, K.T. Silva, A.D. De Figueiredo, On the use of blast-furnace slag in sprayed concrete applications, Constr. Build. Mater. 218 (2019) 543–555. https://doi.org/10.1016/j.conbuildmat.2019.05.132.
[297] F. Avet, K. Scrivener, Investigation of the calcined kaolinite content on the hydration of Limestone Calcined Clay Cement (LC3), Cem. Concr. Res. 107 (2018) 124–135. https://doi.org/10.1016/j.cemconres.2018.02.016.
[298] M.. Trezza, A.. Lavat, Analysis of the system $3CaO{\cdot}Al_2O_3$–$Ca_SO_4{\cdot}2H_2O$–$CaCO_3$–H_2O by FT-IR spectroscopy, Cem. Concr. Res. 31 (2001) 869–872. https://doi.org/10.1016/S0008-8846(01)00502-6.
[299] I. Pajares, S. Martínez-Ramírez, M.T. Blanco-Varela, Evolution of ettringite in presence of carbonate, and silicate ions, Cem. Concr. Compos. 25 (2003) 861–865. https://doi.org/10.1016/S0958-9465(03)00113-6.
[300] M. Wu, Y. Zhang, Y. Jia, W. She, G. Liu, Z. Yang, Y. Zhang, W. Zhang, W. Sun, Effects of sodium sulfate on the hydration and properties of lime-based low carbon cementitious materials, J. Clean. Prod. 220 (2019) 677–687. https://doi.org/10.1016/j.jclepro.2019.02.186.
[301] R. Ylmén, U. Jäglid, B.-M. Steenari, I. Panas, Early hydration and setting of Portland cement monitored by IR, SEM and Vicat techniques, Cem. Concr. Res. 39 (2009) 433–439. https://doi.org/10.1016/j.cemconres.2009.01.017.
[302] T. Matschei, B. Lothenbach, F.P. Glasser, The role of calcium carbonate in cement hydration, Cem. Concr. Res. 37 (2007) 551–558. https://doi.org/10.1016/j.cemconres.2006.10.013.
[303] D. Wang, C. Shi, N. Farzadnia, H. Jia, R. Zeng, Y. Wu, L. Lao, A quantitative study on physical and chemical effects of limestone powder on properties of cement pastes, Constr. Build. Mater. 204 (2019) 58–69. https://doi.org/10.1016/j.conbuildmat.2019.01.154.
[304] A. Arora, G. Sant, N. Neithalath, Ternary blends containing slag and interground/blended limestone: Hydration, strength, and pore structure, Constr. Build. Mater. 102 (2016) 113–124. https://doi.org/10.1016/j.conbuildmat.2015.10.179.
[305] G. Puerta-Falla, M. Balonis, G. Le Saout, G. Falzone, C. Zhang, N. Neithalath, G. Sant, Elucidating the Role of the Aluminous Source on Limestone Reactivity in Cementitious Materials, J. Am. Ceram. Soc. 98 (2015) 4076–4089. https://doi.org/10.1111/jace.13806.
[306] S.M. Bushnell-Watson, J.H. Sharp, The detection of the carboaluminate phase in hydrated high alumina cements by differential thermal analysis., Thermochim. Acta. 93 (1985) 613–616.
[307] D. Madej, Hydration , carbonation and thermal stability of hydrates, J. Therm. Anal. Calorim. 131 (2018) 2411–2420. https://doi.org/10.1007/s10973-017-6726-1.
[308] J. Zhang, G.W. Scherer, Comparison of methods for arresting hydration of cement, Cem. Concr. Res. 41 (2011) 1024–1036. https://doi.org/10.1016/J.CEMCONRES.2011.06.003.
[309] F. Avet, E. Boehm-Courjault, K. Scrivener, Investigation of C-A-S-H

composition, morphology and density in Limestone Calcined Clay Cement (LC3), Cem. Concr. Res. 115 (2019) 70–79. https://doi.org/10.1016/j.cemconres.2018.10.011.
[310] Y. Dhandapani, M. Santhanam, Investigation on the microstructure-related characteristics to elucidate performance of composite cement with limestone-calcined clay combination, Cem. Concr. Res. 129 (2020). https://doi.org/10.1016/j.cemconres.2019.105959.
[311] L. Montanaro, A. Negro, M. Regourd, Action de $CaCO_3$, $CaSO_4$ et $CaSO_4 \cdot 2H_2O$ sur l'hydratation de C_3S, Cem. Concr. Res. 18 (1988) 431–437.
[312] P.T. Durdziński, M. Ben Haha, M. Zajac, K.L. Scrivener, Phase assemblage of composite cements, Cem. Concr. Res. 99 (2017) 172–182. https://doi.org/10.1016/j.cemconres.2017.05.009.
[313] M. Zajac, A. Rossberg, G. Le Saout, B. Lothenbach, Influence of limestone and anhydrite on the hydration of Portland cements, Cem. Concr. Compos. 46 (2014) 99–108. https://doi.org/10.1016/j.cemconcomp.2013.11.007.
[314] F. Avet, K. Scrivener, Investigation of the calcined kaolinite content on the hydration of Limestone Calcined Clay Cement (LC3), Cem. Concr. Res. 107 (2018) 124–135. https://doi.org/10.1016/j.cemconres.2018.02.016.
[315] M. Horgnies, J.J. Chen, C. Bouillon, Overview about the use of Fourier Transform Infrared spectroscopy to study cementitious materials, WIT Trans. Eng. Sci. 77 (2013) 1743–3533. https://doi.org/10.2495/MC130221.
[316] J. Bensted, Some applications of infrared and raman spectroscopy in cement chemistry. Part 3 - hydration of portland cement and its constituents, Cem. Technol. (1974). http://www.urbis-libnet.org/vufind/Record/ICCROM.ICCROM38513 (accessed May 21, 2019).
[317] S. Krishnan, A.C. Emmanuel, S. Bishnoi, Hydration and phase assemblage of ternary cements with calcined clay and limestone, Constr. Build. Mater. 222 (2019) 64–72. https://doi.org/10.1016/j.conbuildmat.2019.06.123.
[318] F. Avet, X. Li, K. Scrivener, Determination of the amount of reacted metakaolin in calcined clay blends, Cem. Concr. Res. 106 (2018) 40–48. https://doi.org/10.1016/j.cemconres.2018.01.009.
[319] M.M. Ul Islam, K.H. Mo, U.J. Alengaram, M.Z. Jumaat, Durability properties of sustainable concrete containing high volume palm oil waste materials, J. Clean. Prod. 137 (2016) 167–177. https://doi.org/10.1016/j.jclepro.2016.07.061.
[320] X. Liu, B. Ma, H. Tan, H. Li, J. Mei, T. Zhang, P. Chen, B. Gu, Chloride immobilization of cement-based material containing nano-Al2O3, Constr. Build. Mater. 220 (2019) 43–52. https://doi.org/10.1016/j.conbuildmat.2019.05.148.
[321] P. Chen, B. Ma, H. Tan, X. Liu, T. Zhang, H. Qi, Y. Peng, Q. Yang, J. Wang, Effects of amorphous aluminum hydroxide on chloride immobilization in cement-based materials, Constr. Build. Mater. 231 (2020) 117171. https://doi.org/10.1016/j.conbuildmat.2019.117171.

Appendices

A.1 Rietveld Refinement

The outputs from Rietveld refinement of the various hydrated pastes are presented here. The different cement pastes were analysed and the calculated patterns superimposed on the observed patterns. The background and difference plots are also shown for each of the main composites at 28 days of hydration. The agreement index R_{wp} is also provided for reference.

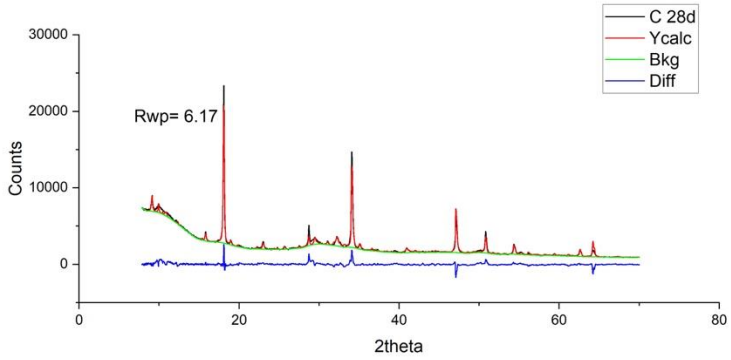
C 28d
Ycalc
Bkg
Diff
Rwp= 6.17
Counts
2theta

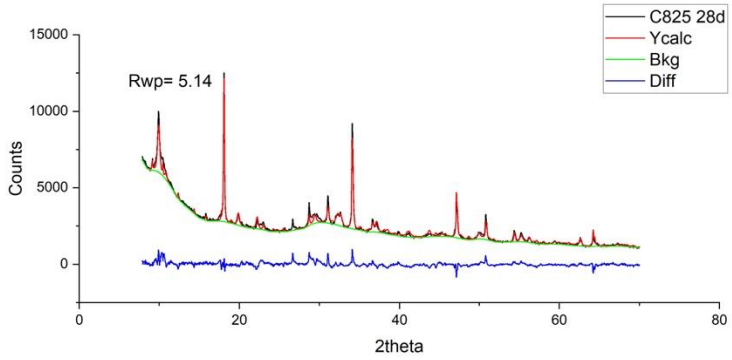
C825 28d
Ycalc
Bkg
Diff
Rwp= 5.14
Counts
2theta

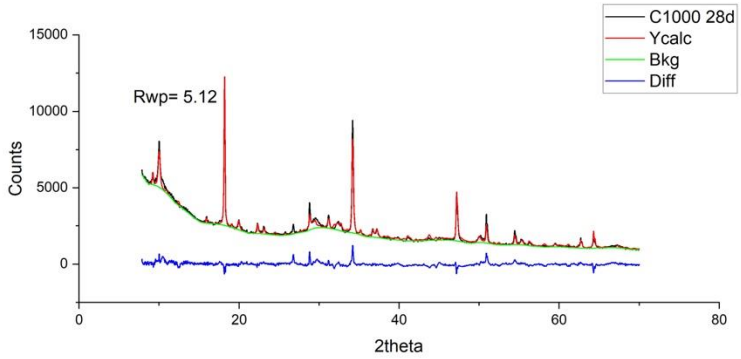
C1000 28d
Ycalc
Bkg
Diff
Rwp= 5.12
Counts
2theta

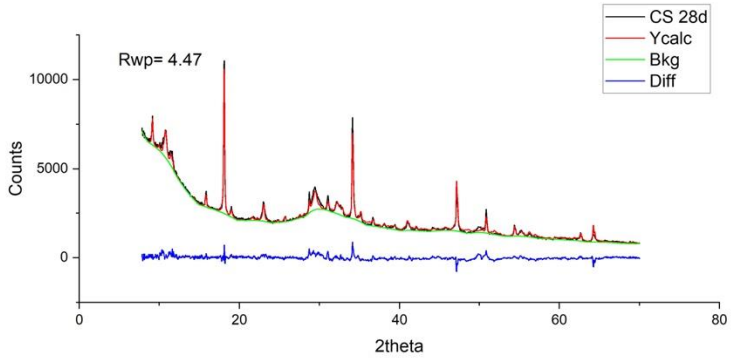
CS 28d
Ycalc
Bkg
Diff
Rwp= 4.47
Counts
2theta

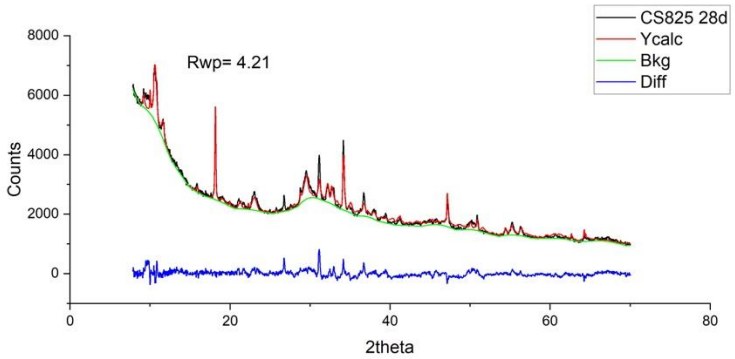
CS825 28d
Ycalc
Bkg
Diff
Rwp= 4.21
Counts
2theta

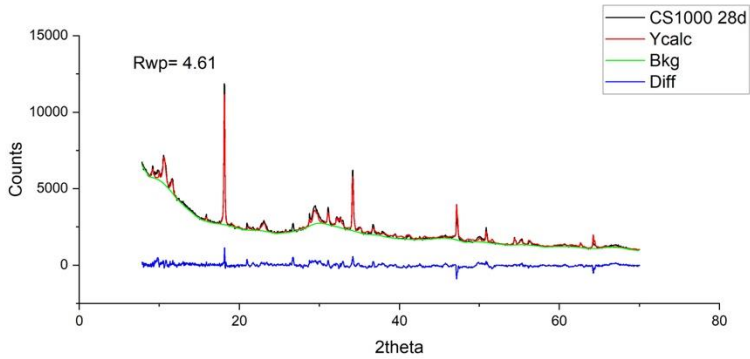
CS1000 28d
Ycalc
Bkg
Diff
Rwp= 4.61
Counts
2theta

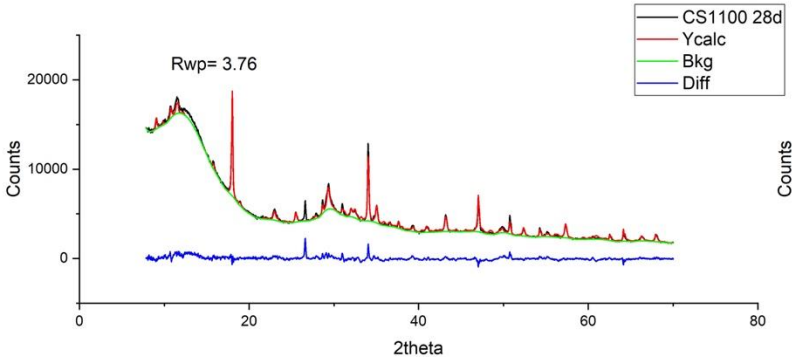
CS1100 28d
Ycalc
Bkg
Diff
Rwp= 3.76
Counts
2theta

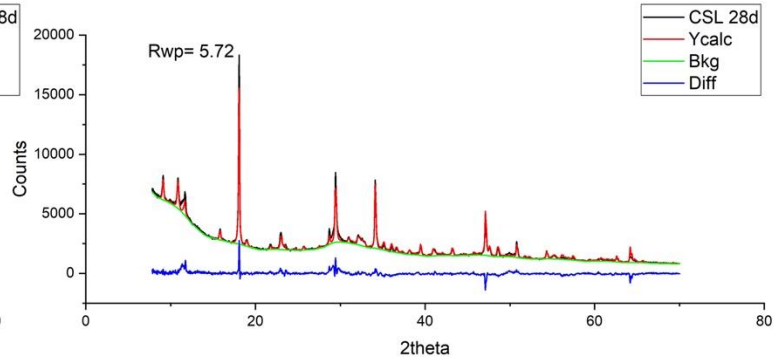
CSL 28d
Ycalc
Bkg
Diff
Rwp= 5.72
Counts
2theta

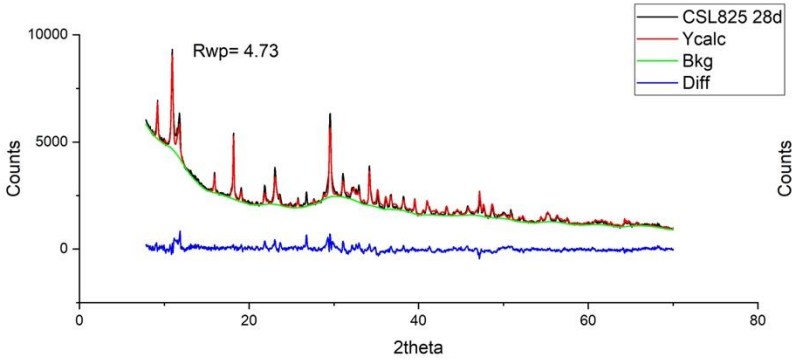
CSL825 28d
Ycalc
Bkg
Diff
Rwp= 4.73
Counts
2theta

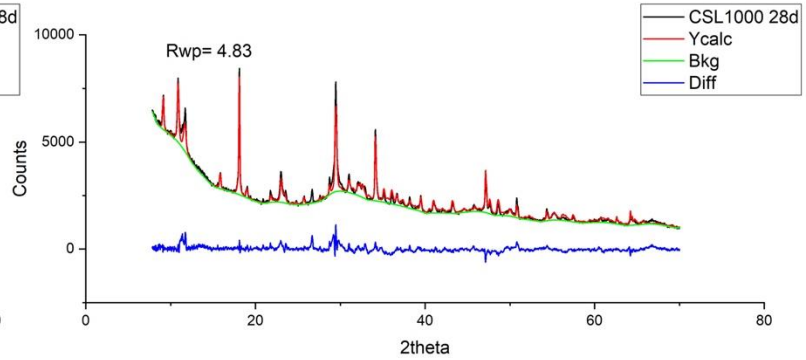
CSL1000 28d
Ycalc
Bkg
Diff
Rwp= 4.83
Counts
2theta

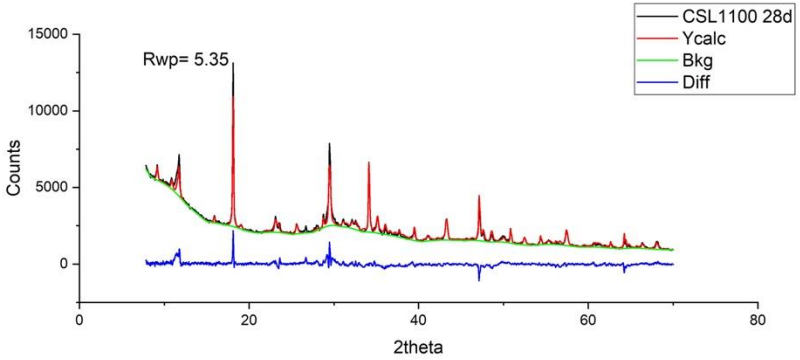
CSL1100 28d
Ycalc
Bkg
Diff
Rwp= 5.35
Counts
2theta

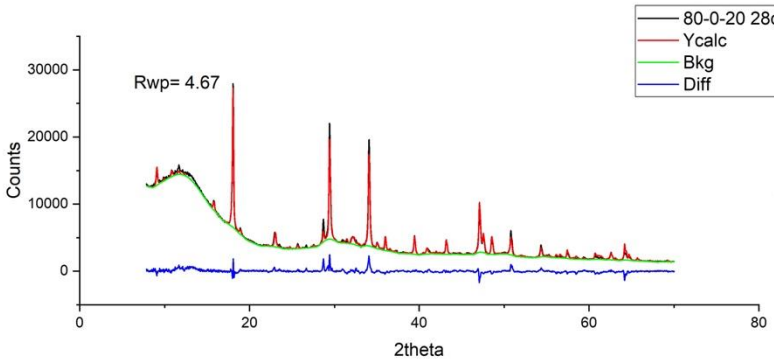
80-0-20 28d
Ycalc
Bkg
Diff
Rwp= 4.67
Counts
2theta

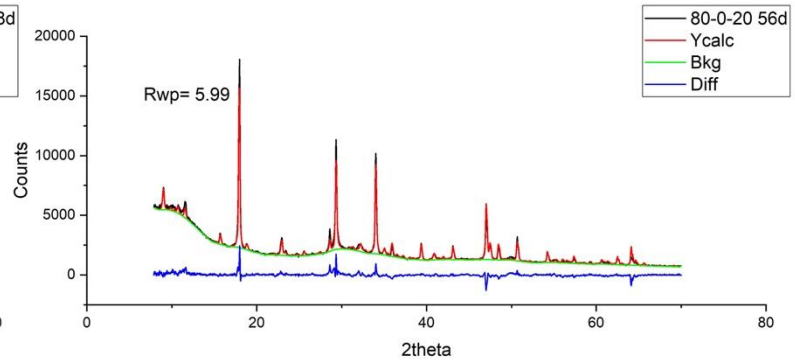
80-0-20 56d
Ycalc
Bkg
Diff
Rwp= 5.99
Counts
2theta

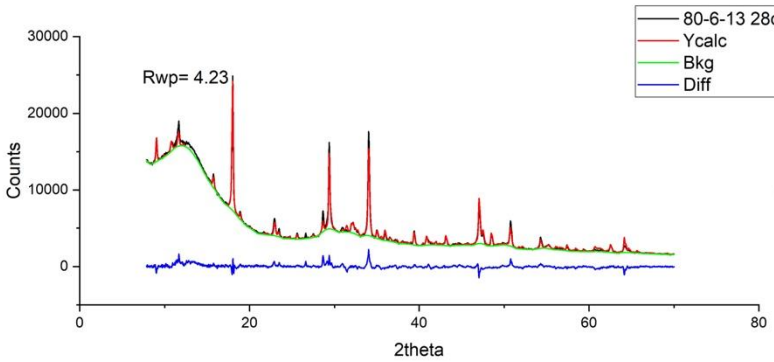
80-6-13 28d
Ycalc
Bkg
Diff
Rwp= 4.23
Counts
2theta

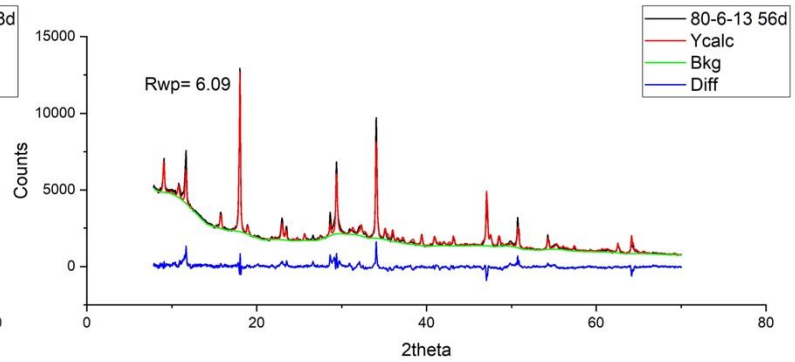
80-6-13 56d
Ycalc
Bkg
Diff
Rwp= 6.09
Counts
2theta

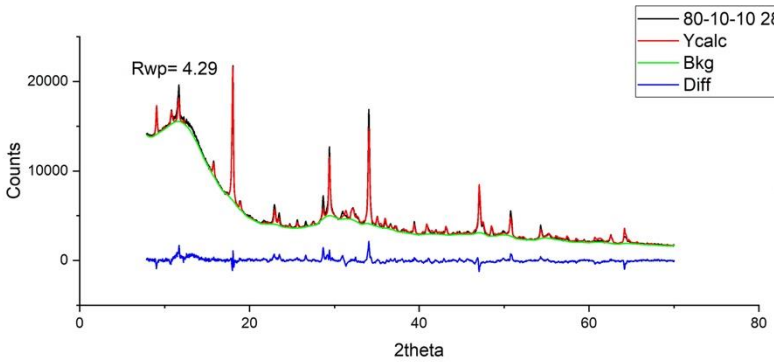
80-10-10 28d
Ycalc
Bkg
Diff
Rwp= 4.29
Counts
2theta

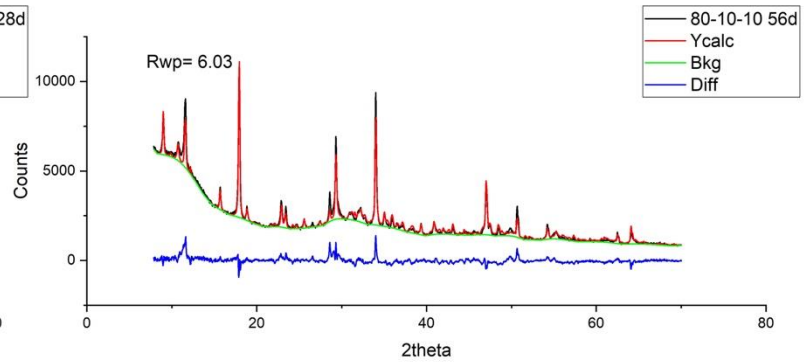
80-10-10 56d
Ycalc
Bkg
Diff
Rwp= 6.03
Counts
2theta

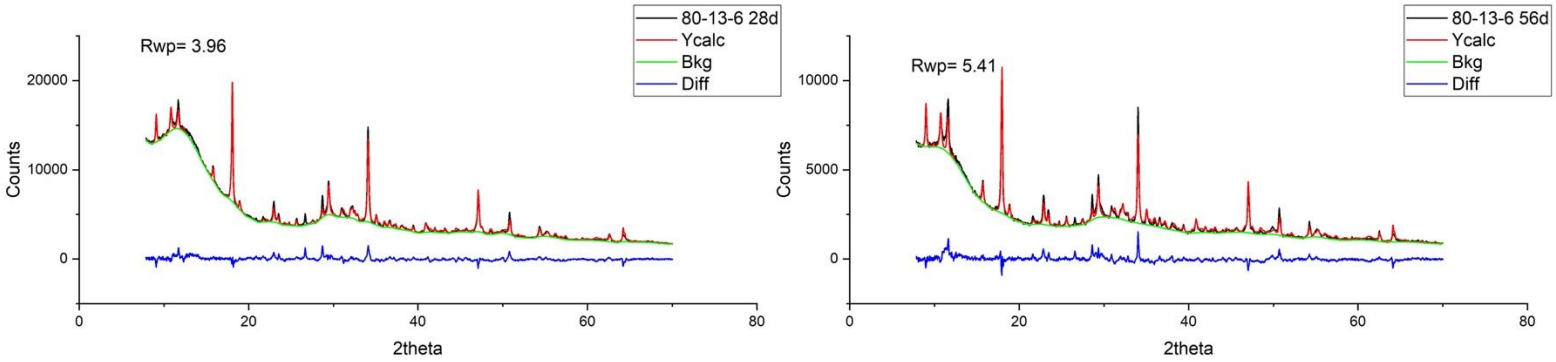
Rwp= 3.96
80-13-6 28d
Ycalc
Bkg
Diff
Counts
2theta
0
10000
20000
0
20
40
60
80
Rwp= 5.41
80-13-6 56d
Ycalc
Bkg
Diff
Counts
2theta
0
5000
10000
0
20
40
60
80

A.2 Backscattered SEM images and thresholding for quantitative analysis

These figures presented supplement the SEM results presented in the Chapter 5 and 6. The figures below show the quantification of cement grains by image analysis:

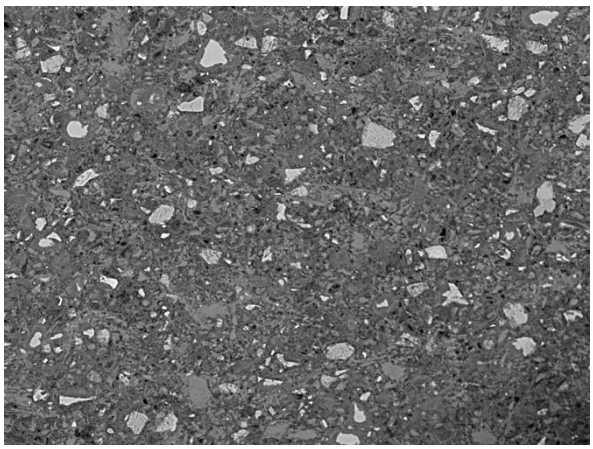
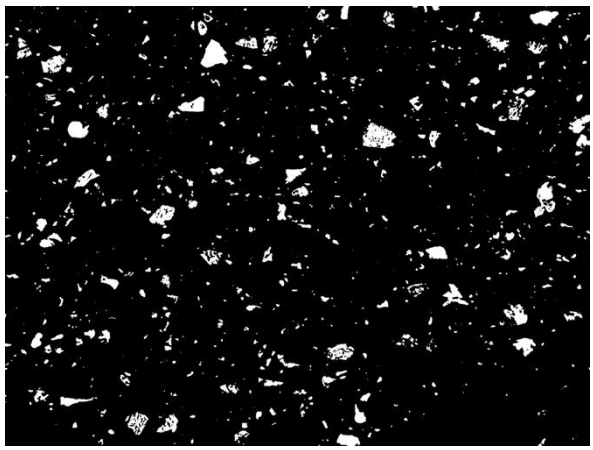

C 28d

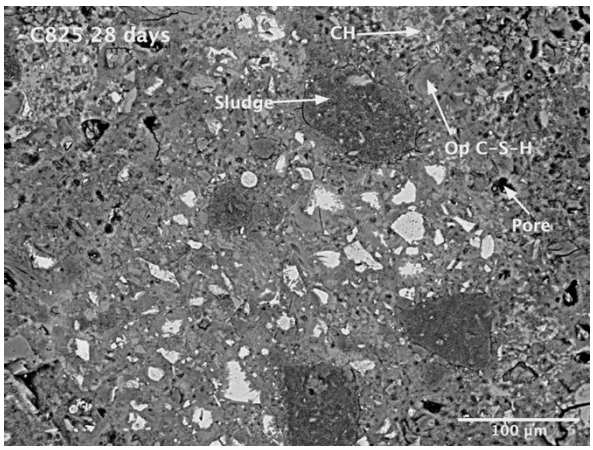

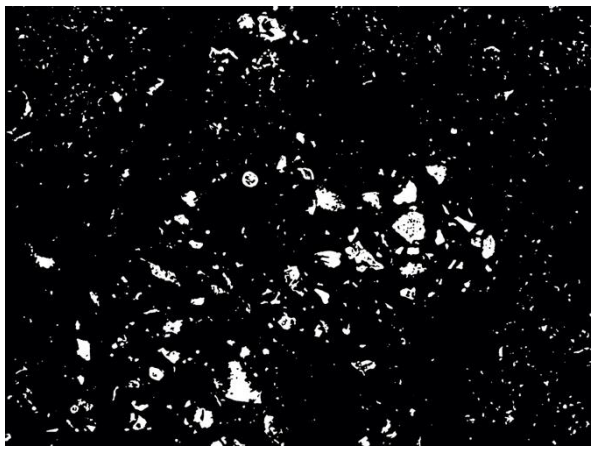

C825 28d

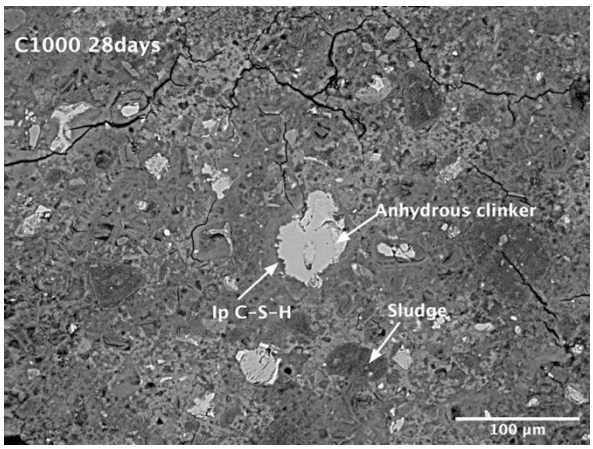

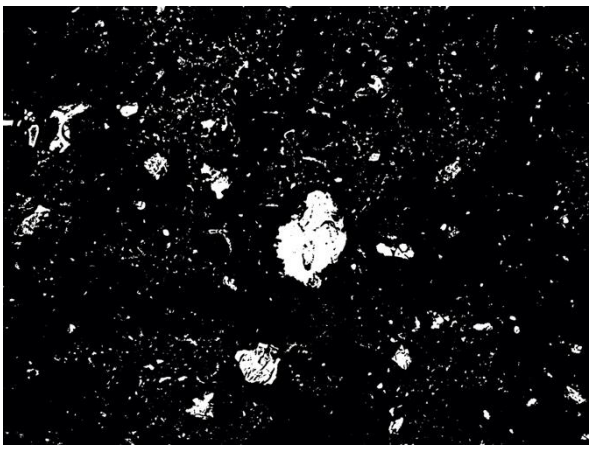

C1000 28d

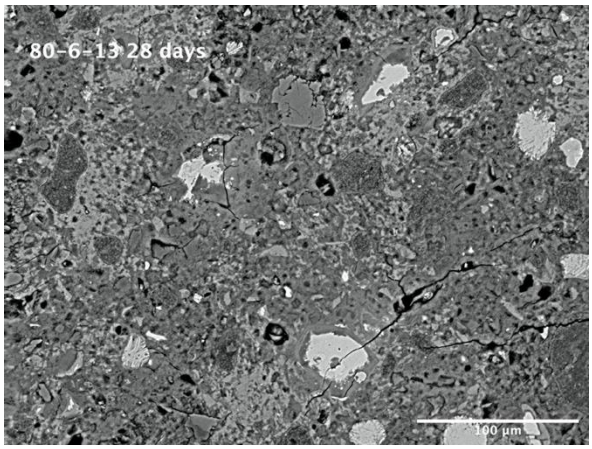

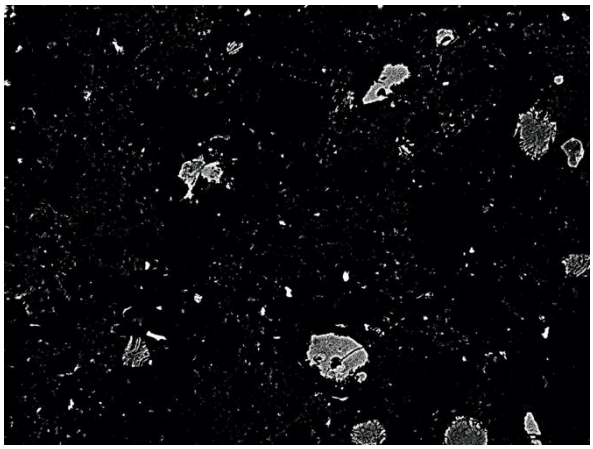

80-6.7-13.3 28d

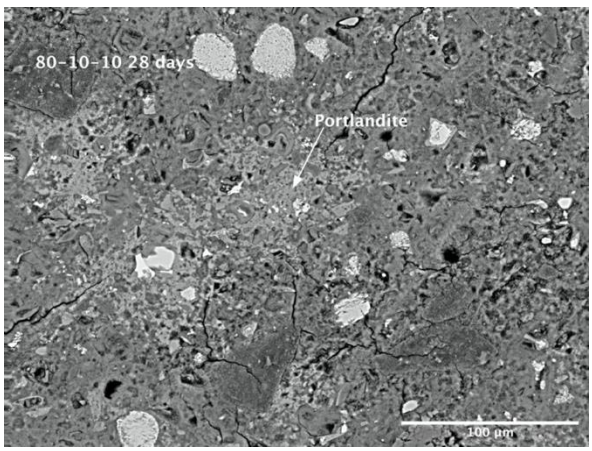

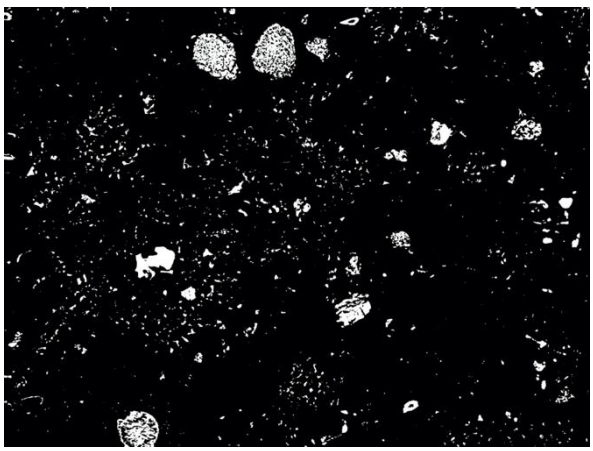

80-10-10 28d

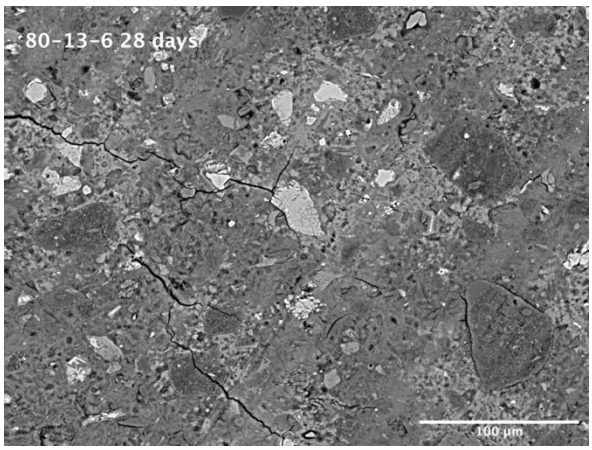

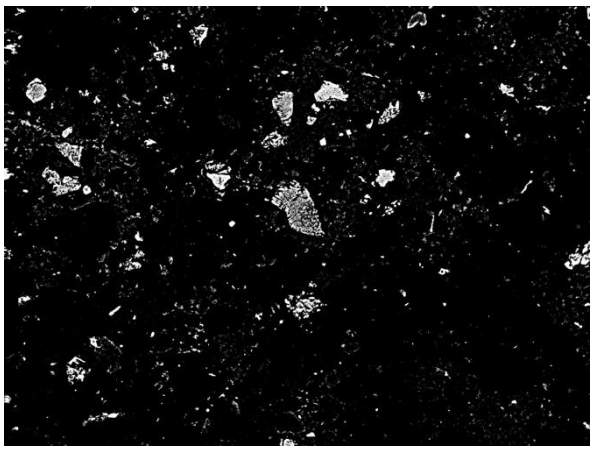

80-13.3-6.7 28d

The figures below show the quantification of anhydrous slag grains by image analysis:

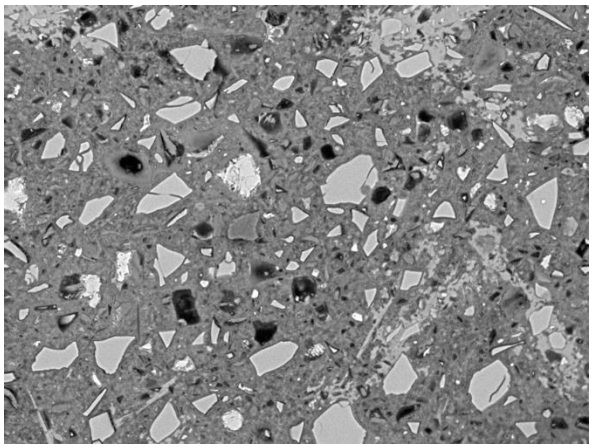
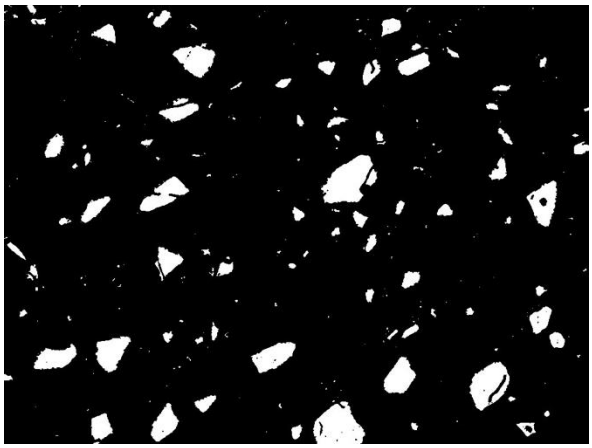

CS 28d

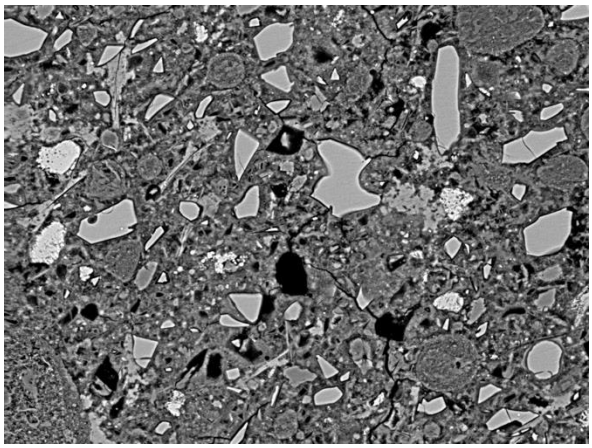
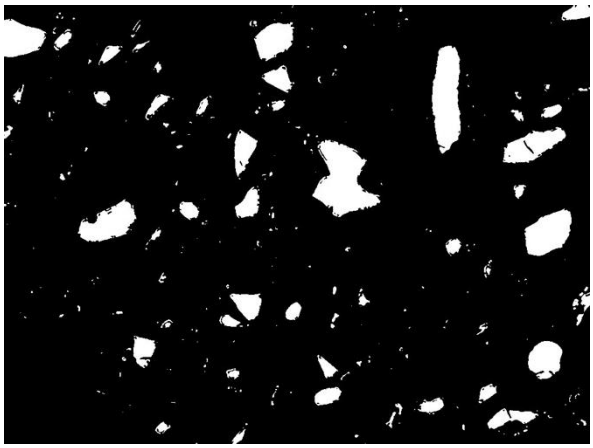

CS825 28d

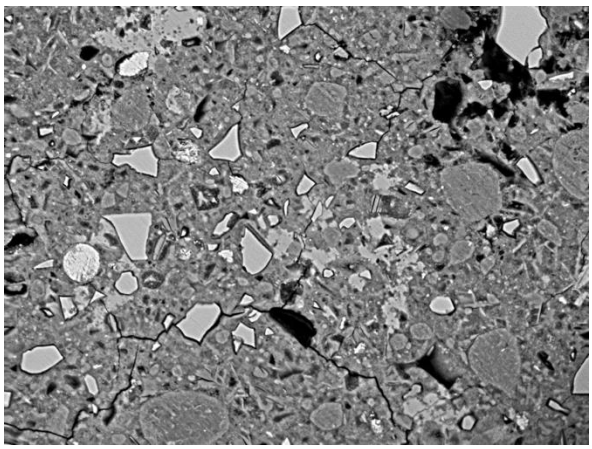
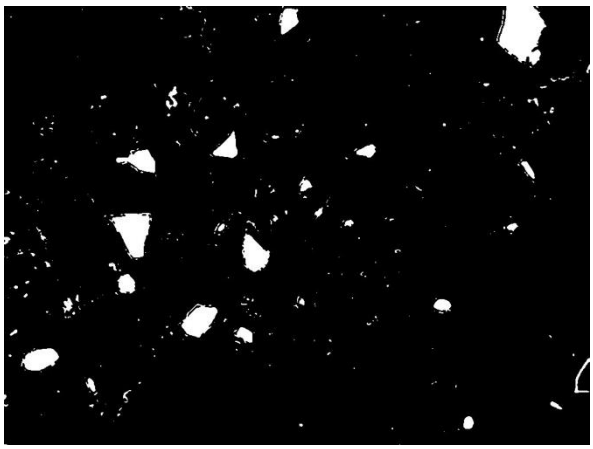

CS825 28d

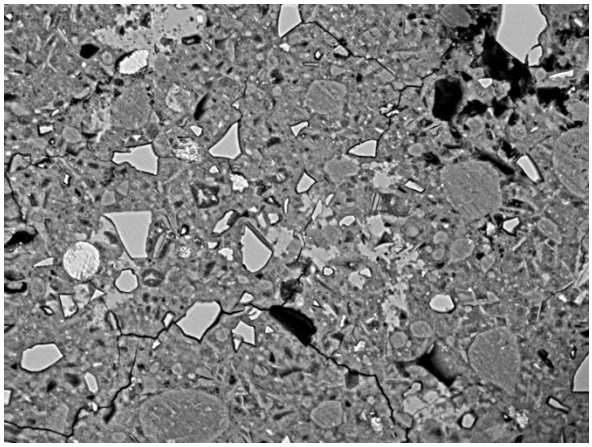
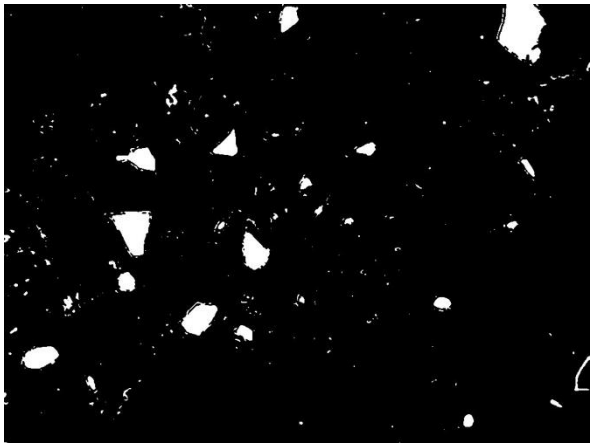

CS1000 28d

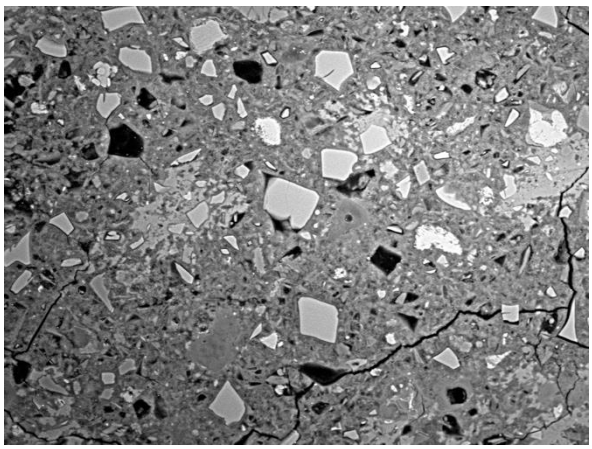
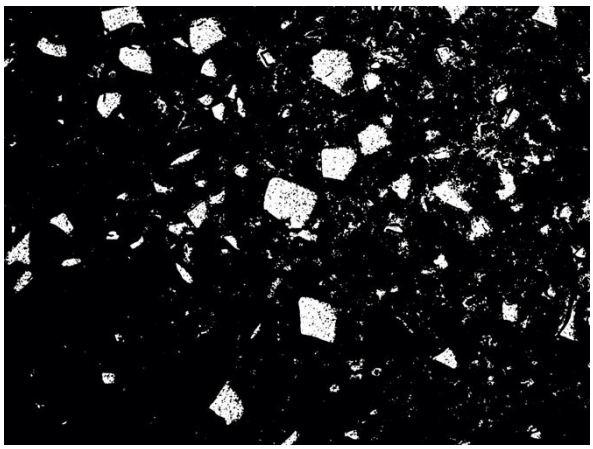

CSL 28d

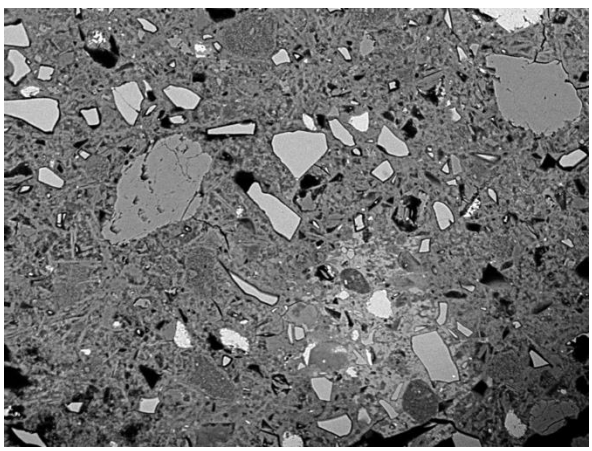
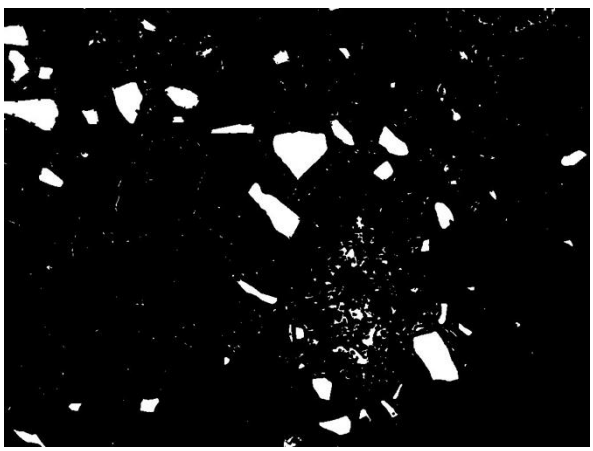

CSL825 28d

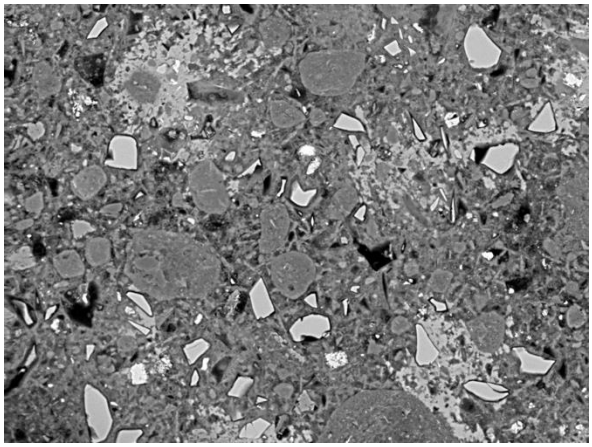
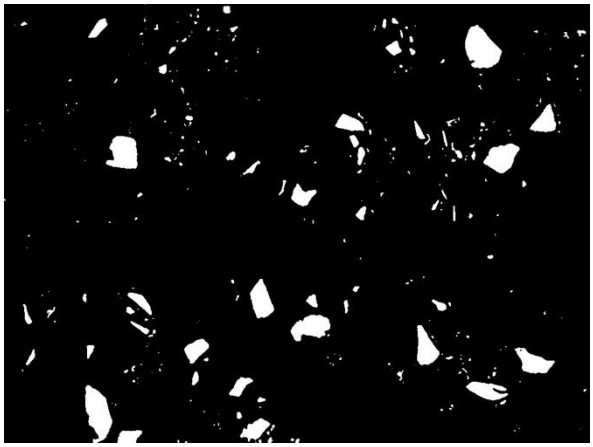

CSL1000 28d

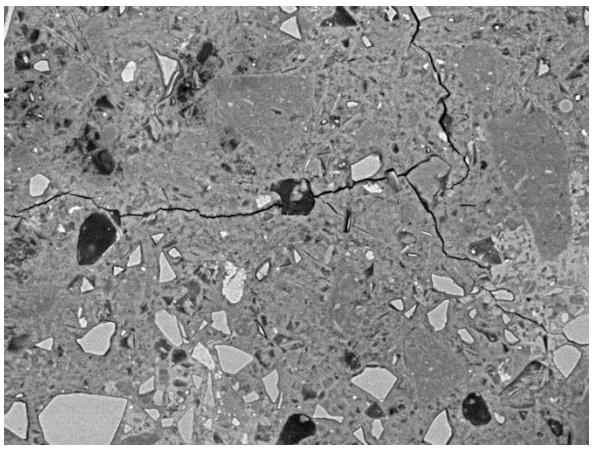
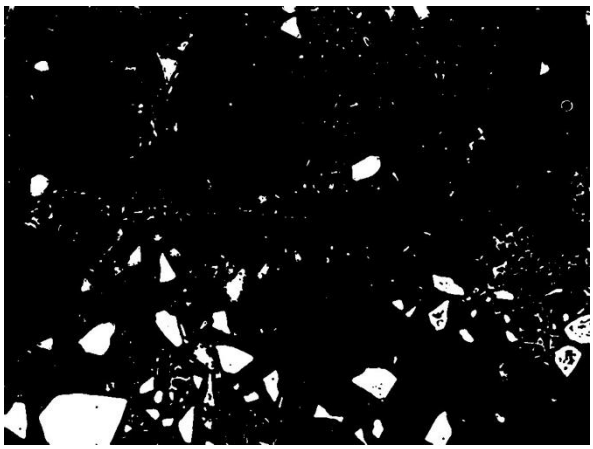

CSL1100 28d

A.3 Sorptivity Determination

The figures below illustrate the relation between water absorption per unit area and time as well as the sorptivity calculation procedure by regression analysis:

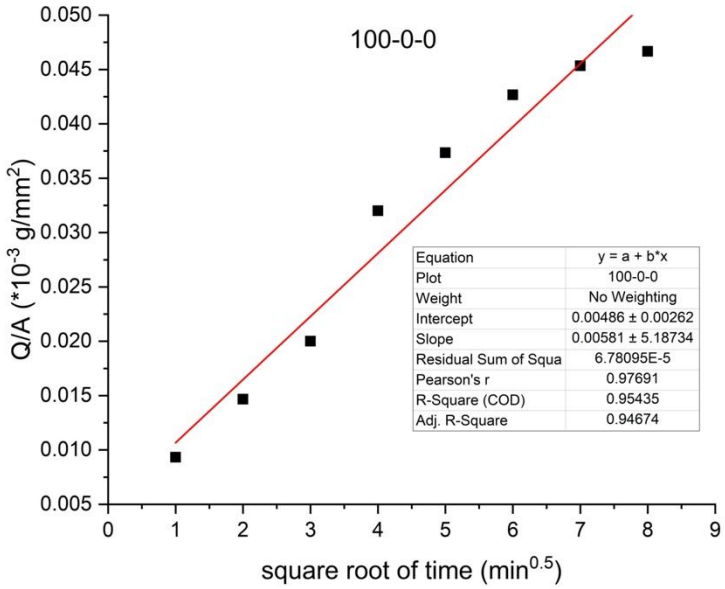

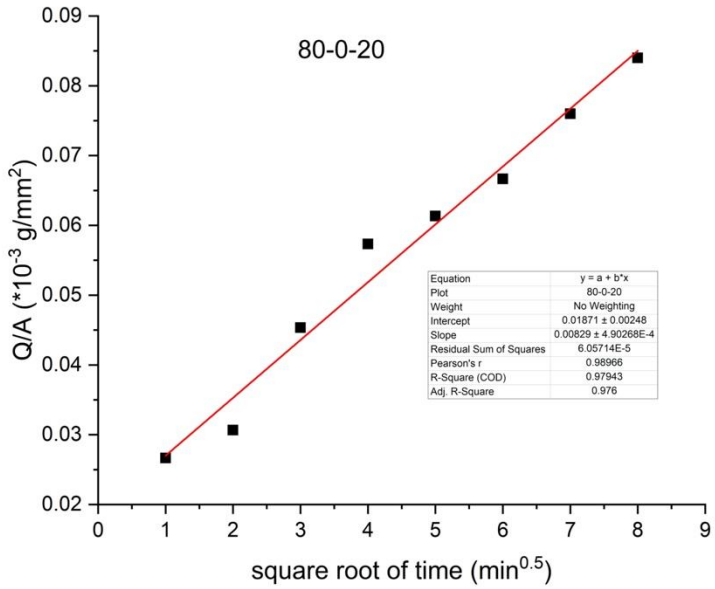

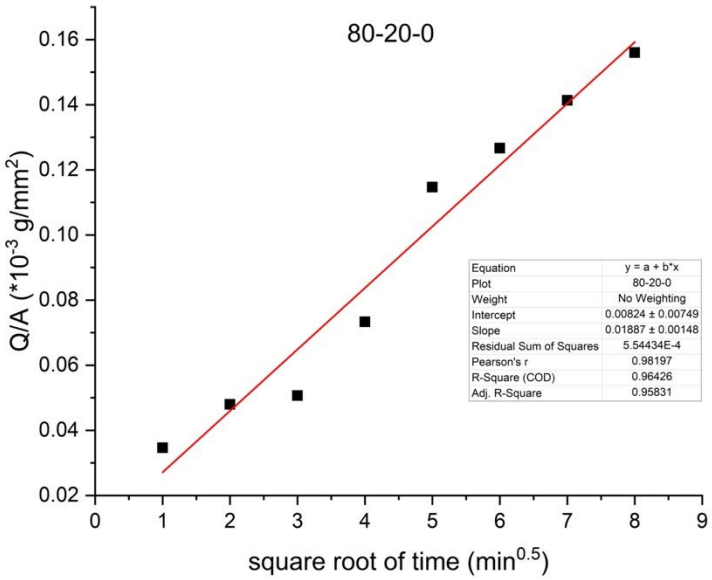
80-20-0
Q/A (*10-3 g/mm2)
square root of time (min0.5)
Equation y = a + b*x
Plot 80-20-0
Weight No Weighting
Intercept 0.00824 ± 0.00749
Slope 0.01887 ± 0.00148
Residual Sum of Squares 5.54434E-4
Pearson's r 0.98197
R-Square (COD) 0.96426
Adj. R-Square 0.95831

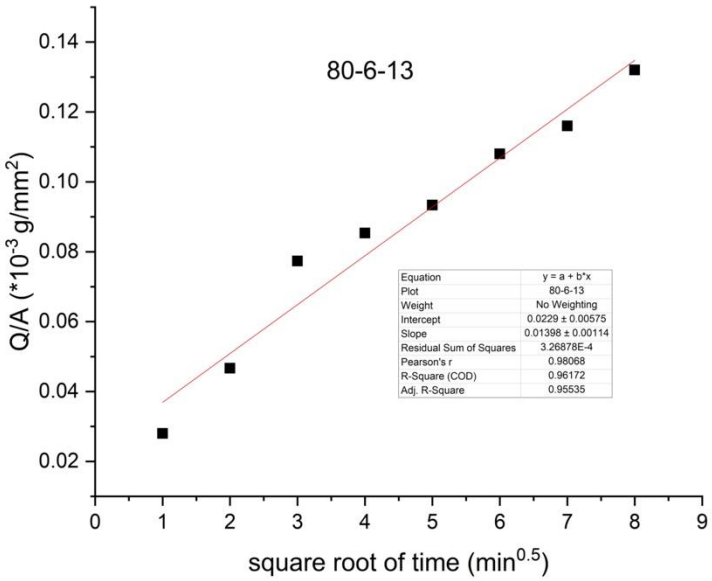
80-6-13
Q/A (*10-3 g/mm2)
square root of time (min0.5)
Equation y = a + b*x
Plot 80-6-13
Weight No Weighting
Intercept 0.0229 ± 0.00575
Slope 0.01398 ± 0.00114
Residual Sum of Squares 3.26878E-4
Pearson's r 0.98068
R-Square (COD) 0.96172
Adj. R-Square 0.95535

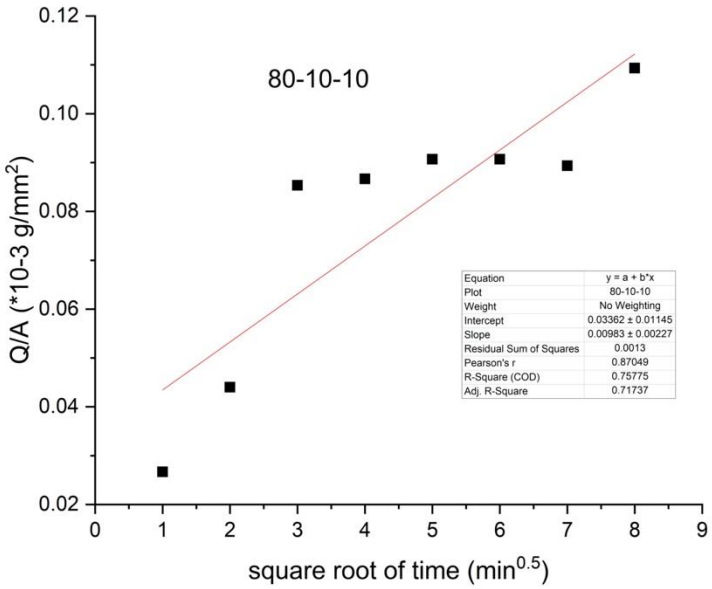
80-10-10
Q/A (*10-3 g/mm2)
square root of time (min0.5)
Equation y = a + b*x
Plot 80-10-10
Weight No Weighting
Intercept 0.03362 ± 0.01145
Slope 0.00983 ± 0.00227
Residual Sum of Squares 0.0013
Pearson's r 0.87049
R-Square (COD) 0.75775
Adj. R-Square 0.71737

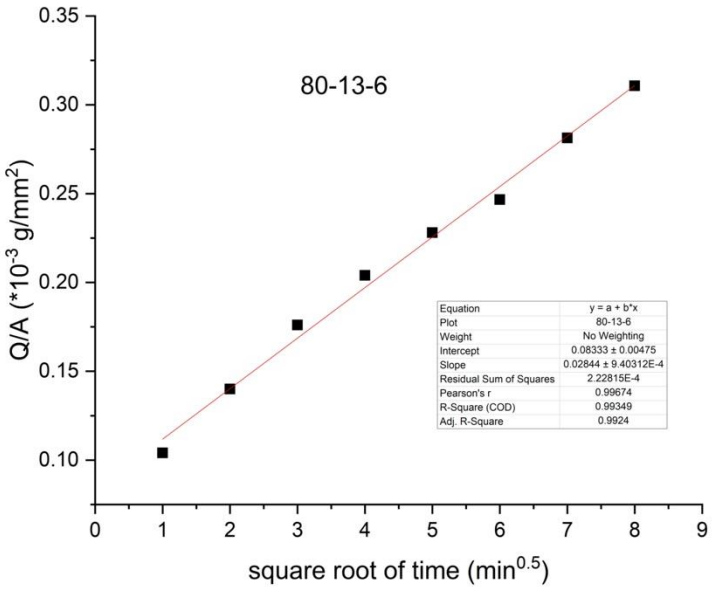
80-13-6
Q/A (*10-3 g/mm2)
square root of time (min0.5)
Equation y = a + b*x
Plot 80-13-6
Weight No Weighting
Intercept 0.08333 ± 0.00475
Slope 0.02844 ± 9.40312E-4
Residual Sum of Squares 2.22815E-4
Pearson's r 0.99674
R-Square (COD) 0.99349
Adj. R-Square 0.9924

A.4 Gas Permeability Determination

The figures below show the relation between the K and $1/P_m$ as well as the regression line for the determination of the corrected value of the gas permeability (Kg) in ternary limestone cements:

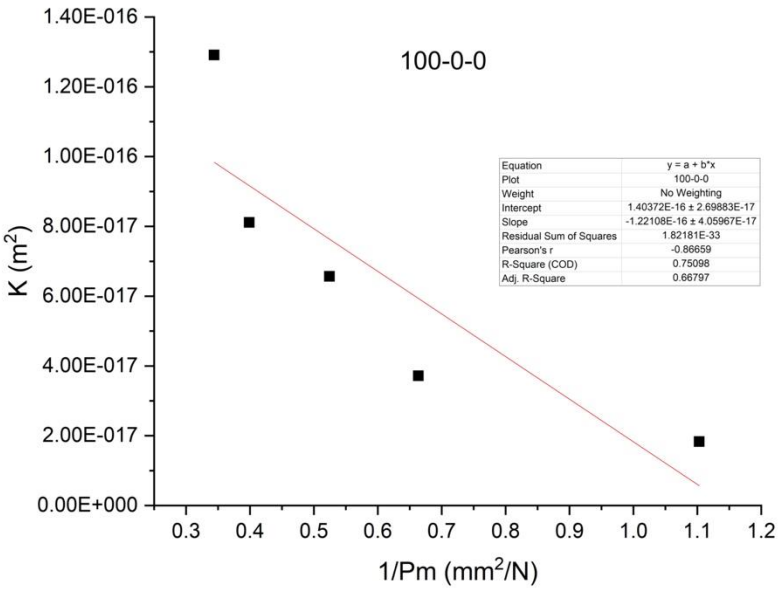

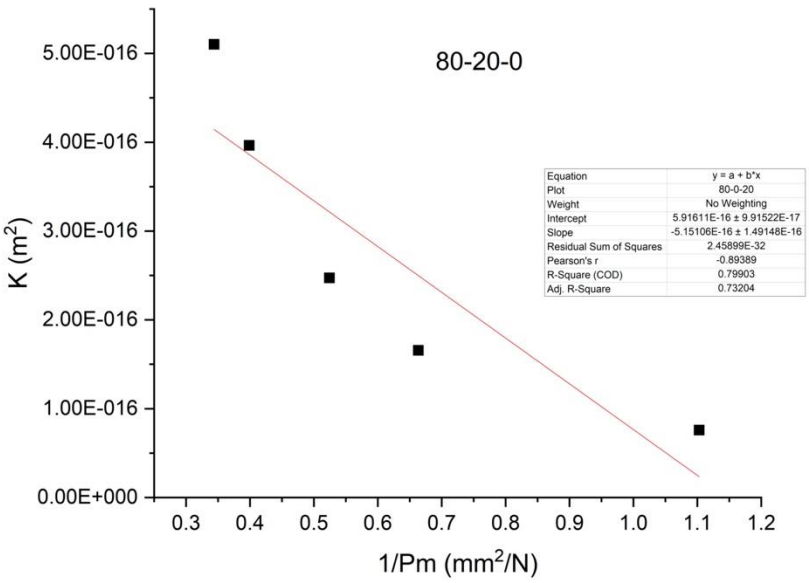

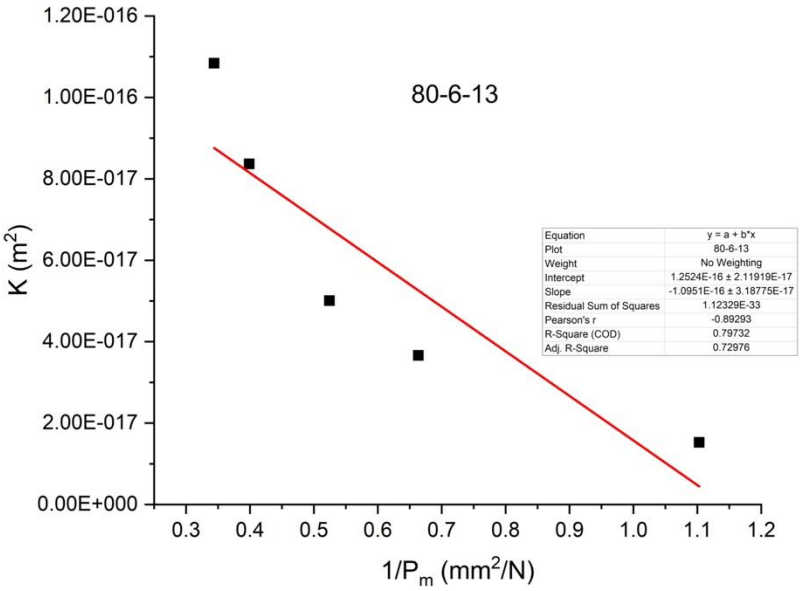
80-6-13
K (m²)
1/P_m (mm²/N)
1.20E-016
1.00E-016
8.00E-017
6.00E-017
4.00E-017
2.00E-017
0.00E+000
0.3
0.4
0.5
0.6
0.7
0.8
0.9
1.0
1.1
1.2
Equation y = a + b*x
Plot 80-6-13
Weight No Weighting
Intercept 1.2524E-16 ± 2.11919E-17
Slope -1.0951E-16 ± 3.18775E-17
Residual Sum of Squares 1.12329E-33
Pearson's r -0.89293
R-Square (COD) 0.79732
Adj. R-Square 0.72976

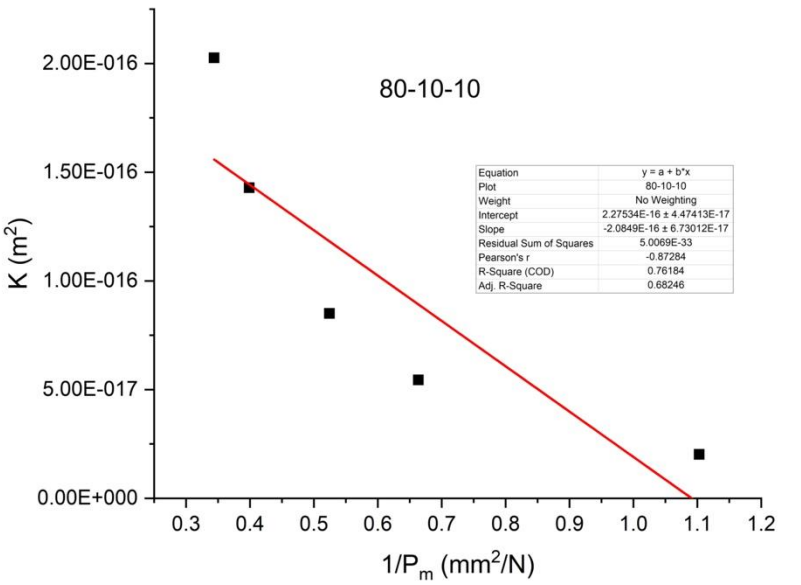
80-10-10
K (m²)
1/P_m (mm²/N)
2.00E-016
1.50E-016
1.00E-016
5.00E-017
0.00E+000
0.3
0.4
0.5
0.6
0.7
0.8
0.9
1.0
1.1
1.2
Equation y = a + b*x
Plot 80-10-10
Weight No Weighting
Intercept 2.27534E-16 ± 4.47413E-17
Slope -2.0849E-16 ± 6.73012E-17
Residual Sum of Squares 5.0069E-33
Pearson's r -0.87284
R-Square (COD) 0.76184
Adj. R-Square 0.68246

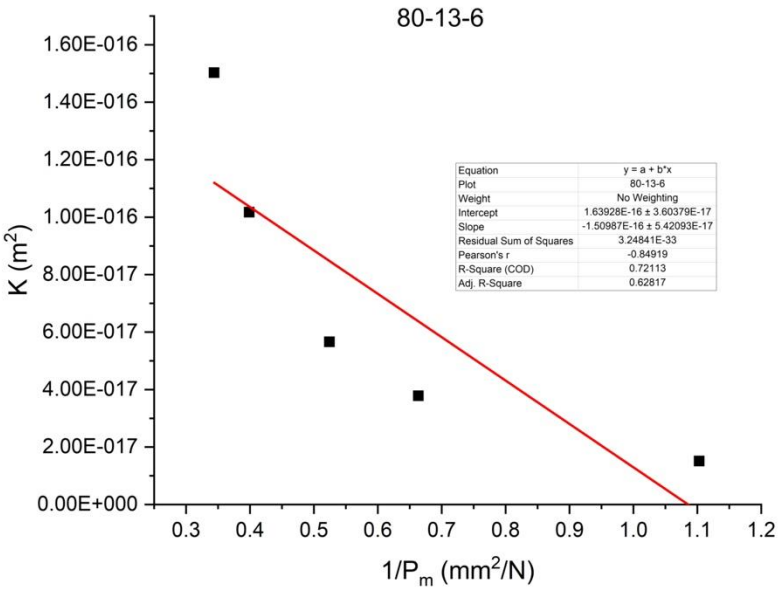
80-13-6
1.60E-016
1.40E-016
1.20E-016
1.00E-016
8.00E-017
6.00E-017
4.00E-017
2.00E-017
0.00E+000
K (m2)
0.3
0.4
0.5
0.6
0.7
0.8
0.9
1.0
1.1
1.2
1/Pm (mm2/N)
Equation y = a + b*x
Plot 80-13-6
Weight No Weighting
Intercept 1.63928E-16 ± 3.60379E-17
Slope -1.50987E-16 ± 5.42093E-17
Residual Sum of Squares 3.24841E-33
Pearson's r -0.84919
R-Square (COD) 0.72113
Adj. R-Square 0.62817

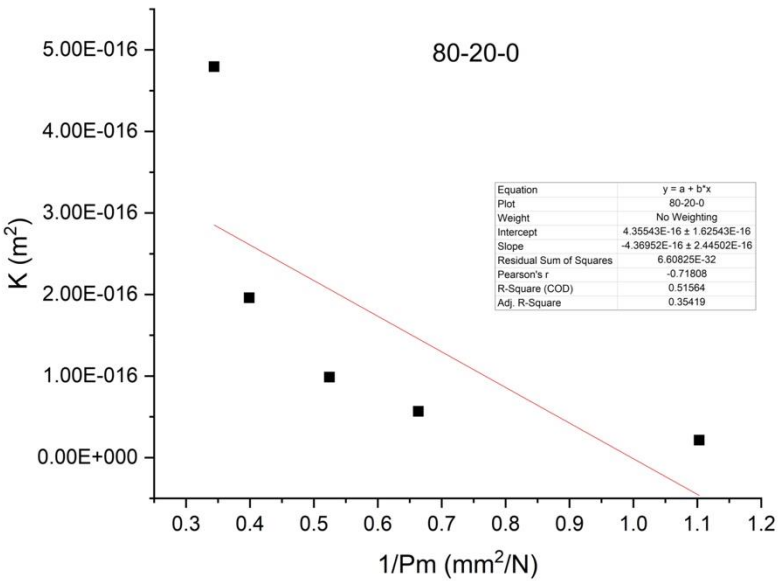
80-20-0
5.00E-016
4.00E-016
3.00E-016
2.00E-016
1.00E-016
0.00E+000
K (m2)
0.3
0.4
0.5
0.6
0.7
0.8
0.9
1.0
1.1
1.2
1/Pm (mm2/N)
Equation y = a + b*x
Plot 80-20-0
Weight No Weighting
Intercept 4.35543E-16 ± 1.62543E-16
Slope -4.36952E-16 ± 2.44502E-16
Residual Sum of Squares 6.60825E-32
Pearson's r -0.71808
R-Square (COD) 0.51564
Adj. R-Square 0.35419